

***Reversible Polymeric Actuators:
Bidirectionality of the thermally induced
two-way shape memory effect of
semicrystalline polymer networks under
constant strain conditions***

DISSERTATION

zur Erlangung des akademischen Grades eines

Doktors der Naturwissenschaften (Dr. rer. Nat.)

im Promotionsprogramm „Polymer Science“

in der Bayreuther Graduiertenschule für Mathematik und Naturwissenschaften

(BayNAT)

der Universität Bayreuth

vorgelegt von

Andrés Fernando Posada Murcia

aus Bogotá, Kolumbien

Bayreuth, 2022

The work presented in this dissertation started in October 2018 and was finished in January 2022; it was carried out in the Biofabrication group at the University of Bayreuth under the supervision of Prof. Leonid Ionov.

Date of submission: 17.05.2022

Date of defense: 02.11.2022

Acting Director: Prof. Dr. Hans Keppler

Doctoral committee:

Prof. Dr. Leonid Ionov (reviewer)

Prof. Dr.-Ing. Holger Ruckdäschel (reviewer)

Prof. Dr. Markus Retsch (chairman)

Prof. Dr. Seema Agarwal

*Me er eit gamalt tre
Med nysprungene knoppar
Mot sola me strekk oss
Fram for å vekse
Langt need i rot
og i ringar av år
Kved dei gamle
Høyr!
Sjå meg djupt i augene
du må forstå
Hugs at alle
eingong forlét
Natta den kjem
Hugs, ta ikkje meir
enn du orkar å bere
For kvar einaste spire
Vert me høgare og djupare*

Einar Selvik

Table Of Contents

Summary	1
Zusammenfassung	4
1.Introduction	7
1.1 Smart Materials	7
1.2 Smart Polymers	9
1.3 Shape Changing Polymers (SCPs)	11
1.4 Shape-memory Polymers (SMPs)	13
1.4.1 One-way Shape-memory Effect (SME)	15
1.4.2 Two-way shape memory polymers.....	17
1.4.2.1 2W-SME: From the LCEs to Semicrystalline Polymers.....	19
1.4.2.2 2W-SME on Semicrystalline Polymer Networks.....	20
1.4.2.3 Rubber Elasticity: The Entropic Contribution to the SME	23
1.4.2.3a The Ideal Chain Model	23
1.4.2.3b The Rubber Elasticity and the 1W-SME	25
1.4.2.3c The Rubber Elasticity and the 2W-SME.....	27
1.4.2.4 Towards the Molecular Model of the 2W-SME.....	29
1.4.2.5 2W-SME Under Stress-Free Conditions	33
1.4.2.6 Crosslinked PCL Networks and Their Polyurethane Copolymers on 2W-SME.....	35
2. Aim.....	39
3. Synopsis	40
3.1 Two-Way Shape Memory Polymers: Evolution of Stress vs Evolution of Elongation.....	40
3.2 Mechanism of Behavior of Two-Way Shape Memory Polymer under Constant Strain Conditions	42
3.3 Bidirectional shape memory polymers: effect of molecular architecture over the thermomechanical behavior at constant stress and constant strain conditions.....	44
4. Literature References.....	48
5. Publication List on BTU	57
6. Individual Contribution to Publications/Manuscript as First Author on BTU	58
7. Publications/Manuscripts	60
Publication 1	60
Publication 2	77
Publication 3	102
8. Conclusion.....	164
9. Outlook.....	167
Acknowledgements	168

Summary

Materials science, a central interdisciplinary field that studies the development of new materials as well as the characterization of their properties, applications, and behaviour, has focused since its inception on the usage of man-developed or natural materials to facilitate the realization of quotidian tasks. Among the most relevant and greatly investigated variety of developed materials in the last decades, we find the so-called “smart” materials. These materials are able to emit a response to an external stimulus. Amid this category, we encounter the stimuli-responsive polymers. The vast investigation of their mechanical, physicochemical, and functionality has caused that their application on the programmable matter area surpasses by far the study of other materials able to respond to a stimulus. The smart polymers are able to deliver a well-controlled, programmed, and high amplitude response to a perturbation through their actuation. Therefore, the development of polymeric actuators with the ability to perform even more intricate and specific operations/tasks has been, for more than two decades, the goal of a great portion of the scientific community involved in the material science discipline.^{1,2}

Due to the huge structural variety of polymers, we also encounter a broad categorization of the actuators made from them. The stimuli-responsive polymers based on crosslinked semicrystalline polymer networks and their phase differentiated copolymers, which actuation is triggered by the melting-crystallization phase transition of their crystalline domains, are one of the most relevant kinds of polymeric actuators. Their facile processability, tailorable thermal properties, reversible actuation in dry/wet environments, and the possibility of autonomous/stand-alone actuation have drawn the researcher’s attention towards these materials. Despite their extensive investigation, a formal and complete description of their actuation mechanism has remained, until today, evasive. The lack of clarity on the physical origin of their reversible actuation unequivocally hinders the design and further development of more robust and advanced actuators, truncating the progress of the programmable matter study.

For all the aforementioned, the aim of this dissertation was to contribute to the understanding of the reversible actuation of semicrystalline polymer networks, specifically focusing on the study of the mechanism behind the thermally triggered two-way shape memory effect (2W-SME) exhibited by these materials. This investigation was performed on high molecular weight crosslinked poly(ϵ -caprolactone) (PCL) networks and poly(ϵ -caprolactone)-based urethane derivatives. The working/model materials were chosen after considering the topic's current state of the art and their outstanding reversible SME behavior. First, to contribute to the unveiling of the physical origin for the shape-shifting transformation of semicrystalline polymers under load, a conscious rheological study was proposed.

Loaded and unstretched linear PCL samples containing different crosslinking densities subjected to thermal cycling were studied under constant stress and strain conditions. This allowed the identification of the strain degree, the load magnitude, and the effective crosslinking density of the materials as the parameters that have a profound effect on the reversibility of the shape-switching transformation. Additionally, the unprecedented constant strain evaluation of the cured PCL samples facilitated the identification of an unexpected intermediate state in between the cooling process from the molten to the crystalline state. This state is characterized by an odd drop in the measured extensional stress, which becomes sharper as the stretching degree of the sample arises.

After the identification of this unusual intermediate state on constantly drawn PCL, the study of its origin became imperative. Simultaneous thermomechanical and structural analysis, and *in-situ* X-ray scattering measurements, were carried out to identify the correspondence between the shape-switching ability and the evolution of the structural features of a polymer framework under constant strain. A model describing the crystallization behavior of highly strained semicrystalline polymers under constant strain was developed which was supported by the acquired data. The coexistence of two well-distinguishable crystallite families during the crystallization process brings clarity to the first observed odd thermomechanical observations.

As the 2W-SME of crosslinked linear PCL networks was successfully explored and characterized under constant stress and strain conditions, the investigation of the bidirectional SME of PCL-based materials exhibiting varied molecular architectures was driven. A direct comparison between the shape memory features of crosslinked linear PCL, crosslinked PCL-armed star-like polymer, and PCL-urethane copolymers (containing hexamethylene and methylene diphenyl diisocyanate as hard segments, with butanediol as chain extender) under constant stress and constant strain setup was proposed. This approach intends to unify the gathered observations on the reversible shape transformations experienced by semicrystalline polymer networks to develop a critical overview for their further usage and application, emphasizing their thermomechanical, physicochemical, and textural characteristics.

Finally, the ultimate goal of the work contained in this dissertation is to open a new spectrum of possibilities for the design and application of reversible shape-transforming actuating materials/composites based on tailorable thermally active semicrystalline polymer matrixes for different applications, including soft-electronics, medicine, biofabrication, robotics among others by providing a rigorous tensile, thermal and structural description of the stages composing their bidirectional SME behaviour.

Zusammenfassung

Das interdisziplinäre Forschungsgebiet der Materialwissenschaften, das die Entwicklung neuer Materialien und die Charakterisierung ihrer Eigenschaften, Anwendungen und ihres Verhaltens untersucht, hat sich seit ihren Anfängen auf die Verwendung von künstlichen oder natürlichen Materialien konzentriert, um die Umsetzung alltäglicher Aufgaben zu erleichtern. Zu den relevantesten und am intensivsten untersuchten Materialien, die in den letzten Jahrzehnten entwickelt wurden, gehören die sogenannten „intelligenten“ Materialien. Diese Materialien sind in der Lage auf einen äußeren Stimulus zu reagieren und gehören damit in die Kategorie der stimuliresponsiven Polymere. Die umfangreiche Untersuchung ihrer mechanischen, physikochemischen und funktionellen Eigenschaften hat dazu geführt, dass ihre Anwendung auf dem Gebiet der programmierbaren Materie die Untersuchung anderer Materialien, die auf einen Stimulus reagieren können, bei weitem übertrifft. Die intelligenten Polymere sind in der Lage eine präzise kontrollierte Antwort mit hoher Amplitude auf ein externes Signal zu liefern. Die Entwicklung von Polymeraktoren mit der Fähigkeit noch kompliziertere und spezifischere Funktionen bereit zu stellen, ist daher seit mehr als zwei Jahrzehnten das Ziel eines großen Teils der wissenschaftlichen Gemeinschaft, die sich mit den Materialwissenschaften befasst.

Aufgrund der enormen strukturellen Vielfalt von Polymeren existiert bereits eine umfangreiche Kategorisierung der resultierenden Aktoren. Zu den relevantesten Vertretern zählen die stimuliresponsiven Polymere basierend auf vernetzten teilkristallinen Polymernetzwerken und ihren phasendifferenzierten Copolymeren, deren Aktivierung durch den Schmelz-Kristallisations-Phasenübergang ihrer kristallinen Domänen ausgelöst wird. Ihre einfache Verarbeitbarkeit, einstellbaren thermischen Eigenschaften, reversible Funktion in trockener/feuchter Umgebung und die Möglichkeit einer autonomen Aktivierung haben die Aufmerksamkeit der Forscher auf diese Materialien gelenkt. Trotz umfangreicher Untersuchungen gibt es bis heute keine fundierte und vollständige Beschreibung ihres Funktionsmechanismus. Ohne das Wissen über den physikalischen Hintergrund ihrer reversiblen Aktivierung ist die Weiterentwicklung und das Design von robusteren und

fortschrittlicheren Aktuatoren nur beschränkt möglich, was den aktuellen Fortschritt der Erforschung programmierbarer Materie hemmt.

Das Ziel dieser Dissertation war daher einen Beitrag zum Verständnis der reversiblen Aktivierung von teilkristallinen Polymernetzwerken zu leisten. Der Schwerpunkt lag dabei insbesondere auf der Untersuchung des Mechanismus hinter dem thermisch ausgelösten Zwei-Wege-Formgedächtniseffekt (2W-SME). Dafür wurden vernetzte Poly(ϵ -caprolacton) (PCL)-Netzwerke mit hohem Molekulargewicht und Urethanderivate auf Poly(ϵ -caprolacton)-Basis untersucht. Die verwendeten Materialien wurden unter Berücksichtigung des aktuellen Stands der Forschung in diesem Fachbereich und ihres hervorragenden reversiblen SME-Verhaltens ausgewählt. Zunächst wurde eine rheologische Studie entworfen, um den physikalischen Ursprung der Formänderung von teilkristallinen Polymeren unter Belastung zu ermitteln.

Beladene und ungedehnte lineare PCL-Proben mit unterschiedlichen Vernetzungsdichten wurden Temperaturwechseln unterzogen und unter konstanten Spannungs- und Dehnungsbedingungen untersucht. Dies ermöglichte die Identifizierung des Dehnungsgrades, der maximalen Belastung und der effektiven Vernetzungsdichte als die dominierenden Materialparameter für die Umkehrbarkeit der Formänderung. Darüber hinaus ermöglichte die Auswertung der konstanten Dehnungsmessung der gehärteten PCL-Proben die Identifizierung eines bisher unbeschriebenen Übergangszustands im Abkühlprozess zwischen dem geschmolzenen und dem kristallinen Zustand. Dieser Zustand ist durch einen plötzlichen Abfall der gemessenen Dehnspannung gekennzeichnet, der mit zunehmendem Dehnungsgrad der Probe deutlicher ausgeprägt ist.

Nach der Identifizierung dieses ungewöhnlichen Zwischenzustands bei PCL unter konstantem Zug, wurde die Untersuchung seines Ursprungs priorisiert. Gleichzeitig wurden thermomechanische und strukturelle Analysen, sowie in-situ-Röntgenstreuungsmessungen durchgeführt, um den Zusammenhang zwischen der Fähigkeit zur Formänderung und der Entwicklung der strukturellen Merkmale eines Polymergerüsts unter konstanter Dehnung aufzuklären. Basierend auf den gewonnenen Daten wurde ein Modell zur Beschreibung des Kristallisationsverhaltens hochbelasteter teilkristalliner Polymere unter konstanter Dehnung

entwickelt. Die Entdeckung der Koexistenz zweier gut unterscheidbarer Kristallit-Familien während des Kristallisationsprozesses erklärt das zuvor beobachtete unerwartete thermomechanische Verhalten.

Durch die Erforschung und Charakterisierung der 2W-SME von vernetzten linearen PCL-Netzwerken unter konstanten Spannungs- und Dehnungsbedingungen, konnten neue Erkenntnisse über den bidirektionalen SME von PCL-basierten Materialien mit unterschiedlichen molekularen Architekturen gewonnen werden. Es wird ein direkter Vergleich zwischen den Formgedächtniseigenschaften von vernetztem linearem PCL, vernetztem sternförmigem PCL und PCL-Urethan-Copolymeren (mit Hexamethylen- und Methylendiphenyldiisocyanat als harten Segmenten und Butandiol als Kettenverlängerer) unter konstanter Spannung und konstanter Dehnung vorgeschlagen. Dieser Ansatz zielt darauf ab, die gesammelten Beobachtungen zur reversiblen Formänderung teilkristalliner Polymernetzwerke zu vereinheitlichen. Damit soll ein kritischer Überblick für ihre Anwendung ermöglicht werden, wobei der Schwerpunkt auf ihren thermomechanischen, physikochemischen und strukturellen Eigenschaften liegt.

Letztendlich ist das ultimative Ziel dieser Arbeit, ein neues Spektrum an Möglichkeiten für das Design und die Anwendung von reversibel formwandelnden Aktuatormaterialien/Verbundwerkstoffen zu eröffnen. Diese basieren auf maßgeschneiderten und thermisch aktiven teilkristallinen Polymermatrizen für verschiedene Anwendungen wie der Soft-Elektronik, Medizin, Biofabrikation oder Robotik. Ermöglicht wird dies durch die Beschreibung der mechanischen, thermischen und strukturellen Eigenschaften der Phasen, die das bidirektionale SME-Verhalten dieser Materialien bestimmen.

1.Introduction

Historically, materials have played an important role in the progress of humanity and have shaped life as we know it nowadays. From the usage of stone in 2.000 BCE for the fabrication of the first precarious tools, the arrival of the metalworking to the discovery of materials such as bronze and iron. These achievements represented an improvement in the durability and functionality of the everytime more intricate and complex artifacts crafted from them. Also, supposed a benefit for the humankind by supporting the abandonment of a nomad lifestyle to constitute what we know today as civilization.

The urgency of improving the features/properties and creating more versatile and universal materials serves the purpose of suppling and relieving even greater necessities. This urgency has served as the driving force of science and engineering progress until our days, where plastics and composite materials have governed the current era and are present in all modern commodities. The extensive research and uncountable advances in the materials science field have allowed the diversification of these materials, massively produced around the world. It has also allowed them to provide a solution to very specific problems, meet very precise requirements, or fill a particular need.

In recent decades, the development of new components has been focused on the designing and production of biodegradable, environment-friendly, sustainable, and even more functional materials. Nowadays, the modern research on this topic is highly inspired by living organisms, specifically by one of their most primitive yet complex and fascinating features: the response to a perturbation or a stimulation. This line of investigation has given birth to the era of the smart material.³⁻⁵

1.1 Smart Materials

Smart materials are, by definition a sort of materials with the capability to respond to an external stimulus through its reception, transmission, or processing; the effect of this response is used to perform a determined action/task to the material's surroundings while its magnitude and performance through time are tailorable features which are strongly

dependent on the chemical nature of the material, by the sort of the impressed stimuli and of course of its application.

The most common responses obtained from a smart material are: change of color, emission of light, voltage, change of shape or volume and index refraction; this broad variety of responses expands greatly the possible application of the smart materials going from the development of self-healing surfaces, biosensing, smart textile production, components for the aerospace industry, electronics and robotics, smart catalysis, drug delivery systems, biofabrication et cetera. Within the several kinds of applied stimulus triggering the actuation of the smart materials we find mechanical stress, electromagnetic fields, gradient of temperature, change of pH, irradiation with assorted types of radiation, mechanical strain, hydrostatic pressure among others.⁶

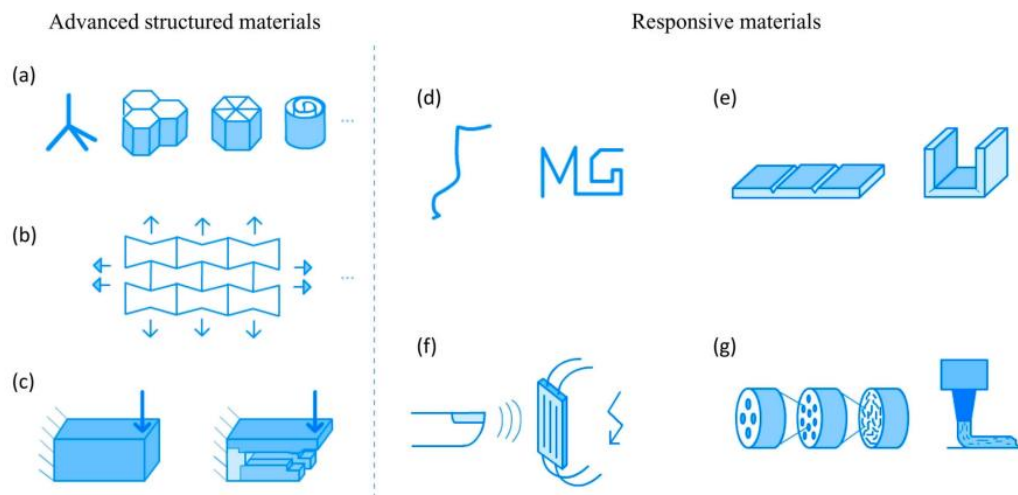


Figure 1. One of many classification systems of smart materials: Advanced structured materials and responsive materials. (a) Specific lattices, (b) Metamaterials and cellular auxetic materials, (c) Multi-materials (topological optimization), (d) Shape memory material on 1D, and (e) 3D self-assembly, (f) Electroactive shape-memory materials, (g) Biomimetic materials with fibrillar structure. Reprinted/adapted by permission from Taylor & Francis Group: Taylor & Francis, *Virtual & Physical Prototyping*, from Gardan, J. Smart materials in additive manufacturing: state of the art and trends. *Virtual and Physical Prototyping* **2019**, *14*(1), pp.1-18., Copyright © 2019, Taylor & Francis Group.⁷

Considering the aforementioned, we can find under the banner of “smart” a great multitude of materials that exhibit halochromism, electrochromism, photochromism, thermochromism, dielectric, piezoelectric, thermoelectric, photomechanical or the magnetocaloric effect. Therefore, their classification is varied as can be performed by taking into account different criteria such as their chemical nature, functionality, purpose/usage, or even their response. One of these classification systems is based on their capability of undergoing a transformation over time or not, dividing them into advanced structured materials or responsive materials (**Fig. 1**). Another interesting approach to categorizing the smart materials is by taking into account their ability or capability to transfer/transmit one or many sorts of energy when perturbed by external stimuli here, they are classified as passive or active smart materials.⁸

Furthermore, in-between the boundaries of the “smart material” designation, we encounter extensively studied materials like hydrogels, shape memory alloys, and finally, the so-called smart polymers. They have been used in the design and fabrication of functional stand-alone actuators, elements for soft electronics, or even components of smart structures. The relative easiness of tailoring their physicochemical/mechanical properties and their versatile processability make smart polymers a very attractive research topic in the smart materials field.⁹

1.2 Smart Polymers

Smart polymers, as well as other smart materials, are able to undergo shifting alterations of their intrinsic properties; these changes are produced by the application of external stimulation. The effect of this response is used to carry out a determined operation that can go from the transmission of mechanical/electrical work to the surroundings to actuation involving swelling or a shape transformation. As discussed in the previous section, there are multiple ways to impart a stimulus upon a smart material that triggers a well-defined and expected response which at the same time is induced by a specific mechanism. The smart polymers suppose an advantage compared with their smart analogs since the production of these materials is comparably cheap, the possibility of their derivatization with multiple functional groups/biomolecules/metal ions and their coupling with other macromolecules.

This chemical adaptability and great structural variety confer them a vast spectrum of properties and, for instance, wide applicability.

The smart polymers are regularly classified by the nature of the stimuli provoking the desired transformation (**Fig. 2**), e.g., the electroactive polymers are a group of smart materials that show a response when under the influence of an electric field; under this category, we find enclosed the electrorheological, dielectric, electrostrictive or the ferroelectric polymers. Amid their multiple applications, they are mainly used in the development of microfluidic devices, chemical sensing, tissue regeneration, and bio-mimic actuation. Other commonly found stimuli-dependent classifications are conductive polymers, thermo-responsive polymers, photo-responsive polymers, pH-sensitive polymers, bio-sensitive polymers, and stress-responsive polymers.¹⁰

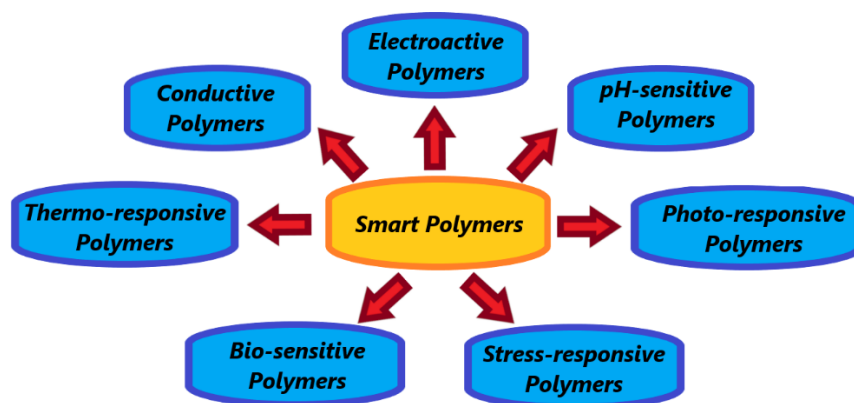


Figure 2. Classification of the so-called smart polymers according to the nature/origin of the stimuli responsible for triggering their desired transformations.

Nevertheless, one of the most studied and representative features of the so-called intelligent polymers, in general, is their ability to change their size or shape as one of the most intuitive and evident responses to an applied stimulus. The shape-morphing phenomena are commonly found in nature, going from microscopic scale, such as amoeboid movement¹¹, to a macroscopic level, such as the elongation/contraction cycle of a muscle¹². Smart polymeric materials with the ability to switch between two or more shapes responding to stimulation are categorized into two groups: the shape-changing polymers (SCPs) and the shape-memory polymers (SMPs).

1.3 Shape-Changing Polymers (SCPs)

Materials based on polymeric/gel networks exhibiting the capability to undergo a shape change are called SCPs and SCGs (shape-changing gels). Their capacity of performing a programmed active motion, as with shape-memory polymers, finds its fundament in the switch-like action of a stimuli-responsive functionality/domain included or present on the macromolecular framework that triggers whenever an appropriate stimulus is applied. The material's shape-changing behavior endures until the stimuli are withdrawn, allowing the polymer/gel to recover its original form in a reversible manner as long as the exposition to the stimulation ends. The shape-transformation process can be performed several times, yet the motion and directionality of this transformation, e.g., bending, folding, bowing, are restricted by the degrees of freedom of its initial shape.¹³

Intrinsically, a shape transformation induces a deformation of the material; the capability of such kind of materials for undergoing an induced form transformation requires a malleable though well-sustained architecture. As bulk materials, the flexible 3D array made of polymer chains on SCPs delivers an elastic functional reversible framework. The elastic behavior of some segments of the polymer chains towards deformation provides the reversibility to the shape switching effect and is typically improved by the addition/inclusion of cleavage points among them. Covalent bonding, copolymerization, crystalline-amorphous domains phase separation, and physical cross-linking processes made by switching electrostatic interactions such as hydrogen bond, ionic bonding, or hydrophilic interactions (mostly for SCGs to control their swelling properties) are used to enhance the connectivity of the polymer network and therefore are a useful tool to design, modify and control the directionality and amplitude of the shape-changing effect per se.^{14,15}

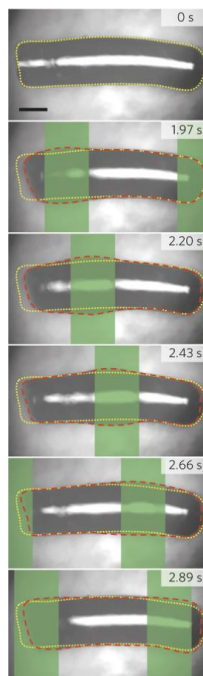


Figure 3. LCE-based microrobot performing biomimetic swimming locomotion propelled by a photoresponsive mechanism, Reprinted/adapted by permission from Nature Publishing Group: Springer Nature, Nature Materials, from Palagi, S.; Mark, A. G.; Reigh, S. Y.; Melde, K.; Qiu, T.; Zeng, H.; Parmeggiani, C.; Martella, D.; Sanchez-Castillo, A.; Kapernaum, N.; Giesselmann, F.; Wiersma, D. S.; Lauga, E.; Fischer, P. Structured Light Enables Biomimetic Swimming and Versatile Locomotion of Photoresponsive Soft Microrobots. *Nature Mater* **2016**, *15* (6), 647–653, Copyright © 2016, Nature Publishing Group.¹⁶

Among the variety of polymeric materials with remarkable programmable shape-changing properties, we find the intelligent hydrogels (both synthetic and natural) and some liquid crystalline elastomers (LCE), which inherently possess different molecular mechanisms of actuation and responsiveness to a great range of stimuli, making them go over the scope of this dissertation. Nevertheless, their study is still an important topic in the materials science discipline, and noteworthy advances have been developed e.g., the production of a microrobot able to mimic the biological locomotion of swimming driven by a photo-stimulation mechanism, as presented in **Figure 3**, or the fabrication of single-layered/multi-layered constructs able to experience several programmed geometrical transformations driven by changes of pH, ionic strength or by the photomechanical effect.^{17–19}

1.4 Shape-memory Polymers (SMPs)

The shape-memory polymers are a type of intelligent material which exhibit a controlled shape-shifting transformation. Although both SMPs and SCPs have an initial and well-defined original shape, the features governing their shape-morphing processes such as 1) The molecular mechanism triggering their motion, 2) the degrees of freedom of the resulting movement originated by the fluctuation between shapes, and 3) the reversibility of the induced effect, differs greatly between them.²⁰

Contrary to SCPs, the original shape of SMPs can be changed and fixed to a temporary shape by means of applying mechanical work in the form of stress or strain. The temporal shape adopted by the material is contained until an appropriate stimulus is provided; then, the reestablishment of the original shape is achieved. The motion created by the shape recovery process is pre-established as it reverses the mechanical work imprinted initially to deform the material. This means that the amplitude and directionality of the movement generated by the recovery of the original shape is dependent on the magnitude of the applied deformation.²¹

As already discussed, the shape-morphing process allowing SCPs to switch between their original form and a second shape is driven by the application of stimuli and ceases by the interruption of this stimulation. For SMPs, the recovery of their original shape from a temporary programmed shape is achieved precisely through their exposition to a stimulus; the driving force behind this process is known as the shape-memory effect (SME). The shape-memory effect is the capability of a material to “remember” its original shape and recover it through stimulation after being deformed. In most cases, SME is triggered directly or indirectly by temperature changes, although the light-induced SME and pH-sensitive SME have been reported for some graft polymers and hydrogels.²²⁻²⁴

The thermally induced shape memory effect and its principles have been greatly studied for more than six decades, initially observed and characterized on the so-called shape-memory alloys. The SME described here is based on the temperature-induced phase shifting between two metastable crystalline structures with different temperatures of transition and crystal lattice parameters. Despite the broad and interesting application potential of these materials,

they count with several disadvantages, which include: short deformation extent, SME taking place at very high temperatures, and a low amplitude response if compared with their polymeric analogs, the SMPs.^{25,26}



Figure 4. Polylactide (PLA) spring exhibiting thermally induced shape memory effect simulating a spiral stent for medical applications, Reprinted/adapted by permission from Springer Science Business Media B.V.: Springer Nature, Journal of Polymer Research, from Huang, W. M.; Zhao, Y.; Wang, C. C.; Ding, Z.; Purnawali, H.; Tang, C.; Zhang, J. L. Thermo/Chemo-Responsive Shape Memory Effect in Polymers: A Sketch of Working Mechanisms, Fundamentals and Optimization. *J Polym Res* **2012**, *19* (9), 9952, Copyright © 2012, Springer Science Business Media B.V.²⁷

The versatility of the SMPs over other shape-memory materials is also notable if compared with shape-memory hydrogels since SMPs can perform actuation in both dry and wet states with superior mechanical properties.^{28,29} SMPs application spectrum has enlarged dramatically in the last decades due to their adaptability, facile processability, a great combination of mechanical features, and biocompatibility. These criteria have strengthened their application in the development of biomedical devices such as spiral stents (**Figure 4**). Until this day, the development of SMPs for diverse purposes and functionalities as in tissue engineering, biofabrication, soft electronics, smart fabric/textile, nanocomposites, optoelectronic and medical fields is flagrant. For all of this, the investigation of SMPs is currently of great relevance and has become a fundamental pillar of the materials science progress.³⁰⁻³⁶

1.4.1 One-way Shape-memory Effect (SME)

The shape memory effect (SME) is not an underlying property of materials, on the contrary, it is a feature that is achieved by the combination of two necessary yet basic structural components: 1) a well-defined and permanent structure consolidated by additive manufacturing or processing which will be re-established after a shape/size modification caused by an applied mechanical stress or strain and 2) stimuli-sensitive molecular functionalities acting as shifting domains able to undergo a reversible transformation which leads to a macroscopically significant change of shape/size of a material from a permanent to a temporary shape and back.³⁷

A typical shape memory run is constituted by two basic stages: First, the material undergoes deformation and is subsequently fixated into a temporary shape. This phase is commonly known as the programming step. Secondly, the material's original shape is reconstituted during the so-called recovery step. The transformation from the temporary to the "memorized" original shape is driven by the exposition of the shape-memory material to an external stimulus that triggers the shape-shifting process. This cyclical procedure can be performed several times as long as the material is forced to adopt a certain temporary shape each time; this means that one programming step is always needed to generate one shape-recovery step (**Figure 5**). Therefore, this course of events is called the one-way shape-memory effect (1W-SME).³⁸

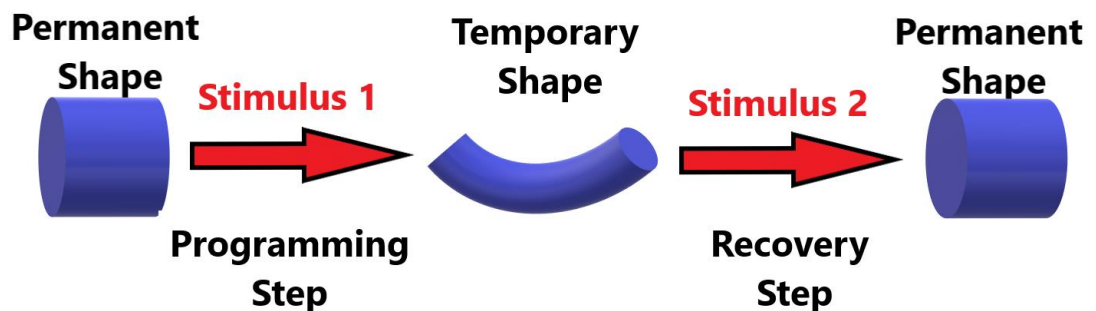


Figure 5. Schematical description of a typical one-way shape memory effect cycle.

As mentioned in the previous sections, the temperature is one of the most common stimuli triggering SME. Therefore, most SMPs demonstrate a thermally induced one-way shape-memory effect, which can be described in a general form as follows: The permanent shape/geometry/architecture of an SMP is set in the early stages of the manufacturing/processing of the material. This is achieved by the formation of cleavage points amid fragments of the chains, which constitute the polymer network by either chemical cross-linking processes or covalent bonding. At the same time, these polymer chains contain either chemical functional groups or domains capable of undergoing reversible conformational or phase transition processes around a transition temperature (T_{trans}) with the application of temperature cycling. These switching segments grant SMPs the possibility of adopting and being set into a temporary shape on the programming step. This shape-programming process is driven by heating the polymer above its T_{trans} where the anchored polymer chains gain mobility and are easily deformed. The deformation leading the material to adopt the transient shape is realized by subjecting the SMP to an external force such as a uniaxial mechanical load. The programming step is completed once the temporary shape is fixed; this is easily achieved by cooling the deformed material below the T_{trans} of its switching segments. This cooling process promotes the creation of physical cross-linking points, e.g., crystallite formation, between the deformed polymer chains, which allows the storing of the distorted chain conformation while the material is released from the external force.

The shape-recovery step, consisting on the restoration of the SMP's original shape from the temporary form, is fulfilled by means of a new thermally driven phase transition process over the aforementioned molecular switching segments. This phase transition restores the polymer chain mobility, which was utterly restricted by the physical cross-linking points created in the programming step. Heating the SMP above its transition temperature will provoke the dissolution of these temporal cleavage points, e.g., melting of the previously formed crystalline domains.³⁹ The melting of the crystallites that kept "frozen" the polymer structure on a distorted temporary shape results in the regeneration of the original shape driven mainly by an entropic effect, which will be expanded in the next chapter (see *1.4.2.3b The Rubber Elasticity and the 1W-SME*)

1.4.2 Two-way shape memory polymers

As the range of applications of the shape-memory polymers became wider and more specific, the necessity of designing and developing new shape-shifting materials able to perform even more complex tasks became evident. Polymers exhibiting a one-way shape-memory effect (1W-SMPs) recover their original form from a temporary shape through the application of an appropriate stimulus. Yet their ability to undergo this shape-shifting transformation is unidirectional as the temporary shape cannot be reestablished by applying a reverse stimulus, a new programming step is always required. The lack of a reversible shape-morphing feature on 1W-SMPs reduced their feasible applications as stand-alone components immensely. This withdrawal was outlasted by the development of the two-way shape-memory polymers (2W-SMPs).

The thermal-cyclic treatment is the most studied and effective way to induce a reversible shape-shifting effect on SMPs, among the most used molecular architectures used to produce thermally triggered 2W-SMPs we find: bi-component polymer laminates, interpenetrated polymer networks (as exemplified on **Figure 6**), liquid crystalline elastomers (LCEs) and the semi-crystalline polymer networks.⁴⁰ We will focus particularly on the latter category of 2W-SMPs as the contribution to the research, detailed description, discussion, and current endeavors towards the unveiling of their molecular mechanism constitute the aims of this dissertation. Semicrystalline polymer networks subdued to thermomechanical cycling are able to efficiently transmit a controlled two-way shape-memory effect (2W-SME) by experiencing a reversible phase transition, most commonly the molten-crystalline phase transition. Amid the semicrystalline polymer systems capable of delivering a reversible shape-shifting transformation, we find the crosslinked elastomers and the phase segregated copolymers derived from them. These two compound families have been largely studied due to their tunable mechanical/physicochemical properties, their relatively easy/cheap production and enhanced stability in a wide range of temperatures.⁴¹⁻⁴³ These features are the reason why most of the investigations on the 2W-SMPs field are based on systems derived from them.

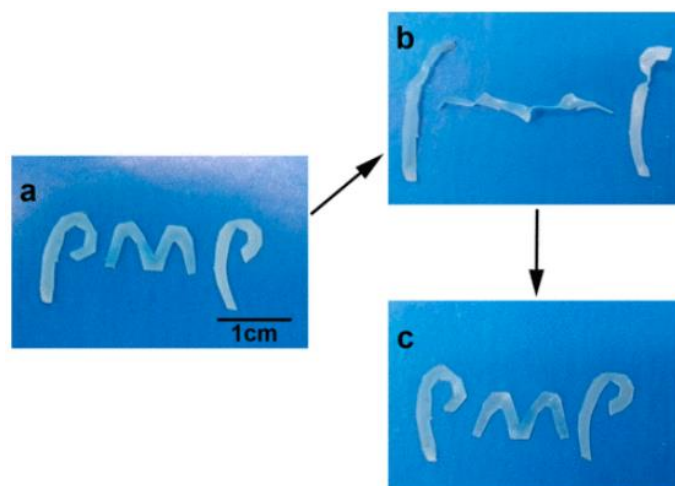


Figure 6. Thermally driven reversible shape memory effect behavior of an interpenetrated double crystalline poly(butylene succinate)-co-poly(ϵ -caprolactone) semicrystalline polymer network, Reprinted/adapted by permission from American Chemical Society: American Chemical Society, Applied Materials, from Huang, M.; Zheng, L.; Wang, L.; Dong, X.; Gao, X.; Li, C.; Wang, D. Double Crystalline Multiblock Copolymers with Controlling Microstructure for High Shape Memory Fixity and Recovery. *ACS Appl. Mater. Interfaces* **2017**, *9* (35), 30046–30055, Copyright © 2017, American Chemical Society.⁴⁴

The two-way shape-memory effect (2W-SME) showed by crosslinked elastomers is rooted in the expansion and contraction of their polymer network upon cooling/heating cycles under external or intrinsic stress. The crosslinked portions act as amorphous bridging zones between the load-orientated polymer chains, which elongate upon crystallization and contract in molten state. This is supported by the entropic nature of the elastic behavior of the polymer's chains. On the other hand, the reversible SME demonstrated by copolymers based on these semicrystalline elastomers is ascribed to the heterogeneity of their molecular structure. Two distinguishable phases are noted here: 1) An elastic semicrystalline phase with low T_{trans} , responsible for the shape transformation through the melting/crystallization of its force-oriented crystalline domains, confined amid 2) An amorphous and rigid phase with high T_{trans} , which supports and maintains the integrity of the polymeric matrix, these amorphous regions function as physical crosslinking zones between the semicrystalline domains ensuring the recovery of the material's original form⁴⁵.

1.4.2.1 2W-SME: From the LCEs to Semicrystalline Polymers

The study of the reversible shape-memory effect on semicrystalline polymer networks was inspired by the ability of LCEs to undergo a 2W-SME while subjected to thermal cycling under constant stress. LCEs experience an extensional elongation whilst being cooled below the temperature, where the phase transition from the isotropic to liquid crystal form takes place. In a complementary way, the material contracts as the temperature is raised above the transition temperature, where the ordering of the liquid crystal phase is disrupted and goes back to an isotropic arrange. The obtention of reversible actuation on LCEs can be achieved by chemically crosslinking flexible side-chain polymer domains (mesogen) to a rigid backbone, ensuring a “controlled” loss of structure on the nematic-isotropic transition of the mesogens. The degree of reversibility and the amplitude of the actuation of LCEs is also dependent on the alignment degree of the LC units. The application of constant uniaxial stress on a lightly cross-linked LCE will lead the LC units to align towards the applied deformation, this anisotropic process will subsequently produce a directed macroscopical coupled effect of elongation/contraction of the LCE upon cooling and heating correspondingly (see **Figure 7**).^{46,47}

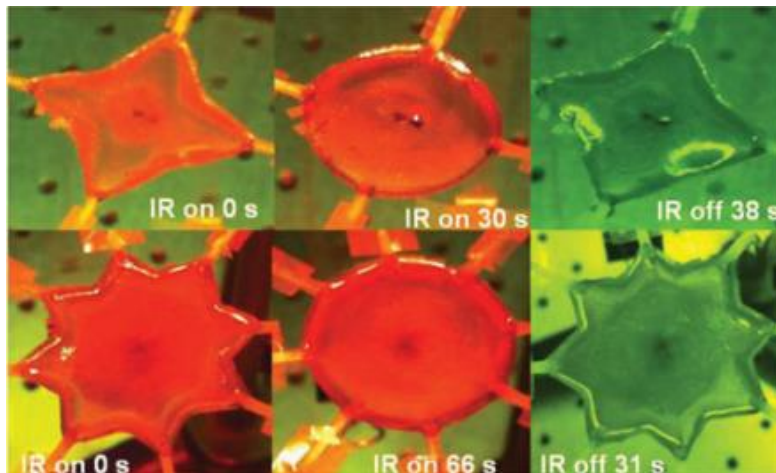


Figure 7. Crosslinked liquid-crystalline elastomer with programmable reversible shape memory features under mechanical load undergoing different shape transformations from varied geometries through the force-directed nematic-isotropic phase transition, Reprinted/adapted by permission from Taylor & Francis Group: Taylor & Francis, *Molecular Crystals & Liquid Crystals*, from Wang, Y.; Huang, X.; Zhang, J.; Bi, M.; Zhang, J.; Niu, H.; Li, C.; Yu, H.; Wang, B.; Jiang, H. Two-Step Crosslinked Liquid-Crystalline Elastomer with Reversible Two-Way Shape Memory Characteristics. *Molecular Crystals and Liquid Crystals* **2017**, *650* (1), 13–22, Copyright © 2017, Taylor & Francis Group.⁴⁶

Accordingly, the main structural requirements for a polymer network to exhibit a 2W-SME are the existence and synergic coupling between a highly stable matrix and shifting domains able to endure a thermally induced reversible phase transition – ultimately allowing them to be programmed into an anisotropic conformation. From the 1W-SMPs it's known that the chemical/physical cross-linking processes are a good way to set the permanent shape of a semicrystalline polymer by producing a highly stable yet flexible network. Inducing a directed crystallization process of the polymer chains by means of a constant deformation, a principle borrowed from the LCEs, effectively grants anisotropy to a semicrystalline polymer network facilitating the adoption of a temporary shape and therefore inducing an elongation of the material. When heated, the melting of the oriented crystalline domains allows the chains to return to their original state (permanent shape), evoking a macroscopical shrinking of the polymer.

1.4.2.2 2W-SME on Semicrystalline Polymer Networks

Following this thread of ideas, a 2W-SME effect was observed for the first time on a crosslinked semicrystalline polymer network when a constantly loaded thermally cured poly(cyclooctene) film was subjected to thermal cycling around the T_{trans} of its crystallization-fusion phase transition.⁴⁸ This thermoset, which already exhibited thermally induced 1W-SME, experienced a great directed elongation/contraction coupled effect upon cooling and heating respectively, under constant stress. The macroscopic reversible shape-switching transformation was explained as the result of two complementary effects: Crystallization-induced elongation (CIE) and the melting-induced contraction (MIC), two effects vastly explored in the study of the 2W-SME exhibited by the LCEs under load.⁴⁹ The crystallization of polymeric semicrystalline materials under load allows the polymer chains to crystallize with a preferred orientation; the newly formed crystallites are directed towards the deformation, promoting an exceptional elongation of the material. The anisotropic effect caused by the aligned crystallization process of the polymer chains upon cooling is the main source of the CIE effect. Correspondingly and during the MIC, a reverse strain effect is observed as the constantly deformed material is heated above its T_{trans} . The drawn polymer

experiences a macroscopically relevant contraction due to the melting of the crystalline domains aligned along the external load.⁵⁰

The characterization and evaluation of the thermally induced 2W-SME on semicrystalline polymers under load is made through the implementation of thermomechanical cycling, each cycle consisting of three stages: Loading, cooling, and heating. The loading step is made by fixing the sample on a typical tensile analyzer setup (one movable and one static clamp), increasing the temperature above the T_m of the material (molten/rubbery state), and applying isothermally a constant load. This produces a uniaxial deformation of the sample as the extensional strain is recorded. The cooling step is realized by decreasing the temperature of the loaded polymer below its T_m allowing the crystallization of the material; the load applied in the previous step is maintained during the course of the cycle. Amid the cooling phase, the probe experiences an unusual straining (CIE) caused by the directed crystallization of the polymer chains. Lastly, the crystallized polymer is heated again above its T_m , provoking its contraction (MIC) as the oriented crystallites melt on the heating course (**Figure 8**). During this step, the odd elongation observed upon cooling is reversed. Following cycles consist of consecutive cooling-heating processes as the load is maintained during the whole experiment.^{43,51}

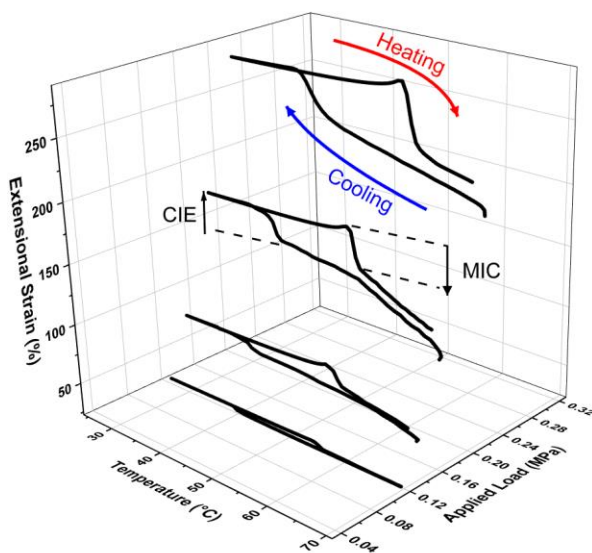


Figure 8. Two-way shape memory behavior of crosslinked PCL under different constant loads. The probes were loaded at ca 70°C. The loading step is followed by cyclic cooling and heating processes under constant stress. CIE and MIC effects are observed upon cooling and heating, respectively.

It must be noted that an analogue yet unexplored thermomechanical characterization of the 2W-SME can be performed under constant strain conditions, meaning that the sample in the molten state is drawn and kept extended to a certain degree on the loading step before the following cooling-heating cycling is made. Therefore, the evolution of the extensional stress as a function of temperature is evaluated. All semicrystalline polymers exhibiting a reversible shape-shifting transformation are studied under constant stress conditions, so during the execution of this dissertation, we explored the behaviour of these materials under a constant strain scenario.

The magnitude of the applied force influenced the amplitude severely and the extent of the observed elongation/contraction, probes under higher loads underwent sharper elongations upon cooling and contractions upon heating. The study of the tensile properties of this cured polymer was revolutionary as it demonstrated three great points: 1) A crosslinked semicrystalline polymer network able to perform a 1W-SME can produce a 2W-SME by inducing anisotropy on its matrix by constantly applying an external force. 2) The measured strain of the constantly loaded materials was increasing as the sample was being cooled below its melting temperature, this supposed a deviation from the typical linear viscoelastic behaviour of elastomeric materials as the extensional strain is supposed to decrease on constant stress experiment in this range of temperatures. 3) Extensively crosslinked samples exhibited hindered strain changes in comparison with their less crosslinked analogs when subjected to the same load. Greater loads needed to be applied to highly crosslinked materials to achieve, to a certain extent, the same elongation/contraction degree of less crosslinked samples.⁴⁸

These observations supported the idea that the induced anisotropy of the polymer chains was not solely responsible for both CIE and MIC processes on the cured semicrystalline polymers networks. The antagonism between the crosslinking density and the elongation suffered by the material upon cooling, which induces a notable deviation in the behaviour of the extensional strain with temperature, thus of the material's elastic modulus, could be explained through the rubber elasticity model. Therefore, it was inferred that the 2W-SME exhibited by semicrystalline polymers under non-zero stress conditions is also supported by an entropic contribution. This means that the change of the conformational entropy of the polymer chains under deformation supports the CIE and MIC processes thermodynamically.

1.4.2.3 Rubber Elasticity: The Entropic Contribution to the SME

The ability to elongate upon cooling and shrinking upon heating under external load is not a unique feature of the 2W-SMPs; as a matter of fact, this unusual behaviour was already studied on the materials known as rubbers. Rubbers are elastomers able to bear tensile deformations of great magnitude and recover their original shape once this deformation is released under isothermal conditions. A constantly loaded rubber contracts when subjected to a heating process; correspondingly, while the rubber is allowed to cool down, the contractions are reverted by an expansion process restoring the original length of the material. This specific feature is observed especially on vulcanized synthetic rubbers; the vulcanization process generates randomly chemical joints between the lengthy rubber chains (net points), creating a continued network of polymer chains defining the original shape of the rubbery material. This irreversible crosslinking method is directly comparable to the processing stage of crosslinked semicrystalline polymers, as, in both cases leads to the production of thermosets. Thus, crosslinked semicrystalline polymers are rubber-like materials able to crystallize. The entropic contribution to the molecular mechanism behind the 2W-SME of cross-linked semicrystalline polymers under load can be intuitively described in terms of the rubber elasticity theory⁵²⁻⁵⁴

1.4.2.3a The Ideal Chain Model

This theory describes the polymer chains as a flexible and free rotating conglomerate composed of rigid sections called Kuhn segments; each Kuhn segment represents a monomer unit. These segments are bonded through rotatable bonds, which grant the polymer chains the possibility of reticular motion. This model does not consider any kind of interaction between the mers or any kind of steric effect between the polymer chains, this is then so-called the ideal chain model. The mers change their orientation and position promptly allowing the polymer chains to adopt random conformations as they entwine and entangle between each other - this is valid for high molecular weight polymers. Following this premise, the length of a polymer chain is simplified as a random walk or a succession of Kuhn segments with an independent and random spatial conformation, making the trajectory from one end of the chain to the other (end-to-end) completely arbitrary. This state is

discretized by a probability distribution where the root mean square of the director describing the trajectory of the end-to-end will allow the calculation of the distance between both ends as showed on **Equation 1**. This parameter defines the equilibrium state of the polymer chains: their conformational entropy is at its maximum and the energy of all the possible conformations is practically the same.⁵⁵

$$P(N, \vec{R}) = \left(\frac{3}{2\pi N b^2} \right)^{\frac{3}{2}} \cdot \exp \left(- \frac{3\vec{R}^2}{2N b^2} \right) \quad (\text{Eq. 1})$$

This expression is the description of the Gaussian approximation used to describe the arbitrary distribution of the chain ends conformations for ideal rubbery chains composed by N number of Kuhn segments with length b, P is the probability that the distance between both ends of the chains could be R and Nb² is the average of the squares of the end-to-end distances of the relaxed chains.

If the end-to-end distance arises, meaning that the polymer chains are being stretched, then the overall free energy will increase by the reduction of the possible chain spatial conformations caused by the stretching. A straightforward equivalence between Boltzmann's expression of entropy and the decrease of the polymer chain's conformational entropy caused by deformation is intrinsic (**Eq.2 and 3**).

$$S(N, \vec{R}) = \kappa_B \ln \Omega(N, \vec{R}) \quad (\text{Eq. 2})$$

$$S(N, \vec{R}) = - \frac{3}{2} \kappa_B \frac{3\vec{R}^2}{N b^2} + S(N, 0) \quad (\text{Eq. 3})$$

Here the multiplicity term on Boltzmann's entropy equation (Ω) is proportional to the number of possible conformations of an extended ideal polymer chain with an end-to-end distance of R. Thus, $\Omega = Z^n 4\pi R^2 P(R, N)$, where Z^n is the total number of conformations. As $\Omega \propto P(N, R)$ we obtain from the equivalence of Eq. 1 and Eq. 2 the Equation 3.

The elongation of the polymer chains is almost solely an entropic contribution as the interactions between them are completely obviated, and therefore, there is no enthalpic contribution to the free energy change; the internal energy of the system is independent of the stretching of the polymer chains (**Equation 4 and 5**).

$$F(N, \vec{R}) = U(N, \vec{R}) - T \cdot S(N, \vec{R}) \quad (\text{Eq. 4})$$

$$F(N, \vec{R}) = \frac{3}{2} \kappa_B \cdot T \frac{\vec{R}^2}{Nb^2} + F(N, 0) \quad (\text{Eq. 5})$$

The expression for the Helmholtz free energy of the polymer's chains as a function of their stretching to a distance R is depicted in equation 4. By introducing the obtained expression describing the reduction of the polymer chains conformational entropy caused by their elongation (Eq. 3) and considering the ideal chain assumption, then equation 4 is rewritten as equation 5.

In the end, this correlation demonstrates that each polymer chain can be described as an entropic spring. This means that the force necessary to strain a polymer chain or what is the same increase its end-to-end length to a certain distance complies with Hooke's law. Therefore, a model describing the linear correlation between the degree of deformation of a polymer chain and the force inducing this deformation is established on **Equation 6**.^{56,57}

$$\vec{f} = - \frac{\delta F(N, \vec{R})}{\delta R} = - \frac{3\kappa_B T}{Nb^2} \cdot \vec{R} \quad (\text{Eq. 6})$$

The derivative for extended polymer's chains Helmholtz free energy expression with respect to their elongation distance allows the estimation of the necessary force to extend them to an end-to-end distance of R through equation 6. This equivalence satisfies spring Hooke's law, here the entropic spring constant is $3\kappa_B T/Nb^2$.

1.4.2.3b The Rubber Elasticity and the 1W-SME

This model is applicable to crosslinked polymers as the crosslinking process ideally forms a 3D continuous molecular network constituted by highly entangled polymer chains (original shape). Under zero stress conditions, the polymer chains can adopt multiple spatial configurations, which are roughly energetically equivalent, then at least at a molecular level, the polymer matrix behaves as a liquid as the monomeric units (Kuhn segments) move randomly. This is the polymer's equilibrium state; the conformational entropy is at its maximum. The crosslinking process creates short-lengthen polymer chains sections in-between the net points, which can be directed by the application of an external deformation,

creating in-situ a great number of entropic springs. Once the rubber-like material is under a uniaxial deformation, the polymer chains are stretched into a specific conformation, so their overall conformational entropy decreases while the material now behaves as an elastic solid (arise of its elastic modulus), the external force induces a change of length of the polymer chains bringing out a force opposing the deformation: the entropy elasticity or entropic spring force. Once the deformation ceases, the reconstitution of the original shape is entropically favoured by the action of the entropically driven retractive force.

Therefore, the thermodynamic origin of the thermally induced 1W-SME of a crosslinked semicrystalline polymer network under uniaxial deformation finds its roots in the evolution of the conformational entropy of its polymer chains. The adoption of a temporary shape on the programming step of a loaded molten semicrystalline matrix involves the stabilization of an out-of-equilibrium state of the elongated polymer chains facilitated by the crystallization process. This “frozen” structure stores the entropically originated retractive force created by the deformation as the polymer chains behave like entropic springs. Once the constant load is released, the crystallized material will maintain this temporary elongated shape characterized by the low conformational entropy of the polymer chains. By heating the polymer above its T_m under zero stress conditions, the crystalline domains will melt; this will ultimately restore the mobility of the polymer chains and allow the release of the stored entropic retractive force. Subsequently, they will return to their less-energetic random coiled conformational distribution provoking the macroscopical contraction of the material and reverting the fixed deformation. The reconstitution of the material’s original form is an entropically-guided process where the semicrystalline polymer network goes from a temporary entropically unfavoured form (temporally extended shape) to a thermodynamically stable state (original non-elongated shape).⁵⁸

1.4.2.3c The Rubber Elasticity and the 2W-SME

The directed reversible elongation/contraction of a thermally cycled crosslinked semicrystalline network under load is caused by changes in the molecular conformation of the polymer chains facilitated by a phase transition process. We encounter that the stretching of the polymer chains in a molten state implicates an alteration of their conformational entropy, going from a highly entropic entangled equilibrium state to a thermodynamically unfavoured drawn state characterized by a lower conformational entropy called the high-temperature shape (HTS). Here, the “fastening” of the polymer chains becomes imperative as their creeping or slipping will lead to an unreversible non-entropic deformation of the polymer network therefore the cleavage points formed between the polymer chains must be able to remain stable during the thermal cycling allowing them to bear reversible conformational changes.

As the loaded polymer is cooled below its T_{trans} the oriented crystallization of the polymer chains induces a further macroscopical elongation of the material giving origin to the low-temperature shape (LTS). The LTS is characterized by the presence of even furtherly stretched polymer chains than in the HTS, which in principle implies an additional diminishment of their conformational entropy. Heating back the crystallized material under load above its T_{trans} results in the reconfiguration of the polymer chains into the HTS; this naturally leads to the melting of the directed crystallites and reverses the elongation caused by the crystallization process. The reversible SME observed on constantly loaded semicrystalline polymer networks is caused by the shape switching between the HT and LT shapes. This fact lessens the contribution of the entropic elasticity to the 2W-SME considerably as both HTS and LTS are intrinsically oriented states, meaning that the change in the conformational entropy of the polymer chains during the thermal cycling is not that relevant in comparison to the 1W-SME scenario where they go from an oriented conformation to a highly entangled random conformation.

During a reversible shape-shifting process, the polymer chains are constantly oriented towards the deformation, implying a modest change in their conformational entropy. Therefore, most of the contribution to the reversibility of the exhibited shape transformation

process rests on the directed crystallization process upon cooling and the melt of these crystallites directed towards the applied force. The alignment degree of the crystalline domains, as for the LCEs, has a positive effect on the elongation suffered by the material upon cooling. Thus, highly directed crystallization will provide an enhanced macroscopical reversible strain effect. The amplitude and origin of the 2W-SME based on the elongation/contraction of a constantly loaded semicrystalline polymer network under thermal cycling are mainly based on three components: I) An important enthalpic contribution given by the chemical nature of the polymer chains (values of ΔH_c and ΔH_m), II) A less notorious yet existent entropic contribution in the form of entropic elasticity and finally III) The magnitude of the applied force.^{59,60}

As the rubber elasticity theory explains fairly the thermodynamical origin of the thermally induced 1W-SME and, to a certain extent, the reversible shape-changing process of a semicrystalline polymer network under load, it also has its limitations. For example, this model does not take into consideration any sort of interaction between the polymer chains. It also overlooks the enthalpic contribution to the free energy of the stretching/contraction processes of a polymer chain under load, which becomes ultimately important as the observed shape-shifting effect involves reversible phase transitions of the crystalline domains. Additionally, this model restricts the molecular deformation to certain angles of deflection and states that all sections between the anchor points amid the polymer strings are able to elongate during an applied load. Most importantly, the entropic spring model is only valid for polymer chains undergoing small to intermediate deformations. This means that if the elongation experienced by a polymer chain exceeds 1/3 of its length (the sum of the length of all its Kuhn segments), then its response to the applied deformation will not be linear and, therefore will leave the Hookean spring regime⁶¹⁻⁶³

1.4.2.4 Towards the Molecular Model of the 2W-SME

The proposal of a general and unified model able to describe the molecular mechanism behind the reversible shape-memory effect on semicrystalline networks in its entirety has been unsuccessful until this date. The cause for this lies on the fact that polymers exhibit an immense structural variety which confers them to a wide range of physicochemical properties. Also, the 2W-SME is a multifactorial process where multiple phenomena contribute to the different stages of the shape transformation mechanism. On top of that, the limited validation of the proposed models with experimental data is a major factor hindering the complete description of such a complex process. Nevertheless, multiple attempts and valuable contributions have been carried out in recent years to describe and quantify all the possible sources which originate and sustain the 2W-SME on semicrystalline polymer networks. Although these models are based on cured polymer matrixes, as they exhibit simpler structural architectures, the theoretical basis and findings are completely applicable to their copolymer analogues. The main outcome of the first attempt to describe the 2W-SME on crosslinked semicrystalline networks was that the odd thermomechanical behavior of these stretched thermosets is based on the CIE. Also, this elongation effect is strongly and directly correlated with the magnitude of the applied load (see 2W-SME on Semicrystalline Polymer Networks). This study was, beyond any doubt, revolutionary in the investigation of the mechanical properties of the SMPs yet overlooked the existence and possible contribution of other phases to the 2W-SME besides the crystalline domains.

More elaborated models were developed by considering the coexistence of two different phases on the SMPs under thermal cycling: the already characterized crystalline phase and the rubbery phase. The highlight of retaking this phase differentiation, initially considered for the description of the 1W-SME, is the underlying capability of the rubbery phase to actively store and further release the strain, which evokes the expansion/contraction effect of the constantly loaded polymer network upon cooling and heating correspondingly. Therefore, a 3D model considering not solely the contribution of the crystalline domains to the 2W-SME of a polymer framework while thermally cycled undergoing small and large deformations was developed^{64,65}.

Expanding the idea of the coexistence of at least two phases on a polymeric matrix to describe the origin of the thermally induced 2W-SME on SMPs led to the development of more robust models. Some of these models consider the clear differentiation of mechanical features of a semicrystalline network above and below its T_g . Accordingly, it is stated that SMPs, upon cooling, undergo at least one phase transition from an entropically governed state (rubbery-elastic phase) to an enthalpy dominated state (glassy phase). Both phases respond differently and contribute energetically to the applied deformation at specific temperature ranges during the thermomechanical cycle. The formation of an intermediate phase between these two regimes confirms the first-order phase transition character of the transition between a hyperelastic deformed rubbery phase to an undeformed glassy viscoplastic phase (**Figure 9**).⁶⁶

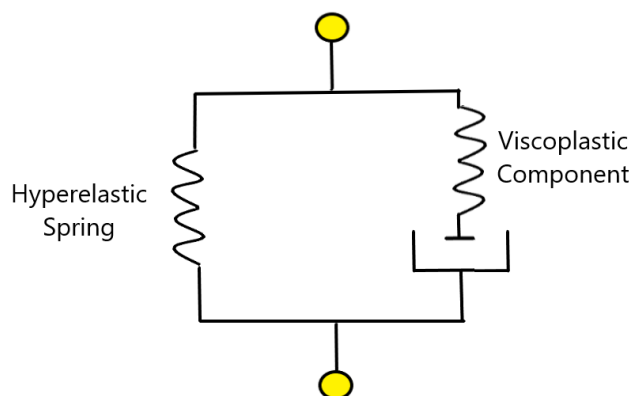


Figure 9. 1D representation of the viscoplastic model for a glassy polymer under stress. The viscoplastic behaviour of a semicrystalline polymer becomes dominant below its glass transition temperature while the hyperelastic component enlarges its contribution above the T_g . The response to an applied load is decomposed into the aforementioned regimes depending on the considered temperature range.

In addition to this approximation, a 1D model was developed and correlated with experimental data to characterize the SME on SMPs under load while being cycled around their fusion temperature (T_f). Above T_f the rubbery phase contributes to the deformation of the material through the entropic elasticity, while below T_f the formation of the oriented crystalline phase is the driving force of the induced crystallization elongation (ICE) effect. The model states that the domains able to produce the ICE effect are formed accordingly to different thermal rates, and therefore, their contribution to the elongation of the polymer chains during the phase transition is dependent on these temperature rates. For instance, at

very high cooling rates, the ability of the rubbery phase to contribute to the ICE through the entropic elasticity is enhanced, but the overall strain experienced by the material upon crystallization diminishes as the formation of large-sized oriented crystalline domains is hindered.⁶⁷

The estimation of the change in the free energy to thermodynamically sustain the odd evolution of stress-strain with a temperature of semicrystalline networks with reversible SME features has also been explored. The stress-induced elongation suffered by the polymer chains upon cooling is mainly caused by the melting-crystallization phase transition. The revealing theoretical outcome of this model allows the prediction of the orientation, structure, size, and number of folds of the incipient crystalline phase. Also enables the estimation of the transference of free energy from the amorphous regions to the directed crystalline phase. Moreover, the implementation of this model also correlated the directionality of the crystalline phase with the 2W-SME. Thus, the anomalous elongation observed on cured elastomers under load while being cooled is only observable when the crystalline domains are parallel or describe a sharp angle with the direction of the applied load (**Figure 10**). Lastly, the model was supported by a good correspondence with the experimental data obtained from the evaluation of the SME on two of the most common crosslinked elastomers to produce SMPs: Polyethylene and PCL.^{68–70}

Finally, the biggest limitation of most of these models is the lack of correspondence with experimental data, making their validation difficult. The design of experiments able to correlate the structural transformation and the thermomechanical features of polymeric networks undergoing a reversible thermally induced shape-shifting transformation process is also not an easy task. Nevertheless, one of the best ways to associate the shape-switching effect with the formation of an oriented crystalline phase is through *in-situ* XRD analysis.⁷¹ Some of the aforementioned models have based their proposals on observations derived from this kind of experiment on crosslinked PCL networks due to their remarkable mechanical properties, easy processing, and notable SM features, making them attractive model objects. Until these days, the challenge of a complete description of the 2W-SME on semicrystalline

polymers networks under constant load still exists; nevertheless, more comprehensive, specific, and robust models/studies are being carried out to shed some light on this topic.

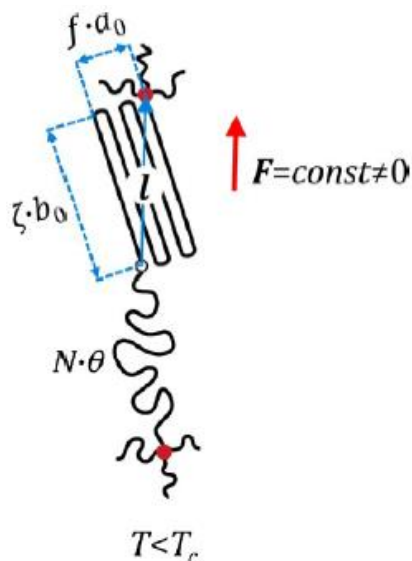


Figure 10. The dimensions of the crystalline segments confined between two crosslink points are mainly given by their thickness (a_0) and length (b_0), and the number of folds (f). The spatial conformation of the crystalline domains along the external stress defines whether a semicrystalline network under load exhibits 2W-SME or not. The crystallographic parameters of the crystalline phase allow the calculation of the free energy change of the system, which gives thermodynamical sustain to the reversible shape transformation mediated by a melting-crystallization phase transition. The transference of free energy from the amorphous to the crystalline segments and the change of entropy on the remanent amorphous regions are parameters that also contribute to the feasibility of a reversible SME on a drawn semicrystalline polymer network, Reprinted/adapted by permission from American Chemical Society: American Chemical Society, *Macromolecules*, from Dolynchuk, O.; Kolesov, I.; Jehnichen, D.; Reuter, U.; Radusch, H.-J.; Sommer, J.-U. Reversible Shape-Memory Effect in Cross-Linked Linear Poly(ϵ -Caprolactone) under Stress and Stress-Free Conditions. *Macromolecules* **2017**, *50* (10), 3841–3854., Copyright © 2017, American Chemical Society.⁷⁰

1.4.2.5 2W-SME Under Stress-Free Conditions

In the previous sections, it has been extensively discussed that the ability of semicrystalline networks to undergo reversible thermally induced shape-changing transformations is tethered by the requirement of an external force. Most of the phenomenological, theoretical, and early developments in the investigation and application of the semicrystalline networks exhibiting 2W-SME have been done for covalently crosslinked polymer matrixes.^{48,59,70,72–76} Suddenly, the application of external stress was replaced by the programming of internal stress on the polymer networks, which delivered an autonomous shape-shifting response under thermal cycling. The intrinsic load on SMPs can be achieved in multiple ways; one of the most direct methodologies is the further crosslinking of a partially crosslinked network under load. Here, the extensive curing methodology creates *in-situ* two different networks containing polymer chains elongated to different strains evocating a shape-shifting effect between these two conformations by thermal cycling⁷⁷.

Another approach to the 2W-SME under zero stress conditions is the fabrication of bi-component polymer laminates or SME composites; the SME shown by this kind of SMPs is based on the transference of internal stress from one component to the other triggered by a phase transition. Typically, the laminates are composed of two not covalently bonded polymer layers with 1W-SME properties or one layer of a 1W-SMP and an elastomeric layer, as illustrated in **Figure 11**.^{78,79}

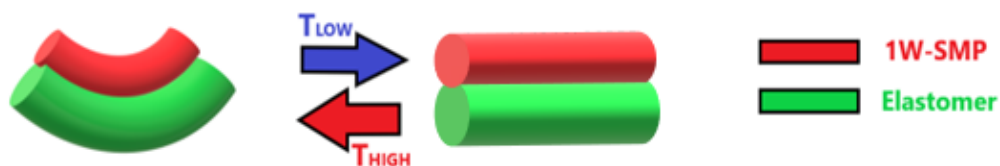


Figure 11. The mechanism of actuation of the polymer laminates is based on the attachment of a deformed 1W-SMP with a low transition temperature to an elastomer with a higher transition temperature in a relaxed state. Although the directionality of the reversible actuation performed by these composites is limited to bending, they are able to endure large reversible strains and are easily fabricated.

The construction of these composites is pretty simple and consists on the binding of a pre-strained crystallized 1W-SMP layer to an unstrained elastomeric polymer layer with an adhesive. By heating above the T_{Trans} of the 1W-SMP, the construct is able to bend due to the contraction of the pre-strained SMP, inducing intrinsic stress to the elastomer laminate; as the composite is cooled down, the elastomeric phase elongates by releasing the stored tension on the heating process, this provokes another bending process which leads to the recovery of the original shape of the composite.

The interpenetrated semicrystalline networks are another alternative toward the autonomous reversible actuation of SMPs; these materials are conformed by two or more polymer networks, which act separately as actuating domains and geometry determining domains. These domains are morphologically separated; both phases can be covalently bonded or embedded among each other depending on the synthesis methodology used to produce this kind of composites. The actuating domains are basically crosslinked semicrystalline networks or copolymers based on these materials able to perform 1W-SME upon thermal cycling; on the other hand, the phase determining the geometry of the composite is an elastomeric material which exhibits a higher T_{trans} than the actuating phase granting stability and intrinsically inducing a load over the crystallizable/melting network.⁸⁰ Some interpenetrated networks consisting of two crystalline phases able to crystallize at different temperatures have demonstrated great 2W-SME under zero-stress conditions. Here the textural structure of the composited network is defined by the crystalline morphology of one of the crystalline phases, while the actuating crystalline domains are confined or micro-confined among the lamellar structures of the latter. The co-crystallization of both phases or the melting/crystallization phase transition of the packed switching domains enables a reversible shape-switching transformation^{44,81,82}.

As it has been demonstrated in the previous chapters regarding the description of the SME and confirmed by checking the current state of the art on this topic, not only crosslinked semicrystalline networks, especially based on poly(ϵ -caprolactone), demonstrate the ability to undergo exceptionally shape-shifting transformations. In fact, their urethane-based copolymers are widely used on most molecular architectures able to demonstrate 1W or 2W-

SME under stress and stress-free conditions as in the laminate composites, interpenetrating polymer networks, and naturally on the semicrystalline polymer networks (**Figure 12**).^{83–91}

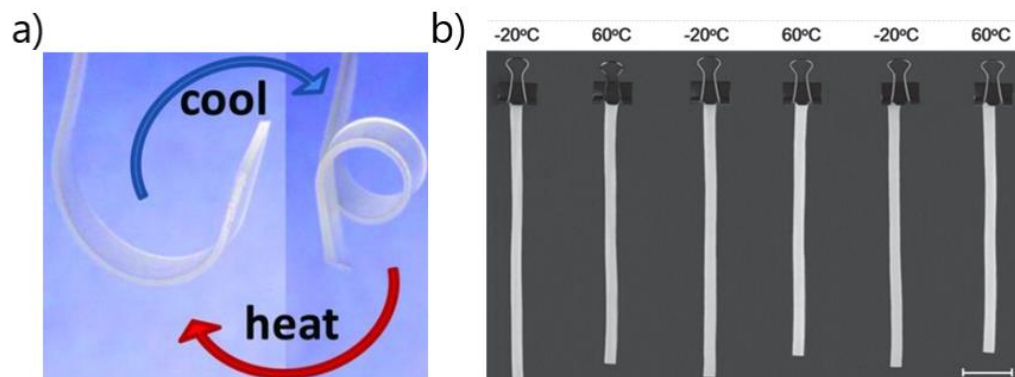


Figure 12. The notable and versatile thermomechanical features of materials derived from poly(ϵ -caprolactone with ester-urethane functionalities have allowed a vast development of self-standing reversible thermal actuators with a great variety of chemical architectures and shape-morphing mechanisms, from **a)** double crystallizable interpenetrated networks to **b)** highly phase segregated phase copolymers, taken from **Left:** Reprinted/adapted by permission from John Wiley and Sons: John Wiley and Sons, Advanced Materials, from Behl, M.; Kratz, K.; Zotzmann, J.; Nöchel, U.; Lendlein, A. Reversible Bidirectional Shape-Memory Polymers. *Advanced Materials* **2013**, 25 (32), 4466–4469., Copyright © 2013 WILEY-VCH Verlag GmbH & Co. KGaA, Weinheim. **Right:** Reprinted/adapted by permission from John Wiley and Sons: John Wiley and Sons, Macromolecular Rapid Communications, from Fan, L. F.; Rong, M. Z.; Zhang, M. Q.; Chen, X. D. A Facile Approach Toward Scalable Fabrication of Reversible Shape-Memory Polymers with Bonded Elastomer Microphases as Internal Stress Provider. *Macromolecular Rapid Communications* **2017**, 38 (16), 1700124., Copyright © 2017 WILEY-VCH Verlag GmbH & Co. KGaA, Weinheim.^{86,89}

1.4.2.6 Crosslinked PCL Networks and Their Polyurethane Copolymers on 2W-SME

The investigation of the design and development of materials exhibiting autonomous reversible shape-shifting transformations strengthened the development and design of multiple urethane-derivate compounds based on crystallizable polymer networks. The polyurethanes (Pus) are a type of alternating copolymers composed of soft segments (most commonly polyester or polyether diol chains with low T_{Trans}) bonded with high melting temperature elastic hard segments (formed from diisocyanate groups and typically coupled with small glycols as chain extenders). These interesting materials have demonstrated high thermal stability, great resistance against a broad selection of organic solvents, relatively easy obtention, enhanced processability, biocompatibility, and highly tailorable mechanical

properties. Those features grant sharp and notorious thermal-responsive SME properties to these phase-segregated copolymers, while their applications as shape-memory actuators can go from the construction industry, and the manufacture of autonomous grippers to the development of tissue engineering and further medical applications. Among the Pus the PCL-based polyurethanes (PCL-Pus) are one of the most extensively researched shape-memory materials thanks to their large strain reversibility, facile additive processability, shape stability, and outstanding thermomechanical properties.⁹²⁻⁹⁶

The hard segments contained in the polymer chains can interact through intermolecular hydrogen bonds and create domains called “clusters”. The presence of these amorphous clusters, which typically exhibit less than 1 μ m of extension and a high T_{Trans} , among the crystalline domains creates a phase segregation effect on the copolymer matrix. The plastic cluster domains behave as physical crosslinking points between the crystallizable domains (PCL domains), enhancing the strength, shape-preservation, and stress-storing properties of the material.³⁷ This capacity of association on the molecular level grants PU-based matrixes with the self-assembly effect, which has broadened their applications even into the LCEs field.^{97,98} The PCL semicrystalline domains are the responsible of the reversible/one-way SME following the same molecular behaviour as the cured semicrystalline networks under stress/zero-stress conditions. The selection of an appropriate ratio between amorphous and crystalline phases, chemical nature of the selected diisocyanate and polyol, degree of crystallinity of the soft segments, and compelling phase segregation facilitated by the addition of semicrystalline networks with high M_n are among the most important criteria on the preparation of PCL-PU_s able to deliver a controllable and effective 2W-SME^{83,99}.

By virtue of its tunable physical-chemical properties and its processability, Poly (ϵ -caprolactone) has proven to be a suitable material for the investigation of the SME and the revealing of the molecular mechanism behind it. PCL is an easily cross-linkable biocompatible and biodegradable semicrystalline polymer used for several purposes going from tissue engineering, and drug-delivery systems to its application on prosthetic joints and food packaging.^{100,101} The ability of crosslinked PCL networks to provide extraordinary

thermally induced one-way and two-way shape memory effects, by themselves or involved in complex molecular arrays, has been broadly investigated^{75,76,102} and applied to the production of polymeric programmable components for soft robots, biocompatible self-healing elastomers for 3D printing, the development of biomedical devices and biocompatible shape memory engineered scaffolds^{103–108} as exemplified on **Figure 13**.

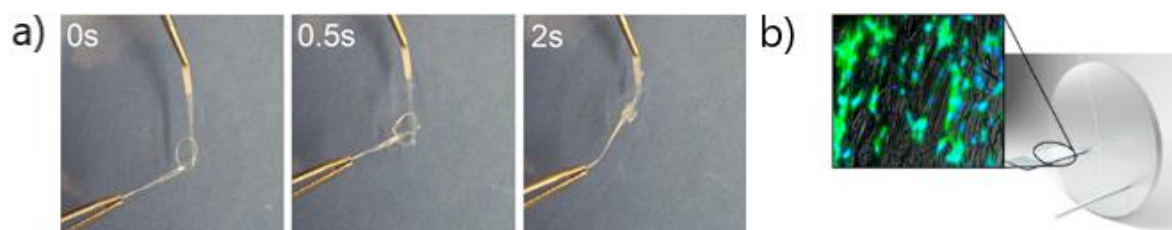


Figure 13. PCL-PU's remarkable biocompatibility and biodegradability, along with their facile processing, have encouraged the production of a) self-knotting sutures to b) suitable fibrous scaffolds for the cell culturing of muscle cells just to name some of the promising applications of these materials on the biomedical field and materials science in general, images are taken from **Left:** Reprinted/adapted by permission from Elsevier: Elsevier, *Journal of the Mechanical Behavior of Biomedical Materials*, from Jing, X.; Mi, H.-Y.; Huang, H.-X.; Turng, L.-S. Shape Memory Thermoplastic Polyurethane (TPU)/Poly(ϵ -Caprolactone) (PCL) Blends as Self-Knotting Sutures. *Journal of the Mechanical Behavior of Biomedical Materials* **2016**, *64*, 94–103, © 2016 Elsevier Ltd. All rights reserved. **Right:** Reprinted/adapted by permission from American Chemical Society: American Chemical Society, *ACS Applied Bio Materials*, from Uribe-Gomez, J.; Posada-Murcia, A.; Shukla, A.; Alkhamis, H.; Salehi, S.; Ionov, L. Soft Elastic Fibrous Scaffolds for Muscle Tissue Engineering by Touch Spinning. *ACS Appl. Bio Mater.* **2021**, *4* (7), 5585–5597 Copyright © 2021, American Chemical Society.^{105,108}

The mechanism behind the 2W-SME and its multiple applications through the development of PCL-based derivate actuators under external or intrinsic constant stress conditions has been exhaustively investigated, yet in almost all the cases, the required locomotion of the synthesized actuators to achieve a determinate functionality does not involve a longitudinal elongation of the sample. Curving, spiraling, bending, and twisting constitute the preferred and most commonly used shape-shifting transitions in the applications of SMPs.^{50,109,110} Therefore, the investigation of the thermomechanical properties of these materials under constant strain conditions while enduring a 2W-SME run is more than necessary and, until today, an outlooked topic.

For all the previously mentioned, the main scope of this work is to contribute to the understanding of the actuation mechanism of reversible thermally induced SME of cross-linkable semicrystalline polymer networks constituted by poly (ϵ -caprolactone) and their corresponding polyurethane-based copolymers. To achieve this relevant task, a structured and comparative investigation of their thermal and mechanical properties under constant stress and constant strain conditions on melting-crystallization cycling is driven. The identification and evaluation of relevant parameters and their effect on the 2W-SME performance of these materials, such as the crosslinking density, degree of crystallinity, rate of heating-cooling, the magnitude of applied load, and strain degree, are proposed.

Once the unexplored thermomechanical behavior of the materials under constant strain is described, the necessity of correlating the acquired tensile macroscopic observables with the structural evolution of the semicrystalline polymer networks undergoing a reversible shape-switching transformation will become evident. Therefore, the correlation between the crystallinity, polymer chain's orientation, sample's drawing upon cooling, and tensile features is pretended to be achieved by performing *in situ* SAXS and WAXS analysis of stretched materials on a constant strain setup and simultaneously measuring the extensional stress evolution with temperature. The endowed observations and their exegesis will eventually allow the development and proposal of a model to contribute to the understanding of the 2W-SME on semicrystalline polymer networks.

2. Aim

The aim of the present dissertation was to provide new insights into the understanding of the mechanism behind the thermally induced reversible shape memory effect (2W-SME) of semicrystalline polymers by carrying out a detailed study of the mechanical, physicochemical and structural features of self-made polymeric actuators based on chemically crosslinked PCL networks and PCL-polyurethane copolymers under, until today overlooked constant strain conditions.

The selected materials for this project are, until this date, relevant to the current state of art and scope of the investigation of the shape memory polymers due to their:

- ❖ Tailorable physicochemical and mechanical properties
- ❖ High processability and wide additive manufacture possibilities
- ❖ Large spectrum of applications
- ❖ Reversible and large amplitude of actuation in dry and wet states

For these reasons, the fulfilment of the established goal in this dissertation was supported by the following objectives:

- 1) The study of the mechanical properties of unstretched and stretched crosslinked PCL under thermal cycling allows the investigation of the evolution of extensional stress and strain upon cooling and heating. Correlate parameters such as the crosslinking density, strain degree, and load magnitude with the reversibility of the thermally induced SME of crosslinked semicrystalline polymers under constant stress and constant strain conditions.
- 2) Expand the feasible correspondence between the shape-shifting transformation ability and the structural rearrangement endured by crosslinked semicrystalline polymers amid the thermally triggered 2W-SME. The usage of *in-situ* X-ray scattering techniques to give a structural explanation to the thermomechanical behaviour of crosslinked PCL under constant strain conditions allows the proposal of a model able to describe the reversible actuation of semicrystalline polymer networks.
- 3) Comparison between the tensile and the 2W-SME properties of cured semicrystalline networks and phase-segregated copolymers based on PCL. Exploration of the effect over the reversibility of the SME, thermomechanical properties, and processability caused by the variation of the chemical nature of the hard segments and their mass content on synthesized PCL-based polyurethanes.

3. Synopsis

The present work was realized with the aim of investigating the mechanism of the thermally induced reversible shape memory effect exhibited by semicrystalline actuators composed of chemically crosslinked PCL and some of its ester-urethane derivatives. Their obtention followed by their thermomechanical and physicochemical characterization, the comparative study of their 2W-SME behavior under constant stress and constant strain conditions, the correlation of their tensile features with the reorganization of their structure while under thermal cycling, and the influence of the composition/architecture of these semicrystalline networks on the reversible SME was thoroughly carried out.

The aforementioned studies were carried in the University of Bayreuth under the supervision of Prof. Dr. Leonid Ionov, head of the Professorship of Biofabrication. The main outcomes of this investigation are presented and consigned in this dissertation on three papers (two already published full papers and one submitted manuscript) which are directly correlated with the three objectives proposed in the chapter 2 of this document.

3.1 Two-Way Shape Memory Polymers: Evolution of Stress vs. Evolution of Elongation

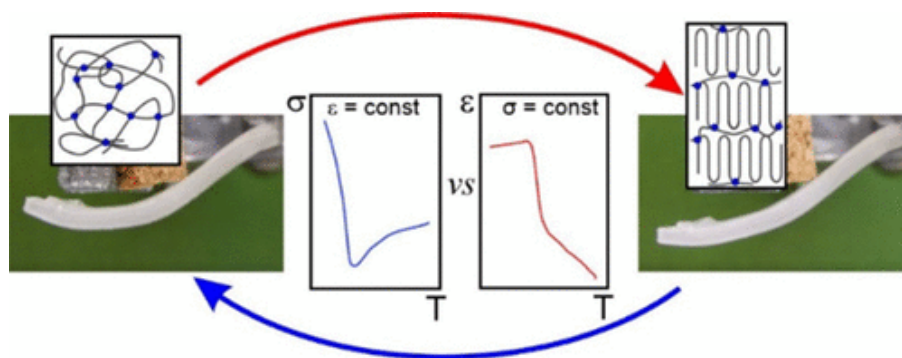


Figure 14. Representation of the evolution of a reversible shape-switching crosslinked PCL semicrystalline networks under constant stress and constant strain conditions upon thermal cycling along with a constantly stretched PCL-based bilayer undergoing an autonomous thermally induced 2W-SME. Reprinted/adapted by permission from American Chemical Society: American Chemical Society, *Macromolecules*, from Posada-Murcia, A., Uribe-Gomez, J. M., Sommer, J. U., & Ionov, L. Two-Way Shape Memory Polymers: Evolution of Stress vs. Evolution of Elongation. *Macromolecules* **2021**, *54* (12), 5838-5847, Copyright © 2021, American Chemical Society.¹¹¹

The first full paper, entitled “Two-Way Shape Memory Polymers: Evolution of Stress vs. Evolution of Elongation.” was published on June 2 of 2021, in the ACS Macromolecules journal.

In this manuscript, the production of semicrystalline actuators based on chemically crosslinked linear high molecular weight (80 kDa) PCL networks able to perform 2W-SME under load upon thermal cycling was reported. A set of materials containing different amounts of the crosslinking agent were obtained through a thermal annealing process using separately dicumyl peroxide (DCP) and 2,5-Bis(tert-butylperoxy)-2,5-dimethylhexane (TBP) as thermal crosslinking agents. The tensile characterization of these materials in the molten state allowed the estimation of their crosslinked density, in the form of the molecular weight of polymer chains between the crosslinking points, by means of the rubber elasticity theory on molten state^{56,112}.

The thermal and thermomechanical properties of these materials were correlated with their performance by undergoing a typical run of reversible SME under constant stress. It was found that the polymers crosslinked with DCP exhibited a higher effective crosslinking density (enhanced storage and elastic modulus) than their analogues containing TBP. The possibility of investigating the tensile behavior of the synthesized thermosets under constant strain setup was explored; by doing so it was encountered that the constantly drawing cured elastomers show an unexpected intermediate behavior between the rubbery and the crystalline state upon cooling characterized by an observable stress-drop. The magnitude of this stress drop is strongly correlated with the strain degree of the sample and seems to be independent of the crosslinking density for equally stretched samples; therefore, its origin was attributed to the reduction of the conformational entropy of the polymer chains under strain.

As the bidirectional SME of thermally cycled crosslinked PCL networks was characterized under constant stress and constant strain conditions, an application of the anomalous intermediate state was assessed through the design of a functional bilayer-construct able to reversibly bend/unbend upon multiple thermal cycling. The heating and cooling processes around the T_{trans} induce the contraction and elongation of a constantly strained cured PCL

laminate adhered to an elastomer strip; this laminate composite delivers an effective and reproducible thermally induced bidirectional SME.

3.2 Mechanism of Behavior of Two-Way Shape Memory Polymer under Constant Strain Conditions

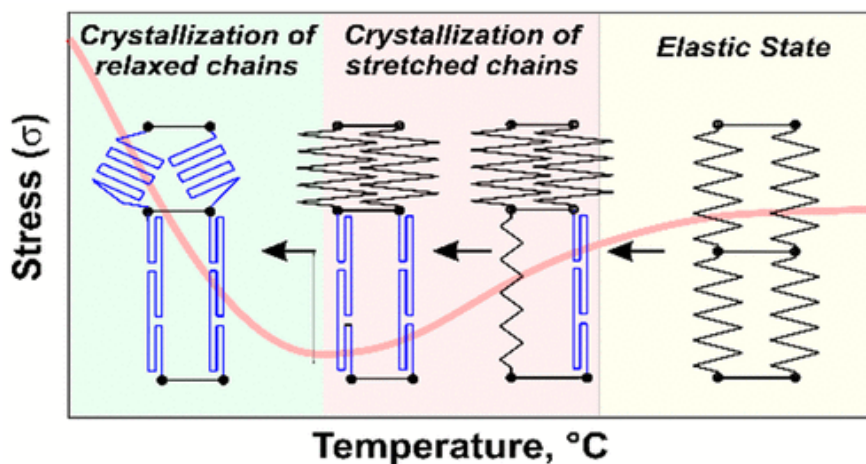


Figure 15. A diagrammatic representation of the proposed molecular mechanism for the crystallization process of a constantly stretched semicrystalline polymer network upon cooling, the presented model is based on the simultaneous acquisition and correlation of thermomechanical and structural parameters of crosslinked PCL probes stretched up to 200 and 300% of their original length. Reprinted/adapted by permission from American Chemical Society: American Chemical Society, *Macromolecules*, from Posada-Murcia, A., Uribe-Gomez, J.M., Förster, S., Sommer, J.U., Dulle, M. and Ionov, L., Mechanism of Behavior of Two-Way Shape Memory Polymer under Constant Strain Conditions. **2022**, *Macromolecules*, 55 (5), pp.1680-1689, Copyright © 2021, American Chemical Society¹¹³

The second manuscript, titled “Mechanism of Behavior of Two-Way Shape Memory Polymer under Constant Strain Conditions” was published in the ACS *Macromolecules* journal on February 14, 2022.

The description of the mechanical features of crosslinked PCL networks exhibiting 2W-SME under constant strain upon cooling was driven in the first paper. This new panorama allowed the identification of an unexpected stress drop region before the crystallization of the material. Although a conscious mechanical study of this odd behavior was provided, its mechanism and origin were merely discussed as their unraveling stayed out of the outlook of the paper. This second paper attempted to supply an answer for these unsolved questions

therefore, it expands the investigation of the thermomechanical evolution of constantly strained cured linear PCL upon cooling by realizing a series of kinetic studies and *in-situ* SAXS/WAXS analysis to establish the temporal stability and structural origin of the observed anomalous stress drop regime.

The kinetic investigation of the unknown transient state between the molten and crystalline state of cured PCL networks under constant load consisted of the evaluation of the recorded extensional stress upon cooling by applying very long cooling/annealing steps on the temperature range where the drop on stress was observed. This allowed to reach the conclusion that this transient state is as a matter of fact, a stable intermediate phase/conformation of the polymer chains as the drop in the measured stress was observed for about 3 hours; this state cannot be avoided by rapidly cooling the sample below the onset temperature for this regime.

Furthermore, the *in-situ* SAXS/WAXS essays made on the extended crosslinked PCL samples revealed that the crystallization process of constantly strained semicrystalline polymer networks upon cooling (which represents the half of a typical thermally induced 2W-SME run) occurs in two-steps. On the temperature range where the stress drop is being recorded (above PCL's T_{cry}), the appearance of a highly ordered family of crystalline domains is detected on the WAXS pattern as very intense anisotropic reflections upon further cooling signals corresponding to isotropic scattering patterns are observed as the extensional stress arises sharply indicating the inception of non-oriented crystallites. These results are in total accordance with the data collected from SAXS experiments where meridional spots appear at the onset of the intermediate state, confirming the formation of oriented lamellae. As the cooling process follows its course and the stress arises below PCL's T_{cry} , equatorial spots come into sight, corresponding to the formation of non-oriented lamellae domains.

Therefore, a good correlation between the simultaneous measurement of the unusual thermomechanical properties and the structural rearrangement suffered by the polymer chains upon cooling permitted the development of a model. This model describes the previously reported 2W-SME of semicrystalline polymer networks on a constant strain setup. The oriented polymer chains crystallize first from the molten state, producing crystalline

domains aligned towards the deformation. This crystallization process evokes a stress distribution on the polymer network forcing the stretching and further crystallization of the adjacent polymer strands provoking the unusual observed stress drop. The magnitude of this drop is strongly dependent on the amount of oriented polymer chain segments, which at the same time are strongly correlated with the crosslinking density of the material and the magnitude of the stretching. As the sample is cooled below its T_{cry} and its length stays constant, the crystallization of non-stretched polymer chains occurs, producing unoriented crystalline domains, which induce a rise of the measured extensional stress.

3.3 Bidirectional shape memory polymers: effect of molecular architecture over the thermomechanical behavior at constant stress and constant strain conditions

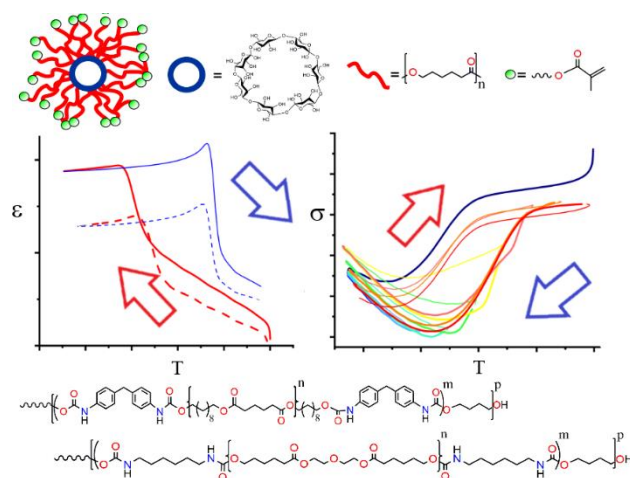


Figure 16. Depiction of the driven thermomechanical characterization essays on multiple semicrystalline polymer networks with varied molecular architecture and crosslinking mechanisms to evaluate and compare their thermally triggered two-way shape memory effect properties under constant stress and constant strain conditions.

The third paper is based on the characterization and direct comparison of the thermally induced 2W-SME of PCL-based semicrystalline networks with diverse chemical functionalities/molecular architectures under constant stress and constant strain conditions. The manuscript under the title “Bidirectional shape memory polymers: effect of architecture on behavior at constant stress and constant strain conditions” will be submitted to ACS Macromolecules.

A straightforward analogy between the reversible thermally guided shape-switching features of a) crosslinked linear PCL, b) crosslinked star-like PCL network based on a functionalized β -cyclodextrin nuclei grafted with acrylate-terminal polycaprolactone arms (β -CD-PCL), and c) ester-urethane PCL-derived copolymers containing different mass percentages of hard segment content was carried out. This final report intended to revise and gather the evolution of the reversible shape transformations experienced by semicrystalline polymer networks with varied chemical structures. With this, the development of a critical and generalized overview for their further application as polymeric actuators was pursued.

First, the synthesis of high molecular weight hydroxyl-ended poly(ϵ -caprolactone) by the solvent-free ring-opening polymerization of ϵ -caprolactone monomer was successful. From this diol, four different polycaprolactone-urethane copolymers (PCL-PUs) were obtained. The PCL-PUs contained either hexamethylene diisocyanate (HDI) or methylene diphenyl diisocyanate (MDI) as hard urethane segments. Butanediol (BD) was used as a chain extender in all cases, while the mass ratio between the hard segment (HSC) and the soft segment (SSC) content was varied in all copolymers.

The spectroscopic, analytical, and thermal characterization of the produced PCL-PUs was carried out; the obtained data were in complete agreement with the proposed composition for these materials. Of all four PCL-PUs just two of them could be processed as films. Therefore, only PCL-PU(HDI+BD) and PCL-PU(MDI+BD) 70:30 (SSC:HSC, %wt) were suitable for the evaluation of their bidirectional shape memory properties. For the sake of comparison, the properties of both PCL-PUs were contrasted with the tensile and thermomechanical features of a polyester urethane with excellent 2W-SME behavior, TPU-PDA 25. This SMP contains poly(1,10-decylene adipate) diol as the soft segment and MDI+BD as the hard segment on a mass ratio of 75:25 (SSC:HSC, %wt).

The PCL-based copolymer derived from MDI+BD is way stiffer and less elastic than its analogue with HDI+BD despite the fact of containing a PCL soft segment with the same

molecular weight and exhibiting the largest M_n among all synthesized PUs. Also, PCL-PU(MDI+BD) exhibits a smaller degree of crystallinity in comparison with PCL-PU(HDI+BD). The rigidity of this material impeded the evaluation of its 2W-SME behaviour at large deformations. PCL-PU(HDI+BD), PCL-PU(MDI+BD) 70:30, and TPU-PDA 25 demonstrated a bidirectional shape memory effect under constant stress and strain conditions. The PDA-based urethane proved to be the softest and most elastic urethane-copolymer tested, this material exhibited superior thermomechanical properties in comparison with PCL-PU(HDI+BD) when extended or loaded equally on a 2W-SME run. Thus, the observed stress drop and the strain increment, origin of the reversibility of the SME upon cooling under constant strain and stress conditions correspondingly, of TPU-PDA 25 were superior. The cause for this is the complementary effect between its high enthalpy of melting/crystallization and the flexibility of the PDA monomer unit in comparison with the short-lengthened PCL repeating units.

Among the chemically crosslinked elastomers, the linear PCL probes showed a more noticeable creep effect under constant stress conditions as the difference between the initial and final recorded strain during the heating/cooling cycle is larger when compared to the star-like PCL. This observation can be interpreted as the linear PCL networks under load are more likely to undergo plastic deformations due to chain slipping than their more cleaved multi-armed analogues, increasing the reversibility of the bidirectional SME on the latter. The acquired data on constant strain conditions support the aforementioned observations. The stress drop magnitude of the β -CD-PCLs is slightly higher and sets in at higher temperatures than in the case of equally extended linear PCLs. Therefore, the degree of orientation of the polymer chains on the cyclodextrin-PCL materials under a uniaxial deformation is higher, improving the amplitude and reversibility of its shape-shifting transformation.

In general, the crosslinked networks showed an inferior nominal stress drop value than the PUs stretched at the same degree under constant strain conditions. Therefore, the phase-segregation effect on the PCL copolymers proved to have a stronger synergic

repercussion on the reversibility of their 2W-SME. The segregation of the amorphous-urethane phase in-between a strained semicrystalline polymer network allows a better orientation of its crystalline domains generated upon cooling towards an applied deformation than net points originated by a chemical crosslinking process.

4. Literature References

- (1) Samui, A. B. *Smart Polymers: Basics and Applications*; CRC Press, 2022.
- (2) Galaev, I.; Mattiasson, B. *Smart Polymers: Applications in Biotechnology and Biomedicine, Second Edition*; CRC Press, 2007.
- (3) Godavitarne, C.; Robertson, A.; Peters, J.; Rogers, B. Biodegradable Materials. *Orthopaedics and Trauma* **2017**, *31* (5), 316–320. <https://doi.org/10.1016/j.mporth.2017.07.011>.
- (4) Nguyen, P. Q.; Courchesne, N.-M. D.; Duraj-Thatte, A.; Praveschotinunt, P.; Joshi, N. S. Engineered Living Materials: Prospects and Challenges for Using Biological Systems to Direct the Assembly of Smart Materials. *Advanced Materials* **2018**, *30* (19), 1704847. <https://doi.org/10.1002/adma.201704847>.
- (5) Cao, W.; Cudney, H. H.; Waser, R. Smart Materials and Structures. *Proceedings of the National Academy of Sciences* **1999**, *96* (15), 8330–8331. <https://doi.org/10.1073/pnas.96.15.8330>.
- (6) Shahinpoor, M. *Fundamentals of Smart Materials*; Royal Society of Chemistry, 2020.
- (7) Gardan, J. Smart Materials in Additive Manufacturing: State of the Art and Trends. *Virtual and Physical Prototyping* **2019**, *14* (1), 1–18. <https://doi.org/10.1080/17452759.2018.1518016>.
- (8) Bahl, S.; Nagar, H.; Singh, I.; Sehgal, S. Smart Materials Types, Properties and Applications: A Review. *Materials Today: Proceedings* **2020**, *28*, 1302–1306. <https://doi.org/10.1016/j.matpr.2020.04.505>.
- (9) Addington, D. M.; Schodek, D. L. *Smart Materials and New Technologies: For the Architecture and Design Professions*; Routledge, 2005.
- (10) García, J. M.; García, F. C.; Ruiz, J. A. R.; Vallejos, S.; Trigo-López, M. *Smart Polymers: Principles and Applications*; Walter de Gruyter GmbH & Co KG, 2022.
- (11) Yoshida, K.; Soldati, T. Dissection of Amoeboid Movement into Two Mechanically Distinct Modes. *Journal of Cell Science* **2006**, *119* (18), 3833–3844. <https://doi.org/10.1242/jcs.03152>.
- (12) Fukutani, A.; Joumaa, V.; Herzog, W. Influence of Residual Force Enhancement and Elongation of Attached Cross-Bridges on Stretch-Shortening Cycle in Skinned Muscle Fibers. *Physiological Reports* **2017**, *5* (22), e13477. <https://doi.org/10.14814/phy2.13477>.
- (13) Iqbal, D.; Samiullah, M. H. Photo-Responsive Shape-Memory and Shape-Changing Liquid-Crystal Polymer Networks. *Materials* **2013**, *6* (1), 116–142. <https://doi.org/10.3390/ma6010116>.
- (14) Raghavan, S. R.; Fernandes, N. J.; Cipriano, B. H. Shape-Changing Tubular Hydrogels. *Gels* **2018**, *4* (1), 18. <https://doi.org/10.3390/gels4010018>.
- (15) Kirillova, A.; Ionov, L. Shape-Changing Polymers for Biomedical Applications. *J. Mater. Chem. B* **2019**, *7* (10), 1597–1624. <https://doi.org/10.1039/C8TB02579G>.
- (16) Palagi, S.; Mark, A. G.; Reigh, S. Y.; Melde, K.; Qiu, T.; Zeng, H.; Parmeggiani, C.; Martella, D.; Sanchez-Castillo, A.; Kapernaum, N.; Giesselmann, F.; Wiersma, D. S.; Lauga, E.; Fischer, P. Structured Light Enables Biomimetic Swimming and

- Versatile Locomotion of Photoresponsive Soft Microrobots. *Nature Mater* **2016**, *15* (6), 647–653. <https://doi.org/10.1038/nmat4569>.
- (17) Wei, Z.; Bai, R. Temperature-Modulated Photomechanical Actuation of Photoactive Liquid Crystal Elastomers. *Extreme Mechanics Letters* **2022**, *51*, 101614. <https://doi.org/10.1016/j.eml.2022.101614>.
- (18) Delgado, S. M.; Norris, S. C. P.; Kasko, A. M. Photodegradation Actuated Shape-Changing Hydrogels. *Journal of Polymer Science* **2022**, *60* (5), 825–841. <https://doi.org/10.1002/pol.20210787>.
- (19) Boothby, J. M.; Gagnon, J. C.; McDowell, E.; Van Volkenburg, T.; Currano, L.; Xia, Z. An Untethered Soft Robot Based on Liquid Crystal Elastomers. *Soft Robotics* **2022**, *9* (1), 154–162. <https://doi.org/10.1089/soro.2020.0135>.
- (20) Behl, M.; Lendlein, A. Actively Moving Polymers. *Soft Matter* **2007**, *3* (1), 58–67. <https://doi.org/10.1039/B610611K>.
- (21) Hager, M. D.; Bode, S.; Weber, C.; Schubert, U. S. Shape Memory Polymers: Past, Present and Future Developments. *Progress in Polymer Science* **2015**, *49–50*, 3–33. <https://doi.org/10.1016/j.progpolymsci.2015.04.002>.
- (22) Gall, K.; Yakacki, C. M.; Liu, Y.; Shandas, R.; Willett, N.; Anseth, K. S. Thermomechanics of the Shape Memory Effect in Polymers for Biomedical Applications. *Journal of Biomedical Materials Research Part A* **2005**, *73A* (3), 339–348. <https://doi.org/10.1002/jbm.a.30296>.
- (23) Qiao, L.; Liu, C.; Liu, C.; Zong, L.; Gu, H.; Wang, C.; Jian, X. Self-Healing, PH-Sensitive and Shape Memory Hydrogels Based on Acylhydrazone and Hydrogen Bonds. *European Polymer Journal* **2022**, *162*, 110838. <https://doi.org/10.1016/j.eurpolymj.2021.110838>.
- (24) Samui, A. B. Shape Memory Polymers. In *Smart Polymers*; CRC Press, 2022.
- (25) Mohd Jani, J.; Leary, M.; Subic, A.; Gibson, M. A. A Review of Shape Memory Alloy Research, Applications and Opportunities. *Materials & Design (1980-2015)* **2014**, *56*, 1078–1113. <https://doi.org/10.1016/j.matdes.2013.11.084>.
- (26) Tobushi, H.; Pieczyska, E.; Ejiri, Y.; Sakuragi, T. Thermomechanical Properties of Shape-Memory Alloy and Polymer and Their Composites. *Mechanics of Advanced Materials and Structures* **2009**, *16* (3), 236–247. <https://doi.org/10.1080/15376490902746954>.
- (27) Huang, W. M.; Zhao, Y.; Wang, C. C.; Ding, Z.; Purnawali, H.; Tang, C.; Zhang, J. L. Thermo/Chemo-Responsive Shape Memory Effect in Polymers: A Sketch of Working Mechanisms, Fundamentals and Optimization. *J Polym Res* **2012**, *19* (9), 9952. <https://doi.org/10.1007/s10965-012-9952-z>.
- (28) Han, X.-J.; Dong, Z.-Q.; Fan, M.-M.; Liu, Y.; Li, J.-H.; Wang, Y.-F.; Yuan, Q.-J.; Li, B.-J.; Zhang, S. PH-Induced Shape-Memory Polymers. *Macromolecular Rapid Communications* **2012**, *33* (12), 1055–1060. <https://doi.org/10.1002/marc.201200153>.
- (29) Gu, L.; Jiang, Y.; Hu, J. Bioinspired Poly(Vinyl Alcohol)-Silk Hybrids: Two-Way Water-Sensitive Shape-Memory Materials. *Materials Today Communications* **2018**, *17*, 419–426. <https://doi.org/10.1016/j.mtcomm.2018.10.005>.

- (30) Zhao, W.; Liu, L.; Zhang, F.; Leng, J.; Liu, Y. Shape Memory Polymers and Their Composites in Biomedical Applications. *Materials Science and Engineering: C* **2019**, *97*, 864–883. <https://doi.org/10.1016/j.msec.2018.12.054>.
- (31) Bao, M.; Lou, X.; Zhou, Q.; Dong, W.; Yuan, H.; Zhang, Y. Electrospun Biomimetic Fibrous Scaffold from Shape Memory Polymer of PDLA-Co-TMC for Bone Tissue Engineering. *ACS Appl. Mater. Interfaces* **2014**, *6* (4), 2611–2621. <https://doi.org/10.1021/am405101k>.
- (32) Sonatkar, J.; Kandasubramanian, B.; Ismail, S. O. 4D Printing: Pragmatic Progression in Biofabrication. *European Polymer Journal* **2022**, *169*, 111128. <https://doi.org/10.1016/j.eurpolymj.2022.111128>.
- (33) Ionov, L. 4D Biofabrication: Materials, Methods, and Applications. *Advanced Healthcare Materials* **2018**, *7* (17), 1800412. <https://doi.org/10.1002/adhm.201800412>.
- (34) Gök, M. O.; Bilir, M. Z.; Gürcüm, B. H. Shape-Memory Applications in Textile Design. *Procedia - Social and Behavioral Sciences* **2015**, *195*, 2160–2169. <https://doi.org/10.1016/j.sbspro.2015.06.283>.
- (35) Liu, T.; Zhou, T.; Yao, Y.; Zhang, F.; Liu, L.; Liu, Y.; Leng, J. Stimulus Methods of Multi-Functional Shape Memory Polymer Nanocomposites: A Review. *Composites Part A: Applied Science and Manufacturing* **2017**, *100*, 20–30. <https://doi.org/10.1016/j.compositesa.2017.04.022>.
- (36) Subramani, N. K.; Siddaramaiah, M. R.; Lee, J. H. *Polymer-Based Advanced Functional Composites for Optoelectronic and Energy Applications*; Elsevier, 2021.
- (37) Lendlein, A.; Kelch, S. Shape-Memory Polymers. *Angewandte Chemie International Edition* **2002**, *41* (12), 2034–2057. [https://doi.org/10.1002/1521-3773\(20020617\)41:12<2034::AID-ANIE2034>3.0.CO;2-M](https://doi.org/10.1002/1521-3773(20020617)41:12<2034::AID-ANIE2034>3.0.CO;2-M).
- (38) Zhou, J.; Sheiko, S. S. Reversible Shape-Shifting in Polymeric Materials. *Journal of Polymer Science Part B: Polymer Physics* **2016**, *54* (14), 1365–1380. <https://doi.org/10.1002/polb.24014>.
- (39) Heuchel, M.; Sauter, T.; Kratz, K.; Lendlein, A. Thermally Induced Shape-Memory Effects in Polymers: Quantification and Related Modeling Approaches. *Journal of Polymer Science Part B: Polymer Physics* **2013**, *51* (8), 621–637. <https://doi.org/10.1002/polb.23251>.
- (40) Zare, M.; Prabhakaran, M. P.; Parvin, N.; Ramakrishna, S. Thermally-Induced Two-Way Shape Memory Polymers: Mechanisms, Structures, and Applications. *Chemical Engineering Journal* **2019**, *374*, 706–720. <https://doi.org/10.1016/j.cej.2019.05.167>.
- (41) Li, J.; Rodgers, W. R.; Xie, T. Semi-Crystalline Two-Way Shape Memory Elastomer. *Polymer* **2011**, *52* (23), 5320–5325. <https://doi.org/10.1016/j.polymer.2011.09.030>.
- (42) Wang, T.; Liu, Y.; Zhao, J.; Zhang, H.; Zhang, Z. A Facile Approach to Fabricate Two-Way Shape Memory Polyurethane with Large Reversible Strain and High Shape Stability. *Smart Mater. Struct.* **2020**, *29* (5), 055033. <https://doi.org/10.1088/1361-665X/ab7f40>.
- (43) Bothe, M.; Pretsch, T. Bidirectional Actuation of a Thermoplastic Polyurethane Elastomer. *Journal of Materials Chemistry A* **2013**, *1* (46), 14491–14497. <https://doi.org/10.1039/C3TA13414H>.

- (44) Huang, M.; Zheng, L.; Wang, L.; Dong, X.; Gao, X.; Li, C.; Wang, D. Double Crystalline Multiblock Copolymers with Controlling Microstructure for High Shape Memory Fixity and Recovery. *ACS Appl. Mater. Interfaces* **2017**, *9* (35), 30046–30055. <https://doi.org/10.1021/acsami.7b08403>.
- (45) Behl, M.; Razzaq, M. Y.; Lendlein, A. Multifunctional Shape-Memory Polymers. *Advanced Materials* **2010**, *22* (31), 3388–3410. <https://doi.org/10.1002/adma.200904447>.
- (46) Wang, Y.; Huang, X.; Zhang, J.; Bi, M.; Zhang, J.; Niu, H.; Li, C.; Yu, H.; Wang, B.; Jiang, H. Two-Step Crosslinked Liquid-Crystalline Elastomer with Reversible Two-Way Shape Memory Characteristics. *Molecular Crystals and Liquid Crystals* **2017**, *650* (1), 13–22. <https://doi.org/10.1080/15421406.2017.1318025>.
- (47) Wermter, H.; Finkelmann, H. Liquid Crystalline Elastomers as Artificial Muscles. *e-Polymers* **2001**, *1* (1). <https://doi.org/10.1515/epoly.2001.1.1.111>.
- (48) Chung, T.; Romo-Uribe, A.; Mather, P. T. Two-Way Reversible Shape Memory in a Semicrystalline Network. *Macromolecules* **2008**, *41* (1), 184–192. <https://doi.org/10.1021/ma071517z>.
- (49) Thomsen, D. L.; Keller, P.; Naciri, J.; Pink, R.; Jeon, H.; Shenoy, D.; Ratna, B. R. Liquid Crystal Elastomers with Mechanical Properties of a Muscle. *Macromolecules* **2001**, *34* (17), 5868–5875. <https://doi.org/10.1021/ma001639q>.
- (50) Behl, M.; Kratz, K.; Noechel, U.; Sauter, T.; Lendlein, A. Temperature-Memory Polymer Actuators. *Proceedings of the National Academy of Sciences* **2013**, *110* (31), 12555–12559. <https://doi.org/10.1073/pnas.1301895110>.
- (51) Atli, B.; Gandhi, F.; Karst, G. Thermomechanical Characterization of Shape Memory Polymers. *Journal of Intelligent Material Systems and Structures* **2009**, *20* (1), 87–95. <https://doi.org/10.1177/1045389X07086689>.
- (52) Flory, P. J. Molecular Theory of Rubber Elasticity. *Polymer* **1979**, *20* (11), 1317–1320. [https://doi.org/10.1016/0032-3861\(79\)90268-4](https://doi.org/10.1016/0032-3861(79)90268-4).
- (53) Wall, F. T.; Flory, P. J. Statistical Thermodynamics of Rubber Elasticity. *J. Chem. Phys.* **1951**, *19* (12), 1435–1439. <https://doi.org/10.1063/1.1748098>.
- (54) Kuhn, W. Dependence of the Average Transversal on the Longitudinal Dimensions of Statistical Coils Formed by Chain Molecules. *Journal of Polymer Science* **1946**, *1* (5), 380–388. <https://doi.org/10.1002/pol.1946.120010505>.
- (55) Gao, J.; Weiner, J. H. Excluded-Volume Effects in Rubber Elasticity. 2. Ideal Chain Assumption. *Macromolecules* **1987**, *20* (10), 2525–2531. <https://doi.org/10.1021/ma00176a035>.
- (56) Gedde, U. W.; Hedenqvist, M. S. Rubber Elasticity. In *Fundamental Polymer Science*; Gedde, U. W., Hedenqvist, M. S., Eds.; Springer International Publishing: Cham, 2019; pp 75–111. https://doi.org/10.1007/978-3-030-29794-7_3.
- (57) Gao, J.; Weiner, J. H. Nature of Stress on the Atomic Level in Dense Polymer Systems. *Science* **1994**, *266* (5186), 748–752. <https://doi.org/10.1126/science.266.5186.748>.
- (58) Beloshenko, V. A.; Varyukhin, V. N.; Voznyak, Y. V. The Shape Memory Effect in Polymers. *Russ. Chem. Rev.* **2005**, *74* (3), 265. <https://doi.org/10.1070/RC2005v074n03ABEH000876>.

- (59) Pandini, S.; Dioni, D.; Paderni, K.; Messori, M.; Toselli, M.; Bontempi, E.; Riccò, T. The Two-Way Shape Memory Behaviour of Crosslinked Poly(ϵ -Caprolactone) Systems with Largely Varied Network Density. *Journal of Intelligent Material Systems and Structures* **2016**, *27* (10), 1388–1403. <https://doi.org/10.1177/1045389X15591384>.
- (60) Kolesov, I.; Dolynchuk, O.; Borreck, S.; Radusch, H.-J. Morphology-Controlled Multiple One- and Two-Way Shape-Memory Behavior of Cross-Linked Polyethylene/Poly(ϵ -Caprolactone) Blends. *Polymers for Advanced Technologies* **2014**, *25* (11), 1315–1322. <https://doi.org/10.1002/pat.3338>.
- (61) Ullman, R. Small-Angle Neutron Scattering from Elastomeric Networks. Application to Labeled Chains Containing Several Crosslinks. *Macromolecules* **1982**, *15* (5), 1395–1402. <https://doi.org/10.1021/ma00233a035>.
- (62) Beltzung, M.; Picot, C.; Herz, J. Investigation of the Chain Conformation in Uniaxially Stretched Poly(Dimethylsiloxane) Networks by Small-Angle Neutron Scattering. *Macromolecules* **1984**, *17* (4), 663–669. <https://doi.org/10.1021/ma00134a024>.
- (63) Flory, P. J. *Principles of Polymer Chemistry*; Cornell University Press, 1953.
- (64) Chen, Y.-C.; Lagoudas, D. C. A Constitutive Theory for Shape Memory Polymers. Part I: Large Deformations. *Journal of the Mechanics and Physics of Solids* **2008**, *56* (5), 1752–1765. <https://doi.org/10.1016/j.jmps.2007.12.005>.
- (65) Chen, Y.-C.; Lagoudas, D. C. A Constitutive Theory for Shape Memory Polymers. Part II: A Linearized Model for Small Deformations. *Journal of the Mechanics and Physics of Solids* **2008**, *56* (5), 1766–1778. <https://doi.org/10.1016/j.jmps.2007.12.004>.
- (66) Qi, H. J.; Nguyen, T. D.; Castro, F.; Yakacki, C. M.; Shandas, R. Finite Deformation Thermo-Mechanical Behavior of Thermally Induced Shape Memory Polymers. *Journal of the Mechanics and Physics of Solids* **2008**, *56* (5), 1730–1751. <https://doi.org/10.1016/j.jmps.2007.12.002>.
- (67) Westbrook, K. K.; Parakh, V.; Chung, T.; Mather, P. T.; Wan, L. C.; Dunn, M. L.; Qi, H. J. Constitutive Modeling of Shape Memory Effects in Semicrystalline Polymers With Stretch Induced Crystallization. *Journal of Engineering Materials and Technology* **2010**, *132* (4). <https://doi.org/10.1115/1.4001964>.
- (68) Dolynchuk, O.; Kolesov, I.; Radusch, H.-J. Theoretical Description of an Anomalous Elongation During Two-Way Shape-Memory Effect in Crosslinked Semicrystalline Polymers. *Macromolecular Symposia* **2014**, *346* (1), 48–58. <https://doi.org/10.1002/masy.201400065>.
- (69) Kolesov, I.; Dolynchuk, O.; Jehnichen, D.; Reuter, U.; Stamm, M.; Radusch, H.-J. Changes of Crystal Structure and Morphology during Two-Way Shape-Memory Cycles in Cross-Linked Linear and Short-Chain Branched Polyethylenes. *Macromolecules* **2015**, *48* (13), 4438–4450. <https://doi.org/10.1021/acs.macromol.5b00097>.
- (70) Dolynchuk, O.; Kolesov, I.; Jehnichen, D.; Reuter, U.; Radusch, H.-J.; Sommer, J.-U. Reversible Shape-Memory Effect in Cross-Linked Linear Poly(ϵ -Caprolactone) under Stress and Stress-Free Conditions. *Macromolecules* **2017**, *50* (10), 3841–3854. <https://doi.org/10.1021/acs.macromol.7b00481>.

- (71) Huang, M.; Dong, X.; Wang, L.; Zhao, J.; Liu, G.; Wang, D. Two-Way Shape Memory Property and Its Structural Origin of Cross-Linked Poly(ϵ -Caprolactone). *RSC Advances* **2014**, *4* (98), 55483–55494. <https://doi.org/10.1039/C4RA09385B>.
- (72) Kalita, H. *Shape Memory Polymers: Theory and Application*; De Gruyter, 2018. <https://doi.org/10.1515/9783110570175>.
- (73) Behl, M.; Zotzmann, J.; Lendlein, A. One-Way and Reversible Dual-Shape Effect of Polymer Networks Based on Polypentadecalactone Segments. *Int J Artif Organs* **2011**, *34* (2), 231–237. <https://doi.org/10.5301/IJAO.2011.6424>.
- (74) Lee, K. M.; Knight, P. T.; Chung, T.; Mather, P. T. Polycaprolactone–POSS Chemical/Physical Double Networks. *Macromolecules* **2008**, *41* (13), 4730–4738. <https://doi.org/10.1021/ma800586b>.
- (75) Pandini, S.; Passera, S.; Messori, M.; Paderni, K.; Toselli, M.; Gianoncelli, A.; Bontempi, E.; Riccò, T. Two-Way Reversible Shape Memory Behaviour of Crosslinked Poly(ϵ -Caprolactone). *Polymer* **2012**, *53* (9), 1915–1924. <https://doi.org/10.1016/j.polymer.2012.02.053>.
- (76) Pandini, S.; Baldi, F.; Paderni, K.; Messori, M.; Toselli, M.; Pilati, F.; Gianoncelli, A.; Brisotto, M.; Bontempi, E.; Riccò, T. One-Way and Two-Way Shape Memory Behaviour of Semi-Crystalline Networks Based on Sol–Gel Cross-Linked Poly(ϵ -Caprolactone). *Polymer* **2013**, *54* (16), 4253–4265. <https://doi.org/10.1016/j.polymer.2013.06.016>.
- (77) Meng, Y.; Jiang, J.; Anthamatten, M. Shape Actuation via Internal Stress-Induced Crystallization of Dual-Cure Networks. *ACS Macro Lett.* **2015**, *4* (1), 115–118. <https://doi.org/10.1021/mz500773v>.
- (78) Zhang, C.-S.; Ni, Q.-Q. Bending Behavior of Shape Memory Polymer Based Laminates. *Composite Structures* **2007**, *78* (2), 153–161. <https://doi.org/10.1016/j.compstruct.2005.08.029>.
- (79) Chen, S.; Hu, J.; Zhuo, H.; Zhu, Y. Two-Way Shape Memory Effect in Polymer Laminates. *Materials Letters* **2008**, *62* (25), 4088–4090. <https://doi.org/10.1016/j.matlet.2008.05.073>.
- (80) Wu, Y.; Hu, J.; Han, J.; Zhu, Y.; Huang, H.; Li, J.; Tang, B. Two-Way Shape Memory Polymer with “Switch–Spring” Composition by Interpenetrating Polymer Network. *Journal of Materials Chemistry A* **2014**, *2* (44), 18816–18822. <https://doi.org/10.1039/C4TA03640A>.
- (81) Zhou, J.; Turner, S. A.; Brosnan, S. M.; Li, Q.; Carrillo, J.-M. Y.; Nykypanchuk, D.; Gang, O.; Ashby, V. S.; Dobrynin, A. V.; Sheiko, S. S. Shapeshifting: Reversible Shape Memory in Semicrystalline Elastomers. *Macromolecules* **2014**, *47* (5), 1768–1776. <https://doi.org/10.1021/ma4023185>.
- (82) Wang, K.; Jia, Y.-G.; Zhu, X. X. Two-Way Reversible Shape Memory Polymers Made of Cross-Linked Cocrystallizable Random Copolymers with Tunable Actuation Temperatures. *Macromolecules* **2017**, *50* (21), 8570–8579. <https://doi.org/10.1021/acs.macromol.7b01815>.
- (83) Chen, S.; Hu, J.; Zhuo, H. Properties and Mechanism of Two-Way Shape Memory Polyurethane Composites. *Composites Science and Technology* **2010**, *70* (10), 1437–1443. <https://doi.org/10.1016/j.compscitech.2010.01.017>.

- (84) Bothe, M.; Pretsch, T. Two-Way Shape Changes of a Shape-Memory Poly(Ester Urethane). *Macromolecular Chemistry and Physics* **2012**, *213* (22), 2378–2385. <https://doi.org/10.1002/macp.201200096>.
- (85) Wang, C.; Zhang, Y.; Li, J.; Yang, Z.; Wang, Q.; Wang, T.; Li, S.; Chen, S.; Zhang, X. Shape Memory Properties of Interpenetrating Polymer Networks (IPNs) Based on Hyperbranched Polyurethane (HBPU). *European Polymer Journal* **2020**, *123*, 109393. <https://doi.org/10.1016/j.eurpolymj.2019.109393>.
- (86) Fan, L. F.; Rong, M. Z.; Zhang, M. Q.; Chen, X. D. A Facile Approach Toward Scalable Fabrication of Reversible Shape-Memory Polymers with Bonded Elastomer Microphases as Internal Stress Provider. *Macromolecular Rapid Communications* **2017**, *38* (16), 1700124. <https://doi.org/10.1002/marc.201700124>.
- (87) Fan, L. F.; Rong, M. Z.; Zhang, M. Q.; Chen, X. D. A Very Simple Strategy for Preparing External Stress-Free Two-Way Shape Memory Polymers by Making Use of Hydrogen Bonds. *Macromolecular Rapid Communications* **2018**, *39* (12), 1700714. <https://doi.org/10.1002/marc.201700714>.
- (88) Schönfeld, D.; Chalissery, D.; Wenz, F.; Specht, M.; Eberl, C.; Pretsch, T. Actuating Shape Memory Polymer for Thermoresponsive Soft Robotic Gripper and Programmable Materials. *Molecules* **2021**, *26* (3), 522. <https://doi.org/10.3390/molecules26030522>.
- (89) Behl, M.; Kratz, K.; Zotzmann, J.; Nöchel, U.; Lendlein, A. Reversible Bidirectional Shape-Memory Polymers. *Advanced Materials* **2013**, *25* (32), 4466–4469. <https://doi.org/10.1002/adma.201300880>.
- (90) Kim, B. K.; Lee, S. Y.; Xu, M. Polyurethanes Having Shape Memory Effects. *Polymer* **1996**, *37* (26), 5781–5793. [https://doi.org/10.1016/S0032-3861\(96\)00442-9](https://doi.org/10.1016/S0032-3861(96)00442-9).
- (91) Ansari, M.; Golzar, M.; Baghani, M.; Soleimani, M. Shape Memory Characterization of Poly(ϵ -Caprolactone) (PCL)/Polyurethane (PU) in Combined Torsion-Tension Loading with Potential Applications in Cardiovascular Stent. *Polymer Testing* **2018**, *68*, 424–432. <https://doi.org/10.1016/j.polymertesting.2018.04.032>.
- (92) Wei, Z. G.; Sandstrom, R.; Miyazaki, S. Shape Memory Materials and Hybrid Composites for Smart Systems: Part II Shape-Memory Hybrid Composites. *Journal of Materials Science* **1998**, *33* (15), 3763–3783. <https://doi.org/10.1023/A:1004674630156>.
- (93) Lorenzo, V.; Díaz-Lantada, A.; Lafont, P.; Lorenzo-Yustos, H.; Fonseca, C.; Acosta, J. Physical Ageing of a PU-Based Shape Memory Polymer: Influence on Their Applicability to the Development of Medical Devices. *Materials & Design* **2009**, *30* (7), 2431–2434. <https://doi.org/10.1016/j.matdes.2008.10.023>.
- (94) Walter, M.; Friess, F.; Krus, M.; Zolanvari, S. M. H.; Grün, G.; Kröber, H.; Pretsch, T. Shape Memory Polymer Foam with Programmable Apertures. *Polymers* **2020**, *12* (9), 1914. <https://doi.org/10.3390/polym12091914>.
- (95) Baer, G.; Wilson, T. S.; Matthews, D. L.; Maitland, D. J. Shape-Memory Behavior of Thermally Stimulated Polyurethane for Medical Applications. *Journal of Applied Polymer Science* **2007**, *103* (6), 3882–3892. <https://doi.org/10.1002/app.25567>.
- (96) Biswas, A.; Aswal, V. K.; Sastry, P. U.; Rana, D.; Maiti, P. Reversible Bidirectional Shape Memory Effect in Polyurethanes through Molecular Flipping.

- Macromolecules* **2016**, *49* (13), 4889–4897. <https://doi.org/10.1021/acs.macromol.6b00536>.
- (97) Srinivasan, K. S. V.; Padmavathy, T. Liquid Crystalline Properties of Unsegmented and Segmented Polyurethanes Synthesised from High Aspect Ratio Mesogenic Diols. *Macromolecular Symposia* **2003**, *199* (1), 277–292. <https://doi.org/10.1002/masy.200350924>.
- (98) Padmavathy, T.; Srinivasan, K. S. V. Liquid Crystalline Polyurethanes—A Review. *Journal of Macromolecular Science, Part C: Polymer Reviews* **2003**, *43* (1), 45–85. <https://doi.org/10.1081/MC-120018021>.
- (99) Li, F.; Hou, J.; Zhu, W.; Zhang, X.; Xu, M.; Luo, X.; Ma, D.; Kim, B. K. Crystallinity and Morphology of Segmented Polyurethanes with Different Soft-Segment Length. *Journal of Applied Polymer Science* **1996**, *62* (4), 631–638. [https://doi.org/10.1002/\(SICI\)1097-4628\(19961024\)62:4<631::AID-APP6>3.0.CO;2-U](https://doi.org/10.1002/(SICI)1097-4628(19961024)62:4<631::AID-APP6>3.0.CO;2-U).
- (100) Woodruff, M. A.; Hutmacher, D. W. The Return of a Forgotten Polymer—Polycaprolactone in the 21st Century. *Progress in Polymer Science* **2010**, *35* (10), 1217–1256. <https://doi.org/10.1016/j.progpolymsci.2010.04.002>.
- (101) Labet, M.; Thielemans, W. Synthesis of Polycaprolactone: A Review. *Chemical Society Reviews* **2009**, *38* (12), 3484–3504. <https://doi.org/10.1039/B820162P>.
- (102) Defize, T.; Riva, R.; Raquez, J.-M.; Dubois, P.; Jérôme, C.; Alexandre, M. Thermoreversibly Crosslinked Poly(ϵ -Caprolactone) as Recyclable Shape-Memory Polymer Network. *Macromolecular Rapid Communications* **2011**, *32* (16), 1264–1269. <https://doi.org/10.1002/marc.201100250>.
- (103) Scalet, G. Two-Way and Multiple-Way Shape Memory Polymers for Soft Robotics: An Overview. *Actuators* **2020**, *9* (1), 10. <https://doi.org/10.3390/act9010010>.
- (104) Malikmammadov, E.; Tanir, T. E.; Kiziltay, A.; Hasirci, V.; Hasirci, N. PCL and PCL-Based Materials in Biomedical Applications. *Journal of Biomaterials Science, Polymer Edition* **2018**, *29* (7–9), 863–893. <https://doi.org/10.1080/09205063.2017.1394711>.
- (105) Jing, X.; Mi, H.-Y.; Huang, H.-X.; Turng, L.-S. Shape Memory Thermoplastic Polyurethane (TPU)/Poly(ϵ -Caprolactone) (PCL) Blends as Self-Knotting Sutures. *Journal of the Mechanical Behavior of Biomedical Materials* **2016**, *64*, 94–103. <https://doi.org/10.1016/j.jmbbm.2016.07.023>.
- (106) Kuang, X.; Chen, K.; Dunn, C. K.; Wu, J.; Li, V. C. F.; Qi, H. J. 3D Printing of Highly Stretchable, Shape-Memory, and Self-Healing Elastomer toward Novel 4D Printing. *ACS Appl. Mater. Interfaces* **2018**, *10* (8), 7381–7388. <https://doi.org/10.1021/acsami.7b18265>.
- (107) Pisani, S.; Calcaterra, V.; Croce, S.; Dorati, R.; Bruni, G.; Genta, I.; Avanzini, A.; Benazzo, M.; Pelizzo, G.; Conti, B. Shape Memory Engineered Scaffold (SMES) for Potential Repair of Neural Tube Defects. *Reactive and Functional Polymers* **2022**, *173*, 105223. <https://doi.org/10.1016/j.reactfunctpolym.2022.105223>.
- (108) Uribe-Gomez, J.; Posada-Murcia, A.; Shukla, A.; Alkhamis, H.; Salehi, S.; Ionov, L. Soft Elastic Fibrous Scaffolds for Muscle Tissue Engineering by Touch Spinning. *ACS Appl. Bio Mater.* **2021**, *4* (7), 5585–5597. <https://doi.org/10.1021/acsabm.1c00403>.

- (109) Tamagawa, H. Thermo-Responsive Two-Way Shape Changeable Polymeric Laminate. *Materials Letters* **2010**, *64* (6), 749–751. <https://doi.org/10.1016/j.matlet.2009.12.053>.
- (110) Bai, Y.; Zhang, X.; Wang, Q.; Wang, T. A Tough Shape Memory Polymer with Triple-Shape Memory and Two-Way Shape Memory Properties. *Journal of Materials Chemistry A* **2014**, *2* (13), 4771–4778. <https://doi.org/10.1039/C3TA15117D>.
- (111) Posada-Murcia, A.; Uribe-Gomez, J. M.; Sommer, J.-U.; Ionov, L. Two-Way Shape Memory Polymers: Evolution of Stress vs Evolution of Elongation. *Macromolecules* **2021**, *54* (12), 5838–5847. <https://doi.org/10.1021/acs.macromol.1c00568>.
- (112) Ferry, J. D. *Viscoelastic Properties of Polymers*; John Wiley & Sons, 1980.
- (113) Posada-Murcia, A.; Uribe-Gomez, J. M.; Förster, S.; Sommer, J.-U.; Dulle, M.; Ionov, L. Mechanism of Behavior of Two-Way Shape Memory Polymer under Constant Strain Conditions. *Macromolecules* **2022**, *55* (5), 1680–1689. <https://doi.org/10.1021/acs.macromol.1c02564>.

5. Publication List on BTU

- **Posada-Murcia, A., Uribe-Gomez, J.M., Förster, S., Sommer, J.U., Dulle, M. and Ionov, L., 2022. Mechanism of Behavior of Two-Way Shape Memory Polymer under Constant Strain Conditions. *Macromolecules*, 55(5), pp.1680-1689.**
- *Uribe-Gomez, J., Schönfeld, D., Posada-Murcia, A., Roland, M.M., Caspari, A., Synytska, A., Salehi, S., Pretsch, T. and Ionov, L., 2022. Fibrous Scaffolds for Muscle Tissue Engineering Based on Touch-Spun Poly (Ester-Urethane) Elastomer. *Macromolecular Bioscience*, p.2100427.*
- **Posada-Murcia, A., Uribe-Gomez, J.M., Sommer, J.U. and Ionov, L., 2021. Two-Way Shape Memory Polymers: Evolution of Stress vs Evolution of Elongation. *Macromolecules*, 54(12), pp.5838-5847.**
- *Uribe-Gomez, J., Posada-Murcia, A., Shukla, A., Alkhamis, H., Salehi, S. and Ionov, L., 2021. Soft Elastic Fibrous Scaffolds for Muscle Tissue Engineering by Touch Spinning. *ACS Applied Bio Materials*, 4(7), pp.5585-5597.*
- *Uribe-Gomez, J., Posada-Murcia, A., Shukla, A., Ergin, M., Constante, G., Apsite, I., Martin, D., Schwarzer, M., Caspari, A., Synytska, A. and Salehi, S., 2021. Shape-morphing fibrous hydrogel/elastomer bilayers fabricated by a combination of 3D printing and melt electrowriting for muscle tissue regeneration. *ACS Applied Bio Materials*, 4(2), pp.1720-1730.*
- *Apsite, I., Uribe, J.M., Posada, A.F., Rosenfeldt, S., Salehi, S. and Ionov, L., 2019. 4D biofabrication of skeletal muscle microtissues. *Biofabrication*, 12(1), p.015016.*
- ***In revision before submission: Posada-Murcia, A., Schönfeld, D., Zhang, Y., Uribe-Gomez, J.M., Pretsch, T., and Ionov, L. Bidirectional shape memory polymers: effect of molecular architecture over the thermomechanical behavior at constant stress and constant strain conditions. *Macromolecules*.***

6. Individual Contribution to Publications/Manuscript as First Author on BTU

- **Publication 1. Title:** Two-Way Shape Memory Polymers: Evolution of Stress vs Evolution of Elongation. **Authors:** Andrés Posada-Murcia, Juan Manuel Uribe Gomez, Jens-Uwe Sommer, and Leonid Ionov. **Journal:** Macromolecules. **Publication Date:** June 2, 2021. **DOI:** 10.1021/acs.macromol.1c00568.

Authors Contribution. Andrés Posada-Murcia: Investigation concept, synthesis/preparation of samples, thermomechanical characterization and preparation of manuscript. **Juan Manuel Uribe-Gomez:** Support on thermomechanical characterization, scientific/theoretical discussion and preparation of manuscript. **Jens-Uwe Sommer:** Investigation concept, scientific/theoretical discussion, and preparation of manuscript. **Leonid Ionov:** Investigation concept, project supervision, scientific/theoretical discussion, and preparation of manuscript.

- **Publication 2. Title:** Mechanism of Behavior of Two-Way Shape Memory Polymer under Constant Strain Conditions. **Authors:** Andrés Posada-Murcia, Juan Manuel Uribe Gomez, Stephan Förster, Jens-Uwe Sommer, Martin Dulle and Leonid Ionov. **Journal:** Macromolecules. **Publication Date:** February 14, 2022. **DOI:** 10.1021/acs.macromol.1c02564.

Authors Contribution. Andrés Posada-Murcia: Investigation concept, synthesis/preparation of samples, thermomechanical characterization, and preparation of manuscript. **Juan Manuel Uribe-Gomez:** Support on thermomechanical characterization, scientific/theoretical discussion and preparation of manuscript. **Stephan Förster:** Anisotropic spinodal decomposition mechanism proposal, SAXS/WAXS results interpretation, preparation of manuscript. **Jens-Uwe Sommer:** Investigation concept, scientific/theoretical discussion, and preparation of

manuscript. **Martin Dulle:** SAXS/WAXS experiments, XRD results treatment and interpretation, Scientific/theoretical discussion, and preparation of manuscript. **Leonid Ionov:** Investigation concept, project supervision, scientific/theoretical discussion, and preparation of manuscript.

- **Manuscript 3. Title:** *Bidirectional shape memory polymers: effect of molecular architecture over the thermomechanical behavior at constant stress and constant strain conditions* **Authors:** Andrés Posada-Murcia, Dennis Schönfeld, Yaoming Zhang, Juan Manuel Uribe-Gomez, Thorsten Pretsch and Leonid Ionov. **Journal:** N/A. **Submission Date:** Yet to be submitted.

Authors Contribution. **Andrés Posada-Murcia:** Investigation concept, synthesis/preparation of linear PCL samples, thermomechanical characterization of all samples, and preparation of manuscript. **Dennis Schönfeld:** TPU-PDA 25 synthesis, physicochemical/thermal characterization, scientific/theoretical discussion and preparation of manuscript. **Yaoming Zhang:** Star PCL synthesis, physicochemical characterization, and preparation of manuscript. **Juan Manuel Uribe-Gomez:** Support on thermomechanical characterization, scientific/theoretical discussion and preparation of manuscript. **Thorsten Pretsch:** Investigation concept, scientific/theoretical discussion preparation of manuscript. **Leonid Ionov:** Investigation concept, project supervision, scientific/theoretical discussion, and preparation of manuscript.

7. Publications/Manuscripts

Publication 1

Two-Way Shape Memory Polymers: Evolution of Stress vs Evolution of Elongation.

Andrés Posada-Murcia, Juan Manuel Uribe Gomez, Jens-Uwe Sommer, and Leonid Ionov

Macromolecules

Publication Date: June 2, 2021.

DOI: 10.1021/acs.macromol.1c00568

Two-Way Shape Memory Polymers: Evolution of Stress vs Evolution of Elongation

Andrés Posada Murcia, Juan Manuel Uribe Gomez, Jens-Uwe Sommer, and Leonid Ionov*



Cite This: *Macromolecules* 2021, 54, 5838–5847



Read Online

ACCESS |



Metrics & More

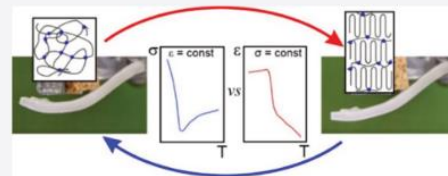


Article Recommendations



Supporting Information

ABSTRACT: Stimuli-responsive polymers are a subject of numerous studies in recent decades due to its variety of possible applications ranging from nanomedicine, drug delivery systems, biosensing, to smart textile development and aerospace engineering. The current demand of reliable and easy-programmable polymeric-actuating components underlines the necessity to understand the mechanism that governs the actuation of materials. This work sheds new light on the understanding of the two-way shape memory effect (2W-SME) of cross-linked semicrystalline polymers. We investigated and compared melting/crystallization of cross-linked polycaprolactone under constant stress and constraint strain conditions. We observed three regions of behavior upon cooling: rubbery, semicrystalline, and an intermediate one associated with entropic softening of the network prior to crystallization. Based on obtained observations, we proposed possible mechanisms for the processes occurring in cross-linked polymers upon their crystallization/melting and quantitatively investigated the effects of applied stress, elongation, and cross-linking density to allow programmable design of reversible actuators.



1. INTRODUCTION

Development of polymers that are able to undergo programmed shape transformations is of paramount importance for soft robotics, tissue engineering, smart textile applications, and for microfabrication technologies such as 4D printing, biofabrication, and others.^{1–6} There are many kinds of materials with shape-changing properties.^{7–10} Each of them has advantages and disadvantages, which define the fields of their possible applications. For example, while hydrogels¹¹ have the largest amplitude of actuation, their usage is limited to wet environments. Moreover, hydrogels are also very soft and brittle. Shape memory polymers¹² and liquid crystalline elastomers are stiffer than hydrogels and are able to actuate in both dry and wet environments. On the other hand, shape memory polymers require manual deformation from a permanent to a temporary shape, while liquid crystalline elastomers¹³ require relatively high temperatures (above 100 °C) for actuation. All these factors restrict practical application of these polymers.

Two-way shape memory polymers (2W-SMP) are a particular case of shape memory polymers.^{14–23} They can be defined as cross-linked semicrystalline polymers that can be deformed manually at elevated temperature and can be frozen in a permanent shape upon cooling and that are able to undergo a reversible shape transformation in the deformed/extended state upon crystallization/melting. Thus, contrary to conventional shape memory polymers (SMP), 2W-SMP are able to undergo reversible deformation with relatively large amplitude in one programming step that generates multiple shape memory cycles. On the other hand, contrary to hydrogels, 2W-SMP do not require the presence of a solvent and are able to actuate in both wet and dry environments. All

these properties make 2W-SMP highly attractive for robotic applications. There are 2W-SMP, which require applying external stress, and 2W-SMP, which undergo reversible deformation in stress-free conditions.^{24–28} 2W-SMP that require applying external stress are stretched elastomers, which are able to crystallize/melt upon cooling/heating. A large amplitude of actuation is achieved when constant stress is applied, and actuation does not occur without a constant applied stress.^{29–33} 2W-SMP, which do not require external stress during the repetitive temperature change, can be realized using two key structural elements. Actuation domains, which are initially stretched, reversibly melt and crystallize upon cyclic heating and cooling, while skeleton forming domains ensure the orientation/stretching of the actuation domains. Both domains are covalently linked to each other.

The practical applications of both kinds of 2W-SMP are substantially limited by the difficulty in predicting their actuation due to a weak understanding of their mechanism. In particular, there are few papers proposing models to explain and predict behavior of 2W-SMP and allowing obtaining of physicochemical parameters of polymers from fitting of the strain–temperature curve. For example, Chung *et al.*³⁴ argued that both rubber elasticity and our observed crystallization-induced elongation contribute to elongation on cooling and

Received: March 12, 2021

Revised: May 11, 2021

Published: June 2, 2021



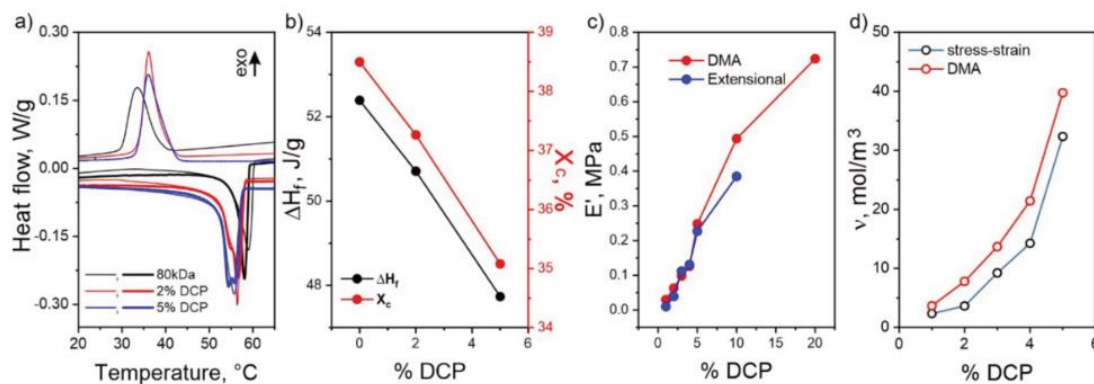


Figure 1. Properties of non-cross-linked and cross-linked polycaprolactones: (a) DSC results for cross-linked PCL 80 kDa containing 2 and 5% DCP, heating/cooling rate 1 °C min⁻¹; (b) degree of crystallinity and enthalpy of crystallization derived from DSC results for PCL 80 kDa containing 2 and 5% DCP (c) extensional storage modulus obtained from tensile and DMA experiments at 70 °C at 0.1 Hz; (d) values of cross-linking density (ν) obtained from extensional and DMA experiments.

contraction on heating. Westbrook *et al.*³⁵ proposed a model to describe the behavior of reversible shape memory polymers. The model is based on the evolution of the deformation energy from an entropy-dominated state to an enthalpy-dominated state, which was modeled as a coexistence of two phases, one dominated by entropic energy and one dominated by enthalpic energy. The model however does not consider that formed crystallites can act as physical cross-linking points and influence the elastic modulus of the rubbery part. This contribution of crystallites must depend not on their volume fraction but on their number. Kolesov *et al.*³⁶ and Dolynchuk *et al.*³⁷ proposed another model. They considered that the free energy change of a deformed polymer network undergoing crystallization consists of the free energy of transmitting statistical segments from the amorphous region to the crystals, the fold surface free energy of a crystal (or lateral surface free energy in the case of the extended-chain crystal), and the entropy change in the remaining amorphous segments.

In many cases, understanding of processes occurring during actuation under constant stress is hampered by the presence of multiple components, which change their properties during actuation and obstruct elucidation of effects produced by each component. Therefore, in order to understand the mechanism, one needs to simplify 2W-SMP to a single actuating component—cross-linked semicrystalline polymer. For simplicity, it can be polycaprolactone since it has been often used as 2W-SMP.^{38,39} While structural and length evolution of cross-linked PCL as 2W-SMP with temperature has been reported,⁴⁰ the change of length can hardly be a criterion for discussion of the process occurring in shape memory polymers as stress–strain dependence is nonlinear at large deformations, the degree of elongation of the polymer chain changes, and there is no clear explanation and no clear model of the process occurring right before crystallization when length changes. On the contrary, in a constant strain experiment, the degree of elongation of polymer chains remains constant, while their conformation and stiffness may change. Moreover, 2W-SMP, especially those that do not require applying of constant stress, change their shape while their perimeter length remains constant. This means that actuation of such polymers occurs in a different regime from the ones widely discussed in the literature. Thus, understanding of behavior of reversible shape memory polymers in constant strain mode is highly important but has not been addressed up to now.

In this paper, we focus on force measurements and for the first time report a detailed investigation and comparison of measurements of reversible shape memory polymers in constant strain and constant stress modes. These measurements allow deeper understanding of the process occurring in shape memory polymers that allows their programmable design.

2. EXPERIMENTAL SECTION

2.1. Materials and Preparation of Samples. Commercially available polycaprolactone homopolymer (PCL) (average $M_n = 80$ kDa, Sigma-Aldrich) was used. 2,5-Bis(*tert*-butylperoxy)-2,5-dimethylhexane (TBP) (Luperox 101, Sigma-Aldrich) and dicumyl peroxide (DCP) (98%, Sigma-Aldrich) were used as thermal cross-linking agents. PCL pellets were dissolved in chloroform (99%, Sigma-Aldrich) before being mixed with different amounts of DCP and TBP (Table S1). These solutions were poured and dried overnight in flat glass to yield homogeneous waxy solid films, from which 10 × 8 mm pieces (average thickness of 0.7 mm) were cut. Finally, the probes were thermally cross-linked in a vacuum oven for 2 h at 160 and 180 °C for samples containing DCP and TBP, respectively.

2.2. Differential Scanning Calorimetry (DSC). DSC analysis of the cross-linked PCL DCP and TBP samples was performed using a DSC3 (Mettler Toledo, USA) under a nitrogen atmosphere. 5–7 mg samples were placed on aluminum crucibles and subjected to a three-step program: first heated from 0 to 200 °C, then cooled from 200 to 0 °C, and finally heated again from 0 to 200 °C at a heating–cooling rate of 10 °C min⁻¹ and additionally 1 °C min⁻¹ for PCL 80 kDa containing 2 and 5% DCP. The crystallinity (X_c) of each sample was also determined (Figure S1).

2.3. Dynamic Mechanical Analysis. The rheological behavior of PCL DCP and TBP probes was studied using a Dynamic Mechanical Analyzer MCR 702 MultiDrive (Anton Paar, Austria) equipped with Solid Rectangular Fixtures (SRF5) and a temperature-controlled chamber (CTD 600 TDR). The cross-linking density (ν) of the materials was assessed by the measurement of the extensional storage modulus (E') (Figure S2) and tensile elastic modulus (E) from extensional stress–strain curves (Figure S3). The effective cross-linking density (ν), which can be defined in the form of the molecular weight of polymer chains between cross-linking/entanglement points (M_c) by considering the rubber elasticity theory approximation in the molten state, was estimated as follows: $\frac{E'}{3RT} = \frac{\rho}{M_c} = \nu$, where ρ is the density of rubber, R is the gas constant, and T is the temperature.⁴¹

2.4. Thermomechanical Cycle under Constant Strain and Constant Stress. Evolution of force during thermal cycling at constant elongation of cross-linked and non-cross-linked polymers was studied as follows: the PCL films were fixed, melted, and

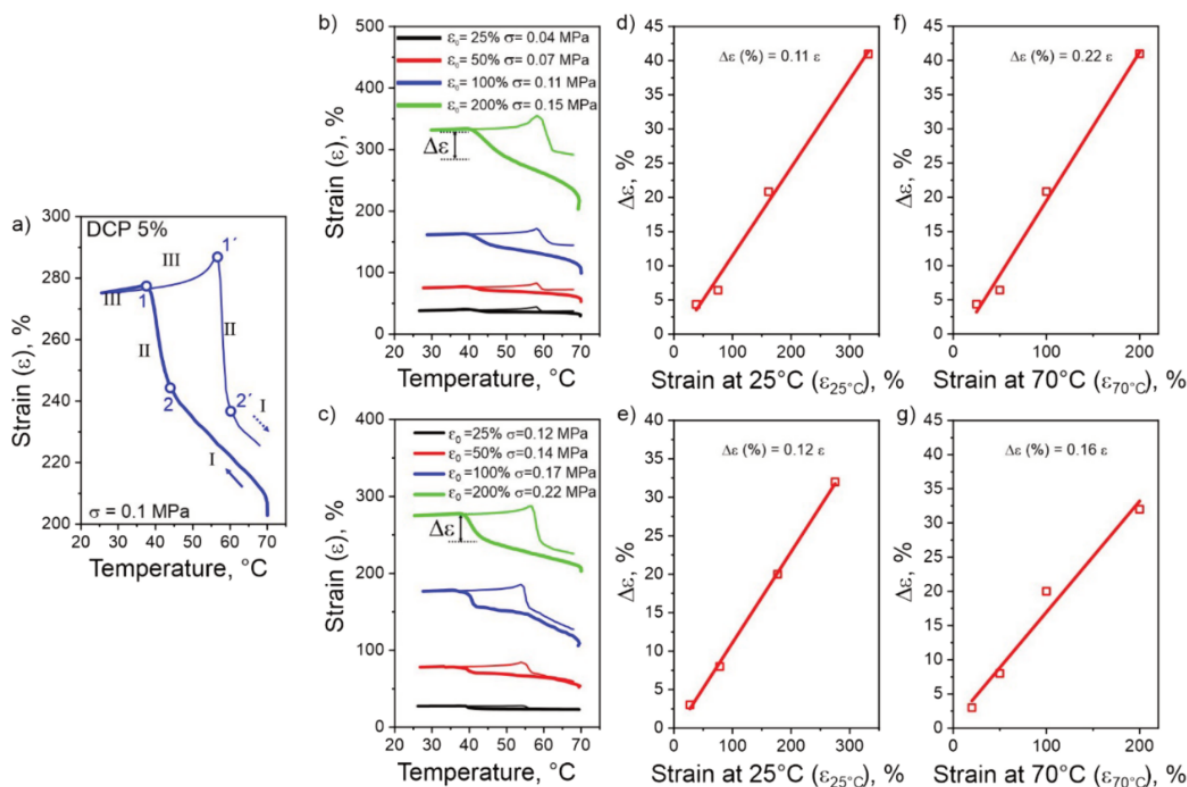


Figure 2. Thermomechanical cycling of cross-linked PCL DCP 5% at constant stress denoting the two-way shape memory effect (2W-SME). Measurements in constant stress mode of stretched cross-linked crystallizing PCL ($\nu = 8$ (upper panel) and 40 mol m^{-3} (lower panel): (a,b) effect of stress on change of length; dependence of relative elongation of samples on strain at 25 (c,d) and 70 °C (e,f).

extended at 70 °C to different strains ϵ (25, 50, 100, and 200%). The extended samples were cooled to ca. 25 °C. Finally, the crystallized probes were heated again to 70 °C to melt, and cooling and heating ramps of 1 °C min^{-1} were used.

Elongation at constant stress of cross-linked polymers was measured using the same thermal-mechanical cycle as mentioned above. The values of constant stress to extend the samples ($\nu = 8$ and 40 mol m^{-3} obtained from DMA) by ca. 25, 50, 100, and 200% were taken from the results acquired from constant strain experiments. Measurements of non-cross-linked polymer under constant load were not performed as it flows irreversibly in the melt state when load is applied.

3. RESULTS AND DISCUSSION

3.1. Effect of Cross-Linking Density on Thermal and Mechanical Properties. In this work, we have used non-cross-linked PCL with a molecular weight of 80 kDa and the same polymer with different degrees of chemical cross-linking. The cross-linked PCL samples were prepared by high-temperature annealing of the polymer, which was blended with peroxides (DCP and TBP). The degree of crystallinity decreases with the increase of the amounts of cross-linkers as it was revealed by DSC (Figure S1, Figure 1a,b, Table S1). The mechanical properties above the melting point were characterized using tensile testing and dynamic mechanical analysis. We observed that non-cross-linked PCL demonstrates a rapid decrease of both storage and loss moduli with the decrease of the frequency, which is due to the relaxation process in polymers (Figure S2). The values of the storage modulus of cross-linked polymers with a low amount of cross-linker also decrease with the decrease of the frequency (Figure S2), and this tendency becomes less pronounced with the increasing

amount of cross-linker. The decrease is however not that pronounced as in the case of non-cross-linked polymer. The reason for the decrease of the modulus with the decrease of frequency at low cross-linking density is relaxation processes due to chain dynamics and dynamics of larger polymer clusters on longer length and time scales. One structural element, which contributes to mechanical properties, is chain entanglements, and their contribution for the equilibrium modulus is high for weakly cross-linked networks.^{42–44}

Since actuation of polymers is relatively slow and takes several seconds/minutes, the values of the storage modulus at low frequency (0.1 Hz) are considered. It was found that the elastic modulus linearly increases with the amount of added cross-linker (Figure 1c, Figure S4a) as expected from the theory. The value of the elastic modulus obtained from extensional experiments (Figure S3) correlates very well with the value of the storage modulus obtained from DMA at lowest frequency (0.1 Hz) at which both fast and slow relaxation processes do not contribute to the modulus. The obtained values of the storage modulus (E') allowed the estimation of effective cross-linking density (ν) (Figure 1d, Figure S4b), which increases with the amount of cross-linking agent.^{45,46} The cross-linking density (ν) values determined from DMA experiments that correlate well with the thermomechanical cyclic analysis were used further.

3.2. Constant Stress Cycling. We performed measurements of strain under constant stress (Figure 2), which are usually reported in the literature to evaluate and demonstrate the two-way shape memory effect triggered by temperature.^{47,48} A typical 2W-SME cycle is depicted in Figure 2a and described as follows: Initially, the cured PCL probe is

molten and constantly loaded at 70 °C. Dropping the temperature down to ca. 45 °C slowly increases the specimen's length (the decrease of the elastic modulus of rubbers upon cooling in regime I, thicker line). Cooling to 37 °C results in a sharp increase of length (regime II, thicker line). Further cooling results in minor shrinking of the sample due to crystallization (regime III, thicker line). Heating from room temperature up to ca. 55 °C results in a slight increase of the sample's length (regime III, thinner line), which can be attributed to thermal expansion of solid polymer. A sustained increment of temperature up to ca. 60 °C results in a sharp decrease of length (regime II, thinner line). Finally, further heating results in a linear decrease of the polymer's length, which is an intrinsic feature of elastomers (regime I, thinner line).

The rapid increments/drops of strain between 45 and 37 °C (cooling) and 55 and 60 °C (heating), here described as regime II, are crystallization-induced expansion (CIE) and melting-induced contraction (MIC) of polymer chains, respectively. These phenomena allow reversible thermally activated actuation of cross-linked PCL under constant load around melting/crystallization temperatures (Figure 1).

We carried out a thorough investigation of reversible shape memory behavior of cross-linked PCL under constant stress (Figure 2b,c). Loading of molten PCL samples ($\nu = 8$ and 40 mol m⁻³) at 70 °C allowed their stretching by ca. 25, 50, 100, and 200% of their original length. The observed behavior in constant stress mode is similar to that observed in previous reports:^{33–37,40} the larger the stress, the stronger the polymer is being stretched and the more pronounced the cooling-induced extension and heating-induced contraction are around the crystallization/melting point.

The change of the sample's length around 37 °C ($\Delta\epsilon$, CIE effect) is linearly proportional to applied stress (Figure S5) and to the strain of the sample at 25 (Figure 2d,e) and 70 °C (Figure 2f,g). The $\Delta\epsilon$ normalized to the length of samples after cooling-induced elongation is nearly independent of cross-linking density ($\Delta\epsilon \approx 0.11 \cdot \epsilon$) illustrated in Figure 2d,e. On the other hand, the change of length around 37 °C normalized to the length of samples at 70 °C depends on cross-linking density—a larger change of the length is observed at lower cross-linking density (Figure 2f,g). This can be related with the lower elastic modulus and thus with a larger initial extension in the soft rubbery state (hindered reversibility for less cross-linked samples). The obtained results are consistent with previous observations.

3.3. Constant Strain Cycling. Next, we studied the behavior of polymers under constant strain conditions. The development of extensional stress for stretched non-cross-linked and cross-linked PCL along a constant strain thermal cycle is presented in Figure 3. We used non-cross-linked PCL with a molecular weight of 80 kDa as the reference material because it was used for making of cross-linked samples. According to existing models, the mechanical properties of elastomers depend on the molecular weight of chain strands between cross-linking points. Of course, freely dangling chain ends do not contribute to elasticity. Performing the experiment with PCL of lower molecular weight (40 kDa) was not possible as the polymer has almost no elastic behavior in the molten state in the temperature range (50–100 °C) and simply flows. Non-cross-linked PCL demonstrates zero stress in the molten state (Figure 3a). Cooling of molten non-cross-linked PCL results in a linear increase of stress starting from $T = 37$ °C due

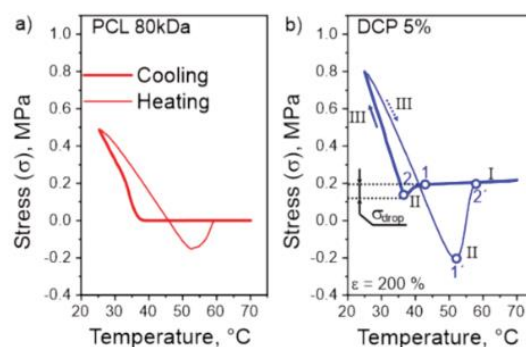


Figure 3. Thermomechanical cycling of non-cross-linked (a) and cross-linked PCL (b) at constant strain.

to the onset of crystallization as DSC assays revealed (Figure 1a). Stress increases below 37 °C due to shrinking of polymer caused by its crystallization. Heating of crystallized and shrunk polymer results first in the decrease of stress that is due to its thermal expansion. The stress becomes even negative at higher temperature, meaning that the still solid polymer sample expands and tends to become larger than the sample in the moment of crystallization upon cooling. This is most probably due to the out-of-equilibrium state—melting of polymer is slow, and polymer is overheated. A further increase of temperature results in a drop of stress to zero, meaning that the polymer is completely melted and flows under external deformation.

The behavior of stretched cross-linked PCL is different from that of non-cross-linked polymers. We observed three distinct regimes in the stress vs temperature curve (Figure 3b). Stretched polymers demonstrate nonzero stress above the melting point at constant elongation. The stress decreases linearly with the temperature decrease (regime I, thicker line). Both these observations indicate that the polymer behaves as an elastomer. Starting from ca. 50 °C, which is above the crystallization temperature of nonstretched polycaprolactone, a decrease of temperature (point 1, Figure 3b) results in a sharp drop of stress (regime II, thicker line). Starting from 37 °C (point 2), at which nonstretched polymer crystallizes, stress increases with a decrease of temperature (regime III, thicker line). This behavior is similar to the behavior of non-cross-linked polymer at low temperature and can be attributed to shrinking of polymer due to crystallization. The increase of temperature starting from room temperature up to 50 °C (point 1') results in a decrease of stress, and it goes to a negative value (regime III, thinner line). This observation can be explained by thermal expansion analogous to non-cross-linked polymer. The increase of temperature to 60 °C (point 2') results in a sharp increase of stress returning to a prior value before the stress drop during the cooling step (regime II, thinner line in Figure 3b). A further increase of temperature results in a slow increase of stress with temperature (regime I, thinner line), which is typical for elastomers.⁴⁹

Different processes can take effect upon cooling including stress “relaxation” upon crystallization, thermal shrinkage in both the rubbery regime and through crystallization, and thermal shrinkage of the DMA grips. Shrinking of DMA grips can be neglected due to small thermal expansion coefficients of metals. A stress decrease upon cooling of strongly stretched elastomers also dominates over their shrinking if polymer is stretched beyond the inversion point, which is at about 10%

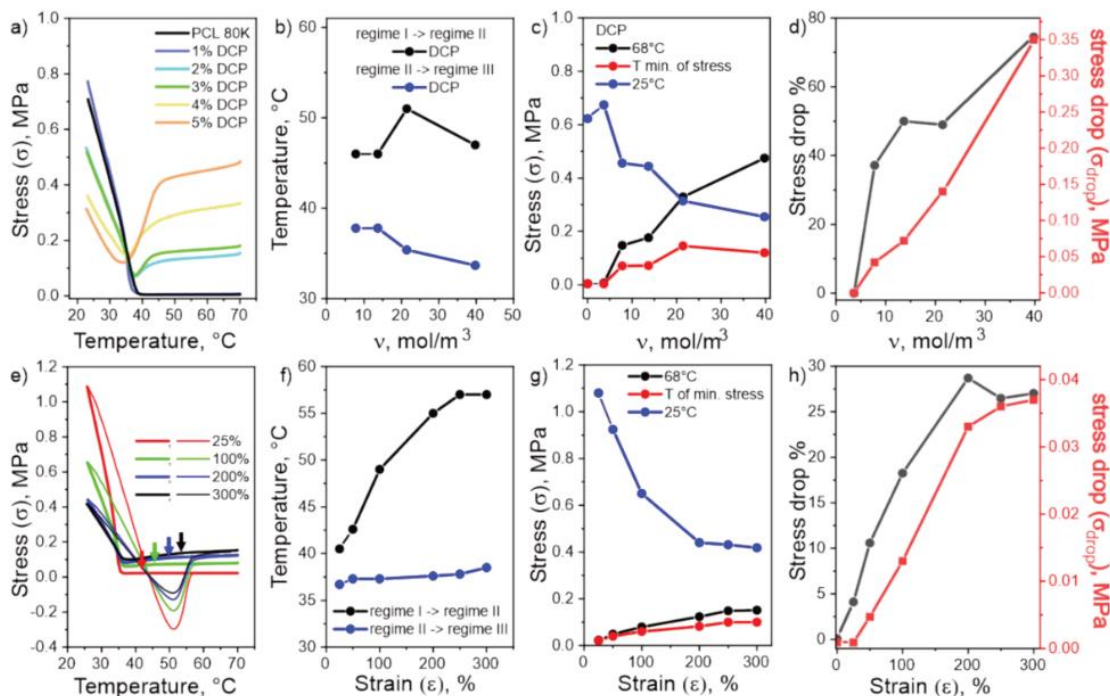


Figure 4. Effect of cross-linking density (obtained from DMA analysis) (top panel) and strain (bottom panel) on stress–temperature behavior of stretched cross-linked PCL crystallizing: (a) effect of cross-linking density on evolution of stress with temperature, PCL was stretched by 200%; (b) dependence of transition temperatures from regimes I to II and from II to III on the cross-linking density; (c) dependence of stress at different temperatures on the cross-linking density; (d) dependence of the stress drop and relative stress drop close to crystallization in regime II on cross-linking density; (e) effect of strain on evolution of stress with temperature (5% DCP); (f) dependence of temperatures of transitions from regimes I to II and from II to III on strain; (g) stress–strain curve for different temperatures derived from panel (e); (h) dependence of the stress drop and relative stress drop in regime II on strain.

elongation. Thus, the main contributors to the change of stress upon cooling are the decrease of rigidity of chains with temperature, stress “relaxation” upon crystallization, and volume shrinking due to the phase transition.

We investigated the effect of cross-linking density at constant elongation (Figure 4a and Figure S6) as well as the effect of elongation at constant cross-linking density on evolution of stress with temperature (Figure 4e and Figure S7). Cross-linking density increases the slope of the stress vs temperature curve (Figure 4a and Figure S6a) in the rubbery state (regime I in Figure 3b) that correlates with statistical theory of rubber elasticity.^{50–52} Temperatures at which the sharp stress drop (σ_{drop}) and minimum of stress are observed (points 1 and 2, respectively, Figure 3b) are nearly independent of cross-linking density at the same degree of stretching (Figure 4b). Stress in the molten state (regime I) increases linearly with cross-linking density (black line, Figure 4c). The minimum of stress (point 2) also increases amidst cross-linking density (red line, Figure 4c). As a consequence, σ_{drop} significantly increases linearly with the cross-linking density (Figure 4d). In contrast, the stress in the stretched polymer at 25 °C (regime III) decreases with the increase of cross-linking density (blue line, Figure 4c).

Strain has also a profound effect on the evolution of stress upon heating and cooling (Figure 4e). First, the temperature at which stress starts to drop upon cooling (transition regime I regime II) increases with the increase of strain from 40 °C at 25% to ca. 55 °C at 300% (Figure 4f). The temperature at which the minimum of stress is observed (transition regime II regime III) remains, meanwhile, constant around 37 °C, which is close to temperature when stress of the non-cross-linked

sample starts to increase upon cooling. The value of stress at 25 °C (crystallization, regime III) decreases with the increase of strain, while values of stress at the point of its minimum (transition regime II regime III) increase (Figure 4g). Stress at 68° (rubbery state, regime I) also increases with strain.

The slope of the stress–strain curve, which can be derived from Figure 4g, depends on temperature. The slope has a lower value at the temperature of minimum of force than at 68 °C (regime I), meaning that stretched elastomer is much softer at the temperature of minimum of stress than at 68 °C. As a result, the value of the sharp stress drop (regime II, see also Figure 3b) increases with strain (Figure 4h). The slope at 25 °C has a negative value—it appears that the crystallized elastomer gets softer with the increase of stretching before crystallization. This statement needs understanding that, although Figure 4g presents a common stress–strain curve, it was derived from crystallization experiments, which are performed in non-isothermal conditions, and the properties of polymer depend on its prehistory. Stress–strain dependence at temperature of minimum of stress and at 68 °C can really represent the mechanical properties of materials—stress increases with elongation. On the other hand, the value of stress in the crystalline state reflects shrinking behavior at different elongation—the stronger the polymer chains are stretched, the smaller the change of conformation upon crystallization is. A semicrystalline polymer stretched at room temperature does not demonstrate this behavior.

3.4. Discussion of Constant Strain Experiments. The essential observations of stress evolution with temperature at constant strain are summarized in Figure 5. Let us first note that the observed stress drop ($\Delta\sigma$) upon cooling is associated

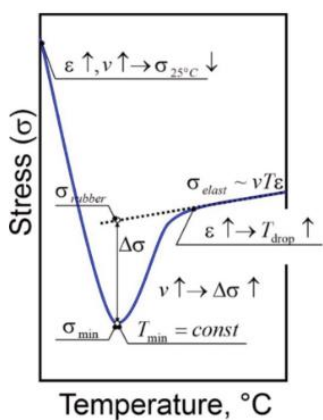


Figure 5. Summary of findings shown in Figures 2 and 4. ϵ – strain, σ – stress, $\Delta\sigma$ – stress drop upon transition from regime I to regime II, T – temperature, ν – cross-linking density.

with processes preceding the crystallization as DSC analysis suggests (Figure 1a, Figure S1). Since the formation of nuclei would correspond to additional physical cross-linking of the network, it should be excluded for the possible explanation of the sudden decrease in stress. Let us note that the stress in the molten rubber is due to the entropy reduction of the chain conformations upon extension and it is proportional to the number of elastically active chains.

A drop in the stress can be explained by a stiffening of the chains, i.e., an increase of persistence length. On the other hand, the thermally induced increase of the persistence length is only a small correction to the dominating linear decrease of the modulus upon cooling and, therefore, cannot serve as an explanation of the occurrence of regime II. Thus, growing interactions between the chains that ultimately force the polymer to crystallize must lead to the decrease of entropy of the coiled polymer chains in a collective manner. We note that the behavior in regime II bears some similarities to the response of main-chain liquid crystalline elastomers,⁵³ but with a much weaker relative extension under constant stretching in the present case. Thus, a possible molecular origin can be the partial alignment of trans-sequences between neighboring chains, but without the formation of crystalline nuclei. The onset of softening upon cooling is nearly independent of the cross-linking density (Figure 4b, Figure S6b), which indicates that the molecular origin of the effect is related to the entropy reduction, i.e., the degree of orientation of the segments rather than the elastic energy stored in the network. This is corroborated with the increase of temperature where the

softening starts with respect to the applied strain (Figure 4e,f, Figure S7). Furthermore, the increase of the stress drop in regime II with the degree of strain (Figure 4h) also points to the role of the segmental orientation for this effect.

Below, we discuss possible explanations to the effects observed in this work. Stress in stretched polymers at room temperature (25 °C) decreases with the increase of cross-linking density. This observation may be related to the decrease of the degree of crystallinity with the increase of cross-linking density (Figure 1b, Figure S1). As a result, the more the crystallization is hindered, the smaller the potential shrinking due to crystallization is, which reduces the measured stress in constant strain mode.

Stress in stretched cross-linked polymers in the semicrystalline state ($\sigma_{25^\circ\text{C}}$) decreases with increasing strain (ϵ). The observed stress at 25 °C is due to shrinking of polymer due to its crystallization. The higher is the stretching degree, the more oriented the polymer chains are and the smaller are conformation changes upon crystallization and the smaller is the resulting stress in the semicrystalline state.

The temperature at which the minimal value of stress is observed (T_{min}) is nearly constant, close to 37 °C. On the other hand, T_{min} indicates the beginning of the crystallization process. Since 37 °C was also determined by DSC as the onset of crystallization in stress-free conditions, this observation indicates that the commencement of crystallization is weakly influenced by the elastic energy stored in the sample at a given strain.

The stress drop ($\Delta\sigma = \sigma_{\text{rubber}} - \sigma_{\text{min}}$) increases with the increase of cross-linking density (ν) at constant stress (σ) and with the increase of strain (ϵ) at constant cross-linking density (ν). The number of elastically active chains increases with cross-linking density; thus, the value of stress in the rubbery regime (σ_{rubber}) before it rapidly drops upon cooling increases with cross-linking density (ν) and strain (ϵ). On the other hand, crystallization brings a major part of the chains into the ordered state (partially folded conformation), which shall be independent of cross-linking density if it does not affect crystallinity. Thus, σ_{rubber} and stress drop ($\Delta\sigma$) must increase with cross-linking density (ν) and strain (ϵ). The energy of the crystalline state depends on enthalpy of crystallization—the larger the absolute value of enthalpy, the lower is the energy of the crystalline state. On the same page, we observed that the increase of the cross-linking degree reduces the enthalpy of crystallization (Figure 1b, Figure S1) while increasing the value of minimal stress (σ_{min}), which can be attributed to hindered crystallization due to cross-linking.

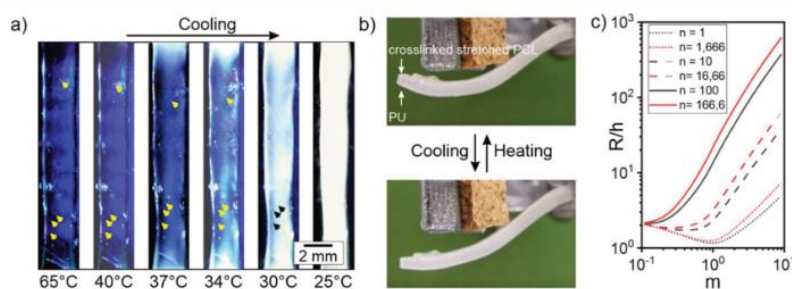


Figure 6. Stretched cross-linked PCL in crossed polarizers upon cooling (a), reversible actuation of a bilayer with cross-linked PCL-hot-melt adhesive (b), and results of a bending bilayer simulation (c) with stretched cross-linked PCL (300%) as the active layer using the Timoshenko equation (eq 1).

We tried to correlate our observation with previously proposed models for the explanation of the nature of the 2W-SMP effect. In order to do it, we investigated the visual changes of stretched cross-linked PCL upon cooling (Figure 6a). The molten cross-linked PCL, which was stretched to 200%, appeared to be transparent, which is an indication of its optical homogeneity—no optically denser crystalline phase is formed that would result in fogginess of the sample due to light scattering on structural inhomogeneity (crystallites). This state remained unchanged upon cooling from 65 to ca. 40 °C with a cooling rate of 1 °C min⁻¹. We observed whitening of polymer at temperatures below 37 °C that is apparently due to crystallization and formation of multiple spherulites.^{54–56} Careful observation of features in samples (defects) upon cooling revealed that fixed samples undergo internal nonuniform motion—the central part of sample contracts. The reason of nonuniform movement is a temperature gradient on the sample—the area close to the clamps has lower temperature than the central part of the sample (whitening from the edges). Thus, cooling results in a scenario where the central part of the sample is amorphous—rubbery state—while the tips of the probe are in the state corresponding to the minimum stress described in Figure 3. As a result, the sample extends from the edges displacing the defects toward the center. This observation is very important. In fact, Westbrook *et al.*³⁵ proposed a model to describe the behavior of reversible shape memory polymers, which assumes that the stress drop must be proportional to the degree of crystallinity and the sample shall actuate as soon as the degree of crystallinity increases. Notably, while the Westbrook *et al.* model³⁵ is able to predict the change of length, there are no *in situ* measurements of the degree of crystallinity upon elongation of SMP and its correlation with length of the sample. On the other hand, Huang *et al.*⁴⁰ reported XRD results during constant stress experiments but did not consider the quantitative evolution of the degree of crystallinity upon cooling. Our observations show that actuation of the sample finished at 37 °C while only a small portion of polymer became white, i.e., the degree of crystallinity is relatively low. The actuation amplitude must, however, be proportional to the degree of crystallinity. This observation indicates that a deeper understanding of the nature of the 2W-SMP effect is required.

3.5. Applications of the Stress Drop. Finally, we demonstrated the fabrication of reversible actuators using stretched cross-linked polycaprolactone making use of our physical understanding of the crystallization process in stretched cross-linked PCL. For this, we fabricated a bilayer of cross-linked polycaprolactone and hot-melt adhesive—ethylene vinyl acetate (EVA). The cross-linked PCL was stretched in the molten state and cooled down to room temperature in the stretched state. Then, hot-melt adhesive was applied to stretched and crystallized PCL. As the obtained sample was straight, exposure to hot water vapor causes bending of the bilayer in the direction of PCL as it contracts in the elastomeric state due to the entropy gain upon disorder of the chains (Figure 6b, up). Removal of hot water vapor results in unbending of the bilayer and a change of its radius of curvature by a factor of 1.34 (Figure 6b, down). The actuation occurs on the time scale of tens of seconds. The process is reversible and can be repeated multiple times. The observed behavior is consistent with the behavior of stretched PCL, which generates large entropic force in the molten state leading to bending of the bilayer. The force drops upon cooling PCL,

which results in unbending of the bilayer. However, the weakening of the PCL elastomer before the onset of crystallization is most notable, i.e., regime-II behavior (see Figure 5) seems to be essential for reversibility of the actuation. Without this particular regime, the reduction in the modulus of the rubbery PCL is only of the order of $(T_H - T_L)/T_H$, where T_H denotes the high temperature and T_L denotes the low temperature of the thermal cycle. Notably, the bilayer with not-stretched un-cross-linked polycaprolactone can demonstrate opposite behavior—the bilayer bends upon crystallization of PCL and straightens upon its melting due to shrinking of the crystalline volume while forming a physical network of nuclei and entanglements.⁵⁷ Thus, the cooling cycle requires expansion of the crystallizable phase acting against the volume contraction of that phase during crystallization—explained by the extraordinary weakening of stretched elastomer before the onset of crystallization. The latter lets the solid adhesive film to mechanically relax before crystallization is completed.

We applied the Timoshenko⁵⁸ equation (eq 1)

$$\frac{1}{R} = \frac{6(\epsilon_{\text{active}} - \epsilon_{\text{passive}})(1 + m)^2}{h(3(1 + m)^2 + (1 + mn)(m^2 + 1/mn))} \quad (1)$$

where $n = \frac{E_{\text{passive}}}{E_{\text{active}}}$, $m = \frac{a_{\text{passive}}}{a_{\text{active}}}$, $h = a_{\text{passive}} + a_{\text{active}}$, E are the elastic moduli, and a are the thicknesses of the layers ($\epsilon_{\text{active}} - \epsilon_{\text{passive}} = 0.33$ that corresponds to 300% elongation and 40% stress drop in regime II that were used for calculations) to estimate the change of the radius of curvature upon stress drop. Due to constraints caused by the adhesive layer, the PCL layer is close to the “constant strain” experiment conditions discussed in this work, i.e., its length is constant, but the stress produced by it changes with temperature. This means that the strain difference between layers before and after the stress drop is the same, and according to the conditions of the experiment, it is 0.33. The only parameter that changes is the ratio between the moduli of both materials—the drop of stress of the PCL layer at constant strain means a decrease of the elastic modulus. We applied experimental results and found out that according to the Timoshenko equation strong bending and no bending upon cooling were observed at small thickness of the passive layer (Figure 6c). The ratio between the radii of curvature in unfolded and folded states increases with thickness of the passive layer and approaches $\frac{R_{\text{folded}}}{R_{\text{unfolded}}} = \frac{100}{100 - \sigma_{\text{drop}}(\%)} = 1.67$, which is in good agreement with experimental observations. The difference between predicted and observed values could be due to (i) the Timoshenko equation that was developed for thin bilayer systems (thickness is much smaller than length) and (ii) nonlinear behavior of the stress–strain profile at large deformations.

4. CONCLUSIONS

We performed a thorough investigation on the thermomechanical properties of cross-linked polycaprolactone as an approach to a better understanding of the behavior and the actuation mechanism of bidirectional shape memory polymers. In particular, we evaluated the development of stress and strain in the polymer upon cooling and heating in constant strain and constant stress experiments, respectively. We proposed an explanation of mechanisms of stress and strain development

upon heating and cooling as well as the explained difference in mechanical properties of not-stretched and stretched cross-linked semicrystalline polymers.

A particular interesting result is the observation of an intermediate behavior of the elastomer between the molten rubbery state and semicrystalline state. Here, we observe a drop in stress (the increase in strain) during cooling under constant strain (constant stress) before the crystalline response can be detected. The amount of the drop in stress upon constant strain appears to be independent of the cross-linking density but increases with the initial strain. Our results indicate a reduction of entropy of the elastic strands due to the interaction between the segments as the most likely origin of this behavior. We harnessed this behavior for the preparation of a reversible shape memory polymer bilayer, which acts against the crystallization-driven contraction of the PCL-phase and reverts the cycle with respect to previously proposed preparation methods.

We believe that the obtained results and their thorough analysis will shed new light on the properties of bidirectional shape memory polymers and will allow more understanding of mechanisms of their actuation. This understanding is vitally important for development of bidirectional shape memory actuators with programmed properties for a variety of applications in robotics, soft electronics, and medicine.

■ ASSOCIATED CONTENT

SI Supporting Information

The Supporting Information is available free of charge at <https://pubs.acs.org/doi/10.1021/acs.macromol.1c00568>.

Properties of cross-linked polycaprolactone (PCL) 80 kDa with different amounts of cross-linker; DSC results, the degree of crystallinity, and enthalpy of crystallization for PCL 80 kDa cross-linked with different amounts of DCP and TBP with a temperature step of 10 °C min⁻¹; DMA results of PCL 80 kDa cross-linked with different amounts of DCP and TBP in the molten state at 70 °C; tensile test of PCL 80 kDa cross-linked with different amounts of DCP and TBP at 70 °C; mechanical properties of PCL TBP samples: (a) extensional storage modulus obtained from tensile and DMA experiments at 70 °C at 0.1 Hz; (b) values of cross-linking density (ν) obtained from extensional and DMA experiments; measurements in constant stress mode of stretched cross-linked crystallizing PCL ($\nu = 8$ (a) and 40 mol m⁻³ (b) dependence of relative elongation of samples on applied stress); effect of cross-linking density from DMA analysis on stress–temperature behavior of stretched cross-linked PCL with TBP crystallizing: (a) effect of cross-linking density on evolution of stress with temperature, PCL was stretched by 200%; (b) dependence of temperatures of transitions from regimes I to II and from II to III on the cross-linking density; (c) dependence of the stress at different temperatures on the cross-linking density; (d) dependence of the stress drop close to crystallization in regime II on cross-linking density; (e) dependence of the relative stress drop on the cross-linking density; effect of elongation at constant cross-linking density on evolution of stress with temperature of cross-linked PCL containing 2% DCP (PDF)

■ AUTHOR INFORMATION

Corresponding Author

Leonid Ionov – Faculty of Engineering Sciences and Bavarian Polymer Institute, University of Bayreuth, 95447 Bayreuth, Germany; orcid.org/0000-0002-0770-6140;
Email: leonid.ionov@uni-bayreuth.de

Authors

Andrés Posada Murcia – Faculty of Engineering Sciences and Bavarian Polymer Institute, University of Bayreuth, 95447 Bayreuth, Germany

Juan Manuel Uribe Gomez – Faculty of Engineering Sciences and Bavarian Polymer Institute, University of Bayreuth, 95447 Bayreuth, Germany

Jens-Uwe Sommer – Leibniz Institute of Polymer Research Dresden e.V., 01069 Dresden, Germany; Faculty of Physics and Cluster of Excellence Physics of Life, TU Dresden, 01069 Dresden, Germany

Complete contact information is available at:

<https://pubs.acs.org/10.1021/acs.macromol.1c00568>

Author Contributions

The manuscript was written through contributions of all authors. All authors have given approval to the final version of the manuscript.

Funding

The authors are grateful to DFG for financial support (grants IO 68/10-1 and IO 68/11-1, SO 277/18-1).

Notes

The authors declare no competing financial interest.

■ ACKNOWLEDGMENTS

Authors thank Andrei Zakharov and Kay Saalwächter for fruitful discussions.

■ ABBREVIATIONS

SMP, shape memory polymers; 2W-SME, two-way shape memory effect; PCL, polycaprolactone; TBP, 2,5-bis(*tert*-butylperoxy)-2,5-dimethylhexane; DCP, dicumyl peroxide; DSC, differential scanning calorimetry

■ REFERENCES

- (1) Cabane, E.; Zhang, X.; Langowska, K.; Palivan, C. G.; Meier, W. Stimuli-Responsive Polymers and Their Applications in Nanomedicine. *Biointerphases* **2012**, *7*, 9.
- (2) Gopalakrishnan, S. Smart Materials Technology for Aerospace Applications. In *Micro and Smart Devices and Systems*; Vinoy, K. J., Ananthasuresh, G. K., Pratap, R., Krupanidhi, S. B., Eds.; Springer: New Delhi, 2014; pp. 423–437, DOI: 10.1007/978-81-322-1913-2_25.
- (3) Hu, J.; Meng, H.; Li, G.; Ibeke, S. I. A Review of Stimuli-Responsive Polymers for Smart Textile Applications. *Smart Mater. Struct.* **2012**, *21*, No. 053001.
- (4) Oksuka, K.; Wayman, C. M. *Shape Memory Materials*; Cambridge University Press: 1999.
- (5) Leng, J.; Lu, H.; Liu, Y.; Huang, W. M.; Du, S. Shape-Memory Polymers—A Class of Novel Smart Materials. *MRS Bull.* **2009**, *34*, 848–855.
- (6) Wei, M.; Gao, Y.; Li, X.; Serpe, M. J. Stimuli-Responsive Polymers and Their Applications. *Polym. Chem.* **2017**, *8*, 127–143.
- (7) Gracias, D. H. Stimuli Responsive Self-Folding Using Thin Polymer Films. *Curr. Opin. Chem. Eng.* **2013**, *2*, 112–119.

- (8) Jeon, S.-J.; Hauser, A. W.; Hayward, R. C. Shape-Morphing Materials from Stimuli-Responsive Hydrogel Hybrids. *Acc. Chem. Res.* **2017**, *50*, 161–169.
- (9) Stoychev, G. V.; Ionov, L. Actuating Fibers: Design and Applications. *ACS Appl. Mater. Interfaces* **2016**, *8*, 24281–24294.
- (10) Wu, Z. L.; Moshe, M.; Greener, J.; Therien-Aubin, H.; Nie, Z.; Sharon, E.; Kumacheva, E. Three-Dimensional Shape Transformations of Hydrogel Sheets Induced by Small-Scale Modulation of Internal Stresses. *Nat. Commun.* **2013**, *4*, 1586.
- (11) Ionov, L. Biomimetic Hydrogel-Based Actuating Systems. *Adv. Funct. Mater.* **2013**, *23*, 4555–4570.
- (12) Löwenberg, C.; Balk, M.; Wischke, C.; Behl, M.; Lendlein, A. Shape-Memory Hydrogels: Evolution of Structural Principles To Enable Shape Switching of Hydrophilic Polymer Networks. *Acc. Chem. Res.* **2017**, *50*, 723–732.
- (13) Liu, D.; Broer, D. J. Liquid Crystal Polymer Networks: Switchable Surface Topographies. *Liq. Cryst. Rev.* **2013**, *1*, 20–28.
- (14) Wang, K.; Jia, Y.-G.; Zhao, C.; Zhu, X. X. Multiple and Two-Way Reversible Shape Memory Polymers: Design Strategies and Applications. *Prog. Mater. Sci.* **2019**, *105*, 100572.
- (15) Fan, L. F.; Rong, M. Z.; Zhang, M. Q.; Chen, X. D. Dynamic Reversible Bonds Enable External Stress-Free Two-Way Shape Memory Effect of a Polymer Network and the Interrelated Intrinsic Self-Healability of Wider Crack and Recyclability. *J. Mater. Chem. A* **2018**, *6*, 16053–16063.
- (16) Han, J.-L.; Lai, S.-M.; Chiu, Y. T. Two-Way Multi-Shape Memory Properties of Peroxide Crosslinked Ethylene Vinyl-Acetate Copolymer (EVA)/Polycaprolactone (PCL) Blends. *Polym. Adv. Technol.* **2018**, *29*, 2010–2024.
- (17) Pandini, S.; Baldi, F.; Paderni, K.; Messori, M.; Toselli, M.; Pilati, F.; Gianoncelli, A.; Brisotto, M.; Bontempi, E.; Riccò, T. One-Way and Two-Way Shape Memory Behaviour of Semi-Crystalline Networks Based on Sol–Gel Cross-Linked Poly(ϵ -Caprolactone). *Polymer* **2013**, *54*, 4253–4265.
- (18) Qi, X.; Yang, W.; Yu, L.; Wang, W.; Lu, H.; Wu, Y.; Zhu, S.; Zhu, Y.; Liu, X.; Dong, Y.; Fu, Y. Design of Ethylene-Vinyl Acetate Copolymer Fiber with Two-Way Shape Memory Effect. *Polymer* **2019**, *11*, 1599.
- (19) Qian, C.; Dong, Y.; Zhu, Y.; Fu, Y. Two-Way Shape Memory Behavior of Semi-Crystalline Elastomer under Stress-Free Condition. *Smart Mater. Struct.* **2016**, *25*, No. 085023.
- (20) Lu, L.; Cao, J.; Li, G. Giant Reversible Elongation upon Cooling and Contraction upon Heating for a Crosslinked Cis Poly(1,4-Butadiene) System at Temperatures below Zero Celsius. *Sci. Rep.* **2018**, *8*, 14233.
- (21) Raquez, J.-M.; Vanderstappen, S.; Meyer, F.; Verge, P.; Alexandre, M.; Thomassin, J.-M.; Jérôme, C.; Dubois, P. Design of Cross-Linked Semicrystalline Poly(ϵ -Caprolactone)-Based Networks with One-Way and Two-Way Shape-Memory Properties through Diels-Alder Reactions. *Chemistry* **2011**, *17*, 10135–10143.
- (22) Pandini, S.; Passera, S.; Messori, M.; Paderni, K.; Toselli, M.; Gianoncelli, A.; Bontempi, E.; Riccò, T. Two-Way Reversible Shape Memory Behaviour of Crosslinked Poly(ϵ -Caprolactone). *Polymer* **2012**, *53*, 1915–1924.
- (23) Kolesov, I.; Dolynchuk, O.; Borreck, S.; Radosch, H.-J. Morphology-Controlled Multiple One- and Two-Way Shape-Memory Behavior of Cross-Linked Polyethylene/Poly(ϵ -Caprolactone) Blends. *Polym. Adv. Technol.* **2014**, *25*, 1315–1322.
- (24) Behl, M.; Kratz, K.; Noechel, U.; Sauter, T.; Lendlein, A. Temperature-Memory Polymer Actuators. *Proc. Natl. Acad. Sci. U. S. A.* **2013**, *110*, 12555–12559.
- (25) Li, Q.; Zhou, J.; Vatankeh-Varnoosfaderani, M.; Nykypanchuk, D.; Gang, O.; Sheiko, S. S. Advancing Reversible Shape Memory by Tuning the Polymer Network Architecture. *Macromolecules* **2016**, *49*, 1383–1391.
- (26) Zhou, J.; Turner, S. A.; Brosnan, S. M.; Li, Q.; Carrillo, J.-M. Y.; Nykypanchuk, D.; Gang, O.; Ashby, V. S.; Dobrynin, A. V.; Sheiko, S. S. Shapeshifting: Reversible Shape Memory in Semicrystalline Elastomers. *Macromolecules* **2014**, *47*, 1768–1776.
- (27) Gong, T.; Zhao, K.; Wang, W.; Chen, H.; Wang, L.; Zhou, S. Thermally Activated Reversible Shape Switch of Polymer Particles. *J. Mater. Chem. B* **2014**, *2*, 6855–6866.
- (28) Westbrook, K. K.; Mather, P. T.; Parakh, V.; Dunn, M. L.; Ge, Q.; Lee, B. M.; Qi, H. J. Two-Way Reversible Shape Memory Effects in a Free-Standing Polymer Composite. *Smart Mater. Struct.* **2011**, *20*, No. 065010.
- (29) Behl, M.; Kratz, K.; Zotzmann, J.; Nöchel, U.; Lendlein, A. Reversible Bidirectional Shape-Memory Polymers. *Adv. Mater.* **2013**, *25*, 4466–4469.
- (30) Farhan, M.; Chaganti, S. R.; Nöchel, U.; Kratz, K.; Lendlein, A. Reversible Shape-Memory Properties of Surface Functionalizable, Crystallizable Crosslinked Terpolymers. *Polym. Adv. Technol.* **2015**, *26*, 1421–1427.
- (31) Saatchi, M.; Behl, M.; Nöchel, U.; Lendlein, A. Copolymer Networks From Oligo(ϵ -Caprolactone) and n-Butyl Acrylate Enable a Reversible Bidirectional Shape-Memory Effect at Human Body Temperature. *Macromol. Rapid Commun.* **2015**, *36*, 880–884.
- (32) Lee, K. M.; Knight, P. T.; Chung, T.; Mather, P. T. Polycaprolactone–POSS Chemical/Physical Double Networks. *Macromolecules* **2008**, *41*, 4730–4738.
- (33) Ge, Q.; Westbrook, K. K.; Mather, P. T.; Dunn, M. L.; Qi, H. J. Thermomechanical Behavior of a Two-Way Shape Memory Composite Actuator. *Smart Mater. Struct.* **2013**, *22*, No. 055009.
- (34) Chung, T.; Romo-Uribe, A.; Mather, P. T. Two-Way Reversible Shape Memory in a Semicrystalline Network. *Macromolecules* **2008**, *41*, 184–192.
- (35) Westbrook, K. K.; Parakh, V.; Chung, T.; Mather, P. T.; Wan, L. C.; Dunn, M. L.; Qi, H. J. Constitutive Modeling of Shape Memory Effects in Semicrystalline Polymers With Stretch Induced Crystallization. *J. Eng. Mater. Technol.* **2010**, *132*, No. 041010.
- (36) Kolesov, I.; Dolynchuk, O.; Jehnichen, D.; Reuter, U.; Stamm, M.; Radosch, H.-J. Changes of Crystal Structure and Morphology during Two-Way Shape-Memory Cycles in Cross-Linked Linear and Short-Chain Branched Polyethylenes. *Macromolecules* **2015**, *48*, 4438–4450.
- (37) Dolynchuk, O.; Kolesov, I.; Jehnichen, D.; Reuter, U.; Radosch, H.-J.; Sommer, J.-U. Reversible Shape-Memory Effect in Cross-Linked Linear Poly(ϵ -Caprolactone) under Stress and Stress-Free Conditions. *Macromolecules* **2017**, *50*, 3841–3854.
- (38) Schuh, C.; Schuh, K.; Lechmann, M. C.; Garnier, L.; Kraft, A. Shape-Memory Properties of Segmented Polymers Containing Aramid Hard Segments and Polycaprolactone Soft Segments. *Polymer* **2010**, *2*, 71–85.
- (39) Stroganov, V.; Al-Hussein, M.; Sommer, J.-U.; Janke, A.; Zakharchenko, S.; Ionov, L. Reversible Thermosensitive Biodegradable Polymeric Actuators Based on Confined Crystallization. *Nano Lett.* **2015**, *15*, 1786–1790.
- (40) Huang, M.; Dong, X.; Wang, L.; Zhao, J.; Liu, G.; Wang, D. Two-Way Shape Memory Property and Its Structural Origin of Cross-Linked Poly(ϵ -Caprolactone). *RSC Adv.* **2014**, *4*, 55483–55494.
- (41) Gedde, U. W.; Hedenqvist, M. S. *Fundamental Polymer Science*; Springer: Cham, 2019. DOI: 10.1007/978-3-030-29794-7.
- (42) Ferry, J. D. *Viscoelastic Properties of Polymers*; John Wiley & Sons; 1980.
- (43) Marvin, R. S.; Oser, H. A Model for the Viscoelastic Behavior of Rubberlike Polymers Including Entanglement Effects. *J. Res. Natl. Bur. Stand.* **1962**, *66B*, 171.
- (44) Tobolsky, A. *Viscoelasticity: Phenomenological Aspects*. J. T. Bergen, Ed. Academic Press, New York–London, 1960. x + 150 pp. \$6.00. *Journal of Polymer Science* **1960**, *46*, 555.
- (45) Charlesby, A.; Hancock, N. H. The Effect of Cross-Linking on the Elastic Modulus of Polythene. *Proc. R. Soc. A* **1953**, *218*, 245–255.
- (46) Nielsen, L. E. Cross-Linking–Effect on Physical Properties of Polymers. *J. Macromol. Sci.* **1969**, *3*, 69–103.
- (47) Dolynchuk, O.; Kolesov, I.; Androsch, R.; Radosch, H.-J. Kinetics and Dynamics of Two-Way Shape-Memory Behavior of Crosslinked Linear High-Density and Short-Chain Branched Poly-

ethylenes with Regard to Crystal Orientation. *Polymer* **2015**, *79*, 146–158.

(48) Pandini, S.; Dioni, D.; Paderni, K.; Messori, M.; Toselli, M.; Bontempi, E.; Riccò, T. The Two-Way Shape Memory Behaviour of Crosslinked Poly(ϵ -Caprolactone) Systems with Largely Varied Network Density. *J. Intell. Mater. Syst. Struct.* **2016**, *27*, 1388–1403.

(49) Wolf, F. P. Elastic Behaviour of Rubber under Small Uniaxial Extension and Compression. *Polymer* **1972**, *13*, 347–354.

(50) Flory, P. J. Molecular Theory of Rubber Elasticity. *Polym. J.* **1985**, *17*, 1–12.

(51) Yoon, D. Y.; Flory, P. J. Moments and Distribution Functions for Polymer Chains of Finite Length II. Polymethylene Chains. *J. Chem. Phys.* **1974**, *61*, 5366–5380.

(52) Flory, P. J. Network Topology and the Theory of Rubber Elasticity. *Br. Polym. J.* **1985**, *17*, 96–102.

(53) Wermter, H.; Finkelmann, H. Liquid Crystalline Elastomers as Artificial Muscles. *e-Polym.* **2001**, *1*, No. 013.

(54) Floudas, G.; Reiter, G.; Lambert, O.; Dumas, P. Structure and Dynamics of Structure Formation in Model Triarm Star Block Copolymers of Polystyrene, Poly (Ethylene Oxide), and Poly(ϵ -Caprolactone). *Macromolecules* **1998**, *31*, 7279–7290.

(55) Qiao, C.; Zhao, J.; Jiang, S.; Ji, X.; An, L.; Jiang, B. Crystalline Morphology Evolution in PCL Thin Films. *J. Polym. Sci., Part B: Polym. Phys.* **2005**, *43*, 1303–1309.

(56) Schultz, J. M. Microstructural Aspects of Failure in Semi-crystalline Polymers. *Polym. Eng. Sci.* **1984**, *24*, 770–785.

(57) Ionov, L.; Stoychev, G.; Jehnichen, D.; Sommer, J. U. Reversibly Actuating Solid Janus Polymeric Fibers. *ACS Appl. Mater. Interfaces* **2017**, *9*, 4873–4881.

(58) Timoshenko, S. Analysis of Bi-Metal Thermostats. *J. Opt. Soc. Am.* **1925**, *11*, 233–255.

Supporting Information for:

Two-Way shape memory polymers: evolution of
stress vs evolution of elongation

Andrés Posada Murcia[§], Juan Manuel Uribe Gomez[§], Jens-Uwe Sommer^{†‡||} and Leonid Ionov^{§}.*

[§]Faculty of Engineering Sciences and Bavarian Polymer Institute
University of Bayreuth
Ludwig Thoma Str. 36A, 95447, Bayreuth, Germany

[†] Leibniz Institute of Polymer Research Dresden e. V., Hohe Straße 6, 01069 Dresden, Germany.

[‡]Faculty of Physics, TU Dresden, Dresden, Germany.

^{||}Cluster of Excellence Physics of Life, TU Dresden, Dresden, Germany.

Table S1. Properties of crosslinked polycaprolactone (PCL) 80kDa with different amount of crosslinker.

Sample	Amount of crosslinker (% w/w)	T_m^a (°C)	T_{cry}^b (°C)	Crystallinity X_c^b (%)
PCL DCP 2%	2	53.8	26.56	41
PCL DCP 3%	3	53.6	23.46	40
PCL DCP 4%	4	52.9	21.55	39
PCL DCP 5%	5	52.0	24.1	38
PCL TBP 2%	2	56.1	30.31	44
PCL TBP 3%	3	55.8	30.48	43
PCL TBP 4%	4	54.7	29.88	40
PCL TBP 5%	5	54.6	28.76	39
PCL 80 kDa	0	56.7	26.19	48

a) Values from the second thermal cycle melting peak obtained by DSC ($10^\circ\text{C min}^{-1}$); b) Values from the first thermal cycle obtained by DSC ($10^\circ\text{C min}^{-1}$).

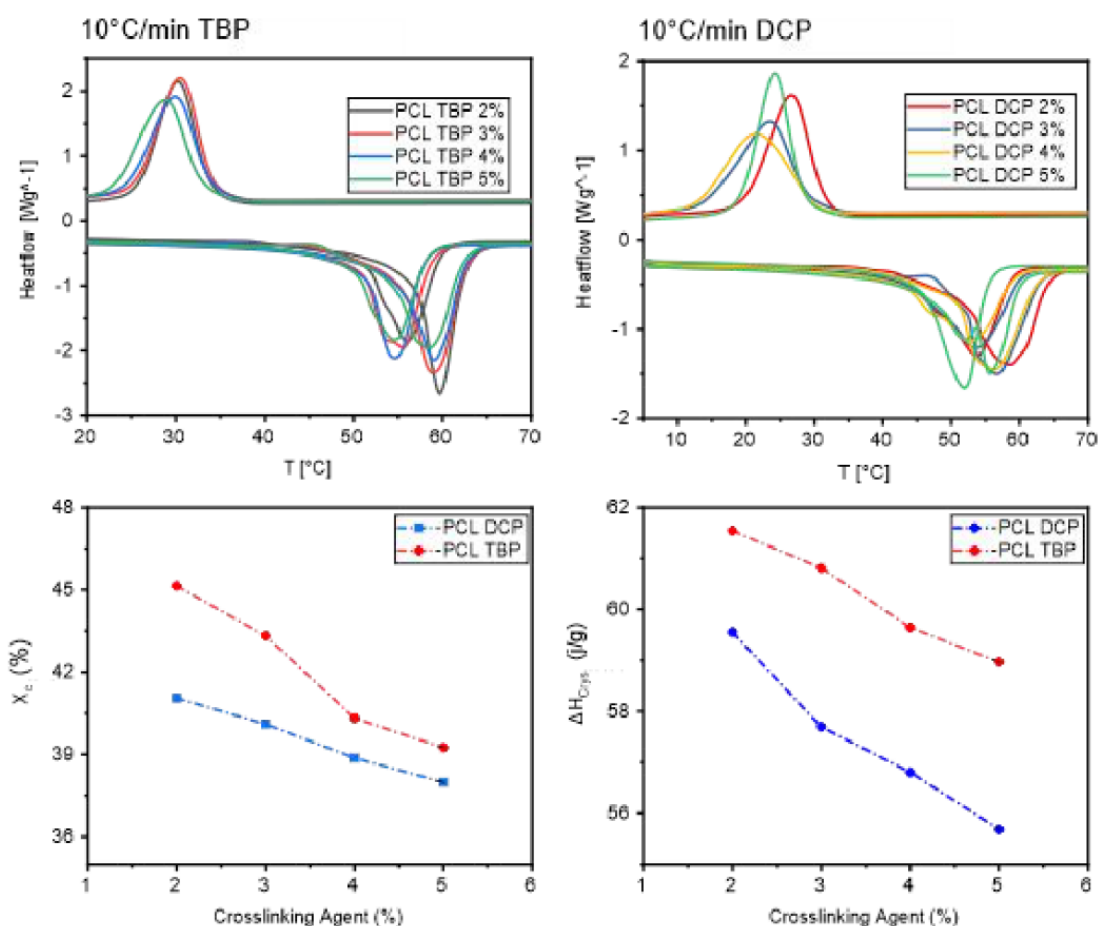


Figure S1. DSC results, degree of crystallinity and enthalpy of crystallization for PCL80KDa cross-linked with different amounts of DCP and TBP with a temperature step of $10^{\circ}\text{C min}^{-1}$.

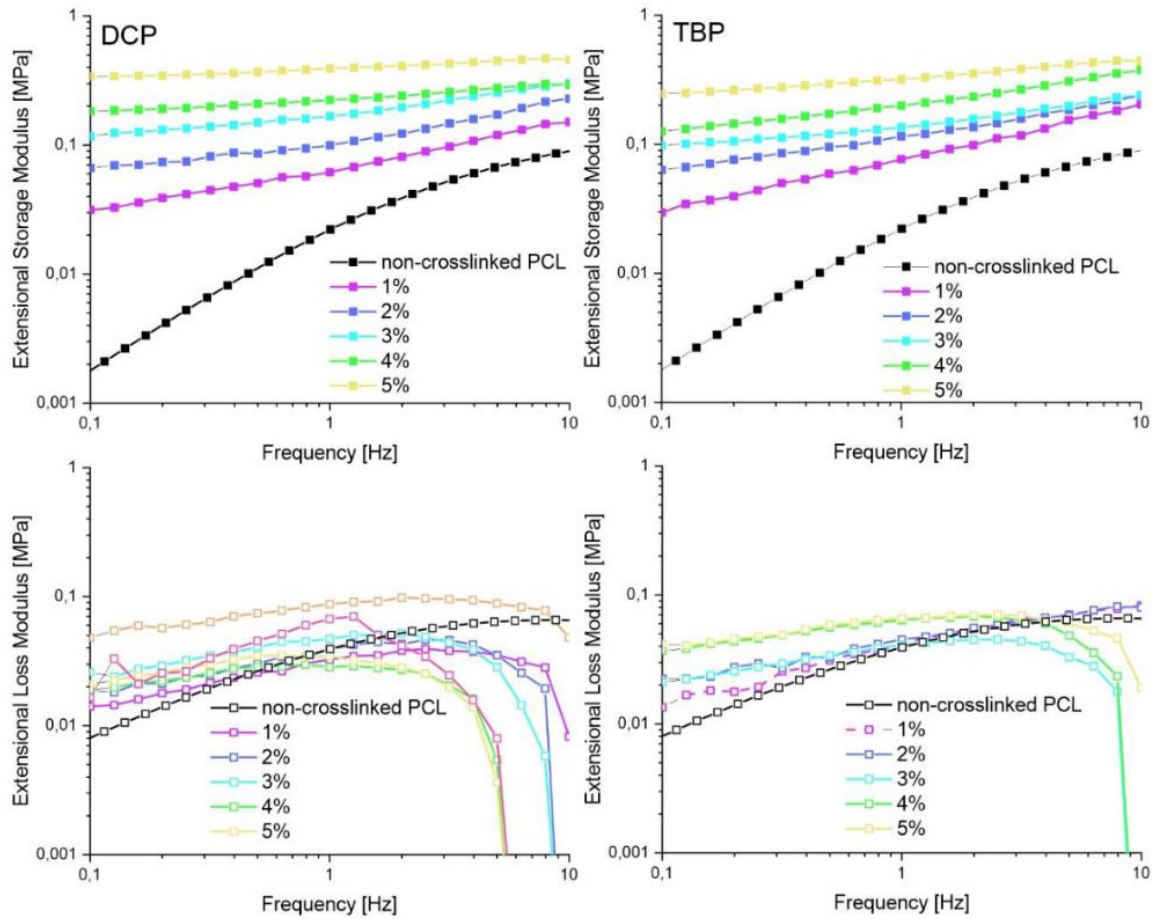


Figure S2. DMA results of PCL 80KDa crosslinked with different amount of DCP and TBP on molten state at 70°C .

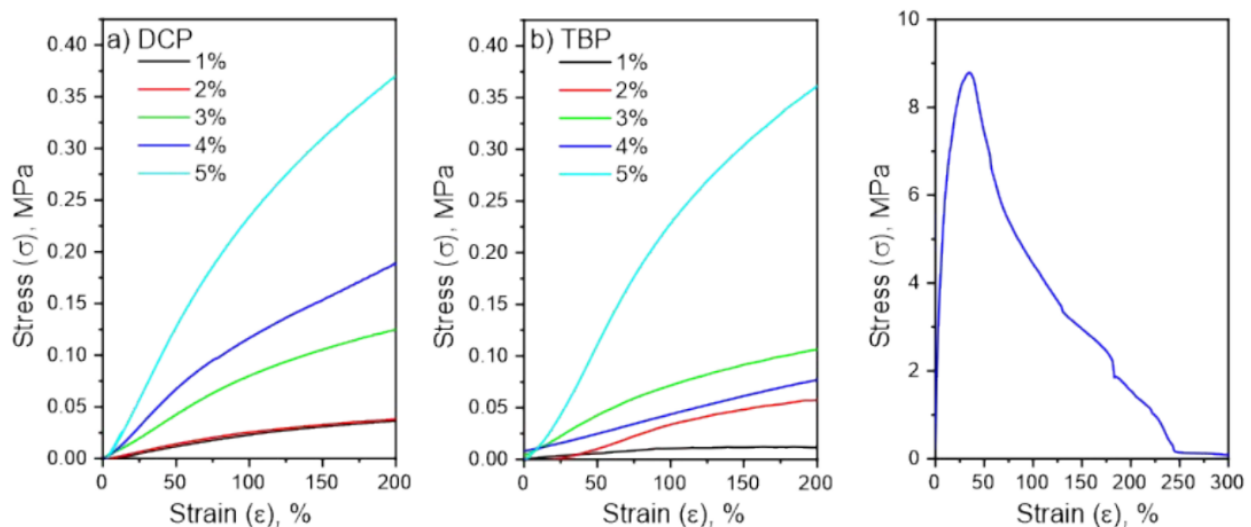


Figure S3. Tensile test of PCL 80KDa crosslinked with different amount of DCP and TBP at 70°C

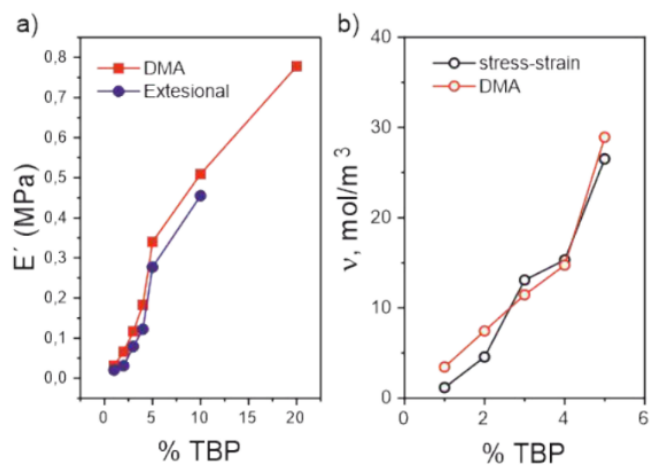


Figure S4. Mechanical properties of PCL TBP samples: (a) – extensional storage modulus obtained from tensile and DMA experiments at 70°C at 0.1 Hz; (b) – values of crosslinking density (ν) obtained from extensional and DMA experiments.

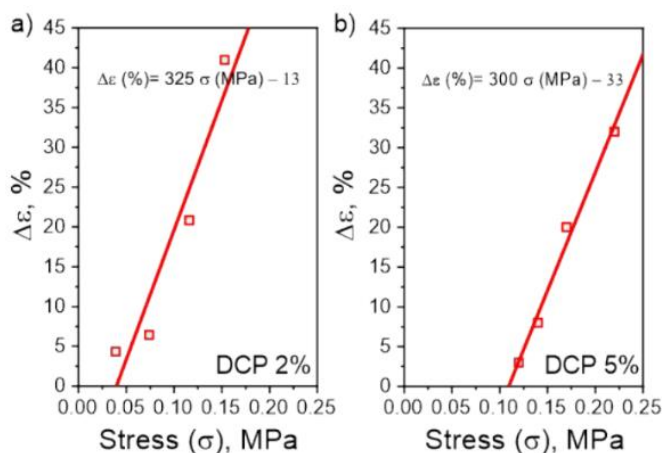


Figure S5. Measurements in constant stress mode of stretched crosslinked crystallizing PCL ($v = 8$ (a) and 40 mol m^{-3} (b)- dependence of relative elongation of samples on applied stress.

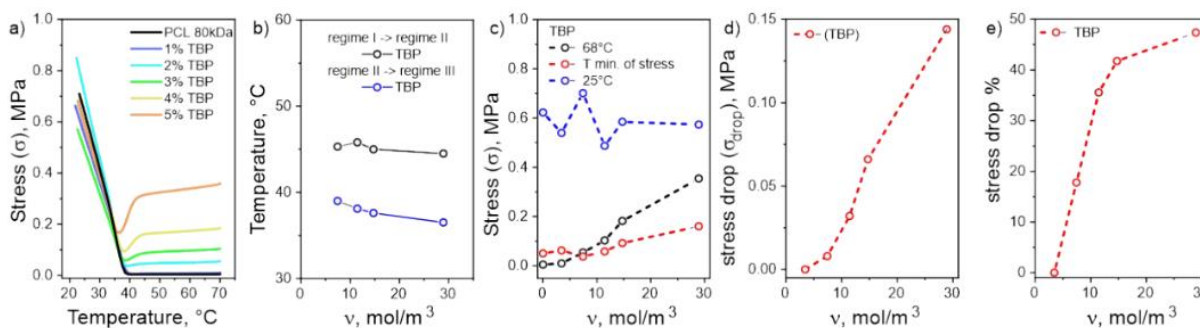


Figure S6. Effect of crosslinking density from DMA analysis on stress-temperature behavior of stretched crosslinked PCL with TBP crystallizing: (a) – effect of crosslinking density on evolution of stress with temperature, PCL was stretched by 200%; (b) – dependence of temperatures of transition from regime I to II and from II to III on the crosslinking density; (c) – dependence of the stress at different temperatures on the crosslinking density. (d) – dependence of stress drop close to crystallization in regime II on crosslinking density; (e) – dependence of relative stress drop on the crosslinking density.

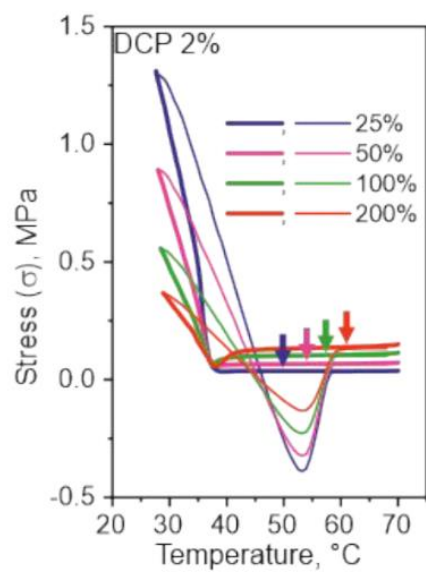


Figure S7. Effect of elongation at constant crosslinking density on evolution of stress with temperature of cross-linked PCL containing 2% DCP.

Publication 2

Mechanism of Behavior of Two-Way Shape Memory Polymer under Constant Strain Conditions

*Andrés Posada-Murcia, Juan Manuel Uribe Gomez, Stephan Förster, Jens-Uwe Sommer,
Martin Dulle and Leonid Ionov.*

Macromolecules

Publication Date: February 14, 2022.

DOI: 10.1021/acs.macromol.1c02564

Mechanism of Behavior of Two-Way Shape Memory Polymer under Constant Strain Conditions

Andrés Posada-Murcia, Juan Manuel Uribe-Gomez, Stephan Förster, Jens-Uwe Sommer, Martin Dulle,* and Leonid Ionov*

Cite This: *Macromolecules* 2022, 55, 1680–1689

Read Online

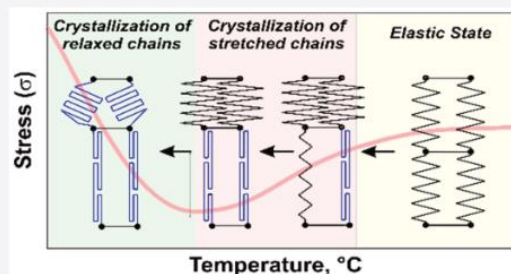
ACCESS |

Metrics & More

Article Recommendations

Supporting Information

ABSTRACT: In this paper, we report detailed investigation of structural changes occurring in two-way shape memory polymers (2W-SMP) upon thermal cycling at constant strain conditions. We demonstrate that cooling of stretched chemically cross-linked polycaprolactone results first in a slow decrease of stress, the stress drops rapidly upon further cooling, and further cooling results in sharp increase of stress. In this paper, we investigated structural changes occurring in each of these three phases using *in situ* force measurements and XRD analysis (SAXS and WAXS). In the first phase, the stress decreases due to decrease of entropic factor in the elastic state. In the second phase, polymer chains start to crystallize in the stretched state as a result of the number of active springs producing stress decreasing. This results in the decrease of the stretching degree of other polymer chains, and finally, unstretched polymer chains crystallize that result in an increase of stress—the polymer simply tends to shrink.



1. INTRODUCTION

Two-way shape memory polymers (2W-SMP) are a promising kind of actuating materials due to their ability to actuate autonomously (without external power source) and reversibly with large amplitude in both wet and dry environments—a combination of properties inaccessible to hydrogels, common shape memory polymers, and piezoelectric polymers.^{1–6} 2W-SMPs that actuate upon thermal cycling undergoing a reversible shape-shifting process can be separated into two classes: ones that require an applied stress for actuating and ones that do not require it.⁷ The 2W-SMPs of the first type consist of single component materials: cross-linked semicrystalline polymers, which change their length during crystallization/melting, when an external force is applied and the polymer is stretched.^{8,9} 2W-SMPs of the second kind are formed by two fundamental structural elements: a scaffold, which plays a passive role in actuation and typically confers enhanced mechanical properties to the material, and a stretched crystallizing elastomer section, which enables the actuation.^{10–14} The stretching of the elastic part is achieved during a shape-programming step, and the passive polymer domains keep the elastic crystallizing component in a stretched state. Crystallization/melting of the stretched elastic component result in its elongation/contraction allowing a shape-shifting effect of the whole sample.

Several models were developed to explain and predict behavior of the 2W-SMP. Chung et al.(2008),¹⁵ for example, argued that elongation of stretched elastomer occurs due to oriented crystallization promoted greatly by the magnitude of

the applied load. Moreover, Westbrook et al.(2010)¹⁶ proposed a 1D model, which describes the coexistence of two phases during crystallization as the origin of two-way shape memory effect (2W-SME) in semicrystalline polymers. The evolution of energy from an entropy governed-phase (rubbery state) to a stretched-induced crystalline phase during thermal cycling allows the reversible actuation of the material to be strongly dependent on the rate of temperature change. A model based in the transition of free energy of a polymeric network under load subjected to crystallization from amorphous to crystalline domains was proposed by Dolynchuk et al. (2014)¹⁷ and Kolesov et al. (2015).¹⁸ This approach, based on the thermodynamic description of the stress-induced crystallization phenomena, established that the elongation observed on cured elastomers under load upon cooling is the driving force of the 2W-SME, and it is noticeable only when the formed crystalline domains are oriented toward or forming an acute angle with the direction of the applied stress. The crystalline domains are alternated with the amorphous phase forming well-defined lamellar structures which stack perpendicularly to the direction of deformation. The model allowed the prediction of relevant crystallographic parameters for high-

Received: December 16, 2021

Revised: January 18, 2022

Published: February 14, 2022



density polyethylene such as the number of crystal folds, size and morphology. Validation of proposed models requires *in situ* experiments allowing a correlation between shape change and structural reorganization. Huang et al. (2014)¹⁹ performed *in situ* X-ray diffraction analysis (XRD) experiments during crystallization-induced elongation confirming that the length of polymer subjected to a constant external load changes while it crystallizes. Meanwhile, a detailed evaluation of the correlation between crystallinity and orientation degree with elongation has not been performed complicating the validation of these models.

Although the behavior of 2W-SMP at constant stress conditions is relatively well studied, most of the 2W-SMP moieties are used in setups, where they undergo out of plane deformation such as bending and twisting,^{20–25} where the length of the whole sample remains nearly unchanged during actuation. This means that such polymers are used under different conditions than 2W-SMPs, which require an external constant force to actuate. Recently, we published a phenomenological comparison of the behavior of 2W-SMP in both regimes:²⁶ in a constant stress setup, the polymer undergoes sharp elongation right before crystallization, while in a constant strain setup, the stretched polymer undergoes an anomalous sharp drop of stress right before crystallization followed then by an expected increase of measured stress upon further cooling. The discussion of the mechanism and behavior of polymers in constant strain mode in thermal cycling remained out of the scope of our work. In this paper, we undertake an attempt to reveal processes occurring in semicrystalline polymers by performing *in situ* XRD studies of stretched cross-linked poly(ϵ -caprolactone) (PCL) in constant strain setup upon cooling, accompanied by simultaneous measurements of extensional stress in polymer.

2. EXPERIMENTAL SECTION

2.1. Materials. Commercially available PCL ($M_n = 80$ kDa), dicumyl peroxide (DCP) (98%), and chloroform (99%) were purchased from Sigma-Aldrich and further used as received without any additional treatment/processing.

2.2. Preparation of Samples. PCL beads were dissolved in chloroform before being mixed with 5 wt % of DCP at room temperature (PCL DCP 5%). After proper homogenization, the viscous solution was poured and let to dry overnight on a flat glass recipient, obtaining a homogeneous solid film from which 10×8 mm rectangular pieces (average thickness of 0.7 mm) were cut. Finally, the probes were thermally cross-linked in a vacuum oven for 2h at 160 °C.

2.3. Thermomechanical Cycle under Constant Strain and Constant Stress. Evolution of extensional stress during thermal cycling at constant elongation was performed, a typical run is described as follows: PCL film is clamped and extended on molten state (70 °C) up to a given strain, 200%, e.g. Then, stretched samples were cooled to ca. 25 °C. Finally, the crystallized probes were heated again up to the molten state, and cooling/heating steps of 1 °C min⁻¹ were used. Strain progression on constant stress experiments was studied by applying an analogous thermal cycle as mentioned above. The value of constant stress to extend a specimen by ca. 200% was obtained from the constant strain experiment while the 2W-SME was demonstrated (Figure 1).

2.4. Kinetic Study of Unstretched/Stretched PCL Crystallization Process. Time dependent analysis of observed stress drop in constant strain experiments upon cooling and its correlation with stretching degree was carried out. Slow cooling program was implemented on stretched cured polymer and described as follows: Specimens were cooled from molten state (70 °C) to 55 °C on a 30 min window, followed by -1 °C cooling and subsequent annealing

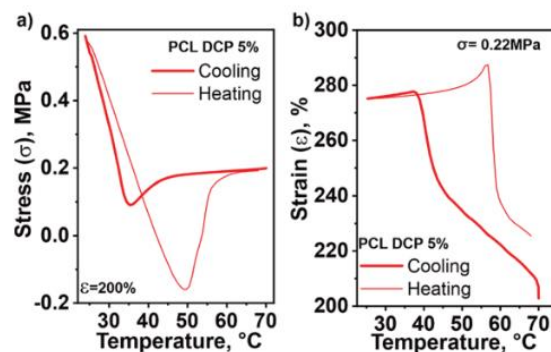


Figure 1. Behavior of cross-linked PCL sample undergoing a thermomechanical cycle under (a) constant strain and (b) constant stress conditions with heating/cooling steps of 1 °C · min⁻¹.

steps for 15 and 30 min correspondingly until 40 °C, these temperature limits are supported on our previous observation of the transient state occurrence where the stress drop is detected. Unstretched and not cross-linked samples were tested as a reference (Figure 2). Additionally, we performed constant strain thermal-analysis of the PCL DCP 5% sample and evaluated force evolution as a function of the applied cooling/heating rate (0.5, 1, and 2 °C min⁻¹) using a homologous program as described above (Figure S1).

2.5. Differential Scanning Calorimetry (DSC). Thermal analysis of uncross-linked and cured PCL specimens was performed using a DSC3 (Mettler Toledo, USA). Samples were subjected to a three step program: first heated from 0 to 200 °C, then cooled from 200 to 0 °C, and finally heated again from 0 to 200 °C at a heating-cooling rate of 1 °C min⁻¹ under nitrogen atmosphere (Figure 2).

2.6. Crossed Polarizers Experiments. A qualitative study of crystallization at constant strain of stretched PCL DCP 5% was carried out using crossed polarizers. Two light polarizers were mounted with a 90° disposition on a self-made device equipped with a LED white light panel, movable clamps, which allowed the extension of the specimen above the light source, and a heating unit. Probes were fastened and subsequently heated to a molten state ~70 °C and then the polymer was extended up to 200% of its original length and fixed as the heating was maintained. At this point, the heating was stopped to allow crystallization of the material while recording temperature. Birefringence changes on the sample were noted and registered along its cooling to room temperature (Figure 3).

2.7. In Situ Wide-Angle and Small-Angle X-ray Scattering Analysis (WAXS and SAXS). Scattering patterns were recorded with the SAXS system “Ganesha-Air” from (SAXSLAB, Xenocs). The X-ray source of this laboratory-based system was a D2-MetalJet (Excillum) with a liquid-metal anode operating at 70 kV and 3.57 mA with Ga K α radiation ($\lambda = 0.13141$ nm) providing a very brilliant and a very small beam (<200 μ m). The beam was focused with a focal length of 55 cm using a specially made X-ray multilayer optic (Xenocs) to provide a very small and intense beam at the sample position.

The prestretched samples (200 and 300% of their original length) were placed in a Linkam TST-350 tensile stage with the glass windows replaced with 10 μ m thick mica windows. All samples were prepared in the same way for the measurement. After fixing the heat-pressed samples on the stage, the blocks were moved apart until a force value of 2 N m was reached. This was done to ensure good contact of the sample with the heating block as well as to have a standardized starting point. This is especially important as it was unavoidable to make two separate measurements for WAXS (0.16 m distance) and SAXS (51 cm) with two separate samples.

Each sample was heated and kept at 70 °C for 5 min. After that, the sample was cooled with a cooling rate of -1 °C/min while being continuously illuminated with X-rays. The scattering was recorded continuously and a separate pattern was saved every 15s for the duration of the cool down. Details to the different data reduction

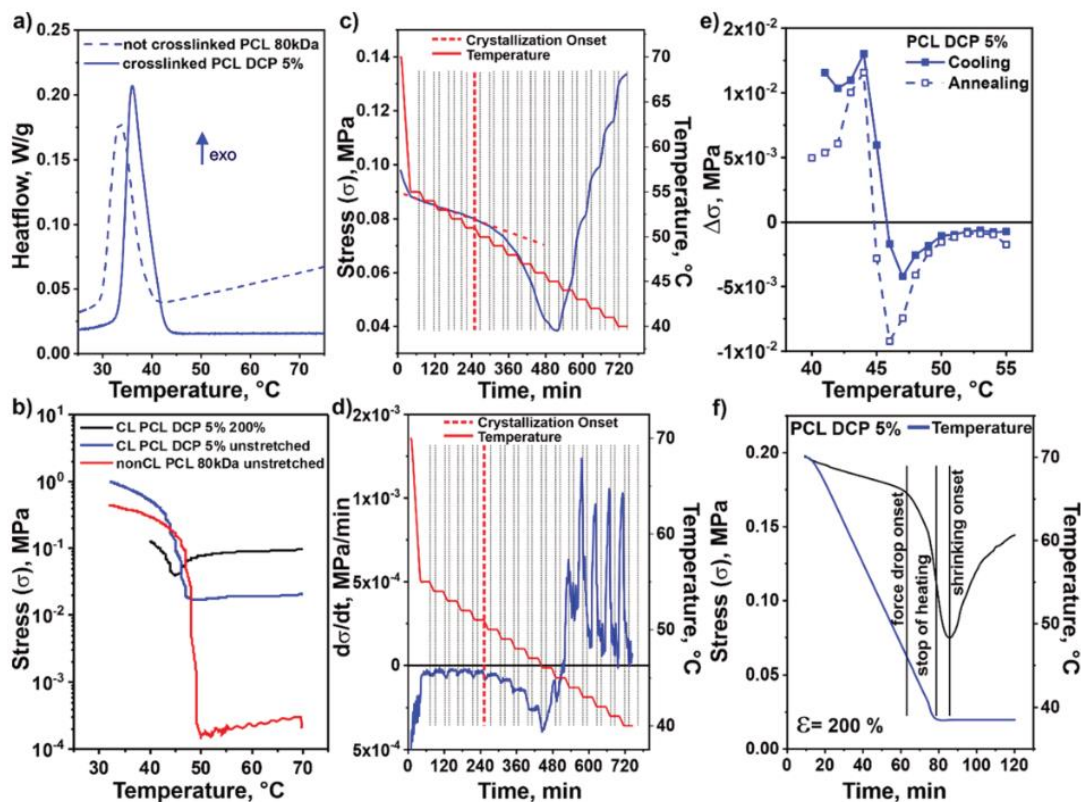


Figure 2. Kinetics of stress evolution upon cooling: (a) DSC of cross-linked and not cross-linked polymers at $1\text{ }^{\circ}\text{C}\cdot\text{min}^{-1}$; (b) evolution of stress with temperature of not stretched polymers $-1\text{ }^{\circ}\text{C}$ each 30 min and (c) evolution of stress with time of stretched polymer during cooling under constant strain; (d) evolution of the slope stress vs time with temperature of stretched polymer during cooling; (e) stress drop in each step of cooling and annealing for a stretched cross-linked PCL sample under constant strain; (f) evolution of stress with time during slow cooling and annealing at constant temperature below the temperature of the onset of crystallization.

procedures as well as the analysis of the data are given in the Supporting Information (Figures S2–S5).

3. RESULTS AND DISCUSSION

For our experiment, we used chemically cross-linked PCL with an initial molecular weight $M_n = 80\text{ kDa}$. The stretched polymer demonstrated an odd evolution of stress upon crystallization under constant strain conditions—stress sharply drops upon cooling until reaches a minimum, then the force increases as expected due to crystallization with further cooling (Figure 1a). On the other hand, the change of length upon crystallization under constant stress has a typical character—the sample undergoes sharp elongation upon cooling followed by a recovery of original length upon heating (Figure 1b).

3.1. Kinetic Evaluation of Crystallization Process under Constant Strain. In order to understand the stability of the anomalous stage upon cooling associated with the stress drop at constant strain, we performed crystallization essays at very slow cooling rate. We first made DSC of not stretched cross-linked as well as not cross-linked polymers at a rate of $1\text{ }^{\circ}\text{C}\cdot\text{min}^{-1}$ to identify the onset of crystallization. It was found from DSC that the onset of crystallization is observed at $40\text{--}42\text{ }^{\circ}\text{C}$, while the crystallization peak is located at ca. $35\text{--}37\text{ }^{\circ}\text{C}$ (Figure 2a). Next, we measured force generated by polymer at very slow cooling rate—the temperature was reduced stepwise by $1\text{ }^{\circ}\text{C}$ each step followed by a 30 min annealing at constant temperature. The experiment was carried out with stretched cross-linked polymers, a nonstretched cross-linked sample and a not cross-linked nonstretched probe were also measured as references. It was observed that the elastic storage modulus of

not stretched cross-linked and not cross-linked polymers starts to increase at ca. $47\text{--}48\text{ }^{\circ}\text{C}$ (Figure 2b). The increase of the storage modulus (E') becomes considerable at $45\text{--}46\text{ }^{\circ}\text{C}$. The difference in the temperature of crystallization onset provided by DSC and the thermomechanical analysis is caused mainly by the sensitivities of the methods. DSC is sensitive to changes on volume/mass of crystallizing materials—formation of a small number of crystallites is not detectable by DSC. On the other hand, mechanical properties are sensitive to the number small crystallites, which act as physical cross-linking points increasing the value of the elastic modulus of elastomers.²⁷

We plotted the evolution of temperature and stress of the stretched cross-linked polymer with time (Figure 2c) as well as the slope of the stress/time curve (first derivative) vs time (Figure 2d) to study the kinetics of the transition. We observed that changes of stress ($\Delta\sigma$) in each cooling step and during annealing remain nearly constant upon cooling from 55 to $52\text{ }^{\circ}\text{C}$. The stress is changing linearly with time during annealing, which means that the relaxation time of the cured polymer after being subjected to stretching is larger than 30 min, which is the duration of each annealing step. At $52\text{ }^{\circ}\text{C}$, we observed the commencement of stress's deviation from the linear behavior until ca. $50\text{ }^{\circ}\text{C}$, where an intense decrease of stress takes place resulting in larger values of $\Delta\sigma$, which became more pronounced for each cooling–annealing step as depicted on Figure 2e. As result, the stress vs time curve becomes steeper. At $47\text{ }^{\circ}\text{C}$, an increase of the stress was observed. Very sharp changes of stress were observed in each step of the cooling. Annealing after each cooling step resulted in relaxation of stress as it tended to approach an equilibrium level. The value

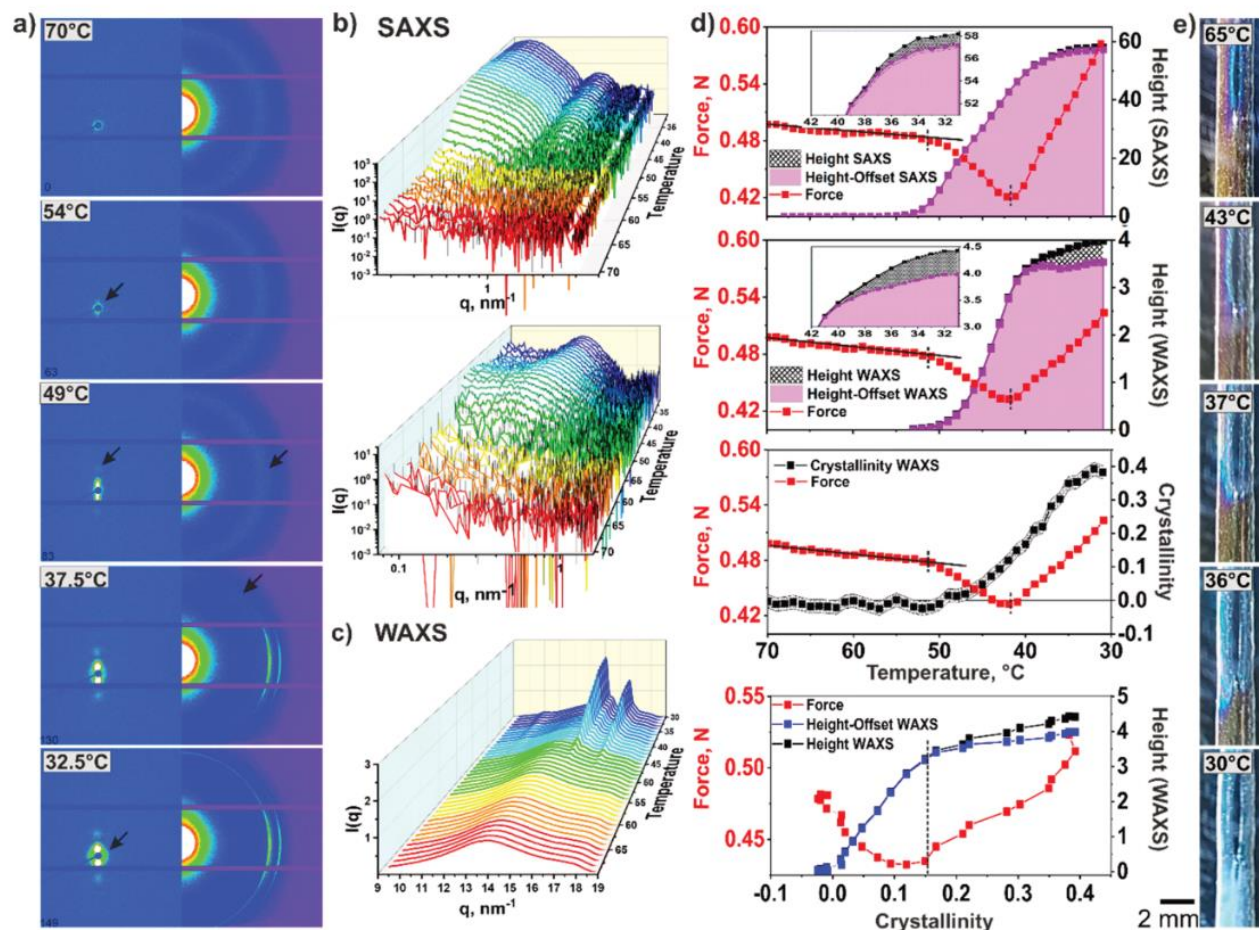


Figure 3. *In situ* structural studies of 200% stretched cross-linked PCL: (a) 2D SAXS (left) and 2D WAXS images (right); temperature evolution of (b) SAXS and (c) WAXS radial patterns; (d) evolution of SAXS and WAXS height and height-offset Voigt fitting parameters and degree of crystallinity with temperature as well as dependence of WAXS Voigt parameters with force on degree of crystallinity; (e) crossed polarizer images.

of stress at equilibrium, which can be achieved in each annealing step, increases with decreasing temperature. The main observation of this experiment is that the transitional state corresponding to the stress drop on stretched polymers at constant strain upon cooling is stable through time—we observed the stress drop over a period of ca. 3 h.

We performed a control experiment to investigate if the course of the stress drop in transitional state is dependent on the change of temperature (Figure 2f). For this, we performed the crystallization of a stretched sample fixed at 200% of its original length and recorded the evolution of stress with temperature upon cooling. It was observed that stress started to rapidly drop at ca. 45 °C. The temperature was further reduced down to 37 °C, which is lower than the temperature at which an increase of stress during stepwise cooling was observed, and annealed at this temperature. The stress continued to further decrease at 37 °C, and after ca. 10 min of annealing, the force started to increase at this temperature. This experiment demonstrated that the transitional state is not strictly determined by temperature but corresponds to an intermediate structure adopted by polymer chains upon transition from amorphous to crystalline states and cannot be avoided at the conditions at which crystallization occurs.

3.2. *In Situ* SAXS and WAXS Structural Analysis.

3.2.1. 200% Elongation. We studied the structural evolution of stretched elastomers with 200% of elongation upon cooling and crystallization by performing *in situ* SAXS and WAXS

measurements at constant strain (Figure 3). The obtained SAXS patterns showed that the polymer is fully amorphous at 70 °C (Figure 3a,b). Decrease of temperature to 58 °C results in appearance of anisotropic scattering at low q , which is usually attributed to density fluctuation.^{28–32} However, the fact that this signal at low q is showing a very strong orientational anisotropy right from the start is remarkable. This can be described by an anisotropic spinodal decomposition.³³ This behavior has been reported already for PCL upon cooling.³⁴ The cross-linked points located within the amorphous regions of the sample have a slightly different density than the rest of the polymer, acting as the driving force for the decomposition. The first discernible SAXS signal shows up at 58 °C, at the point when the stress starts to drop (53 °C) (Figure S6) we observed the appearance of meridional spots on the 2D SAXS pattern at $q = 1.2 \text{ nm}^{-1}$, which indicates the inception of well-defined oriented lamellae. Upon further cooling, a structure factor peak in the meridional direction is developing from stacking of the lamellae as well as continuous increase of scattered intensity (Figure 3a,b). At ca. 43 °C, the minimum of the force was observed; the total force drop was ca. 9%. Below 42 °C an isotropic scattering contribution about 100 times weaker than the signal on the meridian shows up on the equator. This ring is also a structure factor peak from lamellae but this time from the ones not oriented in any particular direction. Although the signals were weak in intensity, we were

able to fit the data well to the same model as the oriented lamellae.

WAXS analysis of the stretched sample showed no observable reflections between 70 and 54 °C, indicating no crystalline phase in this temperature range when the stress versus temperature curve remains linear. However, the appearance of an azimuthally anisotropic reflection at 53 °C evidently indicates the onset of the formation of an oriented crystalline phase (Figure 3a,c; Figure S7) as the force starts to fall. Thus, the measured crystallinity starts to increase while the sample is further cooled. The degree of crystallinity is ca. 10% at the point of minimum force, which corresponds to a 10% drop in force in relation to the force in an elastic regime. Further cooling to 37 °C results in the appearance of the (110) isotropic reflection,³⁵ which could be related to massive formation of disordered crystallites, provoking a sustained further arising of the detected crystallinity until the cooling program is over (Figure 3d).

A Voigt profile fitting model was applied to the obtained SAXS and WAXS azimuthal plots. Azimuthal fitted WAXS profiles of 200% stretched cross-linked PCL revealed that peak's position and width parameters are hardly changing upon cooling (Figure S8). On the contrary, the evolution of the height parameter with temperature follows the same two stage behavior as the simultaneously recorded force (Figure 3d). From 53 to 40 °C, where the fall in force takes place, the peak's height is rapidly growing to about 80% of its final height. Between 40 and 30 °C the height parameter grows modestly while the recorded force increases for both small- and wide-angle scattering data.

The contribution of the oriented crystalline domains to the intensity of the peak's height for SAXS and WAXS measurements was assessed by subtracting the offset criterion, which in an azimuthal plot is a constant (angle independent) background, from the overall height signal. The resulting values and their correlation with the measured stress upon cooling revealed that on the temperature range, where the stress drop is recorded the intensity of oriented crystalline phase grows sharply until the force minimum is reached (ca. 43 °C). Below this temperature, the progression of the signal becomes monotonous, demonstrating that the further increase exhibited by the overall height parameter between 42 and 30 °C is solely a contribution of the offset criterion to the intensity of the peak as depicted on Figure 3d. This observation is way more evident on WAXS experiments as they are carried on a shorter length scale and its signal corresponds to the crystal lattice while SAXS peaks do not answer to a such well-defined structure and are susceptible to slightly shifted positions with temperature due to the change in concentration as well as separation distance.

Therefore, these observations allowed us to associate the anomalous thermomechanical behavior of constantly strained polymers upon cooling with the existence of two different types of crystalline phases on the crystallization process: oriented or with a certain degree of orientation and nonoriented crystalline domains. As the stretched material leaves the rubbery amorphous state (70–54 °C) and enters the transient regime characterized by the stress drop (ca. 53 °C), a highly ordered crystalline phase begins to grow until the force minimum is reached (around 43 °C for 200% strained PCL), signal intensity for both SAXS and WAXS grows sharply as a consequence of this process. Finally, below 42 °C, the measured force rises as the offset parameter becomes the

main contribution to the intensity of the acquired small and wide-angle scattering signals due to unordered crystalline phase formation as depicted in Figures 3d and S9.

We have also observed the stretched polymer sample in crossed polarizers (Figure 3e). The temperature measurements were imprecise, and results can be used for qualitative illustration of process occurring in the polymers. In crossed polarizers, the stretched polymer at 65 °C exhibits a yellowish coloration indicating birefringence of the stretched polymer chains. Cooling the sample under constant strain leads to a reddish to bluish color change in some areas of the sample, which, according to the Michel–Levy diagram, indicates an increase in birefringence.³⁶ This implies an increase in optical anisotropy and, therefore, the degree of orientation of the polymer chains. As the temperature further decreases, the sample becomes slightly hazy, presumably due to massive crystallization. Finally, at 30 °C, the sample becomes completely white and opaque.

3.2.2. 300% Elongation. We studied the effect of the stretching degree on the evolution of structure of the stretched polymer upon its crystallization. Generally, the behavior of the stronger stretched polymer (300%) is qualitatively similar to that discussed above. The main effects of stretching are that, at 70 °C, the SAXS 2D pattern shows already a modest anisotropic reflection corresponding to slightly oriented platelets (Figure S10). Accordingly, the WAXS experiments revealed the inception of an anisotropic reflection ca. 60 °C. The outset of reflections denoting orientation occur at higher temperatures for more stretched samples. This trend continued its course with further cooling developing the same pattern of reflections previously described for less-strained probes (Figures S10 and S11). Even more, a sharper stress drop takes place at higher temperature (ca. 46 °C) exhibiting a force reduction of 15% while the crystallinity at the force minimum is also ca. 15%—the stress drop corresponds to degree of crystallinity as in the case of polymer stretched to 200%. This results are in complete agreement with the observations reported on our previous study and provides an explanation for the anomalous recorded stress drop caused by the onset of crystallization process on constant strain mode and its dependence on stretch degree. Voigt fitting of azimuthal profiles and the associated height and offset parameters for 300% stretched samples followed an analogous evolution upon cooling, suggesting the same two-stepped crystallization course than less stretched specimens but taking place at higher temperatures (Figure S10 and Figure S11). As a final remark, it must be noted that the offset's contribution to the overall SAXS and WAXS intensity for 300% stretched samples is less significant than that for 200% PCL as a consequence of the enhancement of oriented crystallization on a greatly strained probe.

3.3. SAXS Form and Structure Factor Fitting. A simple homogeneous disc form factor³⁷ was used to describe the acquired small-angle scattering of the radially averaged signal for stretched PCL up to 200 and 300% upon cooling under constant strain. For the radial average, a cone shape region of interest was used, encompassing an angle of 20° to only capture the signal from the oriented platelets on the meridian. The scattering intensity is calculated for a flat radially averaged cylinder. We use the fact that we only radially averaged over the region of interest (ROI) to use the form factor without preferred orientation to fit the data.

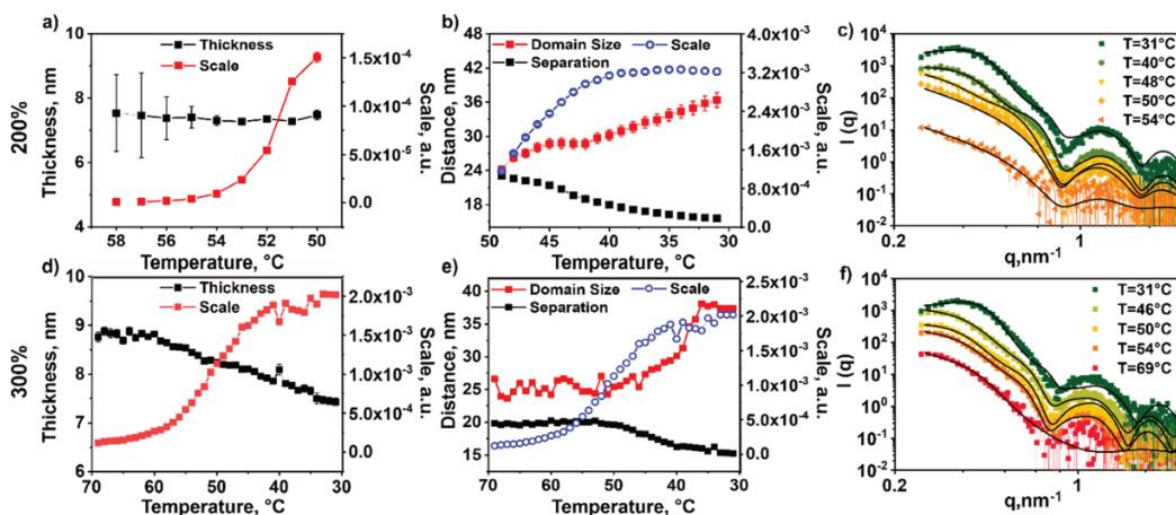


Figure 4. Form and structure factor fitting study of 200% (a) Thickness and scale parameters from disc form factor fitting; (b) separation distance, domain size and scale from stacked disc structure factor fitting; (c) data and fits from form and structure factor models and 300% stretched PCL upon cooling (d) thickness and scale parameters from disc form factor fitting; (e) separation distance, domain size, and scale from stacked disc structure factor fitting; (f) data and fits from form and structure factor models. (c, f) the data and fit for 31 °C were shifted on the y-scale by a factor of 5 for better visibility.

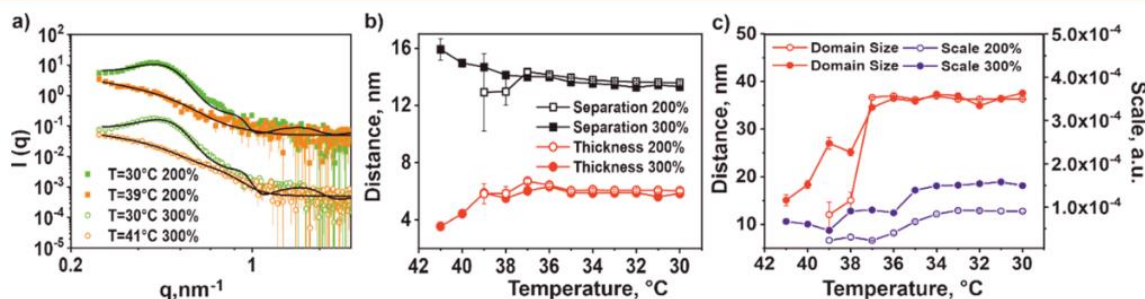


Figure 5. Form and structure factor fitting study of radially averaged equatorial scattering for 200% and 300% stretched PCL. (a) Data and fitting plots from form and structure factor models. Data and plots for 300% sample was shifted on the y-scale by a factor of 100 for better representation. (b) Thickness and separation distance from stacked platelets form factor fitting. (c) Domain size and scale from stacked disc structure factor fitting.

As cooling progressed, the scattering not only showed the features of a disc form factor but also a structure factor from a stacking disc arrangement along the polymer chains stretching orientation; this can be seen in the obtained scattering data as a peak developing toward low q values (Figure S11). To fit this data, we introduced a lamellar structure factor to model the stacked disc conformation. In this case we used the radial structure factor $S(q)$ in powder average of a crystal lattice including the Debye–Waller factor and broadening due to domain size (the technical details are given in Supporting Information).

In the case of elongation of 200%, the first discernible signal shows up around 58 °C, and from 58 to 50 °C, a model without structure factor suited well to fit the data. The threshold of 49 °C, where the introduction of the structure factor was necessary, falls together with the detected decrease in force measured alongside the SAXS data. It was also observed that on the temperature range between 58 and 50 °C from all the fitted parameters only the scale parameter—which corresponds to the concentration—is significantly increasing while the thickness and polydispersity of the discs stayed constant (Figure 4a). The data below 50 °C needed the incorporation of a structure factor model. From this point onward the thickness and polydispersity were kept constant to ensure a faster and more stable fitting since during the

remaining course of the test we found that these parameters exhibited no significant change as temperature was lowered. The structure factor yields mainly two parameters: the distance describing the separation between platelets as well as the domain size for a lamellar crystal.

The increase in domain size together with the decrease in platelets separation distance below 50 °C (Figure 4b) is the result of the increase of order within the polymer chains above the 10 nm size regime. One can understand this behavior the following way: the packed stacks of platelets are solidifying thereby decreasing their separation distance and as a side effect the order within the stacks is increasing which is reflected in the domain size parameter evolution. Overall the applied model could fit the radial averaged data in the meridional direction very well with the smallest amount of possible fit parameters (Figure 4c), the tables containing all parameters for all temperatures and samples are provided in the Supporting Information (Tables S1–S4).

For the 300% PCL sample, the fitting was done the same way as for the 200% sample with the only difference being that structure factor was included for all investigated temperatures (Figure 4d–f). The trends we see here are the same as for the 200% sample, but the final domain size is a little larger, and even at 70 °C, the sample has not fully lost its orientation and still clearly shows oriented spinodal decomposition.

3.4. Nonoriented Platelets (Equatorial Scattering). As mentioned earlier a noticeable isotropic scattering contribution is showing up below 42 °C in SAXS as well as in WAXS (Figure 3a). We attribute this signal to nonoriented but still crystalline lamellae. Again the 300% sample shows this signal at a slightly higher T than its less stretched counterpart. In WAXS, it is pretty clear that the ring comes from the same crystal structure as the main signal as all peak positions in q are the same. For SAXS however there could be several reasons for such behavior, the two most likely are as follows: (I) a structure factor peak due to spatial correlations of the oriented lamellae due to their high relative concentration and close proximity; (II) the same kind of structure factor from stacked lamellae as in the meridional direction but this time without preferred orientation. The first would give only the structure factor without any form factor contribution in the equatorial direction, and the second type would give both but with different structural parameters such as thickness or domain size.

When radially averaging on the equator we got the same type of scattering as for the meridional direction: stacked lamellae, but about a hundred times weaker in intensity as depicted on Figure 5a. We were able to fit these curves with the same model as the oriented platelets. The difference we see in thickness as well as domain size come from the constant strain conditions in which the experiment was conducted, these nonoriented lamellae are less strained and therefore not as stretched as the oriented ones. For instance, the platelets in equatorial scattering are thinner (~ 6 nm) than the ones on the meridian—with a thickness of ~ 7.5 nm—for the same sample (Figure 5b). The domain size is similar for both oriented and nonoriented stacks but slightly larger for the 300% sample, even for nonoriented stacks as shown in Figure 5c. Details on the mechanism behind this behavior are discussed on the next paragraph.

3.5. Crystallization Mechanism of Semicrystalline Cross-Linked Polymers under Constant Strain. Our interpretation of the scattering results leads us to the conclusion that the stress drop during cooling at constant strain has its origin in the formation of oriented crystallites that are formed due to the decrease of free energy of the molten rubber under elongation. In a previous work, Dolynchuk et al.³⁸ has proposed a theoretical model that can quantitatively explain the increase of strain under cooling in the complementary experiment at constant stress; see Figure 1b. The key idea is an extension of the concept proposed by Flory³⁹ and Gaylord,⁴⁰ namely that crystallization of network strands originating from the cross-links can lead to a reduction of the end-to-end distance of noncrystallized chains sequences in stress direction and thus reduce the free energy under constant load. It has been further shown that extended chain crystals and double folded crystals would dominate above a minimal strain of about $\varepsilon = 0.25$.³⁸

This concept may also be applied to understand the stress-drop under cooling at constant strain. However, while in the case of constant stress the formation of oriented crystallites can extend through the sample, in case of constant strain this would result in a relaxation of chains in the direction of stress which would stop the accelerated crystallization process and results in a spontaneous separation into highly oriented crystallites and noncrystallized regions. This idea is schematically sketched on Figure 6a. We note that the formation of highly oriented chain nuclei would exert an extra force on the

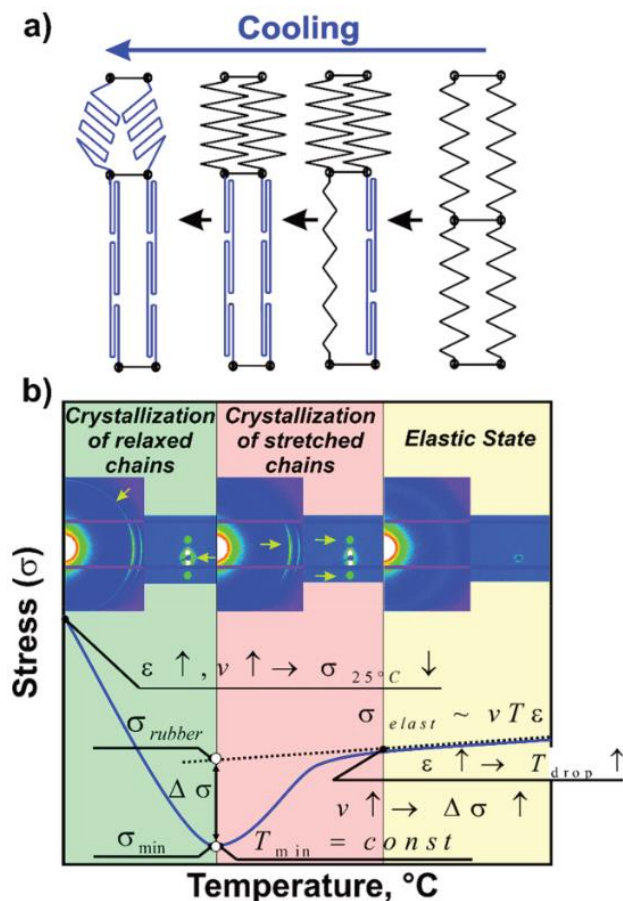


Figure 6. (a) Schematic representation of proposed crystallization mechanism for stretched cross-linked elastomers under constant strain conditions upon cooling. (b) Summary of findings and observations for constant strain experiments.

chains lying parallel to them. This process could promote the lateral extension of the nucleus and the formation of an oriented crystallite. Under further cooling the relaxed chains can eventually crystallize too with orientations in random directions. This can explain the onset of the stress increase at lower temperatures.

We note that this model would lead to a frozen-in two-phase semicrystalline sample: Highly oriented and less folded crystallites which are thermodynamically more stable coexist with a crystalline phase obtained at lower temperatures, see Figure 6a. As a direct result of this model, the degree of orientation of chains in the constant stress experiment must be larger than that in constant strain experiment. The visual analysis of 2D WAXS patterns obtained by Huang et al.¹⁹ provide experimental evidence for this.

This model provides a qualitative explanation to facts reported in our previous paper.²⁶ First, it is necessary to increase the degree of chain stretching (increase stress in the elastic state) in order to increase the stress drop—the more the chains are stretched, the larger is the elastic force provided by each strand and the greater the stress drop will be, which is confirmed by the experimental results published in our previous work.²⁶ The increase of stress in elastic state will cause more strands to crystallize in the stretched state, meaning that the onset of the stress drop shall be observed at a higher temperature, a fact which was also experimentally observed. The thus formed conclusion allows us to assume that

the largest stress drop shall be observed when polymer chains are completely stretched in elastic state. In this case, the stress must drop to zero upon crystallization, and no further increase of stress at low temperature must be observed because all chains crystallize in the stretched state. A summary of the previously mentioned findings and their explanation for the unexpected crystallization behavior of semicrystalline polymers upon constant strain is presented on Figure 6b.

4. CONCLUSIONS

In this study, we carried out a detailed research on the mechanism and characterization of the behavior of reversible shape memory effect of cross-linked PCL on constant strain mode upon cooling. We demonstrated by performing a thorough kinetic study on the crystallization of stretched polymer with very slow cooling/annealing steps that the transient state which leads to the observed stress drop ($\Delta\sigma$) happens to be a stable intermediate phase structure adopted by polymer chains upon transition from amorphous to crystalline state. The stability of this phase was proven to be not strictly conditioned by a further decrease of temperature.

SAXS and WAXS measurements together with a Voigt fitting analysis of the corresponding azimuthal profiles allowed us to determine that crystallization process occurs on a two-step course where two families of crystallites could be identified. As the stress drop is recorded a highly orientated crystalline phase is detected while the intensity of the signal height rapidly grows to ca. 80% of its final height until the force minimum is reached. Further cooling leads the measured force to arise although ordered crystallites contribution to signal's height parameter becomes monotonous from this point—indicating the outset of nonoriented crystalline domains supported on a sharp increase of the offset criterion. It was also found that width and peak position parameters are barely changing on the course of the crystallization process. The aforementioned observations were also noted for even highly stretched PCL samples though their manifestation occur at higher temperatures. Higher strain degree of the sample leads to a sharper stress drop which is proportional to the ordered crystalline phase contribution to the crystallinity degree.

A rigorous form and structure factor fitting study carried out with the collected SAXS data showed an outstanding correlation with a form factor from orientated platelets and a structure factor from a stacking disc arrangement on the meridional direction while the cooling was following its course. It was noted that the isotropic equatorial scattering—observed on 200% and 300% PCL stretched samples—sets in at the same temperature where the minimum of force was recorded; the radial averaging of equatorial response fitted properly with a structure factor from nonoriented stacked lamellae corroborating a two-stepped crystallization process.

Finally, these observations allowed us to propose a model for the crystallization process in the constant strain mode which provides a reasonable explanation to previously reported anomalous behavior. Stretched polymer chains crystallize first from the molten—elastic state producing a redistribution of stress upon the polymer network, which leads to the elongation and further crystallization of parallel-neighboring strands—anomalous stress drop. As the length of the sample remains constant, relaxed polymer chains contract and crystallize, forming unoriented lamellas increasing the measured force upon further cooling.

■ ASSOCIATED CONTENT

SI Supporting Information

The Supporting Information is available free of charge at <https://pubs.acs.org/doi/10.1021/acs.macromol.1c02564>.

Figure S1, constant strain thermal analysis of 200% strained PCL DCP 5% sample with applied cooling/heating rates of 0.5, 1, and 2 °C min⁻¹; Figure S2, ROI for azimuthal averaging in SAXS; Figure S3, ROI for radial averaging in SAXS (meridian); Table S1, fit parameters and values for the 300% sample in equatorial direction; Table S2, fit parameters and values for the 300% sample in meridional direction; Table S3, fit parameters and values for the 200% sample in equatorial direction; Table S4, fit parameters and values for the 200% sample in meridional direction; Figure S4, ROI for radial averaging in WAXS; Figure S5, fits to the radial averages to determine crystallinity; Figure S6, evolution of force first derivative upon cooling of 200% stretched PCL in constant strain; Figure S7, 200% stretched PCL WAXS azimuthal profiles with subtracted background for 55, 54, and 52 °C; Figure S8, evolution of force as well as WAXS (a) width and (b) peak position Voigt fitting parameters with temperature for 200% stretched cross-linked PCL and (c) WAXS azimuthal profiles of cross-linked PCL stretched to 200% upon cooling under constant strain; Figure S9, evolution of 200% stretched PCL (a) SAXS and (b) WAXS Voigt offset parameter as well as force with temperature upon cooling under constant strain; Figure S10, *in situ* structural studies of 300% stretched cross-linked PCL, (a) 2D SAXS (left) and 2D WAXS images (right) and temperature evolution of (b) SAXS and (c) WAXS radial patterns and (d) evolution of SAXS and WAXS height and height-offset Voigt fitting parameters and degree of crystallinity with temperature as well as dependence of WAXS Voigt parameters with force on degree of crystallinity; Figure S11, comparison of WAXS and SAXS radial patterns of cross-linked PCL stretched up to (a) 200% and (b) 300% upon cooling (PDF)

■ AUTHOR INFORMATION

Corresponding Authors

Leonid Ionov — Faculty of Engineering Science, Department of Biofabrication, University of Bayreuth, D-95447 Bayreuth, Germany; Bavarian Polymer Institute, University of Bayreuth, D-95440 Bayreuth, Germany; orcid.org/0000-0002-0770-6140; Email: leonid.ionov@uni-bayreuth.de

Martin Dulle — Jülich Centre for Neutron Science (JCNS-1/IB18), Forschungszentrum Jülich, D-52425 Jülich, Germany; Email: m.dulle@fz-juelich.de

Authors

Andrés Posada-Murcia — Faculty of Engineering Science, Department of Biofabrication, University of Bayreuth, D-95447 Bayreuth, Germany

Juan Manuel Uribe-Gomez — Faculty of Engineering Science, Department of Biofabrication, University of Bayreuth, D-95447 Bayreuth, Germany

Stephan Förster — Jülich Centre for Neutron Science (JCNS-1/IB18), Forschungszentrum Jülich, D-52425 Jülich, Germany; orcid.org/0000-0002-7323-2449

Jens-Uwe Sommer – Leibniz Institute of Polymer Research Dresden e.V., D-01069 Dresden, Germany; Faculty of Physics and Cluster of Excellence Physics of Life, TU Dresden, D-01069 Dresden, Germany; orcid.org/0000-0001-8239-3570

Complete contact information is available at:
<https://pubs.acs.org/10.1021/acs.macromol.1c02564>

Author Contributions

The manuscript was written through contributions of all authors. All authors have given approval to the final version of the manuscript.

Funding

The authors are grateful to the DFG for financial support (Grants IO 68/10-1 and IO 68/11-1, SO 277/18–1).

Notes

The authors declare no competing financial interest.

ACKNOWLEDGMENTS

The authors thank Thomas Thurn-Albrecht, Kay Saalwächter, Eva Bittrich, and Konrad Schneider for the useful discussions on the mechanism proposal and the X-ray data interpretation.

ABBREVIATIONS

2W-SME, two-way shape memory effect; 2W-SMP, two-way shape memory polymers; PCL, poly(ϵ -caprolactone); SME, shape memory effect; DCP, dicumyl peroxide; DSC, differential scanning calorimetry; XRD, X-ray diffraction analysis; WAXS, wide-angle X-ray scattering; SAXS, small-angle X-ray scattering; ROI, region of interest

REFERENCES

- (1) Kaczmarek, H.; Królikowski, B.; Klimiec, E.; Chylińska, M.; Bajer, D. Advances in the Study of Piezoelectric Polymers. *Russ. Chem. Rev.* **2019**, *88* (7), 749.
- (2) Smith, M.; Kar-Narayan, S. Piezoelectric Polymers: Theory, Challenges and Opportunities. *International Materials Reviews* **2022**, *67* (1), 65–88.
- (3) Ionov, L. Hydrogel-Based Actuators: Possibilities and Limitations. *Mater. Today* **2014**, *17* (10), 494–503.
- (4) Le, X.; Lu, W.; Zhang, J.; Chen, T. Recent Progress in Biomimetic Anisotropic Hydrogel Actuators. *Advanced Science* **2019**, *6* (5), 1801584.
- (5) Lv, H.; Leng, J.; Liu, Y.; Du, S. Shape-Memory Polymer in Response to Solution. *Adv. Eng. Mater.* **2008**, *10* (6), 592–595.
- (6) Du, H.; Zhang, J. Solvent Induced Shape Recovery of Shape Memory Polymer Based on Chemically Cross-Linked Poly(Vinyl Alcohol). *Soft Matter* **2010**, *6* (14), 3370–3376.
- (7) Wang, K.; Jia, Y.-G.; Zhao, C.; Zhu, X. X. Multiple and Two-Way Reversible Shape Memory Polymers: Design Strategies and Applications. *Prog. Mater. Sci.* **2019**, *105*, 100572.
- (8) Pandini, S.; Dioni, D.; Paderni, K.; Messori, M.; Toselli, M.; Bontempi, E.; Riccò, T. The Two-Way Shape Memory Behaviour of Crosslinked Poly(δ -Caprolactone) Systems with Largely Varied Network Density. *Journal of Intelligent Material Systems and Structures* **2016**, *27* (10), 1388–1403.
- (9) Dolynchuk, O.; Kolesov, I.; Androsch, R.; Radosch, H.-J. Kinetics and Dynamics of Two-Way Shape-Memory Behavior of Crosslinked Linear High-Density and Short-Chain Branched Polyethylenes with Regard to Crystal Orientation. *Polymer* **2015**, *79*, 146–158.
- (10) Stroganov, V.; Al-Hussein, M.; Sommer, J.-U.; Janke, A.; Zakharchenko, S.; Ionov, L. Reversible Thermosensitive Biodegradable Polymeric Actuators Based on Confined Crystallization. *Nano Lett.* **2015**, *15* (3), 1786–1790.
- (11) Fan, L. F.; Rong, M. Z.; Zhang, M. Q.; Chen, X. D. Dynamic Reversible Bonds Enable External Stress-Free Two-Way Shape Memory Effect of a Polymer Network and the Interrelated Intrinsic Self-Healability of Wider Crack and Recyclability. *J. Mater. Chem. A* **2018**, *6* (33), 16053–16063.
- (12) Biswas, A.; Aswal, V. K.; Sastry, P. U.; Rana, D.; Maiti, P. Reversible Bidirectional Shape Memory Effect in Polyurethanes through Molecular Flipping. *Macromolecules* **2016**, *49* (13), 4889–4897.
- (13) Zharinova, E.; Heuchel, M.; Weigel, T.; Gerber, D.; Kratz, K.; Lendlein, A. Water-Blown Polyurethane Foams Showing a Reversible Shape-Memory Effect. *Polymers* **2016**, *8* (12), 412.
- (14) Bothe, M.; Pretsch, T. Bidirectional Actuation of a Thermoplastic Polyurethane Elastomer. *Journal of Materials Chemistry A* **2013**, *1* (46), 14491–14497.
- (15) Chung, T.; Romo-Urbe, A.; Mather, P. T. Two-Way Reversible Shape Memory in a Semicrystalline Network. *Macromolecules* **2008**, *41* (1), 184–192.
- (16) Westbrook, K. K.; Parakh, V.; Chung, T.; Mather, P. T.; Wan, L. C.; Dunn, M. L.; Qi, H. J. Constitutive Modeling of Shape Memory Effects in Semicrystalline Polymers With Stretch Induced Crystallization. *Journal of Engineering Materials and Technology* **2010**, *132*, 041010.
- (17) Dolynchuk, O.; Kolesov, I.; Radosch, H.-J. Theoretical Description of an Anomalous Elongation During Two-Way Shape-Memory Effect in Crosslinked Semicrystalline Polymers. *Macromol. Symp.* **2014**, *346* (1), 48–58.
- (18) Kolesov, I.; Dolynchuk, O.; Jehnichen, D.; Reuter, U.; Stamm, M.; Radosch, H.-J. Changes of Crystal Structure and Morphology during Two-Way Shape-Memory Cycles in Cross-Linked Linear and Short-Chain Branched Polyethylenes. *Macromolecules* **2015**, *48* (13), 4438–4450.
- (19) Huang, M.; Dong, X.; Wang, L.; Zhao, J.; Liu, G.; Wang, D. Two-Way Shape Memory Property and Its Structural Origin of Cross-Linked Poly(α -Caprolactone). *RSC Adv.* **2014**, *4* (98), 55483–55494.
- (20) Zare, M.; Prabhakaran, M. P.; Parvin, N.; Ramakrishna, S. Thermally-Induced Two-Way Shape Memory Polymers: Mechanisms, Structures, and Applications. *Chemical Engineering Journal* **2019**, *374*, 706–720.
- (21) Bai, Y.; Zhang, X.; Wang, Q.; Wang, T. A Tough Shape Memory Polymer with Triple-Shape Memory and Two-Way Shape Memory Properties. *J. Mater. Chem. A* **2014**, *2* (13), 4771–4778.
- (22) Gao, Y.; Liu, W.; Zhu, S. Polyolefin Thermoplastics for Multiple Shape and Reversible Shape Memory. *ACS Appl. Mater. Interfaces* **2017**, *9* (5), 4882–4889.
- (23) Behl, M.; Kratz, K.; Noechel, U.; Sauter, T.; Lendlein, A. Temperature-Memory Polymer Actuators. *Proc. Natl. Acad. Sci. U.S.A.* **2013**, *110* (31), 12555–12559.
- (24) Tamagawa, H. Thermo-Responsive Two-Way Shape Changeable Polymeric Laminate. *Mater. Lett.* **2010**, *64* (6), 749–751.
- (25) Chen, S.; Hu, J.; Zhuo, H. Properties and Mechanism of Two-Way Shape Memory Polyurethane Composites. *Compos. Sci. Technol.* **2010**, *70* (10), 1437–1443.
- (26) Murcia, A. P.; Gomez, J. M. U.; Sommer, J.-U.; Ionov, L. Two-Way Shape Memory Polymers: Evolution of Stress vs Evolution of Elongation. *Macromolecules* **2021**, *54* (12), 5838–5847.
- (27) Nielsen, L. E. Cross-Linking-Effect on Physical Properties of Polymers. *Journal of Macromolecular Science, Part C* **1969**, *3* (1), 69–103.
- (28) Heeley, E. L.; Poh, C. K.; Li, W.; Maidens, A.; Bras, W.; Dolbnya, I. P.; Gleeson, A. J.; Terrill, N. J.; Fairclough, J. P. A.; Olmsted, P. D.; Ristic, R. I.; Hounslow, M. J.; Ryan, A. J. Are Metastable, Precrystallisation, Density-Fluctuations a Universal Phenomena? *Faraday Discuss.* **2003**, *122* (0), 343–361.
- (29) Heeley, E. L.; Maidens, A. V.; Olmsted, P. D.; Bras, W.; Dolbnya, I. P.; Fairclough, J. P. A.; Terrill, N. J.; Ryan, A. J. Early Stages of Crystallization in Isotactic Polypropylene. *Macromolecules* **2003**, *36* (10), 3656–3665.

- (30) Imai, M.; Kaji, K.; Kanaya, T. Orientation Fluctuations of Poly(Ethylene Terephthalate) during the Induction Period of Crystallization. *Phys. Rev. Lett.* **1993**, *71* (25), 4162–4165.
- (31) Terrill, N. J.; Fairclough, P. A.; Towns-Andrews, E.; Komanschek, B. U.; Young, R. J.; Ryan, A. J. Density Fluctuations: The Nucleation Event in Isotactic Polypropylene Crystallization. *Polymer* **1998**, *39* (11), 2381–2385.
- (32) Zhang, J.; Duan, Y.; Sato, H.; Shen, D.; Yan, S.; Noda, I.; Ozaki, Y. Initial Crystallization Mechanism of Isotactic Polystyrene from Different States. *J. Phys. Chem. B* **2005**, *109* (12), 5586–5591.
- (33) Essery, R. L. H.; Ball, R. C. Anisotropic Spinodal Decomposition. *EPL* **1991**, *16* (4), 379–384.
- (34) Zhang, Y.; Huo, H.; Li, J.; Shang, Y.; Chen, Y.; Funari, S. S.; Jiang, S. Crystallization Behavior of Poly(α -Caprolactone) and Poly(α -Caprolactone)/LiClO₄ Complexes from the Melt. *CrystEngComm* **2012**, *14* (23), 7972–7980.
- (35) Kamal, T.; Shin, T. J.; Park, S.-Y. Uniaxial Tensile Deformation of Poly(α -Caprolactone) Studied with SAXS and WAXS Techniques Using Synchrotron Radiation. *Macromolecules* **2012**, *45* (21), 8752–8759.
- (36) Plesters, J.; McCrone, W. C.; McCrone, L. B.; Delly, J. G. Polarized Light Microscopy. *Studies in Conservation* **1981**, *26*, 85.
- (37) Guinier, A.; Fournet, G. *Small-Angle Scattering of X-Rays*; Wiley: 1955.
- (38) Dolynchuk, O.; Kolesov, I.; Jehnichen, D.; Reuter, U.; Radusch, H.-J.; Sommer, J.-U. Reversible Shape-Memory Effect in Cross-Linked Linear Poly(α -Caprolactone) under Stress and Stress-Free Conditions. *Macromolecules* **2017**, *50* (10), 3841–3854.
- (39) Flory, P. J. Thermodynamics of Crystallization in High Polymers. I. Crystallization Induced by Stretching. *J. Chem. Phys.* **1947**, *15* (6), 397–408.
- (40) Gaylord, R. J. A Theory of the Stress-Induced Crystallization of Crosslinked Polymeric Networks. *J. Polym. Sci., Polym. Phys. Ed.* **1976**, *14* (10), 1827–1837.

Supporting Information for:

Mechanism of behavior of two-way shape memory polymer at constant strain conditions

*Andrés Posada-Murcia[§], Juan Manuel Uribe-Gomez[§], Stephan Förster[#], Jens-Uwe Sommer^{†, ‡, //},
Martin Dulle^{#*}, and Leonid Ionov^{§, ##*}*

[§]Faculty of Engineering Science, Department of Biofabrication, University of Bayreuth, 95447
Bayreuth, Germany

[#]Jülich Centre for Neutron Science (JCNS-1/IB18), Forschungszentrum Jülich, 52425 Jülich,
Germany

[†] Leibniz Institute of Polymer Research Dresden e. V., Hohe Straße 6, D-01069 Dresden,
Germany.

[‡]Faculty of Physics, TU Dresden, D-01069 Dresden, Germany.

^{//}Cluster of Excellence Physics of Life, TU Dresden, D-01069 Dresden, Germany.

^{##}Bavarian Polymer Institute, University of Bayreuth, 95440 Bayreuth, Germany.

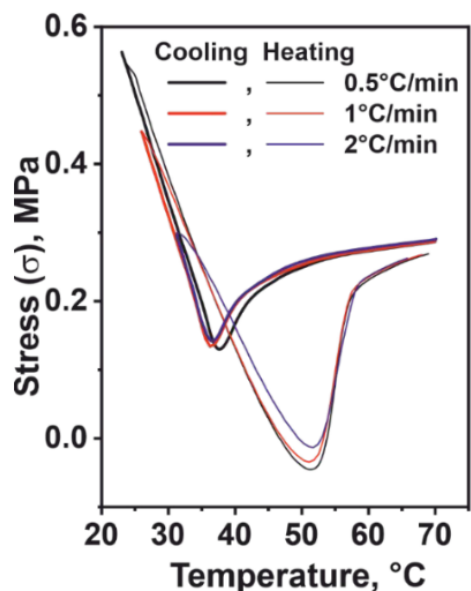


Figure S1. Constant strain thermal analysis of 200% strained PCL DCP 5% sample with applied cooling/heating rates of 0.5, 1 and 2°Cmin⁻¹.

SAXS Data reduction and Fitting Details

The SAXS measurements were recorded as 15s frames with a small dead time of ~50ms between frames. To reduce noise and have a reasonable time resolution 4 consecutive frames were summed pixel wise to yield a pattern averaging over 1minute. This was done for all measurements. These 2D patterns were reduced in two ways.

Azimuthal averaging

To quantify the degree of orientation in the sample as it was cooling down. The 2D patterns were azimuthally averaged using the q- range of the main peak developing at $q=0.4\text{nm}^{-1}$ as the peak shows a slight shift in q over the T range we investigated it we used a q range encompassing all the peak positions ($q=0.3\text{-}0.5$) over 180°.

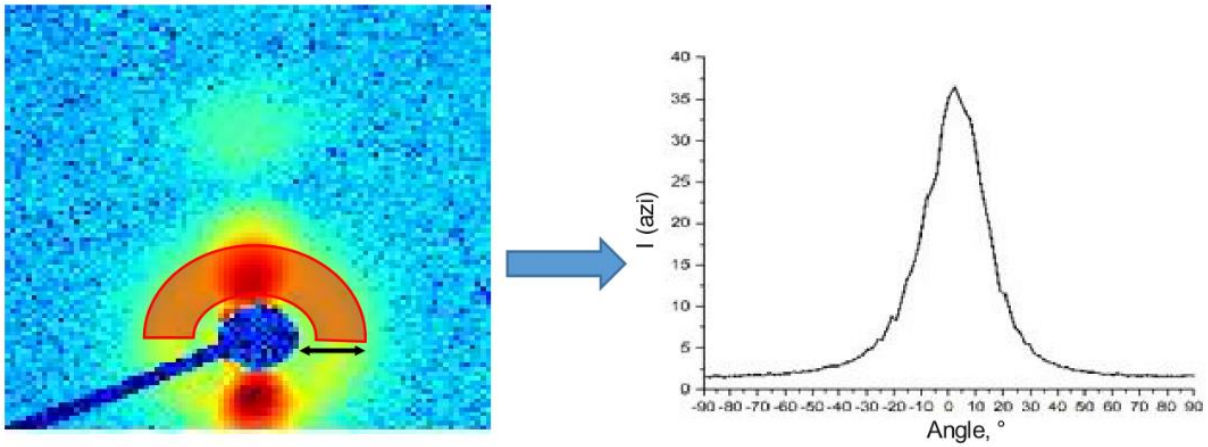


Figure S2: ROI for azimuthal averaging in SAXS.

As background the 2D pattern of the empty camera was used and averaged the same way. After scaling for exposure time the empty camera was subtracted from the sample scattering and used for the peak/orientation analysis.

Radial averaging of ROIs

In order to be able to use isotropic models for fitting the scattering of the oriented platelets has to be separated from the non-oriented and vice versa.

Starting from the last image (to see the extend of scattering around the meridian) wedge was defined and used for radial average. The width was taken from the FWHM of the azimuthally averaged data.

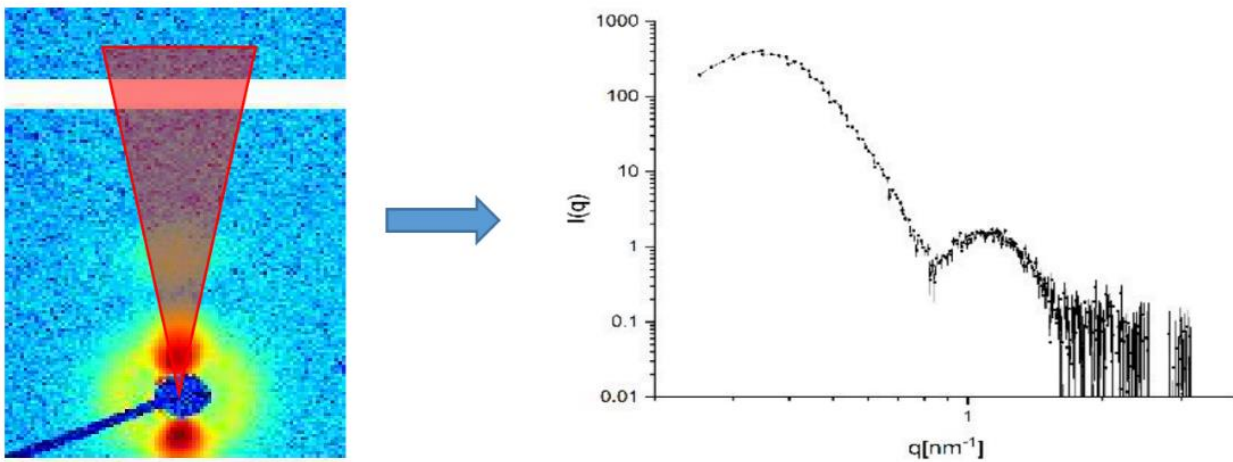


Figure S3: ROI for radial averaging in SAXS (meridian).

The same ROI was taken for the equatorial data just turned 90° clockwise.

Azimuthal peak analysis

The azimuthally averaged files were all fit with a Voigt peak function plus a constant background. This background we dubbed offset in the main text and is the signal from the non-oriented platelets that starts to show at lower T in Form of a ring on the 2D patterns. All the fits were done within Jscatter that uses scipy.optimize. Fits were done with least square method using the following parameters as fit parameters: peak position, fwhm, peak amplitude, offset, ratio of Lorentz to gauss type peak.

Full form and structure factor fitting

The radial averages of the meridional and equatorial ROIs were fit with a model for stacked thin platelets. In both cases the same model was used and due to the modified radial average we could use a radially isotropic model.

The scattering intensity is calculated for a flat radially averaged cylinder. We use the fact that we only radially averaged over the ROI to use the form factor without preferred orientation to fit the data.

$$P(q) = \frac{scale}{V_{cyl}} \int_0^{\pi/2} f^2(q, \alpha) \sin \alpha d\alpha \quad (1)$$

$$f(q, \alpha) = 2(\rho_{cyl} - \rho_{sol}) V_{cyl} j_0(q L_{enght} \cos \alpha) \frac{J_1(q r_{adius} \sin \alpha)}{(q r_{adius} \sin \alpha)} \quad (2)$$

$$V_{cyl} = \pi r^2 L \text{ and } j_0 = \frac{\sin x}{x} \quad (3)$$

Where J_1 is the first order Besselfunction, r is the radius of the disc and L is the thickness.

The scattering for a crystalline domain in the powder average is

$$I(q) = n P(q) S(q) \quad (4)$$

With n being the number density P(q) the disc form factor and S(q) the structure factor.

The structure factor is:

$$S(q) = 1 + \beta(q)(Z_0(q) - 1) * DW(q) \quad (5)$$

With $\beta(q)$ as the asymmetry factor depending on the scattering amplitude and the particle polydispersity, $DW(q)$ Debye-Waller factor.

A more detailed description can be found in Förster *et al*¹. The code to calculate the scattering is included in Jscatter².

The parameters for fitting and their values are shown in the following tables. Radius of the platelet was set to a fixed high value beyond the resolution of the experiment (200nm). The contrast was also fixed to 0.05. D is domain size, S is separation distance, thick is thickness of a single platelet, displacement is the mean square displacement within the domain.

T[°C]	scale [a.u.]	scale err	S [nm]	S_err [nm]	D [nm]	D_err [nm]	dis [nm]	dis_err[nm]	thick [nm]	thick_err [nm]	thick pd	thick pd_err
41	6.64115E-5	7.14464E-6	15.91998	0.74138	15.08029	1.18738	0.16046	0.18258	3.54279	0.29868	1.99751	0.0066
40	6.04945E-5	5.31099E-6	14.97225	0.26594	18.33896	0.8133	0.25339	0.14656	4.43175	0.21604	1.81966	0.01701
39	4.59061E-5	2.64246E-6	14.68707	0.11782	27.01467	1.27007	0.90449	0.08903	5.87983	0.09345	1.29828	0.09901
38	9.06459E-5	2.85572E-6	14.13122	0.10643	25.14894	0.77931	0.20555	0.14324	5.51862	0.08517	0.03	7.72266
37	9.31117E-5	1.96177E-6	14.00845	0.05675	34.54973	0.31101	0.68223	0.03894	6.02823	0.06164	0.66161	0.10824
36	8.65822E-5	5.82992E-6	14	0.14755	36.44167	0.03687	0.89457	0.08238	6.3256	0.12426	0.24478	0.54106
35	1.38817E-4	2.53956E-6	13.63973	0.05042	35.83251	0.02382	0.49883	0.03804	5.88822	0.06724	0.51113	0.14837
34	1.48879E-4	3.0759E-6	13.5396	0.0578	37.33652	0.01181	0.47268	0.04211	5.87343	0.08465	0.69044	0.14466
33	1.50463E-4	3.05295E-6	13.43344	0.05997	37.01439	0.01302	0.44282	0.04269	5.8845	0.08905	0.67714	0.15019
32	1.53756E-4	3.22753E-6	13.26175	0.07107	34.89242	0.07467	0.42416	0.04646	5.89537	0.09631	0.58415	0.17423
31	1.5788E-4	3.44041E-6	13.435	0.06021	36.48732	0.01679	0.35033	0.0582	5.62424	0.08925	0.0302	4.02614

Table S1: Fit parameters and values for the 300% sample in equatorial direction

T[°C]	scale [a.u.]	scale err	S [nm]	S_err [nm]	D [nm]	D_err [nm]	dis [nm]	dis_err[nm]	thick [nm]	thick_err [nm]	thick pd	thick pd_err
69	1.19E-04	3.34013E-06	19.82	0.30	26.61	1.18	0.34	0.05	8.76	0.10	0.07	0.02
68	1.34E-04	3.27126E-06	19.62	0.31	23.96	0.96	0.29	0.04	8.88	0.08	0.06	0.02
67	1.42E-04	3.97537E-06	19.81	0.42	23.62	1.10	0.30	0.05	8.84	0.09	0.04	0.03
66	1.47E-04	3.76316E-06	19.68	0.34	24.66	1.05	0.32	0.04	8.83	0.09	0.03	0.04
65	1.55E-04	3.44404E-06	19.56	0.25	25.97	0.95	0.38	0.04	8.69	0.07	0.05	0.02
64	1.75E-04	4.26723E-06	19.84	0.34	24.76	1.00	0.29	0.04	8.88	0.08	0.05	0.02
63	1.87E-04	3.71861E-06	19.67	0.24	26.06	0.87	0.29	0.04	8.75	0.07	0.04	0.02
62	2.13E-04	4.58573E-06	19.85	0.33	24.45	0.89	0.34	0.03	8.83	0.07	0.04	0.02
61	2.34E-04	4.08908E-06	19.80	0.25	25.17	0.74	0.30	0.03	8.77	0.06	0.04	0.02
60	2.68E-04	4.32748E-06	20.23	0.29	24.22	0.67	0.28	0.03	8.82	0.06	0.06	0.01
59	2.87E-04	4.21692E-06	19.91	0.20	26.36	0.67	0.29	0.03	8.68	0.05	0.03	0.02
58	3.25E-04	4.48842E-06	20.11	0.21	26.61	0.64	0.33	0.02	8.65	0.05	0.04	0.02
57	3.81E-04	4.61692E-06	19.94	0.18	26.31	0.56	0.31	0.02	8.56	0.04	0.04	0.01
56	4.49E-04	5.65263E-06	20.11	0.21	25.51	0.57	0.33	0.02	8.55	0.04	0.06	0.01
55	5.44E-04	7.0171E-06	20.01	0.22	24.72	0.56	0.27	0.02	8.54	0.04	0.08	0.01
54	6.34E-04	8.4158E-06	19.98	0.24	24.72	0.59	0.34	0.02	8.45	0.04	0.07	0.01
53	7.55E-04	8.73846E-06	20.19	0.24	24.40	0.54	0.34	0.02	8.38	0.04	0.06	0.01
52	8.40E-04	1.07617E-05	19.81	0.19	27.03	0.64	0.39	0.02	8.27	0.04	0.00	0.15

51	1.02E-03	1.22187E-05	19.68	0.22	24.31	0.55	0.33	0.02	8.28	0.04	0.06	0.01
50	1.13E-03	1.23282E-05	19.63	0.18	25.40	0.51	0.33	0.01	8.24	0.03	0.06	0.01
49	1.23E-03	1.46328E-05	19.51	0.18	25.60	0.56	0.33	0.02	8.20	0.04	0.07	0.01
48	1.32E-03	1.59219E-05	19.15	0.16	26.33	0.58	0.33	0.02	8.18	0.04	0.05	0.01
47	1.42E-03	1.66473E-05	18.81	0.13	26.99	0.58	0.32	0.02	8.18	0.04	0.06	0.01
46	1.60E-03	3.4692E-05	18.23	0.25	25.39	1.15	0.28	0.03	8.10	0.07	0.05	0.02
45	1.62E-03	2.11592E-05	18.18	0.13	27.35	0.67	0.29	0.02	8.11	0.04	0.04	0.01
44	1.69E-03	2.20322E-05	17.74	0.11	28.01	0.69	0.31	0.02	8.06	0.04	0.06	0.01
43	1.78E-03	2.29991E-05	17.37	0.11	28.26	0.72	0.28	0.02	7.96	0.04	0.00	0.13
42	1.82E-03	2.28023E-05	17.00	0.09	29.13	0.72	0.30	0.02	7.92	0.04	0.01	0.04
41	1.88E-03	2.54417E-05	16.74	0.10	29.44	0.79	0.27	0.02	7.86	0.04	0.04	0.01
40	1.67E-03	5.18412E-05	16.22	0.24	30.13	1.92	0.28	0.06	8.09	0.11	0.05	0.03
39	1.91E-03	2.46744E-05	16.30	0.08	31.30	0.83	0.29	0.02	7.81	0.04	0.03	0.02
38	1.83E-03	3.11149E-05	16.24	0.10	34.62	1.21	0.41	0.02	7.76	0.05	0.06	0.01
37	1.82E-03	3.19714E-05	16.12	0.10	35.70	1.30	0.44	0.02	7.67	0.05	0.00	0.12
36	1.79E-03	4.14699E-05	16.02	0.12	38.08	1.84	0.47	0.03	7.71	0.07	0.08	0.01
35	1.97E-03	3.16938E-05	15.58	0.07	37.70	0.01	0.28	0.04	7.66	0.08	0.05	0.02
34	1.90E-03	4.29368E-05	16.23	0.11	38.00	0.01	0.28	0.06	7.50	0.11	0.05	0.03
33	2.02E-03	3.29285E-05	15.32	0.07	37.40	0.01	0.26	0.04	7.47	0.08	0.03	0.02
32	2.02E-03	3.32774E-05	15.30	0.07	37.40	0.01	0.25	0.04	7.45	0.08	0.03	0.02
31	2.02E-03	3.38706E-05	15.24	0.07	37.40	0.01	0.26	0.04	7.43	0.08	0.03	0.03

Table S2: Fit parameters and values for the 300% sample in meridional direction

T[°C]	scale [a.u.]	scale err	S [nm]	S_err [nm]	D [nm]	D_err [nm]	dis [nm]	dis_err[nm]	thick [nm]	thick_err [nm]	thick pd	thick pd_err
39	2.29E-05	5.56E-06	12.92	2.70	12.01	2.64	0.15	0.82	5.82	0.70	1.93	0.01
38	3.06E-05	4.68E-06	12.97	0.95	15.04	1.73	0.34	0.29	5.84	0.49	1.96	0.01
37	2.26E-05	8.89E-07	14.35	0.17	36.68	0.01	1.24	0.07	6.71	0.15	1.65	0.18
36	4.00E-05	1.10E-06	14.15	0.09	37.00	0.01	0.90	0.04	6.43	0.11	1.40	0.12
35	6.62E-05	1.51E-06	13.94	0.06	36.20	0.02	0.59	0.04	6.03	0.09	0.88	0.13
34	8.36E-05	1.61E-06	13.78	0.06	36.96	0.01	0.55	0.04	6.10	0.08	0.57	0.15
33	9.21E-05	1.66E-06	13.69	0.06	36.26	0.02	0.45	0.04	6.04	0.08	0.04	2.19
32	9.16E-05	1.89E-06	13.65	0.07	36.31	0.02	0.42	0.06	6.07	0.10	0.03	3.65
31	9.07E-05	2.00E-06	13.61	0.08	36.32	0.02	0.37	0.07	6.05	0.12	0.03	4.17

Table S3: Fit parameters and values for the 200% sample in equatorial direction

T[°C]	scale [a.u.]	scale err	S [nm]	S_err [nm]	D [nm]	D_err [nm]	dis [nm]	dis_err[nm]	thick [nm]	thick_err [nm]	thick pd	thick pd_err
58	1.01E-06	2.49E-07	-	-	-	-	-	-	7.54	1.19	0.08	0.73
57	1.13E-06	3.19E-07	-	-	-	-	-	-	7.46	1.32	0.13	0.53
56	1.96E-06	2.72E-07	-	-	-	-	-	-	7.38	0.67	0.04	0.70
55	3.92E-06	2.70E-07	-	-	-	-	-	-	7.41	0.34	0.03	0.46
54	9.44E-06	2.92E-07	-	-	-	-	-	-	7.31	0.15	0.01	0.67
53	2.38E-05	3.86E-07	-	-	-	-	-	-	7.27	0.08	0.06	0.05
52	5.41E-05	5.99E-07	-	-	-	-	-	-	7.36	0.06	0.06	0.03
51	1.26E-04	1.81E-06	-	-	-	-	-	-	7.28	0.07	0.11	0.02
50	1.51E-04	4.94E-06	-	-	-	-	-	-	7.47	0.15	0.01	0.33
49	0.00117	1.48E-05	23.04	0.30	24.17	0.65	0.35	0.02	7.47	0.15	0.01	0.33
48	0.00153	2.09E-05	22.58	0.29	26.30	0.75	0.33	0.02	7.47	0.15	0.01	0.33
47	0.00186	2.56E-05	22.19	0.27	27.03	0.76	0.32	0.02	7.47	0.15	0.01	0.33
46	0.00213	3.07E-05	21.96	0.26	28.05	0.82	0.31	0.02	7.47	0.15	0.01	0.33
45	0.00236	3.59E-05	21.40	0.24	28.71	0.87	0.30	0.02	7.47	0.15	0.01	0.33
44	0.00259	4.16E-05	20.75	0.23	28.81	0.91	0.28	0.03	7.47	0.15	0.01	0.33
43	0.0028	4.32E-05	19.65	0.18	28.70	0.86	0.27	0.03	7.47	0.15	0.01	0.33
42	0.00297	4.60E-05	18.96	0.17	28.69	0.87	0.27	0.03	7.47	0.15	0.01	0.33
41	0.00305	4.65E-05	18.48	0.14	29.70	0.90	0.30	0.02	7.47	0.15	0.01	0.33
40	0.00314	4.58E-05	17.95	0.12	30.22	0.89	0.30	0.02	7.47	0.15	0.01	0.33
39	0.00319	4.64E-05	17.51	0.12	30.96	0.92	0.30	0.02	7.47	0.15	0.01	0.33
38	0.0032	4.67E-05	17.15	0.11	31.65	0.95	0.31	0.02	7.47	0.15	0.01	0.33
37	0.00322	4.71E-05	16.80	0.10	32.46	0.98	0.31	0.02	7.47	0.15	0.01	0.33
36	0.00325	4.90E-05	16.52	0.10	32.91	1.03	0.31	0.03	7.47	0.15	0.01	0.33
35	0.00326	4.95E-05	16.30	0.10	33.77	1.06	0.31	0.03	7.47	0.15	0.01	0.33
34	0.00327	5.26E-05	16.06	0.10	34.40	1.15	0.31	0.03	7.47	0.15	0.01	0.33
33	0.00324	5.33E-05	15.87	0.10	34.98	1.19	0.32	0.03	7.47	0.15	0.01	0.33
32	0.00323	5.58E-05	15.73	0.10	35.77	1.28	0.32	0.03	7.47	0.15	0.01	0.33
31	0.00322	5.67E-05	15.61	0.10	36.39	1.33	0.33	0.03	7.47	0.15	0.01	0.33

Table S4: Fit parameters and values for the 200% sample in meridional direction

WAXS Data reduction and Fitting Details

Radial averaging

As the main WAXS reflexes of the PCL crystal structure are at very high q ($>14\text{nm}^{-1}$) we had to measure them with the detector in an offset position with the primary beam off the detector area. In order to determine the center for radial average we used the final 2D patterns with a ring showing for the main reflex using the form of this ring and taking into account the detector geometry we determined the beam center. This was then used to get the radial averaged curves.

Nearly the whole detector area was used for the radial average.

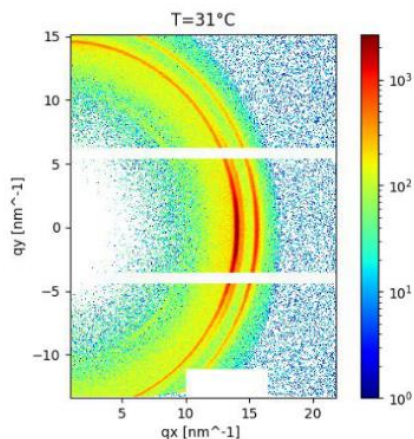


Figure S4: ROI for radial averaging in WAXS.

The radial averaged data was used to determine the degree of crystallinity within the sample. This was done by fitting the radial averages with a sum of six singular peaks, 2 broad peaks for the amorphous background and 4 for the crystalline part. The degree of crystallinity was calculated from the ratio of the areas of the crystalline peaks to the whole area of the radial average. Two examples of a whole fit series are shown here. As the two weak extra peaks were not easy to fit we chose to use the area of the whole curve and the area of the broad peak to determine the degree of crystallinity in the following way:

$$\text{Crystallinity} = \frac{\text{Area}_{full} - \text{Area}_{amorph}}{\text{Area}_{full}} \quad (6)$$

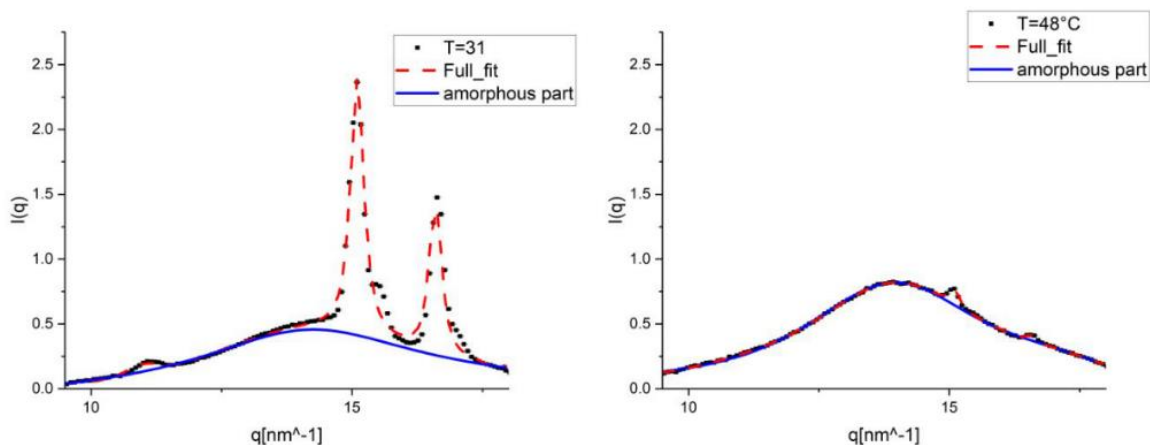


Figure S5: Fits to the radial averages to determine crystallinity.

Areas were calculated with the Simpson numerical integration of the q range from 9.5 to 18nm^{-1}

Azimuthal averaging and analysis for WAXS

We chose the main peak at $q \sim 15\text{nm}^{-1}$ for the azimuthal analysis. The width in q for averaging we got from the width of the peak in the radial average. As background to subtract we chose the average of the azimuthal plots at high T without any crystals. However also this background is changing in magnitude as the sample is cooling down. To account for this, we determined the relative decrease of amorphous background at $q = 14\text{nm}^{-1}$ for the radial average. As this is close to the actual peak and gave a scaling factor for the azimuthal background at high T otherwise the azimuthal plots would become negative except for the peak itself. With this scaling we were able to subtract the amorphous background in a meaningful way without having negative intensities.

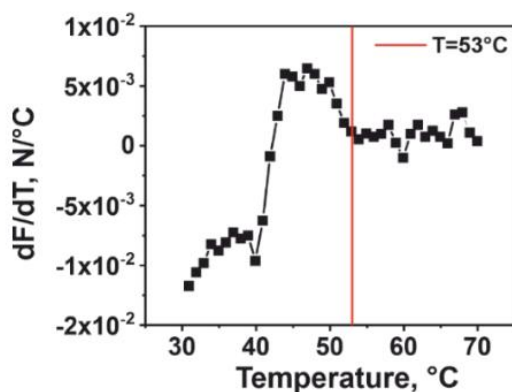


Figure S6. Evolution of force first derivate upon cooling of 200% stretched PCL in constant strain.

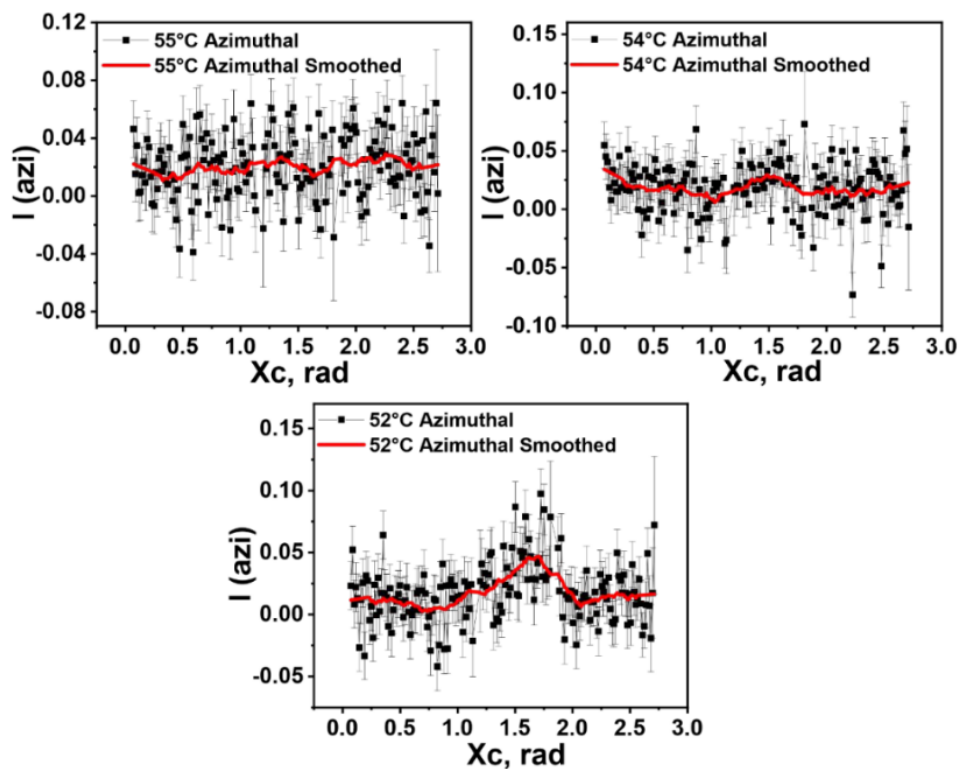


Figure S7. 200% stretched PCL WAXS azimuthal profiles with subtracted background for 55, 54 and 52°C.

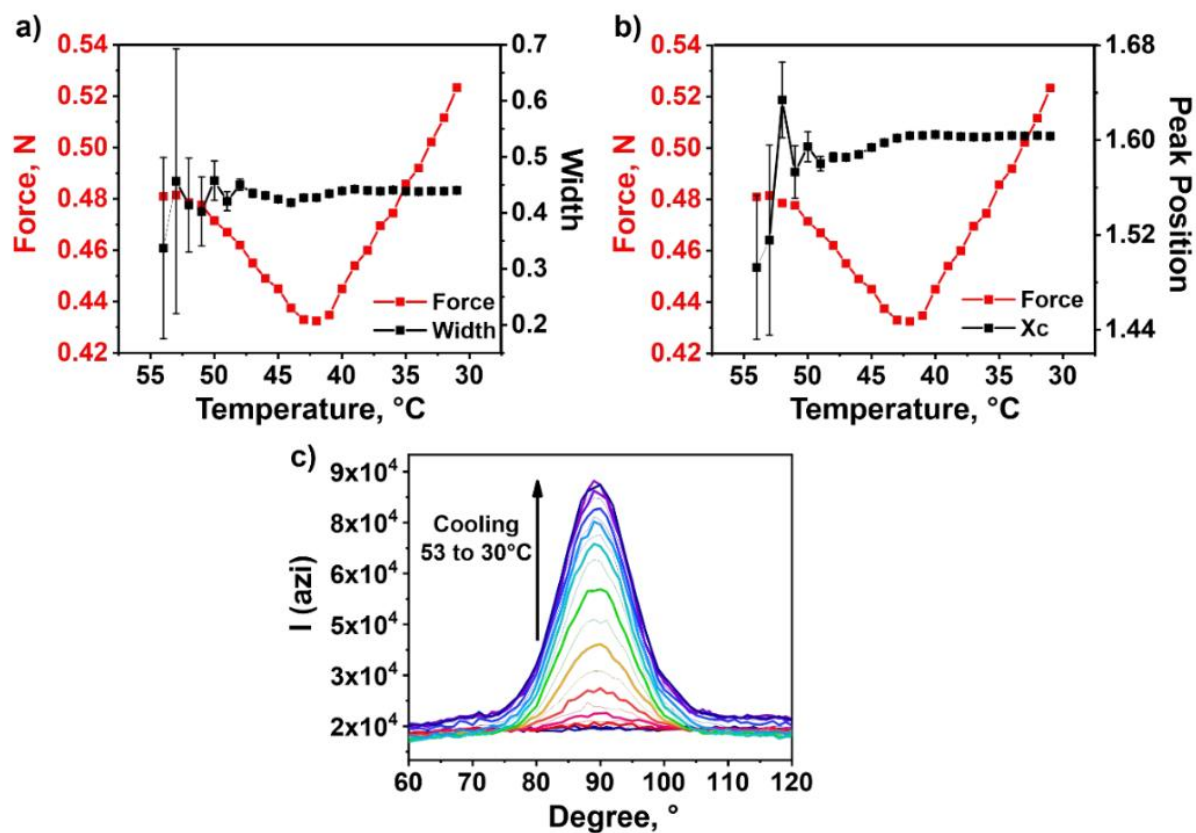


Figure S8. Evolution of force as well as WAXS (a)– width and (b)– peak position Voigt fitting parameters with temperature for 200% stretched crosslinked PCL; (c)– WAXS azimuthal profiles of cross-linked PCL stretched to 200% upon cooling under constant strain.

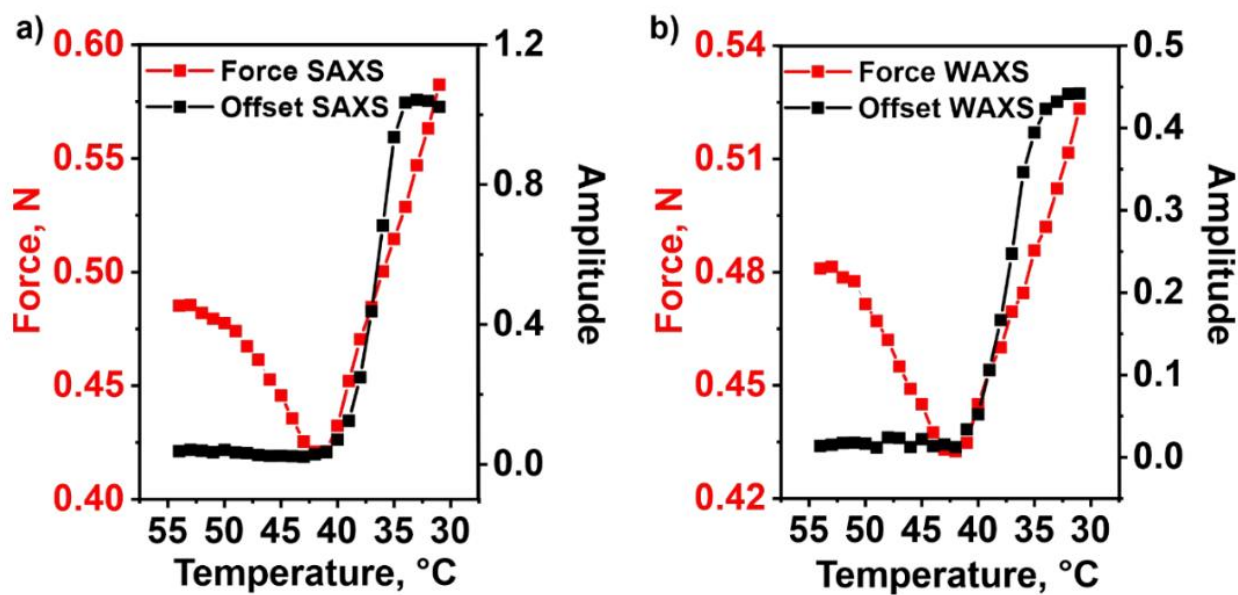


Figure S9. Evolution of 200% stretched PCL (a)–SAXS and (b)–WAXS Voigt offset parameter as well as force with temperature upon cooling under constant strain.

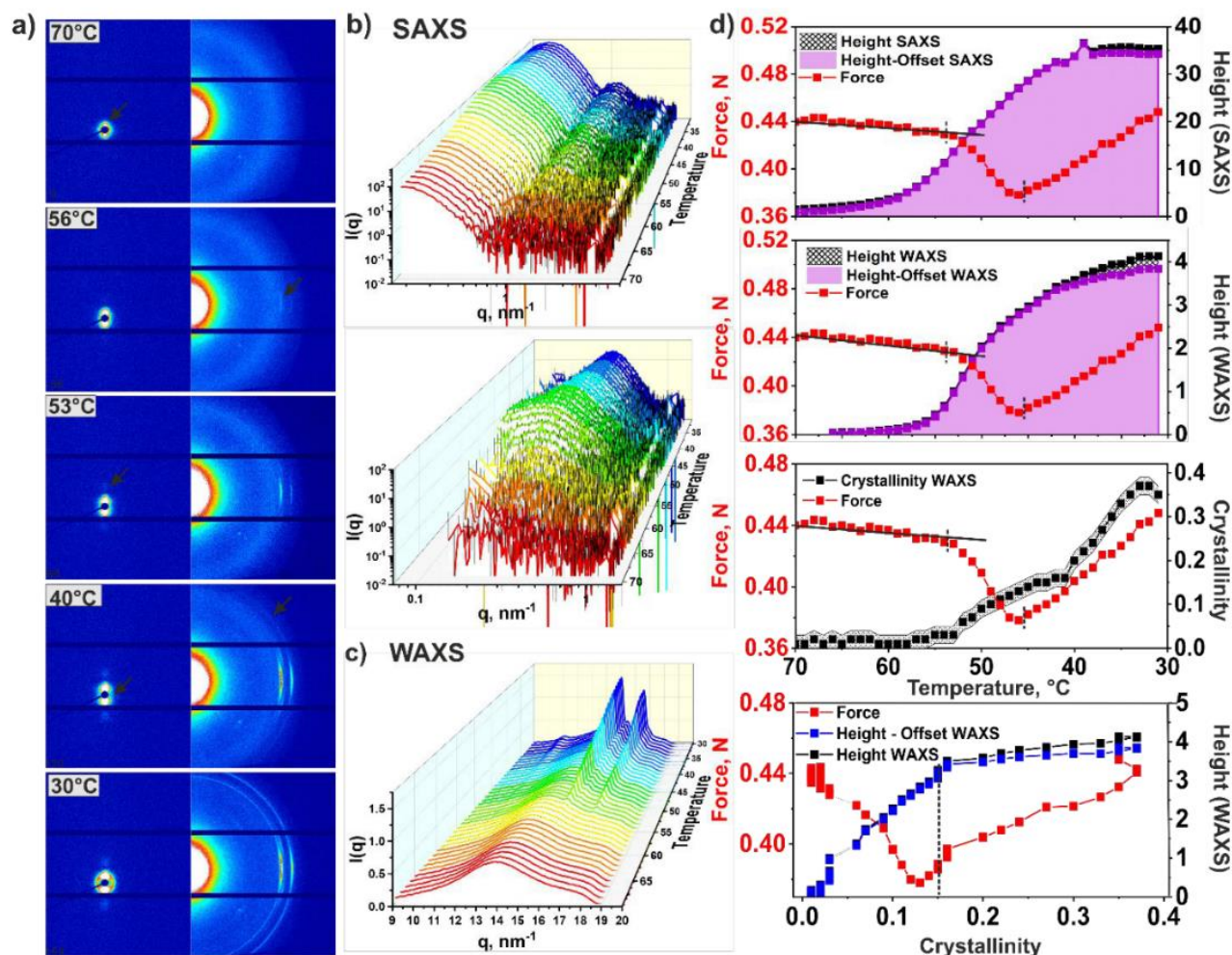


Figure S10. In-situ structural studies of 300% stretched crosslinked PCL: (a)– 2D SAXS (left) and 2D WAXS images (right); temperature evolution of (b)– SAXS and (c)– WAXS radial patterns; (d)– evolution of SAXS and WAXS height and height-offset Voigt fitting parameters and degree of crystallinity with temperature as well as dependence of WAXS Voigt parameters with force on degree of crystallinity

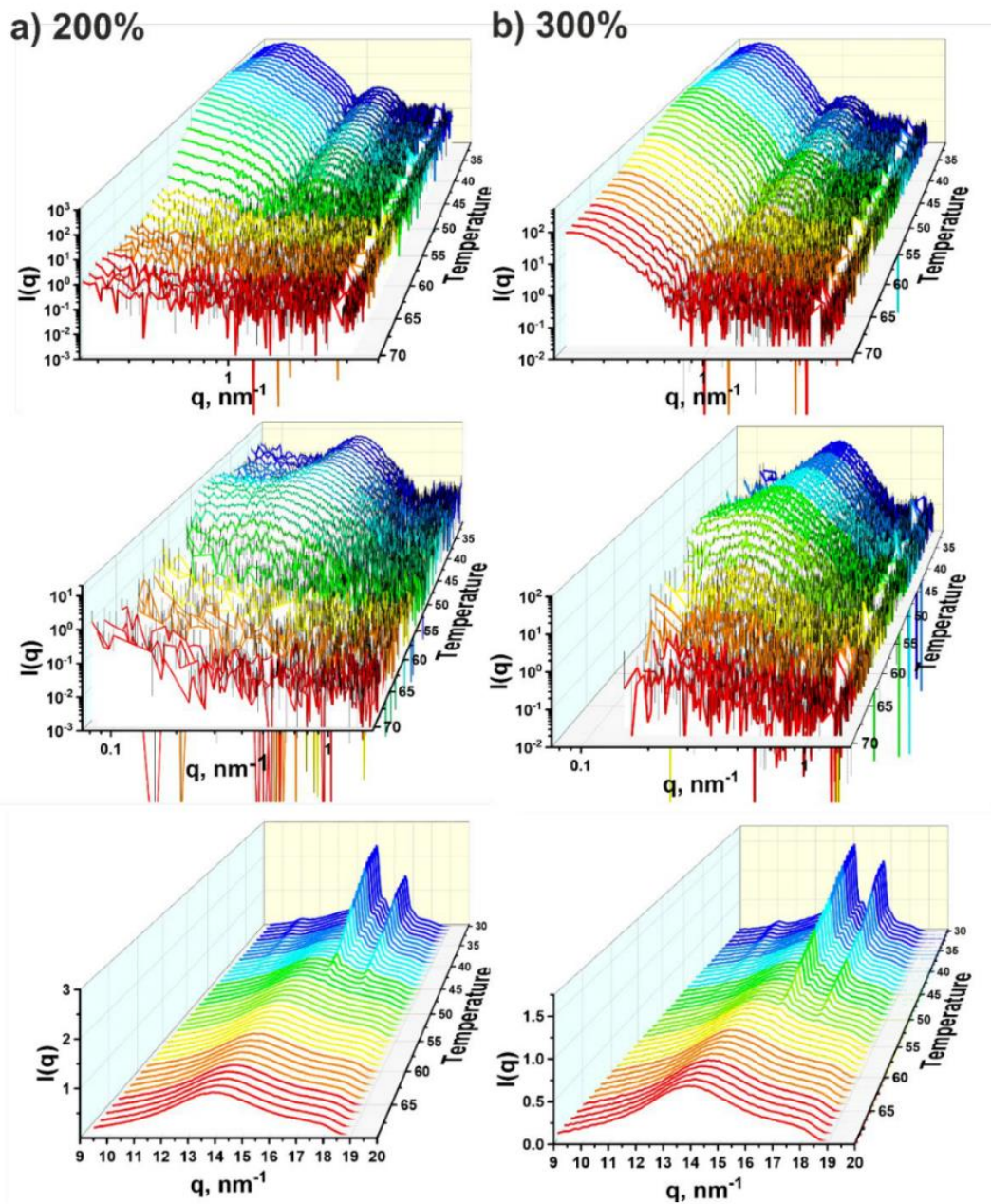


Figure S11. Comparison of WAXS and SAXS radial patterns of cross-linked PCL stretched up to (a)– 200% and (b)–300% upon cooling.

REFERENCES

- (1) Förster, S.; Timmann, A.; Konrad, M.; Schellbach, C.; Meyer, A.; Funari, S. S.; Mulvaney, P.; Knott, R. Scattering Curves of Ordered Mesoscopic Materials. *J. Phys. Chem. B* 2005, *109* (4), 1347–1360. <https://doi.org/10.1021/jp0467494>.

- (2) Biehl, R. Jscatter, a Program for Evaluation and Analysis of Experimental Data. *PLOS ONE* **2019**, *14*(6), e0218789. <https://doi.org/10.1371/journal.pone.0218789>.

Publication 3

Bidirectional shape memory polymers: effect of molecular architecture over the thermomechanical behaviour at constant stress and constant strain conditions

Andrés Posada-Murcia, Dennis Schönfeld, Yaoming Zhang, Juan Manuel Uribe-Gomez, Thorsten Pretsch and Leonid Ionov.

Submission Date: Yet to be submitted

Bidirectional shape memory polymers: effect of molecular architecture over the thermomechanical behaviour at constant stress and constant strain conditions

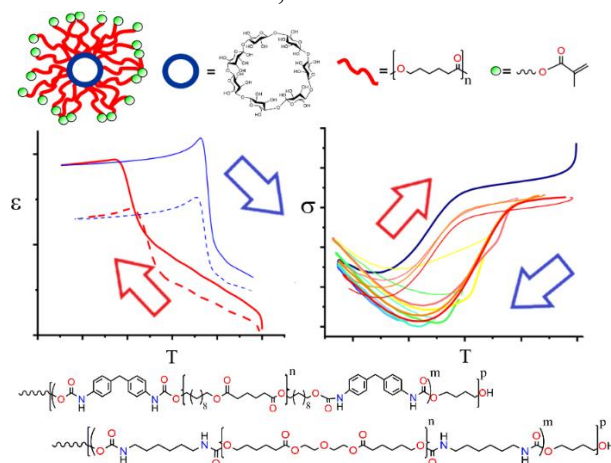
Andrés Posada-Murcia[§], Dennis Schönfeld[#], Yaoming Zhang^{†, ‡}, Juan Manuel Uribe-Gomez[§], Thorsten Pretsch[#] and Leonid Ionov^{§*}

[§]Faculty of Engineering Sciences and Bavarian Polymer Institute, University of Bayreuth, Ludwig Thoma Str. 36A, 95447, Bayreuth, Germany

[#]Fraunhofer Institute for Applied Polymer Research IAP, Geiselbergstr. 69, 14476 Potsdam, Germany

[†]Center of Materials Science and Optoelectronics Engineering, University of Chinese Academy of Sciences, Beijing, 100049, P. R. China.

[‡]State Key Laboratory of Bio-Fibers and Eco-Textiles, Qingdao University, Qingdao, 266071, P. R. China.



KEYWORDS: Actuators; shape-changing; urethanes; crystallization; shape-memory.

ABSTRACT

This report is based on the characterization and direct comparison of the thermally induced 2W-SME of two chemically crosslinked PCL-based polymers, linear and star-like polycaprolactone, together with three physically crosslinked polyurethane copolymers: two containing 14kDa PCL diol as soft segments and the remaining material is an ester urethane with 3.2kDa poly(1,4-butylene adipate) as semicrystalline domains. The PCL-based chemically crosslinked networks presented in general soft elastomeric extensional properties on molten state while the studied polyurethane systems exhibited a stiffer and more rigid character. It was found that the incorporation of the urethane amorphous domains has a stronger crosslinking effect over the thermomechanical and physicochemical properties of semicrystalline polymer networks than the thermal curing process, especially the insertion of the aromatic diphenylmethane diisocyanate. All evaluated materials showed bidirectional shape memory properties under constant stress and strain conditions. The revision of the gathered data allowed the identification of the parameters that primarily rule the reversible shape shifting properties of constantly strained semicrystalline polymer networks regardless their molecular architecture.

1. INTRODUCTION.

Smart or intelligent materials are functional and designed materials able to significantly modify at least one of their properties in a controlled manner as a response to an external stimulus such as change of pH^{1,2}, electric field^{3,4}, magnetic field^{5,6}, light^{7,8} or changes of temperature^{9,10}. The shape memory polymers (SMPs) are one kind of such intelligent polymers. Specifically, SMPs undergo a shape-shifting transformation from one or more

programed temporary shapes to the recovery of their original form, the shape memory effect (SME) on this kind of materials is commonly thermally triggered. In most of the SMPs the shape transformation is typically unidirectional or in one way, meaning that the shifting between the programmed and the original shape is not reversible and requires an external force to cycle^{11,12}. Therefore, two-way shape memory polymers (TW-SMPs), which are able to undergo reversible shape transformation, attract growing attention due to their potential application in soft-robotics, multifunctional optical components, biomedical scaffolds among others¹³⁻¹⁵.

The origin of the thermally induced reversible SME on semicrystalline polymer networks is based on the conformational transformations suffered by polymer chains exposed to mechanical load while undergoing a phase transition e.g., from molten to crystalline state^{16,17}. Loading can be caused by applying of external stress or by using bi-component materials with intrinsic stress: one of the components is programmed and kept on stretched state while its counterpart serves as scaffold. Melting of polymer chains results in the transition to random coil conformation and contraction of polymer that also deforms scaffold, crystallization results in stretching of polymer chains and recovery of deformed scaffold.¹⁸ Other ways to induce residual stress on multicomponent materials are based on the difference between the melting temperatures of their components, the partial melting/crystallization of interpenetrated crystalline domains or the co-crystallization of random copolymers containing crosslinked elastomers¹⁹⁻²⁴.

Any stretched crosslinked crystallizing polymer can act as two-way shape memory polymer. The crosslinking points act as cleavage amorphous zones between the force-orientated semicrystalline domains which expand upon crystallization and contract on molten state supported by the entropic nature of the polymer chains elasticity on a thermal cycle.^{25,26} There are many reports of design and investigation of two-way shape memory actuators based on crosslinked polycaprolactone (PCL) semicrystalline networks. It is widely reported that the amplitude of actuation of these cured PCL network is strongly dependent of the applied load, strain and crosslinking density.²⁷⁻³³ Also, urethane-based polyurethanes copolymers, especially the ones containing PCL (PCL-PU)s, are extensively researched shape-memory materials due to their large strain reversibility, great processability, shape stability and tailorable elastic properties³⁴⁻³⁹. The mechanism behind the actuation of this copolymers lays on their phase segregated morphology: A soft elastic semicrystalline phase with lower transition temperature (T_{trans}) acts as molecular switch through melting/crystallization of its crystalline domains, embowed by an amorphous rigid phase with high T_{trans} which enhances the mechanical properties of the material as maintains its shape integrity during thermal cycling.

Unfortunately, a direct comparison of the 2W-SME features of materials with diverse chemical nature and actuation mechanism is in most of the cases not possible as the experimental setups require specific or way different conditions to be driven along with the great variety of post-processing steps involved on their isolation/manufacture. The goal of this paper is to elucidate the effect of the chemical structure of two-way shape memory polymers on their actuation properties. Thus, a comparative investigation on the

thermomechanical properties between chemically crosslinked PCL-based linear and star-like semicrystalline polymer networks together with physically crosslinked semicrystalline polyurethanes at constant stress and constant strain conditions was driven.

2. EXPERIMENTAL SECTION

2.1 Materials. Linear ϵ -polycaprolactone (PCL) (Average Mn = 80kDa, Sigma-Aldrich), functionalized β -cyclodextrin nuclei-based polymer grafted with 21 acrylate-terminal polycaprolactone arms (CD-PCL) (Average Mn = 386 kDa - supplied by Yaoming Zhang Key Laboratory of Solid Lubrication, Lanzhou Institute of Chemical Physics, Chinese Academy of Sciences, Lanzhou 730000, P. R. China), Dicumyl peroxide (DCP) (98%, Sigma-Aldrich), ϵ -caprolactone (ϵ -CL) (97%), Diethylene glycol (DEG), Ammonium heptamolybdate tetrahydrate ($(\text{NH}_4)_6\text{Mo}_7\text{O}_{24}\cdot 4\text{H}_2\text{O}$), Hexamethylene diisocyanate (HDI) (98%), 4,4'- diphenylmethane diisocyanate (MDI) (98%), 1,4-Butanediol (BD) (99%), Dibutyltin dilaurate (DBTDL) (95%), anhydrous Dimethyl sulfoxide (DMSO) (99.9%), anhydrous N,N-Dimethylformamide (DMF) (99.8%) and 2-Propanol (IPA) acquired from Sigma-Aldrich and subsequently used as received without any additional treatment/processing. Finally, TPU-PDA 25 (Polyester urethane based on poly(1,10-decylene adipate) diol (PDA) as SS and MDI+BD (25wt%) as HS) was supplied by Dr. Thorsten Pretsch and Dennis Schönfeld (Fraunhofer Institute for Applied Polymer Research IAP, Geiselbergstr. 69, 14476 Potsdam, Germany). A summary of the investigated materials is found on **Figure 1**.

2.2 Synthesis of star-like copolymer. CD-PCL was obtained by a multi stepped synthesis methodology⁴⁰, a macrocyclic nucleus of β -cyclodextrin composed by 7 glucose subunits was used as initiator on the ring opening polymerization of ϵ -caprolactone catalyzed by stannous octoate ($\text{Sn}(\text{Oct})_2$) to obtain a 21 PCL hydroxyl terminated-armed star polymer. In a final step, the OH-end groups were methacrylated by an esterification reaction with methacryloyl chloride resulting in the obtention of an acrylate-ended PCL β -cyclodextrin star-like polymer.

2.3 Preparation of chemically cross-linked samples. PCL and CD-PCL were dissolved in chloroform (99%, Sigma-Aldrich) and mixed with different proportions of crosslinking agent (Error! Reference source not found.). Afterwards, these solutions were allowed to dry on flat glass recipients providing uniform solid waxy sheets where 10 x 8mm probes with $\sim 0.7\text{mm}$ of average thickness were obtained for both materials. Lastly, the rectangular samples containing DCP were cured at 160°C 2h in a vacuum oven.

2.4 Synthesis of PCL diol. The synthesis of high molecular weight hydroxyl-ended poly(ϵ -caprolactone) was carried out following a previously reported methodology⁴¹ consisting on the solvent-free ring opening polymerization of ϵ -CL monomer with DEG as initiator and ammonium heptamolybdate tetrahydrate as catalyst (ϵ -CL:DEG:Mo (mmol): $175:1:8.7 \times 10^{-3}$). The obtained material was characterized by ^1H NMR, while its molecular weight was estimated by gel permeation chromatography (GPC) and ^1H NMR.

2.5 Synthesis of PCL diol-based polyester urethanes (PCL-PU). PCL-based polyurethane based materials were synthesized according to the prepolymer method⁴²⁻⁴⁴.

Four HMW PCL diol-based PUs with different hard segment content consisting of HDI+BD and MDI+BD (**Table 1**) were synthesized under inert atmosphere on a two-necked round flask. Pre-polymerization process was carried for 4h at 70°C allowing HMW PCL diol react with the corresponding diisocyanate adding small portions of anhydrous DMSO to allow a proper stirring. After this, BD as chain extender along with DBTDL as catalyst (0.05 wt% with respect to PCL diol) were incorporated dropwise to the mixture containing the prepolymer. The final stage of the reaction lasted 24h at 70°C after the last drop of BD+DBTDL on DMSO was added. The resulting polymers were isolated by precipitation on an excess of distilled water, followed by quenching/washing on IPA for 3 days and finally dried on a vacuum oven at 70°C for 3 days. Estimation of HSC% of dry PCL-PUs along with their characterization was done by ¹H NMR (**Table 1**), without exception all materials exhibited a unimodal molecular weight distribution (**Figure S1**).

2.6 Synthesis of TPU-PDA 25. The synthesis of the PDA-based urethane was also carried out by the prepolymer methodology, first the poly(1,10-decylene adipate) diol (PDA) monomer was synthesized by the reaction of 1,10-Decanediol and adipic acid under nitrogen atmosphere. After the isolation of PDA, its reaction with MDI was allowed permitting the obtention of the corresponding isocyanate-ended prepolymer. By the subsequent addition of 1,4 butanediol as chain extender, the obtention of a polyester urethane with 25%wt of hard segment content was completed.⁴⁵

2.7 Nuclear magnetic resonance (NMR). The characterization of the synthesized materials was accomplished by proton nuclear magnetic resonance (¹H NMR), the essays were performed on a Bruker Avance 500 spectrometer (500.16 MHz for ¹H) (Bruker BioSpin

GmbH, Germany). Proton chemical shifts (δ) are reported in parts per million (ppm) relative to tetramethylsilane (TMS), for PCL diol ^1H NMR spectrum the residual solvent peak used as an internal reference was 7.26ppm (s) as CDCl_3 was used as solvent. On the other hand, the family of synthesized PCL-PU were solubilized on DMSO-d_6 , the materials containing HDI+BD as HS exhibited the following features: (500MHz, DMSO-d_6 , δ): 7.04 (s), 3.94 (s), 2.96 (s), 2.56 (s), 1.59–1.49 (m), 1.35–1.22 (m) corresponding to the polyurethane section while the peaks located on 4.00ppm (t) and 2.28ppm (t) correspond solely to the PCL backbone. Finally, the obtained NMR data for PCL-PU containing MDI+BD is presented as follows: (500MHz, DMSO-d_6 , δ): 9.51 (s), 8.51 (s), 7.34 (t), 7.09 (t), 4.09 (s), 3.78 (s), 2.54 (s) for the hard segment of the copolymer; signals located on 3.97 (t), 2.26 (t), 1.53 (m) and 1.28 (m) belong to the PCL diol. The aforementioned spectra are displayed on **Figure S2**.

2.8 Gel permeation chromatography (GPC). The molecular weight distribution of yielded PCL diol and related PU's was assessed by gel permeation chromatography using a device with the following specifications: 2 PSS-GRAM gel column with a particle size of 10 μm and a porosity ranging from 100 to 3000 \AA (PSS, Mainz, Germany) coupled with a refractive index detector (Agilent Technologies). HPLC grade DMF containing lithium bromide (5 g/L) was used as eluting solvent, a flow rate of 0.5 mL/min was fixed, while toluene (HPLC grade) was used as internal standard. An injection volume of 20 μL was used for performing all the measurements. Prior to injection all samples were dissolved in DMF and filtered through a 0.22 μm PTFE filter. The calibration was performed with a poly(methyl methacrylate) (PMMA) standard (PSS GPC/SEC Calibration Kit). The information extracted from the obtained chromatograms is condensed on **Table S2**.

2.9 Thermogravimetric analysis (TGA). Investigation of the thermal decomposition profiles of all synthesized materials was conducted on a TG 209 F3 Tarsus (NETZSCH, Germany). Probes were heated from 25 to 700 °C at a heating rate of 10 °C/min under N₂ atmosphere while the mass loss was recorded over time, **Table 2** and **Figure S3**. The mass content of HS and SS for PCL-PU was corroborated by the Gaussian fitting of the deconvoluted DTGA curves.

2.10 Differential scanning calorimetry (DSC). Thermal analysis of all materials was performed on a DSC3 (Mettler Toledo, USA) using a three-stepped program: Samples were first heated from 0 to 100 °C then cooled from 100 to 0 °C and finally heated again from 0 to 100 °C with a heating-cooling rate of 1°C min⁻¹ under nitrogen atmosphere. The acquired data for PCL-PU is displayed on **Table 3** while the thermal properties of crosslinked polymers are consigned on **Table S1**. The acquired thermograms and derived data are displayed on **Figure 2** and **Figures S4, S5**.

2.11 Preparation of PCL-PU samples for mechanical testing. Among the produced polymers only PCL-PU(HDI+BD) 70:30 and PCL-PU(MDI+BD) 70:30 were suitable for the production of films. These materials, along with TPU-PDA 25, were dissolved on DMF under magnetic stirring until homogeneous solutions were obtained. These solutions were dried overnight at 80°C on top of a flat glass dish obtaining homogeneous solid films. After drying for 3 days on a vacuum oven at 60°C, 10 x 8mm rectangular specimens were acquired from the dried films with an average thickness of 0.5mm.

In order to accomplish a structured characterization between the selected materials and considering the limited extensional properties of PCL:PU (MDI+BD) 70:30 the mechanical

tests were conducted at low and high strain degrees -50% and 200% of elongation respectively- with the thermal conditions presented on **Table S3**.

2.12 Tensile testing. The mechanical characterization of the studied crosslinked and phase-segregated polymers was driven on a Dynamic Mechanical Analyzer MCR 702 MultiDrive (Anton Paar, Austria) equipped with Solid Rectangular Fixtures (SRF5) and a temperature-controlled chamber (CTD 600 TDR) on tensile testing mode. The non-stretched specimens were heated and annealed for 10min above their corresponding T_m (semicrystalline domains of polymers on molten state according to DSC results) before their stress-strain curves were acquired, the results are displayed in **Figure S6** and **Table S4**. Additionally, the tensile properties of the picked copolymers were studied at room temperature by initially extending the samples up to 5% of their original length with a strain rate of $1\% \text{ min}^{-1}$ followed by a rate of $2000\% \text{ min}^{-1}$ until reaching a final strain of 1200% (**Figure S6**).

2.13 TW-SME evaluation. The thermally-induced reversible shape memory effect of investigated materials under constant strain was demonstrated by applying a cyclic thermomechanical program which goes as follows: (1) An non-stretched clamped specimen was heated and annealed above its transition temperature for 10min (2) The sample was strained to a certain extension degree (in agreement with the previously obtained σ vs ϵ profiles) (3) The strained sample was allowed to crystallize by cooling it down to ca25°C maintaining its length constant while the evolution of the extensional stress upon cooling was being evaluated (4) Lastly, the probe was heated again up to the initial temperature on constant strain as σ was acquired during the heating course. A heating/cooling ramp of 1°Cmin^{-1} was used for all the experiments. Analogously, the mechanical behavior under

constant stress of the polymers was carried out using the same cyclic thermal program. The obtained results of the bidirectional SME evaluation under constant strain and constant stress of the studied materials are depicted on **Figures 3, 4** and consigned on **Table 4**. For comparison purposes, the 2W-SME features of the highly and less crosslinked CD-PCL materials were evaluated.

2.14 Thermomechanical cyclic essays. Constantly strained copolymers were subdued to 8 consecutive thermal cycles in order to evaluate the reversibility of their actuation - represented as reversible response of stress after one heating/cooling step. Initially, all samples were strained on molten state (T_i), accordingly to their stress-strain profiles, and allowed to crystallize under constant strain conditions by cooling them down to 27°C. After cooling, the constantly drawn polymers were subjected to successive thermal cycling; each cycle consisted on a coupled heating/cooling ramp (1°Cmin^{-1}) between a lower and a higher temperature limit, (T_L) and (T_H) correspondingly. T_L on all cases was set to ca27°C while T_H was increased by 5°C after a cycle completion starting from 35°C until 70°C, extensional stress was measured during the whole experiment. Linear PCL DCP5% was tested as a reference. The evolution of extensional stress upon cooling during the successive thermal cycling is shown of **Figure 5** while the complete heating/cooling steps are presented on **Figure S7**.

2.15 Stress relaxation tests. Stress relaxation test were performed for the selected copolymers on molten state (**Figure S8**), the response of the mechanical stress after an applied uniaxial deformation was followed within a window of time as follows: The probes were heated up above their T_m and annealed for 10min, then, the samples were stretched -at the same extension degree used for their evaluation of TW-SME under constant strain and

kept in drawn state while the mechanical stress was isothermally recorded for a period of 10.000s. For the sake of comparison, the relaxation profiles of linear PCL DCP5% and CD-PCL DCP 8% were acquired as well. the stress relaxation profiles of the investigated polymers were fitted using a three exponential decay model, the obtained parameters are presented on **Table 5**.

3.RESULTS AND DISCUSSION

In this paper we compared bidirectional actuation behavior of 5 kinds of shape memory polymers depicted on **Figure 1**. Two of them are chemically crosslinked polymers: (I) linear polycaprolactone (linear PCL); (II) star-like polycaprolactone (CD-PCL). The remaining three polymers are physically crosslinked polyurethane-polyesters: (III) copolymer of PCL diol (MW = 14 kDa), hexamethylene diisocyanate and butanediol (PCL-PU) (HDI+BD); (IV) copolymer of PCL diol (Mn = 14 kDa), methylene diphenyl diisocyanate and butanediol (PCL-PU) (HDI+BD) and (V) copolymer of poly(1,4-butylene adipate) (Mn = 3.2 kDa) with methylene diphenyl diisocyanate and butanediol (TPU-PDA 25).

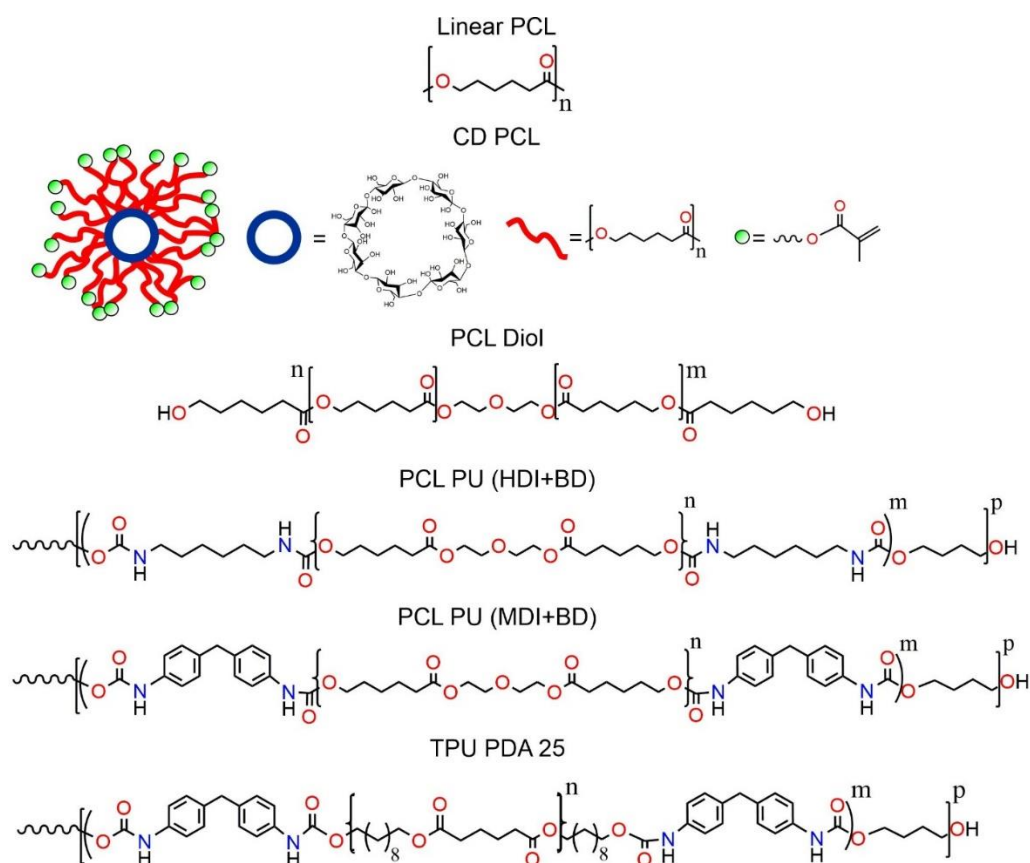


Figure 1. Chemical formulas of bidirectional shape memory polymers

PCL diol used for synthesis of polyurethane was synthesized by ring opening polymerization. The synthesized PCL diol was characterized by ^1H NMR, the obtained spectra exhibited the expected and distinguishable signals for the protons contained on the methylene groups of the PCL backbone, DEG section and the hydroxyl terminal groups⁴⁶; the estimation of its number average molecular mass (M_n) was determined by the end-group analysis methodology^{47,48} ($\approx 1.31 \times 10^4 \text{ g mol}^{-1}$) showing a good correlation with the obtained M_n value assessed by GPC for this material (**Table S2, Figure S1**). Polyurethanes were synthesized according to the prepolymer method which consists on a two-stepped reaction where an

isocyanate-terminated prepolymer is obtained in the first step by the reaction of an hydroxy-terminated oligoester with an excess of a low molecular weight diisocyanate; subsequently a low molecular weight diol is added as chain extender to further couple with the previously obtained pre-polymer and hence, increase the molecular weight of the final ester-urethane copolymer.

Correspondingly, the spectroscopic characterization of the block copolymers derived from PCL allowed the estimation of the hard segment content (HDI/MDI+BD) on each material by means of the integration of isolated signals from the PCL fragment (soft segment) and its correlation with the significance of identifiable signals from BD and HDI/MDI sections on the synthesized materials. The assessed ratios between soft and hard segments showed an excellent correlation with the theoretical composition in mass percentage for all PCL-PU as depicted on **Table 1**, confirming the successful isolation of the desired urethane-copolymers.

Table 1. Proposed and experimentally acquired hard segment composition of synthesized polyurethane-based shape memory polymers by ¹H NMR analysis.

Name	Molar Ratio ^b	Hard segment content (%) ^a	
		Theoretical	Experimental
PCL-PU (HDI+BD) 70:30	0.15 : 3.51 : 3.33	30	27.5
PCL-PU (HDI+BD) 50:50	0.10 : 5.83 : 5.71	50	49.1
PCL-PU (HDI+BD) 30:70	0.06 : 8.15 : 8	70	65.3
PCL-PU (MDI+BD) 70:30	0.15 : 2.67 : 2.56	30	33.7

^aHard segment content mass fraction; ^bPCL: HS: BD mmol

On all cases the obtained PCL-PU exhibited a unimodal distribution profile (**Figure S1**) according to the performed GPC analysis, the obtained dispersity (Đ) values (**Table S2**) denote an intermediate molecular weight distribution (Đ < 2) for these materials. The weight-

average molecular weight of PCL-PU_s (HDI+BD) family increases accordingly as their SS content also increases varying from $M_w \approx 5.0 \times 10^4$ to $8.8 \times 10^4 \text{ g mol}^{-1}$; the copolymer derived from MDI exhibits the narrowest molecular weight distribution among all synthesized PCL-PU_s with a $\bar{D} \approx 1.4$, this fact can be related with the rigidity of aromatic C-C bonds contained on the MDI which leads to the obtention of less branched and more rigid polyurethanes over analogue urethane block polymers containing aliphatic isocyanates such as HDI which are more crystalline, softer and highly elastic^{49,50}.

3.1 Thermal and calorimetric characterization: Data derived from the TGA analysis of the produced materials is presented on **Table 2** and **Figure S3**, the DTGA profile of HMW PCL diol showed a main decomposition process around 400°C featuring a shoulder at lower temperature (ca323°C) which has been reported as a two-stepped decomposition mechanism for analogue PCL⁵¹ and a reasonable range of temperature for PCL diol thermal decomposition⁵². On the other hand, all PCL-PU_s exhibited a three-step decomposition mechanism with temperature as showed on **Figure S3** and thermal stability above 300°C. The first step was identified as dissociation and further cleavage of urethane bonds⁵³, the second and third observable mass loses were assigned to the thermal decomposition of PCL diol on PU block copolymers⁵⁴.

DTGA curves of produced copolymers were deconvoluted using a Gaussian fitting to estimate the percentage of mass loss on each degradation step (**Table 2**), for PCL-PU_s (HDI+BD) family the applied fitting showed that the assigned mass loses are in good agreement with the proposed order and mass content of HS and SS for these materials. Thus, the magnitude of the first degradation step increases as the mass fraction of PU increases.

For PCL-PU (MDI+BD) 70:30 the applied model was not quite accurate as MDI's thermal degradation occurs at higher temperatures overlapping with the SS decomposition temperature range, additionally, its decomposition mechanism involves more steps than its aliphatic counterpart due to its aromatic nature⁵⁵.

Table 2. TGA results of polyurethane-based shape memory polymers

Name	Temperature Degradation Step (°C)			Mass Fraction TGA (%)			Mass Fraction Theoretical (%)	
	Steps			Steps			Segment	
	1	2	3	1	2	3	Hard	Soft
PCL diol 14kDa	323	406	-	20.6	79.4	-	-	-
PCL-PU (HDI+BD) 70:30	387	404	548	31.5	65.2	3.3	30	70
PCL-PU (HDI+BD) 50:50	409	431	542	60.7	34.8	4.5	50	50
PCL-PU (HDI+BD) 30:70	403	432	538	67.1	28.3	4.6	70	30
PCL-PU (MDI+BD) 70:30	399	496	539	91.1	3.5	5.4	30	70

Thermal properties of studied polymer were investigated using differential scanning calorimetry (DSC). It was found that melting and crystallization temperature of chemically crosslinked PCLs decrease as the amount of crosslinker arises (**Figures 2a, 2b** and **S4**). For CD-PCLs this effect is way more notorious than for linear PCLs where the transition temperatures barely vary (transition temperature varies in the range ± 2 °C). On the other hand, it was observed that the crosslinking process decreases considerably the crystallization enthalpy (ΔH_c) and degree of crystallinity (X_c) of linear PCLs in comparison with the CD-PCLs. The progressive diminishment on the transition temperatures, ΔH_c , crystallinity, and

the enthalpy of fusion (ΔH_f), as illustrated on **Figure S5**, with increasing content of crosslinker agent is an expected and well-known effect on semicrystalline networks. The newly formed net points among the polymer chains restrict their mobility inducing a hindered crystallization, thus augmenting the amorphous character of the polymer network.³⁰ In general, the star-like PCL samples exhibited an enhanced crystallinity over their linear analogues, the star-shaped architecture of the CD-PCLs increases the amount of possible molecular conformations lessening partially the restraining effect of the crosslinking process.

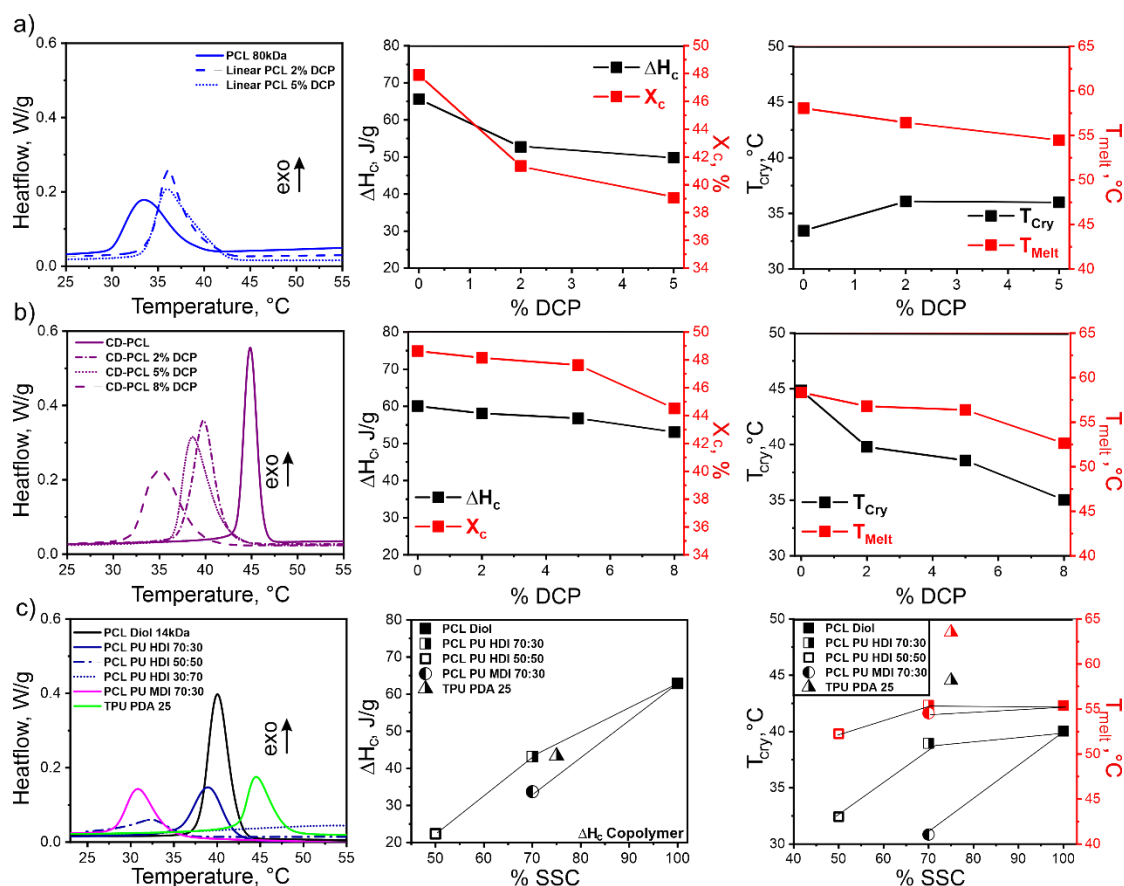


Figure 2. Thermal properties of bidirectional shape memory polymers: Upper panel (a)– Crosslinked Linear PCL; Middle panel (b)– Crosslinked CD-PCLs; Lower Panel (c)– PCL-PU and TPU-PDA 25.

The investigation of thermal properties for the synthesized HMW PCL diol along with its polyurethanes was conducted (**Figures 2c, S4**), while the acquired data is consigned on **Table 3**. The data collected from the calorimetric characterization of TPU-PDA 25 was in complete agreement with the already published results ($T_m=62.4$ and $T_c=44.61$)⁴⁵. As expected, the effect of the hard segment content over the crystallization of the materials was observed, PCL-PU exhibit lower crystallinity than PCL diol. Specifically, in the case of PUs containing HDI+BD, the increase on HSC% diminishes the magnitude of both melting and crystallization enthalpies, thus reducing material's crystallinity degree (X_c), as a result of phase segregation processes⁵⁶. Consequently, the sharp exothermic signal around 40°C (crystallization of crystalline domains on pure PCL diol) becomes broader and shifts to lower temperatures as the HSC% increases until merges with the baseline (see PCL: PU (HDI+BD) 30:70 curve on **Figures 2c** and **S4**). The shifting of the crystallization temperature (T_c) associated with the HSC% has been reported for PCL- polyurethane systems derived from MDI+BD with shorter soft segment lengths ($M_n \approx 4, 5$ and $7.0 \times 10^4 \text{ g mol}^{-1}$), the inclusion of mostly amorphous PU domains hampers the crystallization process of the crystalline domains contained on the PCL matrix although do not modify its crystalline structure⁵⁷.

Table 3. Thermal properties of synthesized PCL-based ester urethanes.

Name	$\Delta H_f \text{ PCL (J g}^{-1}\text{)}$	$\Delta H_c \text{ PCL (J g}^{-1}\text{)}$	$X_c \text{ PCL}^a$	$T_m \text{ (}^\circ\text{C)}$	$T_c \text{ (}^\circ\text{C)}$
PCL diol 14kDa	74.56	62.88	53.45	55.38	40.04
PCL-PU (HDI+BD) 70:30	55.13	61.65	39.52	55.41	38.94
PCL-PU (HDI+BD) 50:50	49.04	44.73	35.15	52.25	32.43
PCL-PU (HDI+BD) 30:70 ^b	-	-	-	-	-

PCL-PU (MDI+BD) 70:30	47.15	48.13	33.80	54.54	30.84
--------------------------	-------	-------	-------	-------	-------

^a X_c was calculated by $X_c = \frac{H_{f,exp}}{w * H_{f,th}^0} * 100$, where w is PCL mass fraction and 139.5 Jg^{-1} was considered as enthalpy of fusion for 100% crystalline PCL.^b There were no measurable signals on this material's thermogram.

Furthermore, the measured T_c of PCL-PU (MDI+BD) 70:30 shifted ca 10°C to lower temperature in comparison with PCL-PU (HDI+BD) 70:30 (**Figure 2c**), this indicates, along with its corresponding assessed X_c , that the integration of MDI as HS on PCL-PU produces a sharper hindering of effective crystallization process of PCL domains than HDI. as M_n of the soft segment remained unchanged and the HSC% is the same for both materials⁵⁸. Among the PUs, TPU-PDA 25 exhibits the highest T_c and T_f due to higher transition temperatures of the PDA segments. Even though PDA-derived copolymer contains the stiffer MDI as hard segment its crystallization enthalpy is comparable with PCL-PU (HDI+BD) 70:30 as shown on **Figure 2c**. The observed strong hindering effect of MDI over the crystallinity on PCL-based copolymers is lessened on TPU-PDA 25 as the PDA segments exhibit larger crystallization and fusion enthalpies, 124.2 and 124.9 Jg^{-1} correspondingly⁴⁵, than PCL diol soft segments (**Table 3**).

Conclusively, the increase of the hard segment fraction has a stronger effect on the reduction of the crystallization temperature than for T_m of the synthesized copolymers. The dependence of the crystallinity of semicrystalline PCL domains with the mass fraction of urethane phase is evident, thus is self-explanatory and expected that the crosslinked networks exhibited greater values of ΔH_c as observed on **Figure 2**.

3.2 Tensile testing: The tensile characterization of the selected copolymers along with the crosslinked PCLs was driven. Based on the observations obtained from their DSC analysis, the determination of the appropriate temperature ranges to measure their corresponding stress-strain profiles on molten state was possible. PCL-PU (MDI+BD) 70:30 became fragile at 70°C breaking at very low strains (1-3% of its original length), thus, its σ - ϵ correlation was evaluated at 60°C. Even under these conditions the MDI-urethane could not be extended further than 60% before failing/breaking with an estimated Young modulus of 3.8MPa. In contrast, TPU-PDA 25 and PCL-PU (HDI+BD) 70:30 showed an enhanced extensional performance at 70°C reaching a strain degree of 200% where TPU-PDA 25 exhibited the lowest elastic modulus followed by PCL-PU (HDI+BD) 70:30 with 1.1 and 2.2 MPa correspondingly (**Table S4** and **Figure S6**).

At lower strain conditions this trend remained unchanged, the PDA-based urethane showed the lowest elastic modulus (E) overpassed by PCL-PU (HDI+BD) 70:30. As expected the values of E for both TPU-PDA 25 and PCL-PU (HDI+BD) 70:30 increased while evaluated at 65 and 60°C correspondingly, the HDI-ester urethane exhibited a sharp stiffening effect as its elastic modulus at 60°C raised up to 3.5 MPa. Correspondingly, the elastic modulus for TPU-PDA arose to 1.9MPa (**Table S4**). Even though both materials are roughly 3-4°C above their T_m at low strain conditions, PDA-based copolymer remained softer than PCL-PU (HDI+BD) 70:30. The softness of TPU-PDA 25 and the marked stiffening of PCL-HDI ester urethane find their origin on the observations obtained from their DSC analysis. The great thermal properties of the poly(1,10-decylene adipate) diol soft segments confers TPU-PDA 25 remarkable elastic properties on a great ranges of temperatures. In contrast, the PCL-based

copolymers are way stiffer at low and high strain thermal conditions due to the strong crosslinking effect of the urethane domains over the PCL diol segments. The observed effect of MDI over the crystallization of PCL phase on the DSC analysis is in complete agreement with the acute stiff extensional behavior of PCL-PU (MDI+BD) 70:30.

According to statistic theory of rubber elasticity, Young's modulus of polymer increases with amount of crosslinker on molten state.⁵⁹ This trend was observed for the tensile characterization of the highly elastic crosslinked PCL networks which were extended up to 200% of their original length. The linear PCLs exhibited lower elastic moduli than CD-PCLs, as a matter of fact the assessed values for E of the star-like cured materials double the Young moduli of linear PCL probes containing the same weight fraction of crosslinking agent (**Table S4**). This is just a consequence of the superior molecular weight of the intricated nuclei-grafted multi-armed architecture of the star-like PCL (Average $M_n = 386$ kDa) in comparison with their linear analogues (80kDa), the tensile properties of elastomers increase with their molecular weight.⁶⁰ Among the studied materials the polyurethanes exhibited the highest elastic moduli values, surpassing the crosslinked PCL networks by a factor of 10. This means that the crosslinking effect caused by the insertion of the urethane domains over a PCL network is stronger and way more effective than the chemical curing process, leading to the production of stiffer yet more elastic/rubbery materials.

Additionally, the tensile features of processable PCL-PU were measured and directly compared to TPU-PDA 25 at room temperature (**Figure S6, Table S5**). The observations derived from these experiments followed the same trend than the tensile essays on molten state, although the samples were able to elongate up to 1200% PCL-PU (MDI+BD) 70:30

presented the highest yield-stress value among the investigated copolymers. The stiffness of this material is followed by the HDI-derived PCL urethane copolymer which leaved the elastic deformation regime by reaching a stress value of 9.67MPa. TPU-PDA 25 proved again to be the softest tested copolymer even at room temperature by yielding at 6.11MPa. As expected, PCL-PU (HDI+BD) 70:30 exhibited the largest strain value before deforming plastically, ca 150.4%. As previously discussed, the aliphatic nature of the HDI segments leads to the production of less rigid copolymers than PUs containing aromatic isocyanates as MDI^{49,50}. Therefore, the yielding strain values for both PDA and PCL-MDI urethanes were inferior, ca 130%, and practically the same. The contrasting chemical nature of the hard segments composing the polyurethanes becomes utterly relevant at temperatures below the transition temperature of their soft segments. Ultimately, the fact that PCL-PU (MDI+BD) is able to elongate further than 1000% at room temperature is remarkable, this demonstrates how acute is the softening effect caused by the melting process of its PCL domains.

3.3 TW-SME Evaluation: We investigated the reversible shape memory effect of the processable polymers by measuring the evolution of stress at constant strain conditions and the evolution of extensional strain at constant stress conditions upon thermal cycling. First, we tested their behaviour at large strains, $\epsilon = 200\%$. The crosslinked PCL networks demonstrated 2W-SME behaviour under constant strain (**Figure 3a**) and constant stress conditions (**Figure 3b**). For comparison purposes, the 2W-SME features of the highly and less crosslinked CD-PCL derived materials were evaluated. On constant strain scenario, the extensional stress of all cured PCLs exhibited an already well studied three-regime evolution upon cooling. At 70°C the stress decreases in a linear way which is a typical feature of

elastomeric materials, then an intermediate regime characterized by a stress drop, associated with the crystallization of the extended polymer chains along the deformation, is observed before the T_c of the stretched materials. Followed by the final cooling phase where an increase of the measured extensional stress is observed, this state corresponds to the massive crystallization of the non-oriented crystalline domains⁶¹.

The initial stress of star-like PCLs is higher than linear PCL samples, this is sustained by the already discussed improved tensile properties of CD-PCL over its linear analogues. The appearance of the intermediate state shifts to higher temperature values as the stretching and orientation degree of the polymer chains increases while its magnitude is strongly dependant on the crosslinking density for equally elongated polymers.⁶² For linear PCLs the stress drop is observed at lower temperatures than for CD-PCLs, ca7°C (**Figure 3a**). This observation means that the polymer chains of the nuclei-grafted PCL orientate more efficiently towards an applied deformation as the cyclodextrin nuclei act as fixated entanglement regions on the polymeric networks reinforcing the elastic character of the materials under load.⁶³ This behaviour is complemented by the enhanced magnitude of the stress drop exhibited by the CD-PCLs in comparison with the linear crosslinked PCL materials (**Table 4**). The cyclodextrin domains act as additional net-points creating a cleavage effect on the polymer network, thus increasing the effective orientation of the polymer chains towards the applied deformation.

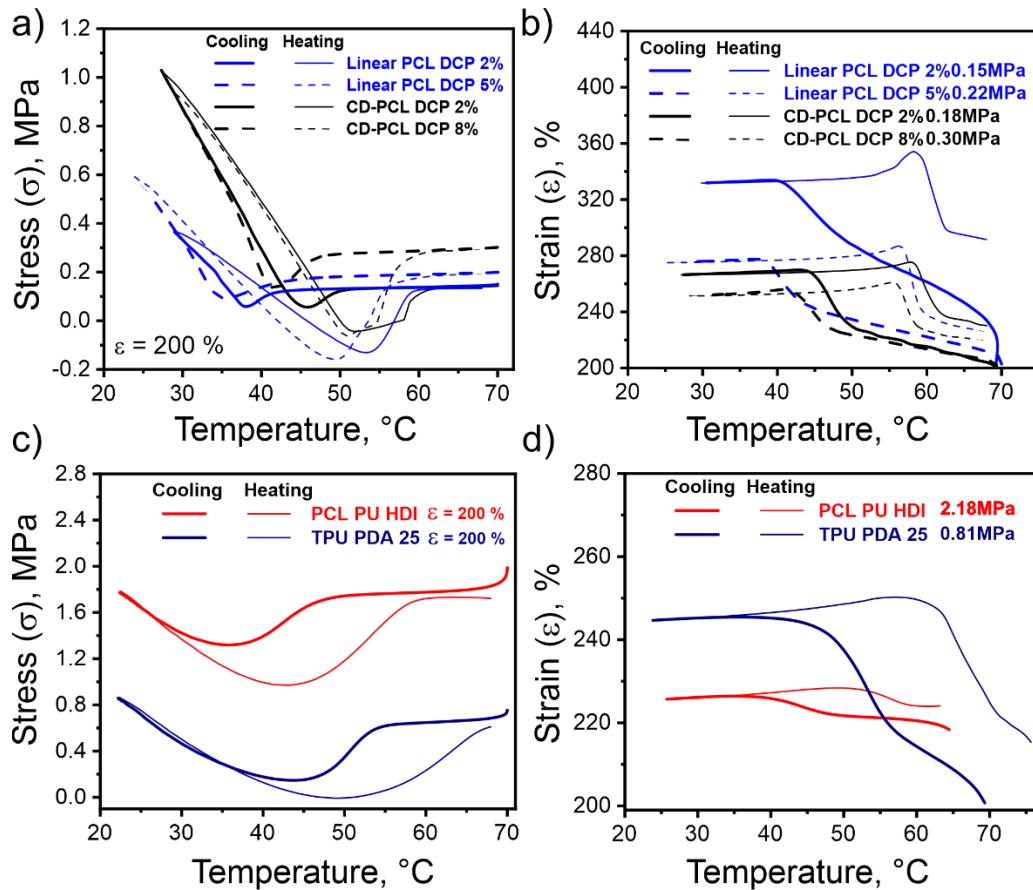


Figure 3. Bidirectional shape-memory properties of investigated polymers: (a)– Crosslinked Linear and star-like PCL networks under constant strain, 200%; (b)– Crosslinked Linear and star-like PCL networks under constant stress conditions; (c)– PCL-PU (HDI+BD)70:30 and TPU-PDA 25 under constant strain, 200%;(d)– PCL-PU (HDI+BD)70:30 and TPU-PDA 25 under constant stress conditions.

The evolution of the extensional strain of thermally cycled crosslinked PCL networks is in complete agreement with the already extensively studied 2W-SME under constant stress conditions. Here two antagonistic effects take place, the crystallization induced elongation (CIE) and the melting induced contraction (MIC) effects underwent by polymer chains upon cooling and heating respectively. The magnitude of the afore mentioned phenomena, and subsequently the reversibility of the 2W-SME process, is dependant on thermal and physicochemical parameters of the polymer networks such as the crystallinity, applied load

and effective crosslinking density. As depicted on **Figure 3b**, highly crosslinked networks undergo less pronounced elongations/ contractions when thermally cycled while greater loads need to be applied on them to achieve an initial strain comparable to less crosslinked materials. Therefore, linear PCL DCP 2% undergoes greater elongations, ca 56%, upon cooling in comparison to PCL DCP5%, ca36%, regardless that the latter is under a higher load.

Table 4. Selected thermomechanical features of highly strained (200%) and moderately strained (50%) crosslinked and PU-based investigated polymers

Name	High Strain Conditions		Low Strain Conditions	
	Stress Drop, $\Delta\sigma$ (MPa)	Strain Change, $\Delta\varepsilon$ (%)	Stress Drop, $\Delta\sigma$ (MPa)	Strain Change, $\Delta\varepsilon$ (%)
PCL-PU (HDI+BD) 70:30	0.44	4.68	0.25	3.93
PCL-PU (MDI+BD) 70:30	-	-	0.22	3.52
TPU-PDA 25	0.50	26.44	0.38	22.27
Linear PCL DCP 2%	0.04	56.87	5×10^{-3}	17.16
Linear PCL DCP 5%	0.10	36.07	0.04	6.57
CD-PCL DCP 2%	0.07	41.72	0.04	12.81
CD-PCL DCP 8%	0.16	28.66	0.05	4.68

Correspondingly, the materials derived from CD-PCL show the same behaviour although the elongations described by these materials are more discreet, ≈ 41 and 28% for CD-PCL2% and 8% respectively, while subdued to even higher loads than linear PCLs. The above-mentioned considerations regarding their thermal, tensile, and structural properties confers a structured explanation for the observed behaviour.

Following the same thread of ideas, the thermomechanical characterization of PCL-PU (HDI+BD)70:30 and TPU-PDA 25 at high strain conditions under constant strain (**Figure 3c**) and constant load (**Figure 3d**) was made. The 2W-SME behavior of constantly strained PUs was in complete correspondence with the collected data from their DSC and tensile essays. The initial stress for HDI-PU is higher than for TPU-PDA 25 due to its higher elastic modulus and stiffer nature. Despite this fact, the stress drop magnitude is higher for the PDA-copolymer than for the PCL-based urethane as consigned on **Table 4**. The reason for this resides on the improved crystallinity of the poly(1,10-decylene adipate) diol segments, although the urethane phase has an effective crosslinking effect upon the PCL crystalline domains also hinders acutely their crystallization extent. Additionally, the stress drop regime appears early on the PDA-copolymer as the material has a higher melting temperature.

The evaluation of these materials under constant stress conditions revealed the extent of the physical crosslinking effect induced upon the crystallizability of the soft segments by the insertion of a rigid urethane-phase. The 2W-SME character of the HDI-urethane was tested starting from 65°C (**Figure 3d**) as above this temperature underwent irreversible strain transformations due to the creeping effect caused by its softening. The cooling-induced elongation of TPU-PDA 25 ($\approx 26\%$) is way larger in comparison with PCL-PU (HDI+BD) 70:30, ca5%, aside from the fact that the PCL-urethane was loaded with almost 3times greater extensional stress during the thermal cycling than the PDA-derivate. The cause for this is the complementary effect between the utterly restriction of the crystallization process of the semicrystalline PCL domains due to the tethering of their chain mobility and the difference

on the flexibility between the PDA monomer unit in comparison with the short-lengthened PCL repeating units.

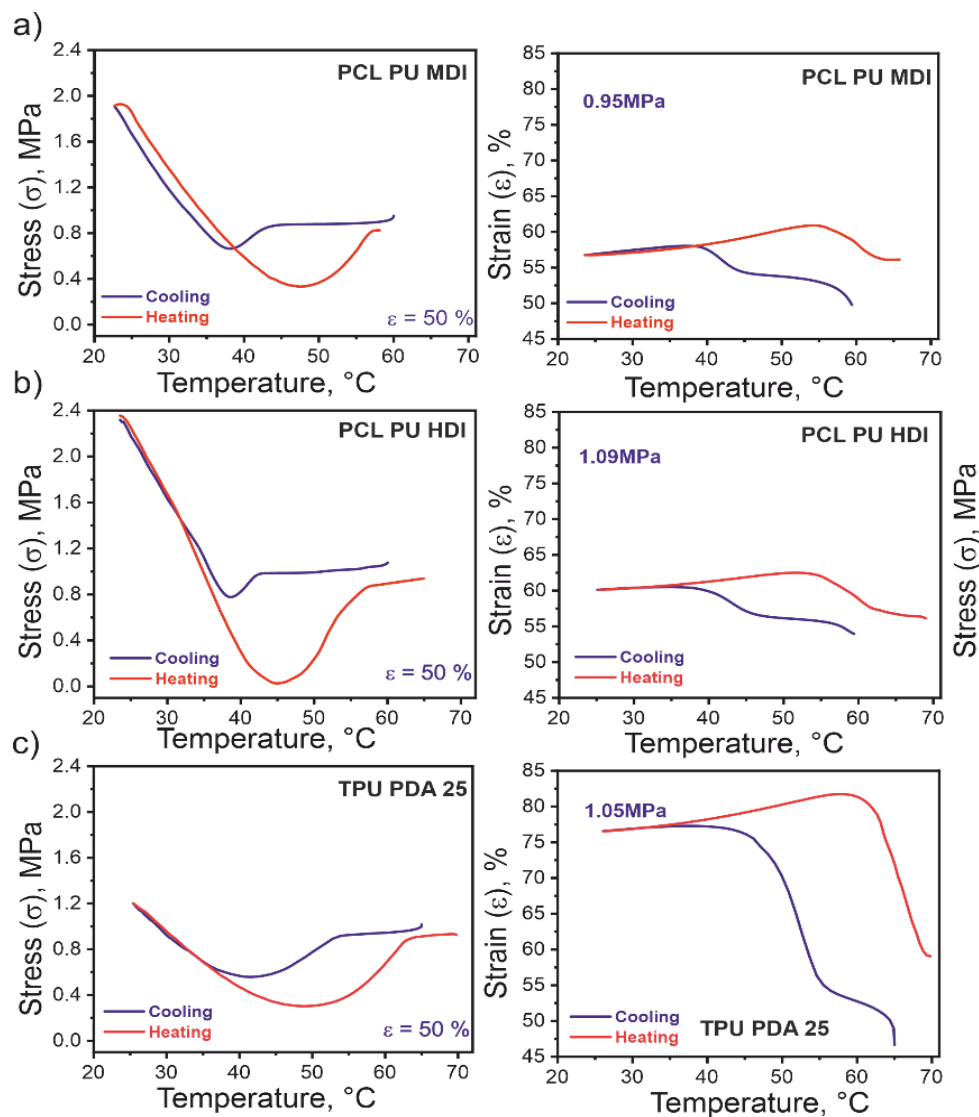


Figure 4. Bidirectional shape-memory properties of selected copolymers under constant strain ($\epsilon=50\%$) left side; and constant stress (ca $\sigma=1\text{MPa}$) right side: (a)– PCL-PU (MDI+BD) 70:30; (b)– PCL-PU (HDI+BD) 70:30; (c)– TPU-PDA 25.

In order to compare the different kinds of PU-based copolymers we repeated the same set of experiments at low strain conditions (**Figure 4**) along with a qualitative contrast with the

PCL crosslinked networks. The data extracted from these essays is also consigned on **Table 4**. In a general form, the 2W-SME behavior of the crosslinked samples at low strains follows the same trends as for high constrain conditions. Under constant strain setup CD-PCLs exhibit higher initial stress values and larger stress drops than linear PCL samples, the magnitude of these parameters decrease accordingly as the polymer networks are less strained by going from 200 to 50% of strain degree. The behavior of the thermomechanical parameters for the crosslinked probes under constant stress at low strain degrees is analogue to the already discussed observation on higher stretching conditions. The strain change associated with the ICE effect is stronger on less crosslinked materials although the reversibility of the shape transformation increases with the increase of crosslinker content. Therefore, linear PCL samples exhibit larger strain changes than the star-like PCLs.

The three investigated PUs showed reversible actuation under constant strain and stress conditions by undergoing moderate deformations, as being subjected to thermal cycling in a constant strain setup the selected urethanes exhibited the expected three-stated stress evolution. Interesting is the fact that by being extended to 50% of their original length with the thermal conditions settled on **Table S3**, the three copolymers have an initial stress of ca 1MPa. The onset temperature of the stress drop for the PCL-based ester urethanes is readily the same, around 45°C, while for TPU-PDA 25 sets-in at ca55°C due to its high melting and crystallization temperatures (**Figure 4a-c; left side**). The magnitude of the observed drop on the stress among the PCL-PUs is nearly identical although for the HDI-derivate is slightly greater, TPU-PDA 25 exhibits the largest value of stress drop with 0.38 MPa. The observed sharp differences between the tensile properties of the PCL urethane copolymers seems to

recede at lower stretched conditions as their thermomechanical parameters at constant strain conditions are very similar.

PCL-PU (HDI+BD) 70:30 shows a higher value of stress at the lower temperature of the thermomechanical cycle than its MDI analogue. This observation along with a wider hysteresis between the cooling and heating runs confirm that the MDI hard segments direct more efficiently the semicrystalline PCL domains than HDI domains as a deformation with the same magnitude is applied, the contribution to the stress corresponding to non-oriented crystalline domains is more important on PCL-PU (HDI+BD) 70:30. The magnitude of this contribution is even way smaller on TPU-PDA 25 (**Figure 4c; left side**) corroborating the important directional modulation effect of the MDI upon soft domains able to crystallize.

The bidirectional shape-memory features of the PCL-based copolymers on constant stress conditions are also very similar (**Figure 4a, b; right side**), the strain change associated with the ICE process for both materials are practically the same, ca 3.5%. In the other hand PDA-derivate material exhibits a notable crystallization-induced elongation – $\approx 22\%$ (**Figure 4c; right side**) due to the enhanced entropic properties of the PDA soft segment over PCL diol. The nominal values of stress drop and strain change for both PCL-PU (HDI+BD) 70:30 and TPU-PDA 25 decrease as the degree of the applied deformation also decreases.

The stress drop increases with crosslinking agent content, in general star PCLs show greater stress-drops than linear PCLs effect associated with a higher entanglement degree of its polymer chains. PUs exhibit larger stress drops than crosslinked materials for all elongations as the addition of the amorphous urethane domains amid a semicrystalline polymer network induces a sharper crosslinking effect upon them, facilitating the orientation of its crystalline

domains towards an applied deformation. TPU-PDA 25 exhibits the highest stress drop among the PUs regardless the strain degree. Larger deformations lead to greater stress drops for all materials. Chemically crosslinked networks exhibit larger strain changes than PUs on large deformations. The crosslinking/stiffening impact of the phase-segregation on the urethane semicrystalline copolymers leads to the hindering of the crystallization process, thus of their CIE effect. On intermediate strain degree conditions, PCL-PUs derived from HDI and MDI exhibit very similar thermomechanical features.

3.4 Thermomechanical Cyclic Essays: The cyclic thermomechanical essays were conducted under the same conditions than the tensile and the 2W-SME evaluation for all samples, naturally the MDI-derivate analysis was carried at low strain conditions (60°C, 50% of strain degree). The trends observed here for the analyzed PUs and linear PCL on constant strain conditions are in complete agreement with their 2W-SME evaluation. As the stretched probes are allowed to crystallize from the molten state a stress drop is noticed above their T_c according to the DSC results. The magnitude of this reduction on extensional stress, associated with the crystallization of oriented polymer chains, is way more significant for the urethane copolymers than for the crosslinked PCL network as depicted on **Figures 5** and **S7** where the cooling steps and the whole thermal cycles are correspondingly showed. In general, as the high temperature limit (T_H) of the thermal cycles is below the melting temperatures of the materials the drop on the extensional stress is not observed, thus, for linear PCL the stress drop is only noticeable as the heating temperature was set at 60° (**Figure 5a**). Respectively, this effect is also evident on the polyurethanes where no stress drop is recorded upon cooling

as T_H is below 55°C for PCL-PU and 65°C for TPU-PDA 25 which is in complete agreement with their calorimetric characterization.

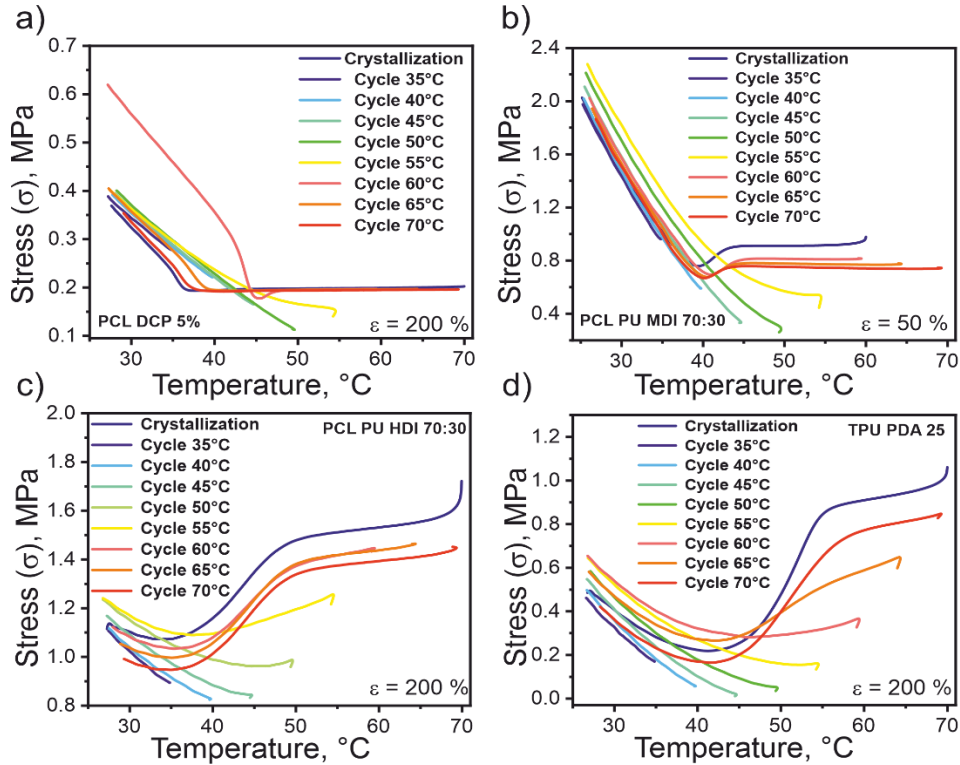


Figure 5. Cooling sections of the thermomechanical cycles of: (a)– PCL DCP 5%; (b)– PCL-PU (MDI+BD) 70:30; (c)– PCL-PU (MDI+BD) 70:30 and (d)– TPU-PDA 25 under constant strain.

As previously mentioned on the 2W-SME section, an increase on the measured stress is expected below the crystallization temperature of a semicrystalline polymer network under constant strain conditions. The cause for this effect is the massive crystallization of the non-oriented crystalline domains, thus highly strained materials will exhibit a less notorious arise of stress. As expected, the PCL-MDI (**Figure 5b**) urethane presented higher values of stress at T_L than the HDI-urethane (**Figure 5c**) as the latter is able to extend up to 200% of its original length. The stress value at T_L (σ_{TL}) increases with every cooling cycle as more PCL

and PDA domains are allowed to crystallize. Also, σ_{TL} becomes larger as the T_H of each cycle is greater, the maximum stress value on semicrystalline state is observed on the cycle where T_H was set on 55°C for PCL-PU_s and 65°C for TPU-PDA 25 (**Figure 5d**). Above these temperatures, σ_{TL} decreases dramatically as the stress drop is observed again due to the softening effect of the complete melting and further directed crystallization of the PCL and PDA crystalline domains. These observations are complemented by the magnitude of the stress drop - directly correlated with the orientation degree of the polymer chains, PCL-PU (HDI+BD) 70:30 exhibited enhanced values of stress drop upon cooling than its less strained aromatic analogue. On the other hand and as expected, the PDA ester urethane displayed the largest stress drop among all evaluated materials accordingly to its previous tensile and bidirectional shape memory characterization.

Another interesting observation extracted from the cyclic thermal experiments is the strong creep effect suffered by the studied polyurethanes in comparison with the chemically crosslinked PCL network. On the first portion of the crystallization curve for the copolymers, a pronounced drop of stress is caused by the stress relaxation process which takes place immediately after the deformation of the urethanes on molten state (see also **Figure S7**). Contrarily, the stress relaxation effect is way less marked for the linear PCL sample due to its inherent softness and elastomeric behavior. Therefore, the final value of stress at 70°C after the course of the eight thermal cycles (cycle 70°C) differs greatly from the initial value of stress at the same temperature on the first crystallization curve for the PU_s – ca 0.2 MPa, while for PCL DCP 5% the stress difference after thermal cycling is $\approx 6.4 \times 10^{-3}$ MPa.

3.5 Stress relaxation test: The stress relaxation profiles of the investigated materials are displayed on **Figure S8** while the parameters obtained from their exponential decay fitting are consigned on **Table 5**. The analysis of the stress relaxation profiles was performed by considering a modified version of Burgers stress relaxation model, which in essence reduces the viscoelastic character of a polymer network to two springs and two restraint elements (dashpots) connected in series (two Maxwell models arranged in series)^{64,65}. As a three exponent exponential decay fitting model was applied, the relaxation profiles of the materials are divided on three portions of time: Right after the deformation where a sharp stress drop takes place, intermediate time values after the deformation took place and very long periods of time where the stress is barely changing. Each of these sections has an associated relaxation time constant (τ_1 , τ_2 and τ_3), every relaxation time constant represents the time at which the stress will reduce to ca36.8% of its initial value (σ_0) on its corresponding portion of the stress-time profile. The evaluation of stress response at short and long-time frames are the most useful aspects to characterize the viscoelastic features of a material, thus the magnitude of τ_1 and τ_3 are of great relevance. The polyurethanes, regardless their elongation degree, exhibit in general greater initial values of stress than highly crosslinked PCL samples, this was expected as their stress-strain evaluation already demonstrated that the urethane-based materials are way stiffer than cured elastomers. Accordingly, the star-like PCL has a greater σ_0 value than its linear analogue.

Table 5. Obtained exponential decay fit parameters of the stress relaxation profiles of the selected semicrystalline polymer networks.

Name	Elongation (%)	Temperature (°C)	τ_1 (s)	τ_2 (s)	τ_3 (s)	σ_0 (Mpa)
PCL-PU (HDI+BD) 70:30	200	70	78.8	583.7	6468.8	2.19
PCL-PU (HDI+BD) 70:30	50	60	80.4	673.0	6178.3	1.10
PCL-PU (MDI+BD) 70:30	50	60	71.8	582.3	5232.5	1.02
TPU-PDA 25	200	70	106.6	753.2	6565.5	0.80
TPU-PDA 25	50	65	117.9	711.8	6516.4	1.08
Linear PCL DCP 5%	200	70	85.2	776.5	14921	0.22
CD-PCL DCP 8%	200	70	41.3	763.8	11682	0.31

The first relaxation time constant (τ_1) is higher for linear PCL DCP 5% than for the cyclodextrin-based PCL, this means that the former requires almost the half of time of the latter to relax to the same extent. The nuclei-grafted architecture of CD-PCL DCP 8% confers this material an extraordinary instantaneous reaction to an applied deformation allowing a sharp relaxation on the early stages of the stress relaxation experiments, as a matter of fact this polymer exhibits the lowest τ_1 among all investigated materials (**Table 5**). Amid the PUs, the PCL-MDI derivate has the lowest relaxation time constant despite the elongation degree. As the most rigid urethane was expected that this copolymer experienced a faster stress reduction than its aliphatic analogue and TPU-PDA 25. By comparing the 200% and 50% elongation scenarios for both PCL-PU (HDI+BD) 70:30 and TPU-PDA 25 its noticeable that the τ_1 for a less stretched material is higher than for a more extended sample. The response

of a constantly drawn rubbery polymer network becomes sharper as the magnitude of the deformation increases, thus an extensively elongated polymer will exhibit larger initial stress values and shorter instantaneous relaxation times than a less stretched network. TPU-PDA 25 has the longest initial relaxation time constant of all studied polymers, this fact corroborates all the previously revised thermomechanical features where the softness and enormous elasticity of this material was demonstrated.

Accordingly, the crosslinked PCL polymers exhibit larger relaxation time constants at large frames of time (τ_3) than the phase-segregated copolymers. These observations were also expected as the crosslinking effect of the urethane-domains over the semicrystalline PCL and PDA domains are sharper than the curing process over PCL networks. Linear PCL DCP 5% has the largest τ_3 outlining the fact that also exhibits the lowest initial stress value, the sliding effect of the polymer chains accompanied by their ineffective fastening and lessened entanglement will increase the plastic character of their elongation enlarging the required time for this material to overcome the applied deformation. Another remarkable annotation is that τ_3 values are readily similar for low and highly strained TPU-PDA 25 and PCL-HDI. Less strained materials will need less time to relax at longer frames of time which is still valid for both materials, yet this relaxation time seems to be not strongly affected by the magnitude of the applied deformation which unequivocally attest the great elastic character of these copolymers. In the case of the PDA-derivate the two τ_3 constants at 50 and 200% of extension are almost identical (see **Table 5**). Lastly, PCL-PU (MDI+BD) 70:30 has also the shortest time relaxation constant on a large time interval. Its already proven stiffness and

strong crosslinking properties facilitate the fast recovery of this material after an applied elongation and sustains its stress relaxation behavior.

3.6 Contribution of stress drop, strain degree and enthalpic properties to bidirectional shape memory effect under constant strain: From all the above mentioned on the previous sections of this comparative study, we were able to identify the strain degree, stress drop and enthalpy of crystallization as the most relevant parameters affecting and modulating the bidirectional shape memory properties of constantly strained chemically/physically crosslinked semicrystalline polymer networks with varied structural architectures under thermal cycling. The preferred orientation of the polymer chains of a semicrystalline polymer under constant load grants such materials the ability to deliver a shape memory transformation while thermally cycled around T_{Trans} of its switching domains. Greater deformations lead to the enhancement of the polymer chains alignment. Thus, the magnitude, amplitude and reversibility of the shape-switching phenomena have a positive correlation with the alignment rate of uniaxially stretched polymer strands⁶⁶.

The extent of the observed drop of stress upon cooling for constantly drawn rubbery elastomeric materials is another important criterion for evaluating the alignment degree of constantly strained polymer chains. Therefore, samples with constant effective crosslinking density undergoing larger strain degrees deliver greater stress drops (**Figure 6**) despite its molecular architecture. The stress value on molten state for constantly loaded materials increases accordingly with the effectiveness of the restrain/entanglement effect of the crosslinking process on a polymer network. This is, highly crosslinked polymers are stiffer on molten state than less crosslinked analogues as they are deformed at the same extent as

depicted on **Figure 6**. For instance, the studied PUs exhibited greater extensional stress values when deformed on molten state to the same degree than the way softer crosslinked PCL networks. The urethane-based copolymers demonstrated superior tensile properties than the cured elastomers thanks to the strong physical crosslinking effect of the urethane phase over the crystalline PDA and PCL domains. On a similar manner, the CD-PCLs showed an enhanced stress drop delivery as well as experiencing larger stresses while deformed on molten state than cured linear PCLs thanks to the radial grafting effect of its cyclodextrin nuclei.

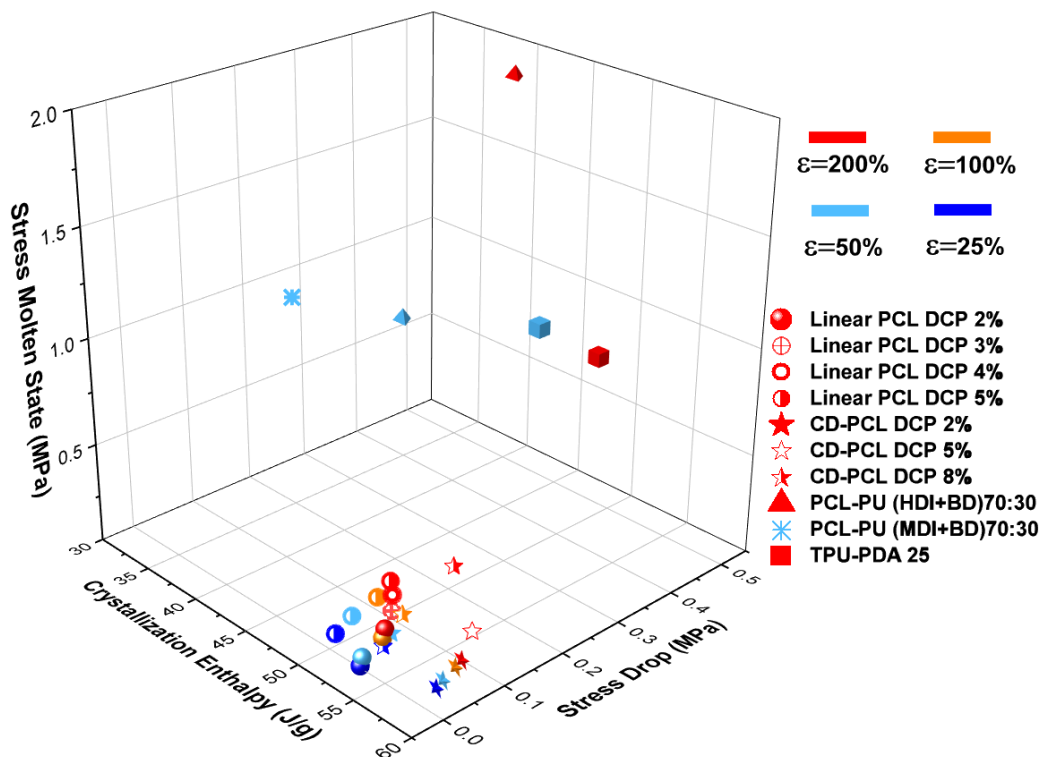


Figure 6. Summary of the collected data from the thermomechanical investigation of the studied semicrystalline systems and its correlation with the most relevant parameters affecting their bidirectional shape memory behavior under constant load.

Finally, the enthalpic properties showed to have an important influence over the two-way shape memory features of semicrystalline polymer networks. It is well-established that the thermally induced bidirectional SEM on loaded semicrystalline polymers is carried along thanks to the directed crystallization/melting of its crystalline domains. Also, that the crosslinking process on a polymer diminishes its inherent crystallinity as the material becomes more amorphous, the hampering effect over crystallization is bulkier with increasing content of crosslinker or by arising the HSC for cured elastomers and phase-segregated copolymers respectively. The restriction of the crystallization process intrinsically evokes a reduction of the crystallization and fusion enthalpies of the crosslinked material, phenomena attested by the data obtained for the studied materials on our investigation (see **Figures 2** and **S5**).

In this order of ideas and by checking **Figure 6**, is notorious that the investigated crosslinked PCLs exhibit larger ΔH_c values than the ester urethanes allowing them to undergo larger reversible deformations while thermally cycled under constant load due to their enhanced crystallinity and intrinsic mechanical softness -lower stress values at molten state than PUs. Additionally, the PCL-MDI copolymer has the lowest crystallization enthalpy amid the probed materials which explains its limited extensional properties and modest deformations upon cycling under load. Moreover, between the polyurethanes the TPU-PDA 25 has the largest crystallization enthalpy-almost the same as linear PCL DCP 5%, this fact clarifies its superior elastic behavior in comparison with the more rigid and less crystalline PCL-based urethanes.

4. CONCLUSIONS

On this report we successfully carried a complete study based on the comparison of the bidirectional actuation behavior of 5 kinds of semicrystalline polymer networks with varied chemical functionalities and architectures. The 2W-SME features of chemically crosslinked linear PCL and star-like PCL (CD-PCLs) networks were evaluated along with a copolymer of poly(1,4-butylene adipate) with methylene diphenyl diisocyanate (MDI) /butanediol (BD) (TPU-PDA 25) and here synthesized PCL diol-based urethane copolymers containing varied mass fractions of hexamethylene diisocyanate (HDI) /BD and MDI/BD as hard segments (PCL-PUs).

PCL diol (14kDa) was successfully synthesized by means of a ring opening polymerization catalyzed by ammonium heptamolybdate tetrahydrate. From this ester diol monomer, we carried out the synthesis of 4 PCL-PUs derived from HDI and MDI containing different hard segment mass contents. The experimental mass fraction content of hard and soft segment for the synthesized copolymers was in accordance with the proposed phase composition for these materials. All urethane-copolymers were thermally stable above 300°C and thermally decompose on at least three-stepped process. The PCL-PUs exhibited a unimodal molecular weight distributions with M_n values between 5.0×10^4 and 1.3×10^5 g mol⁻¹, higher mass fraction of soft segment enhanced the polymerization process enhancing the M_n of synthesized PUs.

The calorimetric characterization of all polymers was also investigated. The thermal properties of crosslinked semicrystalline networks such as T_m , T_c , ΔH_c , ΔH_f and degree of crystallinity (X_c) decreased as the crosslinking agent content arises due to the increment of

their amorphous character. In general CD-PCLs exhibited higher enthalpies and crystallinity than their linear analogues. As for the PCL-PU, the insertion of MDI as urethane phase produces a stronger hindering effect over the crystallinity of the PCL soft domains than the incorporation of HDI on PUs systems with the same hard segment content. TPU-PDA 25 exhibited higher T_c , T_f and crystallization enthalpies than the produced PCL-PU as the PDA monomer count with larger ΔH_c and ΔH_f than PCL diol. Mainly, the crosslinked networks exhibited greater values of ΔH_c than the studied polyurethane systems confirming the sharp abating effect over the crystallinity of a semicrystalline network by bonding to the amorphous urethane phase.

Among the 4 synthesized PCL-PU, just PCL-PU(HDI+BD) 70:30 and PCL-PU(MDI+BD) 70:30 were processable and able to produce homogeneous films. Thus, their tensile and thermomechanical properties were measured alongside TPU-PDA 25. PCL-MDI urethane failed by being stretched up to 60% of its original length, the stiffening effect of MDI over the semicrystalline PCL domains was in evidence as both, TPU-PDA 25 and its HDI analogue, were able to stretch up to 200% while exhibiting lower elastic moduli than the aromatic polyurethane. The PDA-derivate was the softest copolymer amid the studied PUs. Accordingly, linear thermally cured PCLs exhibited lower Young moduli than CD-PCLs. The superior molecular weight and the nuclei-grafted multi-armed architecture of the star-like PCL support these observations. Ultimately, PUs showed higher elastic moduli values on molten state than crosslinked PCL networks, the insertion of urethane domains causes a stronger crosslinking effect than the chemical crosslinking process over a semicrystalline network.

The evaluation of the 2W-SME of the selected materials was carried successfully under constant stress and constant strain conditions. Chemically crosslinked networks displayed larger strain changes than PUs under constant stress due to their softer tensile. Linear PCLs undergo greater deformations than CD-PCLs when thermally cycled under load. Accordingly, TPU-PDA 25 experiences greater strain elongations than PCL-PUs under constant stress mode as the PDA soft segments are more elastic in comparison with the highly restrained short-lengthened PCL segments. On constant strain scenario, the investigated PUs showed larger stress drops than crosslinked materials. The addition of the amorphous urethane domains induces an acuter crosslinking effect upon their soft segments, facilitating the orientation of its crystalline domains towards an applied deformation. Out of the studied ester urethanes TPU-PDA 25 presented the greatest stress drop while the star-like PCLs also showed larger stress drop values than their linear analogues. In general, the stress drop increases with the crosslinking agent content as larger deformations led to greater drops of stress upon cooling for constantly strained materials regardless their chemical structure or crosslinking mechanism.

The observations derived from the tensile and shape memory essays for the selected PUs were confirmed on the thermomechanical cyclic essays performed under constant strain. The less strained and stiffer PCL-MDI showed larger stress values on crystalline state than the highly stretched PCL-PU (HDI+BD) 70:30, TPU-PDA 25 and linear PCL DCP 5%. This fact corroborates that less drawn materials endure sharper increases on their extensional stress below their crystallization temperatures due to the massive crystallization of non-oriented crystalline domains. In fact, after each cooling cycle the stress value at the lower temperature

limit increases for all tested materials due to exhaustive crystallization. Once their melting temperature is reached, this trend ceases as the chain mobility is restored and the polymer strands are allowed to crystallize on a directed manner once again.

The analysis of the stress relaxation profiles of the semicrystalline polymers revealed that crosslinked networks have larger relaxation time constants on long time frames than the urethane-copolymers. Correspondingly, linear PCL DCP 5% exhibits the largest relaxation constant while PCL-PU (MDI+BD) 70:30 the smallest, here the profound stiffening and conformational restrain effect of the aromatic isocyanate over the PCL polymer chains was confirmed backed up by the already collected data. Finally, all the gathered observations derived from the thermomechanical characterization of the investigated materials allowed us to identify that their enthalpy of crystallization, the magnitude of the deformation imposed on them, and the delivered stress drop caused by the effective alignment of their polymer chains are the parameters which mainly govern their bidirectional shape memory properties under constant load. The understanding of the synergic effect between the aforementioned parameters is essential for the development of polymeric actuators based on chemically/physically crosslinked semicrystalline networks able to deliver a controllable reversible shape memory effect. The magnitude, amplitude and actuation temperature of the bidirectional shape-switching transformation is strongly dependent of the structural architecture of the semicrystalline actuator.

ASSOCIATED CONTENT

Supporting Information

Table S1. Crosslinking agent content and thermal properties of crosslinked PCL networks exhibiting 2W-SME.; **Figure S1.** Chromatograms of the synthesized PCL diol and its derivate polyurethanes obtained from their GCP analysis.; **Table S2.** Mass average, number average molecular weight and polydispersity of PCL diol and PCL-based urethane shape memory polymers.; **Figure S2.** ¹H-NMR spectra of the isolated 14kDa PCL diol and its corresponding ester-urethane derivatives.; **Figure S3.** Thermal decomposition curves and deconvoluted DTGA profiles with Gaussian fitting for PCL diol and PCL-PU.s.; **Figure S4.** Complete thermograms obtained from the DSC analysis of the investigated semicrystalline materials with a heating/cooling ramp of 1°C min⁻¹.; **Figure S5.** Evolution of degree of crystallinity (X_c) fusion enthalpy (ΔH_f) and crystallization enthalpy (ΔH_c) with the crosslinking agent content/soft segment content on mass percentage for the studied polymers.; **Table S3.** Thermal conditions used for the mechanical testing at low and high stretching degree of the studied ester urethane polymers.; **Figure S6.** Stress-strain profiles of the selected semicrystalline polymer networks on molten state and at room temperature.; **Table S4.** Assessed Young modulus and selected thermal features of investigated PUs and crosslinked PCL-based networks.; **Table S5.** Tensile features of selected polyurethanes elongated up to 1200% of their original length at room temperature.; **Figure S7.** Complete consecutive thermomechanical cyclic essays performed over the investigated polyurethane systems under constant strain conditions, linear PCL DCP5% as reference.; **Figure S8.** Stress relaxation experiments and their corresponding fitting to a three exponential decay function for highly crosslinked PCL networks and selected PUs at low and high strain degrees.

AUTHOR INFORMATION

Corresponding Author

Leonid Ionov

* E-mail: leonid.ionov@uni-bayreuth.de

Author Contributions

The manuscript was written through contributions of all authors. All authors have given approval to the final version of the manuscript.

Funding Sources

Notes

The authors declare no conflicts of interest.

ACKNOWLEDGMENTS

ABBREVIATIONS

2W-SME, two-way shape memory effect; 2W-SMP, two-way shape memory polymers; PCL, poly(ϵ -caprolactone); CD-PCL, β -cyclodextrin PCL; SME, shape memory effect; DCP, dicumyl peroxide; DSC, differential scanning calorimetry; TGA, thermogravimetric analysis; HDI, Hexamethylene diisocyanate; MDI, 4,4'-diphenylmethane diisocyanate; BD, 1,4-Butanediol; PDA, poly(1,10-decylene adipate) diol; PU, polyurethane; CIE, crystallization induced elongation; MIC, melting induced contraction.

REFERENCES

- (1) Van der Schueren, L.; de Clerck, K. Halochromic Textile Materials as Innovative PH-Sensors. *Advances in Science and Technology* **2013**, *80*, 47–52. <https://doi.org/10.4028/www.scientific.net/AST.80.47>.
- (2) Xie, J.; Li, A.; Li, J. Advances in PH-Sensitive Polymers for Smart Insulin Delivery. *Macromolecular Rapid Communications* **2017**, *38* (23), 1700413. <https://doi.org/10.1002/marc.201700413>.
- (3) Pelrine, R.; Kornbluh, R.; Kofod, G. High-Strain Actuator Materials Based on Dielectric Elastomers. *Advanced Materials* **2000**, *12* (16), 1223–1225. [https://doi.org/10.1002/1521-4095\(200008\)12:16<1223::AID-ADMA1223>3.0.CO;2-2](https://doi.org/10.1002/1521-4095(200008)12:16<1223::AID-ADMA1223>3.0.CO;2-2).
- (4) Ning, C.; Zhou, Z.; Tan, G.; Zhu, Y.; Mao, C. Electroactive Polymers for Tissue Regeneration: Developments and Perspectives. *Progress in Polymer Science* **2018**, *81*, 144–162. <https://doi.org/10.1016/j.progpolymsci.2018.01.001>.
- (5) Hong, C. C. Application of a Magnetostrictive Actuator. *Materials & Design* **2013**, *46*, 617–621. <https://doi.org/10.1016/j.matdes.2012.11.013>.
- (6) Kitanovski, A. Energy Applications of Magnetocaloric Materials. *Advanced Energy Materials* **2020**, *10* (10), 1903741. <https://doi.org/10.1002/aenm.201903741>.
- (7) Kaur, N.; Singh, M.; Pathak, D.; Wagner, T.; Nunzi, J. M. Organic Materials for Photovoltaic Applications: Review and Mechanism. *Synthetic Metals* **2014**, *190*, 20–26. <https://doi.org/10.1016/j.synthmet.2014.01.022>.
- (8) Yao, H.; Wang, J.; Xu, Y.; Zhang, S.; Hou, J. Recent Progress in Chlorinated Organic Photovoltaic Materials. *Acc. Chem. Res.* **2020**, *53* (4), 822–832. <https://doi.org/10.1021/acs.accounts.0c00009>.
- (9) Chen, Z.; Hsu, P.-C.; Lopez, J.; Li, Y.; To, J. W. F.; Liu, N.; Wang, C.; Andrews, S. C.; Liu, J.; Cui, Y.; Bao, Z. Fast and Reversible Thermoresponsive Polymer Switching Materials for Safer Batteries. *Nat Energy* **2016**, *1* (1), 1–2. <https://doi.org/10.1038/nenergy.2015.9>.
- (10) Nagase, K.; Okano, T. Thermoresponsive-Polymer-Based Materials for Temperature-Modulated Bioanalysis and Bioseparations. *Journal of Materials Chemistry B* **2016**, *4* (39), 6381–6397. <https://doi.org/10.1039/C6TB01003B>.
- (11) Gopinath, S.; Adarsh, N. N.; Radhakrishnan Nair, P.; Mathew, S. One-Way Thermo-Responsive Shape Memory Polymer Nanocomposite Derived from Polycaprolactone and Polystyrene-Block-Polybutadiene-Block-Polystyrene Packed with Carbon Nanofiber. *Materials Today Communications* **2020**, *22*, 100802. <https://doi.org/10.1016/j.mtcomm.2019.100802>.
- (12) Hu, J.; Yang, Z.; Yeung, L.; Ji, F.; Liu, Y. Crosslinked Polyurethanes with Shape Memory Properties. *Polymer International* **2005**, *54* (5), 854–859. <https://doi.org/10.1002/pi.1785>.
- (13) Gao, H.; Li, J.; Zhang, F.; Liu, Y.; Leng, J. The Research Status and Challenges of Shape Memory Polymer-Based Flexible Electronics. *Materials Horizons* **2019**, *6* (5), 931–944. <https://doi.org/10.1039/C8MH01070F>.

- (14) Zarek, M.; Layani, M.; Cooperstein, I.; Sachyani, E.; Cohn, D.; Magdassi, S. 3D Printing: 3D Printing of Shape Memory Polymers for Flexible Electronic Devices (Adv. Mater. 22/2016). *Advanced Materials* **2016**, *28* (22), 4166–4166. <https://doi.org/10.1002/adma.201670148>.
- (15) Tippets, C. A.; Li, Q.; Fu, Y.; Donev, E. U.; Zhou, J.; Turner, S. A.; Jackson, A.-M. S.; Ashby, V. S.; Sheiko, S. S.; Lopez, R. Dynamic Optical Gratings Accessed by Reversible Shape Memory. *ACS Appl. Mater. Interfaces* **2015**, *7* (26), 14288–14293. <https://doi.org/10.1021/acsami.5b02688>.
- (16) Meng, Q.; Hu, J. A Review of Shape Memory Polymer Composites and Blends. *Composites Part A: Applied Science and Manufacturing* **2009**, *40* (11), 1661–1672. <https://doi.org/10.1016/j.compositesa.2009.08.011>.
- (17) Dolynchuk, O.; Kolesov, I.; Radusch, H.-J. Theoretical Description of an Anomalous Elongation During Two-Way Shape-Memory Effect in Crosslinked Semicrystalline Polymers. *Macromolecular Symposia* **2014**, *346* (1), 48–58. <https://doi.org/10.1002/masy.201400065>.
- (18) Chen, S.; Hu, J.; Zhuo, H.; Zhu, Y. Two-Way Shape Memory Effect in Polymer Laminates. *Materials Letters* **2008**, *62* (25), 4088–4090. <https://doi.org/10.1016/j.matlet.2008.05.073>.
- (19) Wang, K.; Jia, Y.-G.; Zhu, X. X. Two-Way Reversible Shape Memory Polymers Made of Cross-Linked Cocrystallizable Random Copolymers with Tunable Actuation Temperatures. *Macromolecules* **2017**, *50* (21), 8570–8579. <https://doi.org/10.1021/acs.macromol.7b01815>.
- (20) Behl, M.; Kratz, K.; Zotzmann, J.; Nöchel, U.; Lendlein, A. Reversible Bidirectional Shape-Memory Polymers. *Advanced Materials* **2013**, *25* (32), 4466–4469. <https://doi.org/10.1002/adma.201300880>.
- (21) Saatchi, M.; Behl, M.; Nöchel, U.; Lendlein, A. Copolymer Networks From Oligo(ϵ -Caprolactone) and n-Butyl Acrylate Enable a Reversible Bidirectional Shape-Memory Effect at Human Body Temperature. *Macromolecular Rapid Communications* **2015**, *36* (10), 880–884. <https://doi.org/10.1002/marc.201400729>.
- (22) Li, Q.; Zhou, J.; Vatankhah-Varnoosfaderani, M.; Nykypanchuk, D.; Gang, O.; Sheiko, S. S. Advancing Reversible Shape Memory by Tuning the Polymer Network Architecture. *Macromolecules* **2016**, *49* (4), 1383–1391. <https://doi.org/10.1021/acs.macromol.5b02740>.
- (23) Wu, Y.; Hu, J.; Han, J.; Zhu, Y.; Huang, H.; Li, J.; Tang, B. Two-Way Shape Memory Polymer with “Switch–Spring” Composition by Interpenetrating Polymer Network. *Journal of Materials Chemistry A* **2014**, *2* (44), 18816–18822. <https://doi.org/10.1039/C4TA03640A>.
- (24) Fan, L. F.; Rong, M. Z.; Zhang, M. Q.; Chen, X. D. A Facile Approach Toward Scalable Fabrication of Reversible Shape-Memory Polymers with Bonded Elastomer Microphases as Internal Stress Provider. *Macromolecular Rapid Communications* **2017**, *38* (16), 1700124. <https://doi.org/10.1002/marc.201700124>.
- (25) Behl, M.; Lendlein, A. Shape-Memory Polymers. *Materials Today* **2007**, *10* (4), 20–28. [https://doi.org/10.1016/S1369-7021\(07\)70047-0](https://doi.org/10.1016/S1369-7021(07)70047-0).
- (26) Li, J.; Rodgers, W. R.; Xie, T. Semi-Crystalline Two-Way Shape Memory Elastomer. *Polymer* **2011**, *52* (23), 5320–5325. <https://doi.org/10.1016/j.polymer.2011.09.030>.

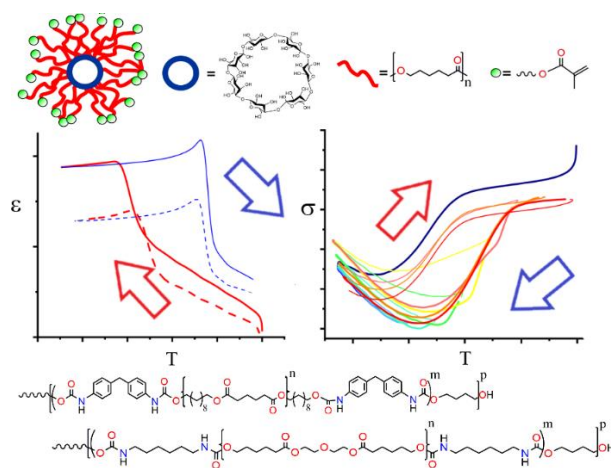
- (27) Chung, T.; Romo-Uribe, A.; Mather, P. T. Two-Way Reversible Shape Memory in a Semicrystalline Network. *Macromolecules* **2008**, *41* (1), 184–192. <https://doi.org/10.1021/ma071517z>.
- (28) Pandini, S.; Passera, S.; Messori, M.; Paderni, K.; Toselli, M.; Gianoncelli, A.; Bontempi, E.; Riccò, T. Two-Way Reversible Shape Memory Behaviour of Crosslinked Poly(ϵ -Caprolactone). *Polymer* **2012**, *53* (9), 1915–1924. <https://doi.org/10.1016/j.polymer.2012.02.053>.
- (29) Dolynchuk, O.; Kolesov, I.; Jehnichen, D.; Reuter, U.; Radusch, H.-J.; Sommer, J.-U. Reversible Shape-Memory Effect in Cross-Linked Linear Poly(ϵ -Caprolactone) under Stress and Stress-Free Conditions. *Macromolecules* **2017**, *50* (10), 3841–3854. <https://doi.org/10.1021/acs.macromol.7b00481>.
- (30) Pandini, S.; Dioni, D.; Paderni, K.; Messori, M.; Toselli, M.; Bontempi, E.; Riccò, T. The Two-Way Shape Memory Behaviour of Crosslinked Poly(ϵ -Caprolactone) Systems with Largely Varied Network Density. *Journal of Intelligent Material Systems and Structures* **2016**, *27* (10), 1388–1403. <https://doi.org/10.1177/1045389X15591384>.
- (31) Raquez, J.-M.; Vanderstappen, S.; Meyer, F.; Verge, P.; Alexandre, M.; Thomassin, J.-M.; Jérôme, C.; Dubois, P. Design of Cross-Linked Semicrystalline Poly(ϵ -Caprolactone)-Based Networks with One-Way and Two-Way Shape-Memory Properties through Diels–Alder Reactions. *Chemistry – A European Journal* **2011**, *17* (36), 10135–10143. <https://doi.org/10.1002/chem.201100496>.
- (32) Han, J.-L.; Lai, S.-M.; Chiu, Y. T. Two-Way Multi-Shape Memory Properties of Peroxide Crosslinked Ethylene Vinyl-Acetate Copolymer (EVA)/Polycaprolactone (PCL) Blends. *Polymers for Advanced Technologies* **2018**, *29* (7), 2010–2024. <https://doi.org/10.1002/pat.4309>.
- (33) Huang, M.; Dong, X.; Wang, L.; Zhao, J.; Liu, G.; Wang, D. Two-Way Shape Memory Property and Its Structural Origin of Cross-Linked Poly(ϵ -Caprolactone). *RSC Advances* **2014**, *4* (98), 55483–55494. <https://doi.org/10.1039/C4RA09385B>.
- (34) Chen, S.; Hu, J.; Zhuo, H. Properties and Mechanism of Two-Way Shape Memory Polyurethane Composites. *Composites Science and Technology* **2010**, *70* (10), 1437–1443. <https://doi.org/10.1016/j.compscitech.2010.01.017>.
- (35) Bothe, M.; Pretsch, T. Bidirectional Actuation of a Thermoplastic Polyurethane Elastomer. *Journal of Materials Chemistry A* **2013**, *1* (46), 14491–14497. <https://doi.org/10.1039/C3TA13414H>.
- (36) Peponi, L.; Navarro-Baena, I.; Sonseca, A.; Gimenez, E.; Marcos-Fernandez, A.; Kenny, J. M. Synthesis and Characterization of PCL–PLLA Polyurethane with Shape Memory Behavior. *European Polymer Journal* **2013**, *49* (4), 893–903. <https://doi.org/10.1016/j.eurpolymj.2012.11.001>.
- (37) Biswas, A.; Aswal, V. K.; Sastry, P. U.; Rana, D.; Maiti, P. Reversible Bidirectional Shape Memory Effect in Polyurethanes through Molecular Flipping. *Macromolecules* **2016**, *49* (13), 4889–4897. <https://doi.org/10.1021/acs.macromol.6b00536>.
- (38) Hong, S. J.; Yu, W.-R.; Youk, J. H. Two-Way Shape Memory Behavior of Shape Memory Polyurethanes with a Bias Load. *Smart Mater. Struct.* **2010**, *19* (3), 035022. <https://doi.org/10.1088/0964-1726/19/3/035022>.

- (39) Gu, X.; Mather, P. T. Entanglement-Based Shape Memory Polyurethanes: Synthesis and Characterization. *Polymer* **2012**, *53* (25), 5924–5934. <https://doi.org/10.1016/j.polymer.2012.09.056>.
- (40) Zhou, Y.; Zhou, D.; Cao, P.; Zhang, X.; Wang, Q.; Wang, T.; Li, Z.; He, W.; Ju, J.; Zhang, Y. 4D Printing of Shape Memory Vascular Stent Based on BCD-g-Polycaprolactone. *Macromolecular Rapid Communications* **2021**, *42* (14), 2100176. <https://doi.org/10.1002/marc.202100176>.
- (41) Báez, J. E.; Marcos-Fernández, Á.; Lebrón-Aguilar, R.; Martínez-Richa, A. A Novel Route to α,ω -Telechelic Poly(ϵ -Caprolactone) Diols, Precursors of Biodegradable Polyurethanes, Using Catalysis by Decamolybdate Anion. *Polymer* **2006**, *47* (26), 8420–8429. <https://doi.org/10.1016/j.polymer.2006.10.023>.
- (42) Mi, H.-Y.; Jing, X.; Napiwocki, B. N.; Hagerty, B. S.; Chen, G.; Turng, L.-S. Biocompatible, Degradable Thermoplastic Polyurethane Based on Polycaprolactone-Block-Polytetrahydrofuran-Block-Polycaprolactone Copolymers for Soft Tissue Engineering. *J. Mater. Chem. B* **2017**, *5* (22), 4137–4151. <https://doi.org/10.1039/C7TB00419B>.
- (43) Kloss, J.; Munaro, M.; De Souza, G. P.; Gulmine, J. V.; Wang, S. H.; Zawadzki, S.; Akcelrud, L. Poly(Ester Urethane)s with Polycaprolactone Soft Segments: A Morphological Study. *Journal of Polymer Science Part A: Polymer Chemistry* **2002**, *40* (23), 4117–4130. <https://doi.org/10.1002/pola.10499>.
- (44) Uribe-Gomez, J.; Posada-Murcia, A.; Shukla, A.; Alkhamis, H.; Salehi, S.; Ionov, L. Soft Elastic Fibrous Scaffolds for Muscle Tissue Engineering by Touch Spinning. *ACS Appl. Bio Mater.* **2021**, *4* (7), 5585–5597. <https://doi.org/10.1021/acsabm.1c00403>.
- (45) Schönfeld, D.; Chalissery, D.; Wenz, F.; Specht, M.; Eberl, C.; Pretsch, T. Actuating Shape Memory Polymer for Thermoresponsive Soft Robotic Gripper and Programmable Materials. *Molecules* **2021**, *26* (3), 522. <https://doi.org/10.3390/molecules26030522>.
- (46) Fernández, M. J.; Fernández, M. D.; Cobos, M. Synthesis, Characterization and Properties of Telechelic Hybrid Biodegradable Polymers Containing Polyhedral Oligomeric Silsesquioxane (POSS). *RSC Adv.* **2014**, *4* (41), 21435–21449. <https://doi.org/10.1039/C4RA02172J>.
- (47) Wackerly, J. Wm.; Dunne, J. F. Synthesis of Polystyrene and Molecular Weight Determination by ¹H NMR End-Group Analysis. *J. Chem. Educ.* **2017**, *94* (11), 1790–1793. <https://doi.org/10.1021/acs.jchemed.6b00814>.
- (48) Pérez, J. M.; Ruiz, C.; Fernández, I. Synthesis of a Biodegradable PLA: NMR Signal Deconvolution and End-Group Analysis. *J. Chem. Educ.* **2022**, *99* (2), 1000–1007. <https://doi.org/10.1021/acs.jchemed.1c00824>.
- (49) Guo, J.; Yin, J.; Feng, Y. Synthesis and Characterization of HDI/MDI-Polycarbonate Urethanes. *Trans. Tianjin Univ.* **2010**, *16* (5), 317–321. <https://doi.org/10.1007/s12209-010-1506-z>.
- (50) Fernández-d'Arlas, B.; Alonso-Varona, A.; Palomares, T.; Corcuera, M. A.; Eceiza, A. Studies on the Morphology, Properties and Biocompatibility of Aliphatic Diisocyanate-Polycarbonate Polyurethanes. *Polymer Degradation and Stability* **2015**, *122*, 153–160. <https://doi.org/10.1016/j.polymdegradstab.2015.10.023>.

- (51) Persenaire, O.; Alexandre, M.; Degée, P.; Dubois, P. Mechanisms and Kinetics of Thermal Degradation of Poly(ϵ -Caprolactone). *Biomacromolecules* **2001**, *2* (1), 288–294. <https://doi.org/10.1021/bm0056310>.
- (52) Haryńska, A.; Kucinska-Lipka, J.; Sulowska, A.; Gubanska, I.; Kostrzewa, M.; Janik, H. Medical-Grade PCL Based Polyurethane System for FDM 3D Printing—Characterization and Fabrication. *Materials* **2019**, *12* (6), 887. <https://doi.org/10.3390/ma12060887>.
- (53) Bajsić, E. G.; Rek, V. Thermal Stability of Polyurethane Elastomers before and after UV Irradiation. *Journal of Applied Polymer Science* **2001**, *79* (5), 864–873. [https://doi.org/10.1002/1097-4628\(20010131\)79:5<864::AID-APP110>3.0.CO;2-D](https://doi.org/10.1002/1097-4628(20010131)79:5<864::AID-APP110>3.0.CO;2-D).
- (54) Askari, F.; Barikani, M.; Barmar, M. Study on Thermal Stability of Polyurethane-Urea Based on Polysiloxane and Polycaprolactone Diols. *Korean J. Chem. Eng.* **2013**, *30* (11), 2093–2099. <https://doi.org/10.1007/s11814-013-0139-z>.
- (55) Rosu, D.; Tudorachi, N.; Rosu, L. Investigations on the Thermal Stability of a MDI Based Polyurethane Elastomer. *Journal of Analytical and Applied Pyrolysis* **2010**, *89* (2), 152–158. <https://doi.org/10.1016/j.jaap.2010.07.004>.
- (56) Van Horn, R. M.; Steffen, M. R.; O'Connor, D. Recent Progress in Block Copolymer Crystallization. *POLYMER CRYSTALLIZATION* **2018**, *1* (4), e10039. <https://doi.org/10.1002/pcr2.10039>.
- (57) Li, F.; Hou, J.; Zhu, W.; Zhang, X.; Xu, M.; Luo, X.; Ma, D.; Kim, B. K. Crystallinity and Morphology of Segmented Polyurethanes with Different Soft-Segment Length. *Journal of Applied Polymer Science* **1996**, *62* (4), 631–638. [https://doi.org/10.1002/\(SICI\)1097-4628\(19961024\)62:4<631::AID-APP6>3.0.CO;2-U](https://doi.org/10.1002/(SICI)1097-4628(19961024)62:4<631::AID-APP6>3.0.CO;2-U).
- (58) Pergal, M. V.; Antić, V. V.; Govedarica, M. N.; Goëvac, D.; Ostojić, S.; Djonlagić, J. Synthesis and Characterization of Novel Urethane-Siloxane Copolymers with a High Content of PCL-PDMS-PCL Segments. *Journal of Applied Polymer Science* **2011**, *122* (4), 2715–2730. <https://doi.org/10.1002/app.33926>.
- (59) Wall, F. T.; Flory, P. J. Statistical Thermodynamics of Rubber Elasticity. *J. Chem. Phys.* **1951**, *19* (12), 1435–1439. <https://doi.org/10.1063/1.1748098>.
- (60) Nunes, R. W.; Martin, J. R.; Johnson, J. F. Influence of Molecular Weight and Molecular Weight Distribution on Mechanical Properties of Polymers. *Polymer Engineering & Science* **1982**, *22* (4), 205–228. <https://doi.org/10.1002/pen.760220402>.
- (61) Posada-Murcia, A.; Uribe-Gomez, J. M.; Förster, S.; Sommer, J.-U.; Dulle, M.; Ionov, L. Mechanism of Behavior of Two-Way Shape Memory Polymer under Constant Strain Conditions. *Macromolecules* **2022**, *55* (5), 1680–1689. <https://doi.org/10.1021/acs.macromol.1c02564>.
- (62) Posada-Murcia, A.; Uribe-Gomez, J. M.; Sommer, J.-U.; Ionov, L. Two-Way Shape Memory Polymers: Evolution of Stress vs Evolution of Elongation. *Macromolecules* **2021**, *54* (12), 5838–5847. <https://doi.org/10.1021/acs.macromol.1c00568>.
- (63) Ziabicki, A. Statistical Theory of Entanglement Density in Linear Polymers and Fiber Systems. I. General Considerations. *J. Chem. Phys.* **1976**, *64* (10), 4100–4106. <https://doi.org/10.1063/1.431977>.

- (64) Hajikarimi, P.; Moghadas Nejad, F. Chapter 3 - Mechanical Models of Viscoelasticity. In *Applications of Viscoelasticity*; Hajikarimi, P., Moghadas Nejad, F., Eds.; Elsevier, 2021; pp 27–61. <https://doi.org/10.1016/B978-0-12-821210-3.00003-6>.
- (65) Malkin, A. Ya.; Isayev, A. 2 - VISCOELASTICITY. In *Rheology (Third Edition)*; Malkin, A. Ya., Isayev, A., Eds.; ChemTec Publishing, 2017; pp 45–128. <https://doi.org/10.1016/B978-1-927885-21-5.50008-4>.
- (66) Zare, M.; Prabhakaran, M. P.; Parvin, N.; Ramakrishna, S. Thermally-Induced Two- Way Shape Memory Polymers: Mechanisms, Structures, and Applications. *Chemical Engineering Journal* **2019**, 374, 706–720. <https://doi.org/10.1016/j.cej.2019.05.167>.

For Table of Contents Only



Supporting Information for:

Bidirectional shape memory polymers: effect of
molecular architecture over the
thermomechanical behaviour at constant stress
and constant strain conditions

*Andrés Posada-Murcia[§], Dennis Schönfeld[#], Yaoming Zhang^{†, ‡}, Juan Manuel Uribe-
Gomez[§], Thorsten Pretsch[#] and Leonid Ionov^{§*}*

[§]Faculty of Engineering Sciences and Bavarian Polymer Institute,
University of Bayreuth, Ludwig Thoma Str. 36A, 95447, Bayreuth, Germany

[#]Fraunhofer Institute for Applied Polymer Research IAP, Geiselbergstr. 69, 14476
Potsdam, Germany

[†]Center of Materials Science and Optoelectronics Engineering, University of Chinese
Academy of Sciences, Beijing, 100049, P. R. China.

[‡]State Key Laboratory of Bio-Fibers and Eco-Textiles, Qingdao University, Qingdao,
266071, P. R. China.

Name	Amount of crosslinker (% wt)	ΔH_f (J g ⁻¹)	ΔH_c (J g ⁻¹)	X_c (%) ^a	T_m (°C)	T_c (°C)
PCL 80 kDa	0	66.81	65.62	47.89	58.06	33.45
PCL DCP 2%	2	57.69	52.70	41.35	56.45	36.07
PCL DCP 5%	5	54.49	49.82	39.06	54.46	36.00
CD-PCL	0	66.18	61.49	47.44	58.34	44.85
CD-PCL DCP 2%	2	65.52	58.11	46.97	56.79	39.78
CD-PCL DCP 5%	5	64.82	56.76	46.46	56.37	38.57
CD-PCL DCP 8%	8	60.58	53.05	43.42	52.63	35.02

^a X_c was calculated by $X_c = \frac{H_{f,exp}}{w \cdot H_{f,th}^0} * 100$, where w is PCL mass fraction and 139.5 Jg⁻¹ was considered as enthalpy of fusion for 100% crystalline PCL¹.

Table S1. Crosslinking agent content and thermal properties of crosslinked PCL networks exhibiting 2W-SME

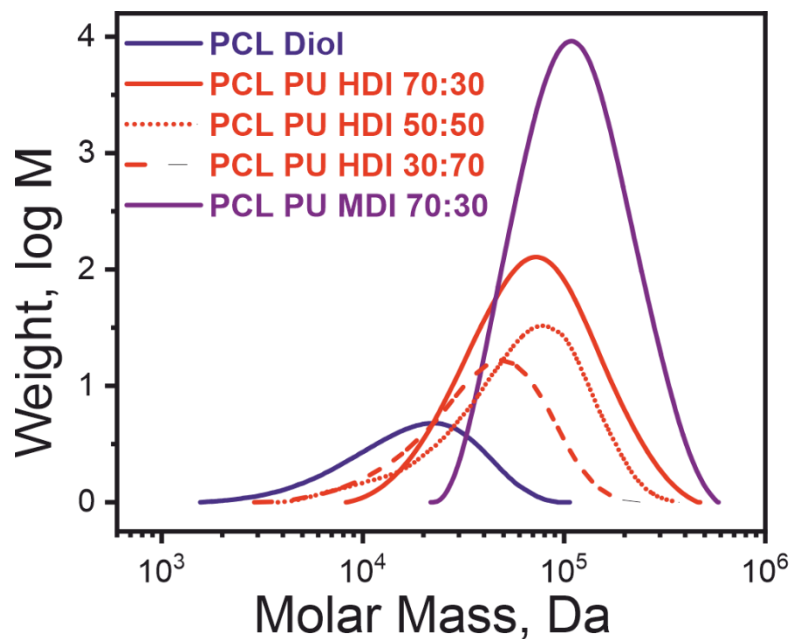


Figure S1. Chromatograms of the synthesized PCL diol and its derivate polyurethanes obtained from their GPC analysis.

Name	M_w (g mol ⁻¹)	M_n (g mol ⁻¹)	Polydispersity (Đ)
PCL diol	2.35×10^4	1.45×10^4	1.61
PCL-PU (HDI+BD) 70:30	8.77×10^4	5.36×10^4	1.64
PCL-PU (HDI+BD) 50:50	7.33×10^4	4.15×10^4	1.76
PCL-PU (HDI+BD) 30:70	5.02×10^4	3.21×10^4	1.56
PCL-PU (MDI+BD) 70:30	1.33×10^5	9.34×10^4	1.42

Table S2. Mass average, number average molecular weight and polydispersity of PCL diol and PCL-based urethane shape memory polymers

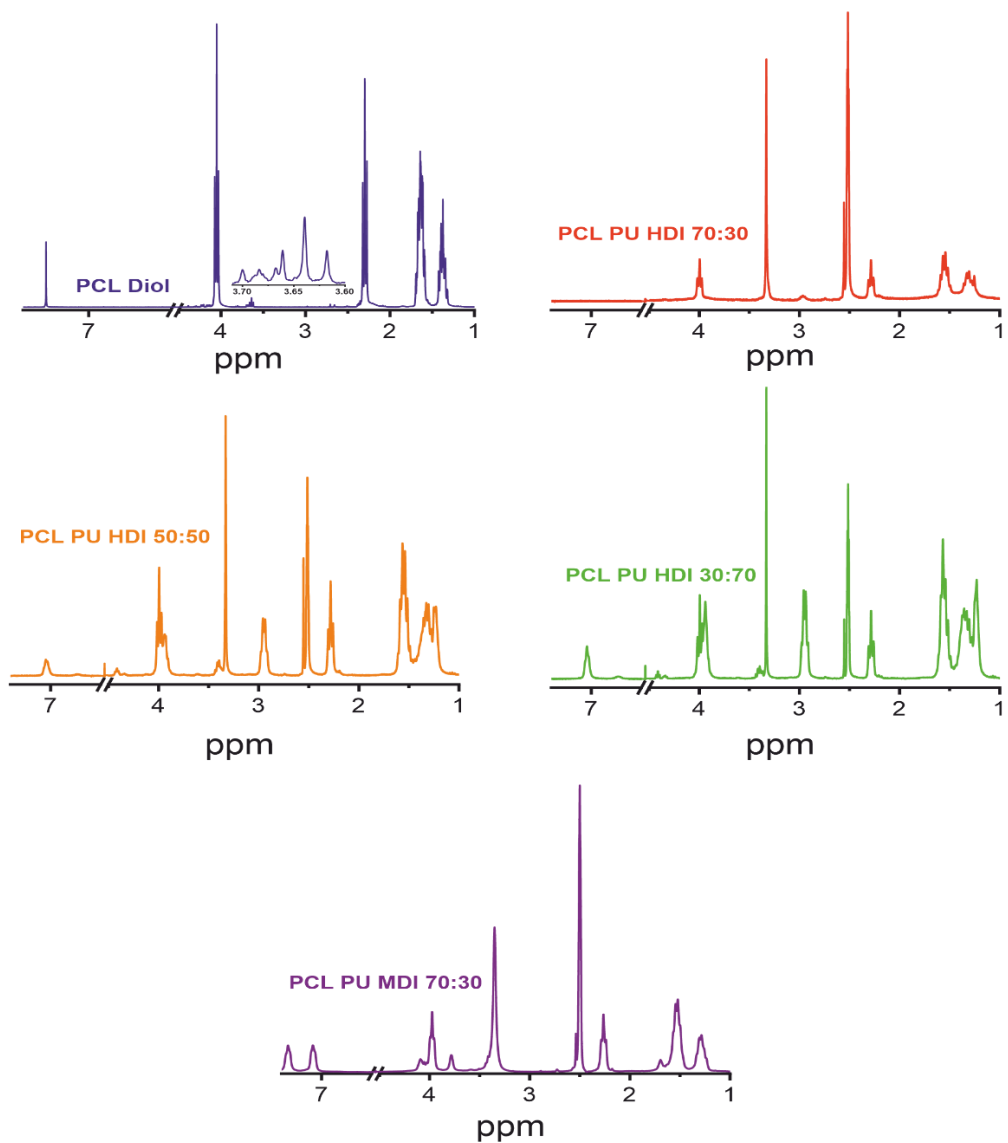


Figure S2. ¹H-NMR spectra of the isolated 14kDa PCL diol and its corresponding ester-urethane derivatives.

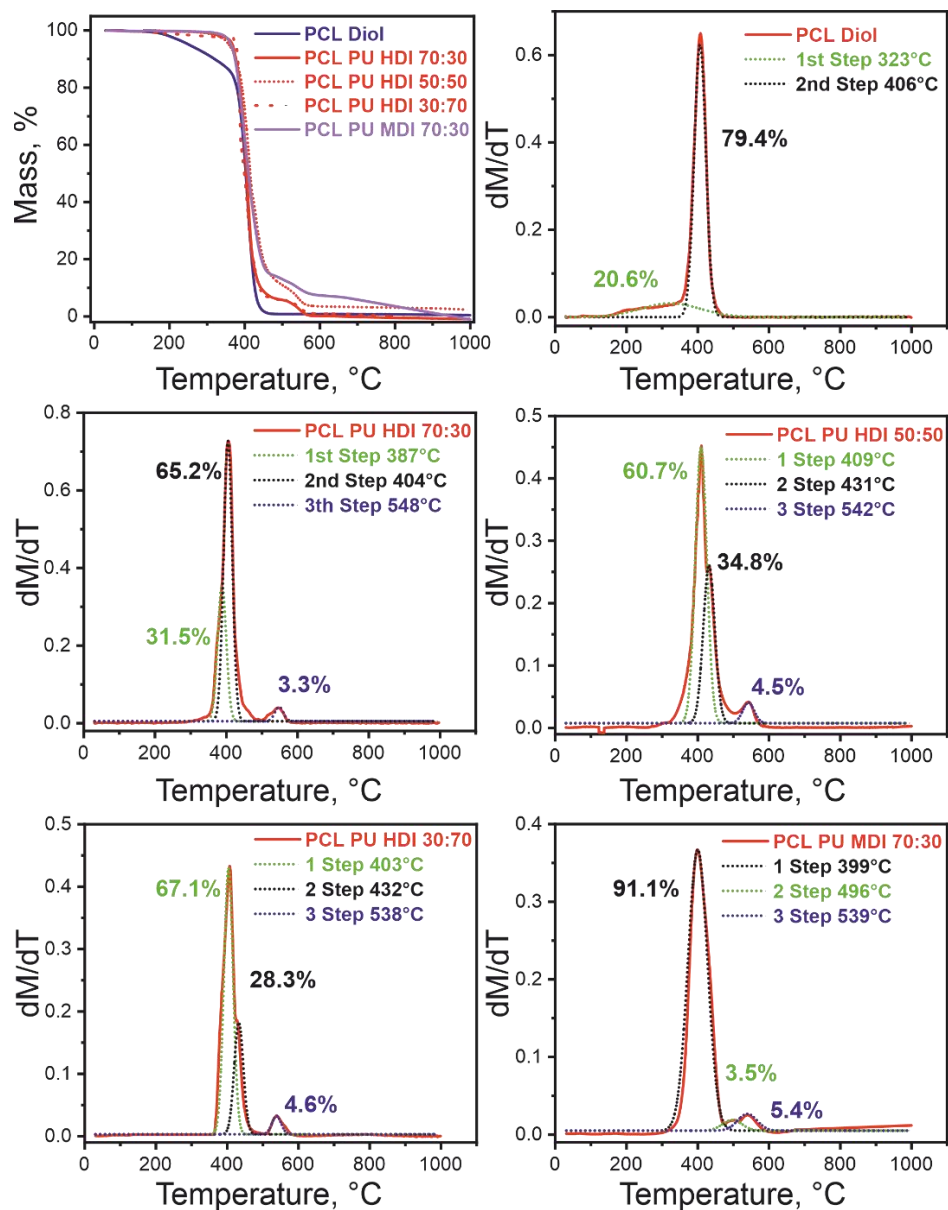


Figure S3. Thermal decomposition curves and deconvoluted DTGA profiles with Gaussian fitting for PCL diol and PCL-PU.

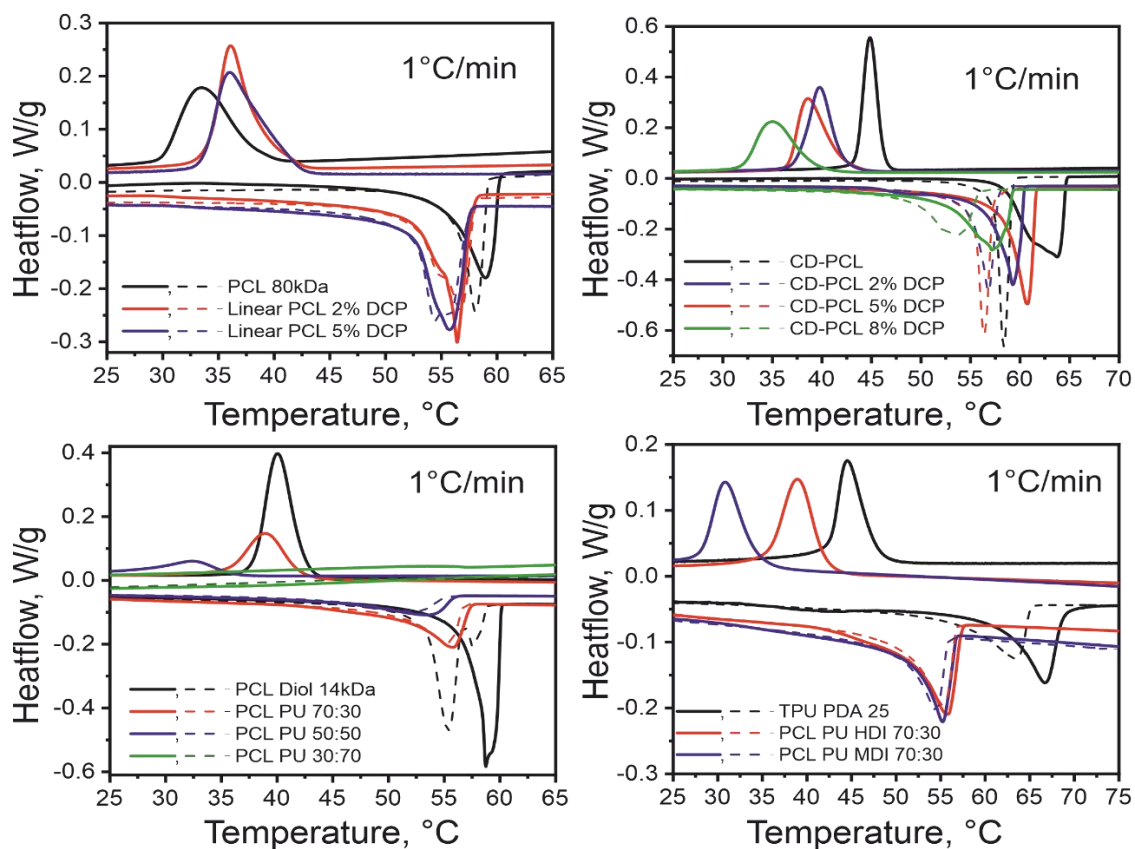


Figure S4. Complete thermograms obtained from the DSC analysis of the investigated semicrystalline materials with a heating/cooling ramp of $1^{\circ}\text{C min}^{-1}$.

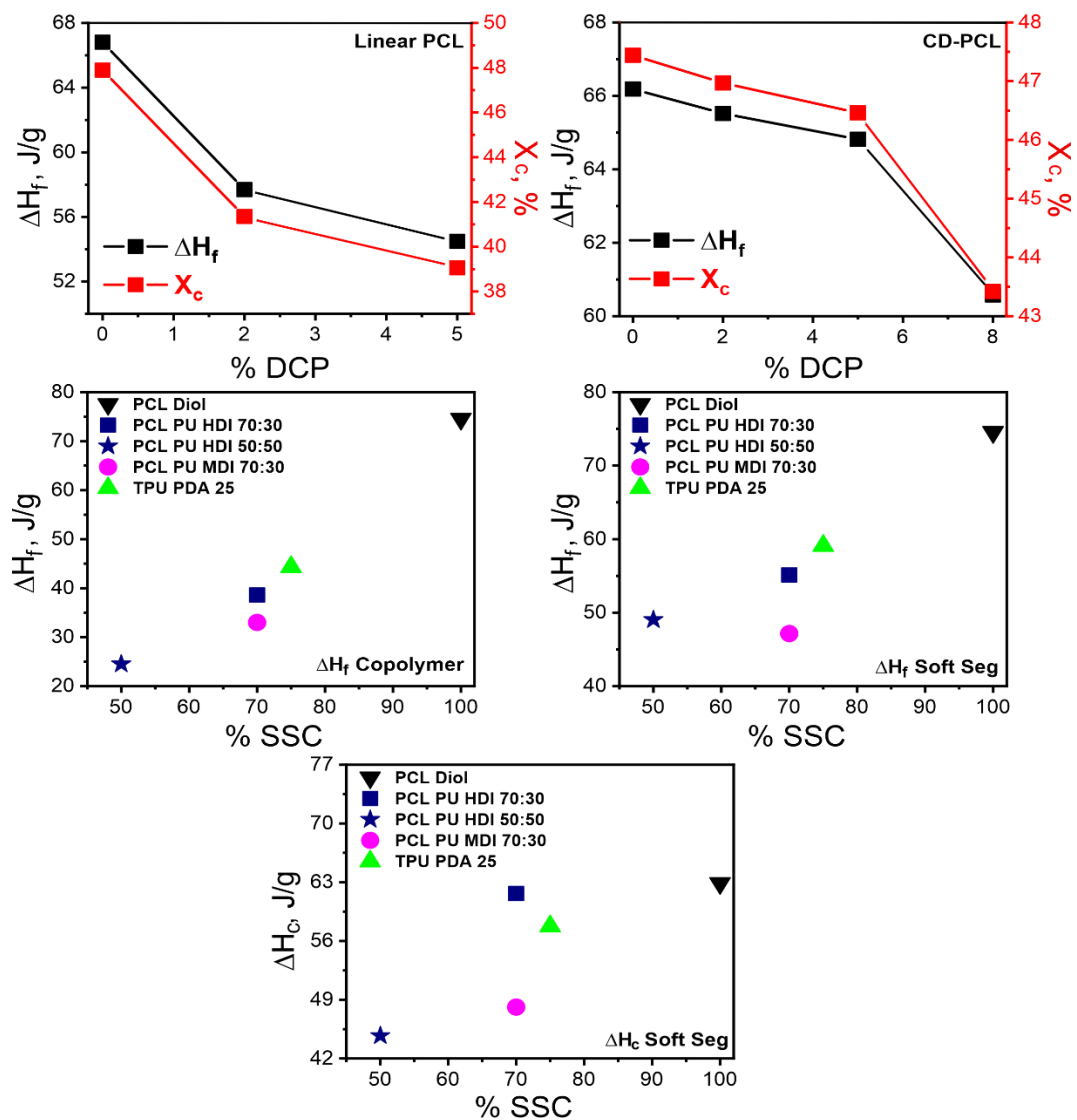


Figure S5. Evolution of degree of crystallinity (X_c) fusion enthalpy (ΔH_f) and crystallization enthalpy (ΔH_c) with the crosslinking agent content/soft segment content on mass percentage for the studied polymers.

	Low Strain Conditions	High Strain Conditions
Material Elongation^a (%)	50	200
Name	Temperature (°C)^b	Temperature (°C)
PCL-PU (HDI+BD) 70:30	60	70
PCL-PU (MDI+BD) 70:30	60	-
TPU-PDA 25	65	70

^a Samples were subdued to stretching or loading processes provoking their elongation to 50 and 200% of their original length. ^b Temperatures used on the mechanical tests involving low strain conditions were selected as PCL-PU (MDI+BD) 70:30 softens and breaks above 60°C. TPU-PDA exhibits higher T_m than PCL-PU. The materials are roughly 3-4°C above their T_m .

Table S3. Thermal conditions used for the mechanical testing at low and high stretching degree of the studied ester urethane polymers.

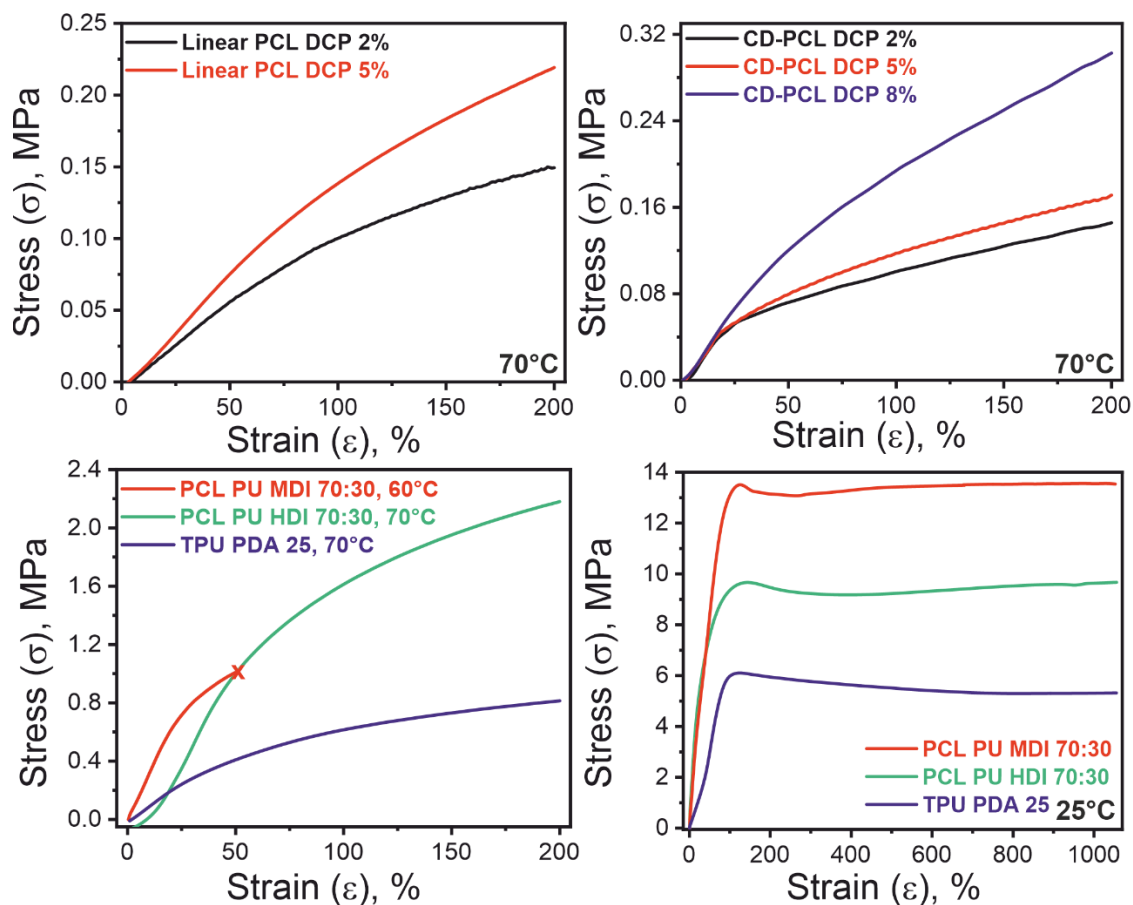


Figure S6. Stress-strain profiles of the selected semicrystalline polymer networks on molten state and at room temperature.

Name	Young Modulus (MPa)	Temperature	ΔH_c Copolymer ($J g^{-1}$)	T_m ($^{\circ}C$)	T_c ($^{\circ}C$)
PCL-PU (HDI+BD) 70:30	2.2	70	43.15	55.41	38.94
PCL-PU (HDI+BD) 70:30	3.5	60	43.15	55.41	38.94
PCL-PU (MDI+BD) 70:30	3.8	60	33.69	54.54	30.84
TPU-PDA 25	1.1	70	43.32	62.37	44.61
TPU-PDA 25	1.9	65	43.32	62.37	44.61
PCL DCP 2%	0.10	70	52.70	56.45	36.07
PCL DCP 5%	0.15	70	49.82	54.46	36.00
CD-PCL DCP 2%	0.22	70	58.11	56.79	39.78
CD-PCL DCP 5%	0.25	70	56.76	56.37	38.57
CD-PCL DCP 8%	0.28	70	53.05	52.63	35.02

Table S4. Assessed Young modulus and selected thermal features of investigated PUs and crosslinked PCL-based networks.

Name	Yield Stress (MPa)	Yield Strain (%)
PCL-PU (HDI+BD) 70:30	9.67	150.4
PCL-PU (MDI+BD) 70:30	13.56	131.3
TPU-PDA 25	6.11	130.4

Table S5. Tensile features of selected polyurethanes elongated up to 1200% of their original length at room temperature.

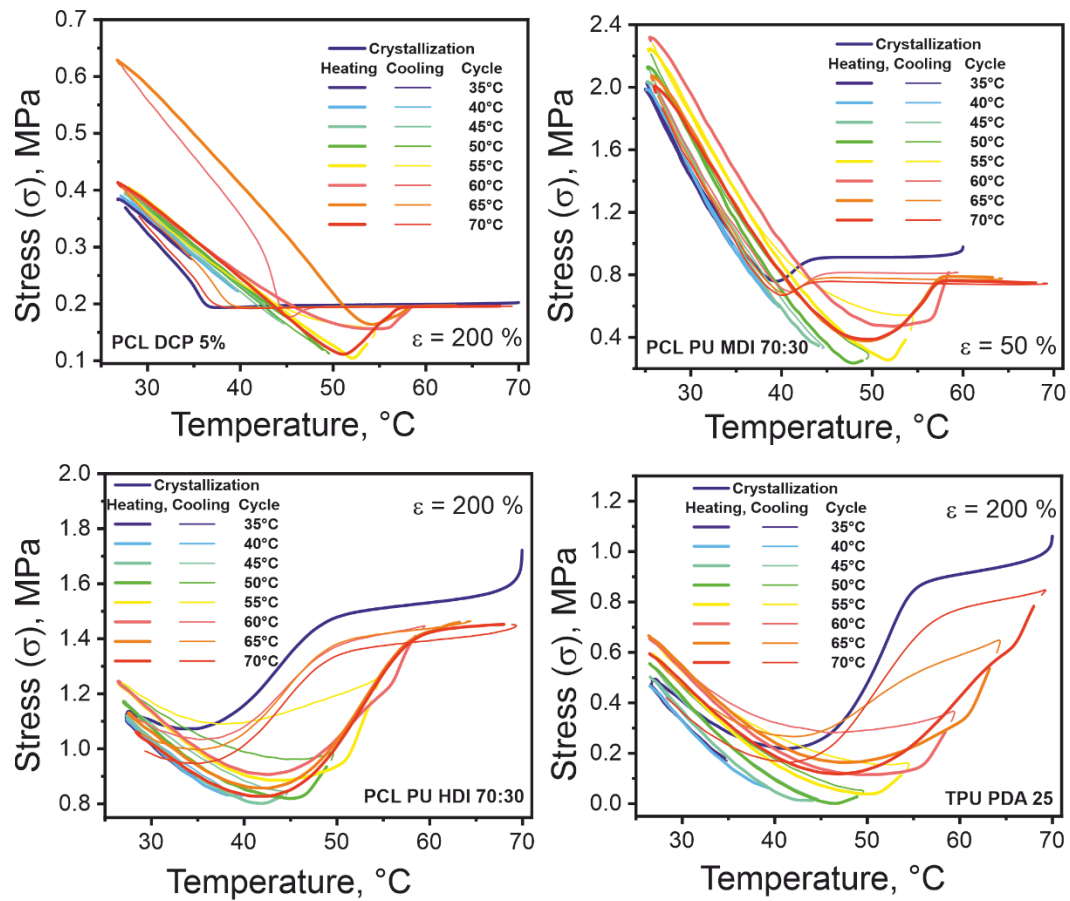


Figure S7. Complete consecutive thermomechanical cyclic essays performed over the investigated polyurethane systems under constant strain conditions, linear PCL DCP5% as reference.

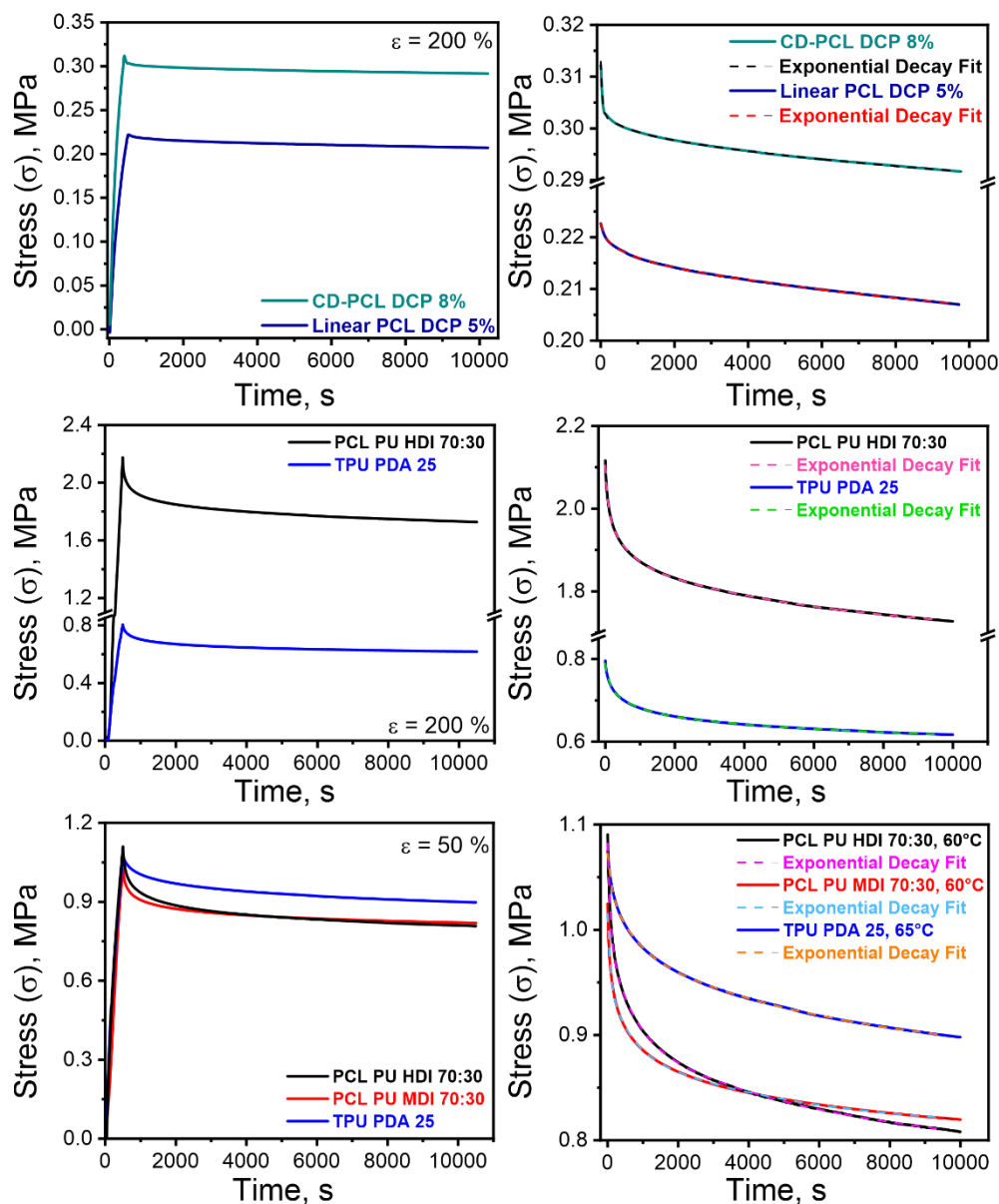


Figure S8. Stress relaxation experiments and their corresponding fitting to a three exponential decay function for highly crosslinked PCL networks and selected PUs at low and high strain degrees.

REFERENCES

- (1) Crescenzi, V.; Manzini, G.; Calzolari, G.; Borri, C. Thermodynamics of Fusion of Poly- β -Propiolactone and Poly- ϵ -Caprolactone. Comparative Analysis of the Melting of Aliphatic Polylactone and Polyester Chains. *European Polymer Journal* **1972**, *8* (3), 449–463. [https://doi.org/10.1016/0014-3057\(72\)90109-7](https://doi.org/10.1016/0014-3057(72)90109-7).

8. Conclusion

An integral investigation of the molecular mechanism responsible for the thermally induced 2W-SME on semicrystalline polymer networks was accomplished. The production of reversible polymeric actuators based on cured PCL networks and PCL-polyurethane copolymers was successful. The study of their tensile, physicochemical and textural properties under thermal cycling and constant strain conditions was meticulously driven, bringing clarity over overlooked/ unexplored aspects of the 2W-SME mechanism. Therefore, the main highlights of this thesis are presented as follows:

- ❖ The parallelism between the evolution of the thermomechanical properties of stretched and unstretched crosslinked PCL films with different crosslinking densities under constant stress and the constant strain was explored. The study of the evolution of the extensional stress for constantly strained cured elastomers upon cooling allowed the identification of an unexpected and unprecedented transitional state between the molten and the crystalline state; this intermediate state is characterized by a strong stress drop before the onset of the crystallization process on the polymeric matrix. The magnitude of this stress drop is proportional to the extent of the strain imposed over cured elastomers.

Another interesting observation extracted from the mechanical characterization of the intermediate state was that its onset temperature is practically independent of the crosslinking density of the materials, but shifts to higher values as the degree of strain also arises. These facts denote that the cause of this intermediate odd mechanical behaviour is strongly correlated with the entropy reduction of the polymer chains caused by the effective orientation of the polymer chains towards the stretching direction. The effect of the degree of orientation on the polymer matrix over the thermomechanical features of constantly strained cured elastomers was way notorious. A sharp correlation between the reduction of the value of stress at the lowest temperature of the thermomechanical cycle with the increase of the extension of the materials was observed; thus, the higher is the stretching degree, the more oriented the polymer chains are, and

therefore smaller are the conformation changes upon crystallization and the smaller is the resulting stress in the semicrystalline state caused by the shrinking of the material.

- ❖ A continuation of the investigation of the newly acknowledged stress drop regime on cured PCL undergoing a thermally induced 2W-SME under constant load was implemented. Supported by *in-situ* SAXS/WAXS measurements, the unrevealing of a two-stepped crystallization mechanism was possible; a highly directed family of crystallites is formed along with the uniaxial deformation as the stress drop is recorded, followed by a massive non-orientated crystallization process upon further cooling. The WAXS essays allowed us to confirm that as the appearance of the stress drop was being measured, a sharp anisotropic signal was also detected. These reflections find their origin in a greatly oriented crystallization process of PCL's crystalline domains. As the minimum of the measured force was recorded, the signal's intensity reached ca 80% of its final height; from this point and as the cooling of the samples proceeded, isotropic reflections corresponding to crystallization of non-oriented crystalline domains were detected on the 2D WAXS pattern.

Additionally, the SAXS measurements together with the form and structure factor fitting studies derived from it, corroborated the aforementioned observations. The appearance of meridional spots on the SAXS 2D pattern at the same temperature range where the WAXS isotropic reflections were noted is caused by the formation of directed platelets stacking on a disc form along the stretching direction. Correspondingly, an isotropic equatorial scattering fitting with the formation of non-oriented lamellae domains were noted as the force reached its minimum value and started to increase. The onset of isotropic reflections for both SAXS and WAXS shifted to higher temperature values for largely strained samples; this validated the observations and correlations made for the thermomechanical features of crosslinked PCL probes in our previous investigations. The development of a model based on these observations allowed a clear and important differentiation between the crystallization mechanism of semicrystalline polymer networks under constant stress and constant strain scenarios.

- ❖ The synthesis and characterization of PCL-based polyurethanes (PCL-PU) with different hard segment content and varied chemical nature was performed. Their 2W-SME was directly compared with chemically crosslinked linear and star-like PCLs derived from β -cyclodextrin (CD-PCL). For linear PCLs the observed stress drop is observed at lower temperatures than for CD-PCLs, also, the star-like PCLs exhibited a larger magnitude of stress in comparison with the linear crosslinked PCL. The reason for this is that the cyclodextrin nuclei act as additional cleavage points, creating a stronger crosslinking effect on the polymer network and subsequently increasing the effective orientation of the polymer chains towards the applied deformation.

During the evaluation of their bidirectional shape memory properties, it was noted that, in general, the PUs exhibited larger storage modulus, greater stress drops upon cooling on the constant strain, and hindered strain deformations under constant stress setups in comparison with their crosslinked analogues. The insertion of PU domains has a sharper crosslinking impact on the physicochemical, thermomechanical, and textural properties of the PCL semicrystalline networks than the curing processes. The mechanical features of the PCL-PU were directly compared with the thermomechanical performance of TPU-PDA 25, a urethane derived from poly(1,10-decylene adipate) diol (PDA) with outstanding shape memory properties. The highlight of this comparative study was that the inclusion of the amorphous urethane phase has a stronger effect on the textural and shape memory properties of PCL's crystalline domains than for PDA. PCL-derived urethanes are way stiffer and more rigid under comparable stress and strain conditions than TPU-PDA 25. The cause for this is the synergic effect between the utter restriction of the crystallization process of the semicrystalline PCL domains due to the tethering of their chain mobility by the insertion of PU's domains and the difference in the flexibility between the PDA monomer unit in comparison with the short-lengthened PCL repeating units with lower transition enthalpies.

9. Outlook

In consideration of the observations and main conclusions obtained from the work contained in the present dissertation, the following perspectives are conferred purposely to serve as a useful outlook and starting point for future studies/investigations focused on the design, production, and application of bidirectional shape memory polymeric actuators based on thermally cycled semicrystalline networks under constant stress and strain conditions.

- ❖ The further study of the thermomechanical properties under constant strain conditions of varied chemically crosslinked semicrystalline polymeric materials with diverse physicochemical/textural features promotes their potential and multiple applications as functional, versatile, and stable actuators.
- ❖ Evaluate the effectiveness of other chemical crosslink methodologies, e.g., UV-crosslinking, on the production of functional polymer actuators through the direct comparison of their thermomechanical performance with their thermally cured semicrystalline analogues under constant stress and strain setups.
- ❖ The structural characterization of the chemically crosslinked star-like PCL materials (CD-PCLs) under constant strain conditions upon cooling by means of small and wide-angle X-ray scattering measurements, followed by a contrasting investigation between the evolution of their textural properties with temperature in comparison with their linear PCL analogues.
- ❖ Investigation of the phase segregation, crystallinity, and further important textural parameters of stretched/unstretched PCL-PU systems with hard segments based on HDI/MDI+BD containing PCL soft segments with variable molecular weight distributions and different mass ratios between both phases by means of SEM, SAXS/WAXS. Correlate the studied structural properties with their ability to undergo reversible shape-switching transformation triggered by thermal cycling and its amplitude under strain and strain-free conditions.

Acknowledgments

Finally, I would like to extend my most sincere gratitude wholeheartedly to:

Prof. Dr. Leonid Ionov for his constant guidance, encouragement, and advice through the realization of this work as my supervisor.

Prof. Dr. Jens-Uwe Sommer for all the fruitful scientific discussions and collaboration on the theoretical aspects of this project.

Dr. Martin Dulle for all his enormous contributions on the realization and processing of the structural studies made on this dissertation.

Juan Manuel Uribe Gómez for his fundamental and important collaboration on the fulfilment of this work. Especially, thanks for always being there despite all the adversities.

Tatiana Albarracin Melo for all the battles, affection, true friendship, and support through all these years.

Diana Marcela Rodriguez for her marvellous friendship and always opportune advice.

Luis Felipe Rico for being the most special and unconditional friend that one person can possibly have.

To my dear friend Michael Karnitzschky and his family for always making me feel like home.

A toda mi familia, a mi padre Harold Posada, a mi madre Olga Marina Murcia, a mis hermanos Felipe Posada y Valentina Posada, mis abuelas, mis tías y primos, sin ustedes nada de esto sería posible. Muchas gracias por tanto amor y apoyo incondicional.

¡A la familia drinkomania por ofrecerme su amistad y hermandad a través de los años, esta va por ustedes también!

To the Ionov Lab staff and work colleagues for all their collaboration during my PhD.

A la Universidad Nacional de Colombia, sede Bogotá y la Universidad de los Andes por mi formación académica, profesional y laboral.

A Ruth Velasquez, Gabriel Roveda, Mayra Rodríguez, Dr. Sahar Salehi-Müller, Hanin Alkhamis, Dr. Elise Liensdorf, Justin Otto, el parche del Agustiniiano, David Sonnleitner y a todas aquellas personas que siempre me apoyaron y creyeron en mí. Ustedes saben quiénes son, muchas gracias.

Lastly, I would like to thank all the collaborators who made possible the realization of this dissertation through their expertise, knowledge, facilitation of facilities/materials, and fructiferous discussions: Dr.-Ing. José Alberto Rodríguez Agudo, Prof. Dr. Stephan Förster, Prof. Dr. Thorsten Pretsch, Dennis Schönfeld, Yaoming Zhang, Prof. Dr. Thomas Scheibel, Prof. Dr. Seema Agarwal, Prof. Dr. Kay Saalwächter, Prof. Dr. Thomas Thurn-Albrecht, Dr. Eva Bittrich, Dr. Konrad Schneider, and Dr. Andrei Zakharov.

(Eidesstattliche) Versicherungen und Erklärungen

(§ 9 Satz 2 Nr. 3 PromO BayNAT)

Hiermit versichere ich eidesstattlich, dass ich die Arbeit selbstständig verfasst und keine anderen als die von mir angegebenen Quellen und Hilfsmittel benutzt habe (vgl. Art. 64 Abs. 1 Satz 6 BayHSchG).

(§ 9 Satz 2 Nr.3 PromO BayNAT)

Hiermit erkläre ich, dass ich die Dissertation nicht bereits zur Erlangung eines akademischen Grades eingereicht habe und dass ich nicht bereits diese oder eine gleichartige Doktorprüfung endgültig nicht bestanden habe.

(§ 9 Satz 2 Nr. 4 PromO BayNAT)

Hiermit erkläre ich, dass ich Hilfe von gewerblichen Promotionsberatern bzw. –vermittlern oder ähnlichen Dienstleistern weder bisher in Anspruch genommen habe noch künftig in Anspruch nehmen werde.

(§ 9 Satz 2 Nr. 7 PromO BayNAT)

Hiermit erkläre ich mein Einverständnis, dass die elektronische Fassung meiner Dissertation unter Wahrung meiner Urheberrechte und des Datenschutzes einer gesonderten Überprüfung unterzogen werden kann.

(§ 9 Satz. 2 Nr. 8 PromO BayNAT)

Hiermit erkläre ich mein Einverständnis, dass bei Verdacht wissenschaftlichen Fehlverhaltens Ermittlungen durch universitätsinterne Organe der wissenschaftlichen Selbstkontrolle stattfinden können.

Bayreuth, 21.11.2022,

.....

Ort, Datum, Unterschrift